Numéro d'ordre : 41639

Université des Sciences et Technologies de Lille
Laboratoire de Mécanique de Lille (UMR CNRS 8107)
Ecole Doctorale Sciences Pour l'Ingénieur - Université Lille Nord de France

THESE

Pour obtenir le grade de

Docteur de l'Université Lille 1 Sciences et Technologies

Discipline : Mécanique, Energétique, Matériaux

Présentée et soutenue publiquement

par

Cristian OVALLE RODAS

1 Décembre 2014

Couplage thermo-mécanique et auto-échauffement en fatigue des élastomères renforcés

Thermo-mechanical coupling and heat build-up of filled rubbers under fatigue

Jury

R. ESTEVEZ	Professeur	Université de Grenoble	
L. LAIARINANDRASANA	Professeur	MINES ParisTech	
N. AIT-HOCINE	Professeur	INSA Centre Val de Loire	
F. ZAIRI	Professeur	Université Lille 1	Codirecteur de thèse
M. NAIT-ABDELAZIZ	Professeur	Université Lille 1	Directeur de thèse

Boulevard Paul Langevin, Cité Scientifique, 59655 VILLENEUVE D'ASCQ CEDEX

CONTENTS

AGRADECIMIENTOS

Sin ti, mi amada esposa, Leidy Cristina Velásquez, este camino estaría falto de amor y belleza. Tu me has apoyado con estoico amor, has hecho tuyos mis sueños haciendo a un lado los tuyos, has llenado de alegría un duro camino. Agradezco con todo mi corazón tu inmenso apoyo y le agradezco a la vida por haberte puesto a mi lado.

Tu, mi princesita Susan Valeria, has invadido nuestros corazones de felicidad y bellos momentos. Al igual que tu mami, sin ti este camino no hubiera sido más que un sendero lleno de maleza y rocas. Espero que esta experiencia te motive a esforzarte por alcanzar tus sueños, sin importar cuán grandes o lejanos parezcan.

Aún no hemos contemplado tu carita pero al soñar ya con ella te amamos con todo el corazón. Tú eres un motivo más que la vida nos obsequia para seguir buscando nuevas metas y ser felices. Ya pronto estarás a nuestro lado y llenaras de más alegría nuestras vidas.

Desde pequeño mis padres, Wuilian Ruiz y María Luisa Rodas, han guiado mis pasos y ahora, como adulto, sus consejos me han enriquecido... Gracias por todo su amor y apoyo, a pesar de la distancia siempre han estado a nuestro lado. Los recuerdos de los momentos juntos, que la vida nos ha obsequiado, han hecho aparecer siempre una sonrisa en mi rostro.

Hemos seguido distintos senderos, pero me alegra grandemente saber que al igual que yo, mis hermanos, Adolfo y Carlos Ovalle, han encontrado el camino de la felicidad y la satisfacción. Somos y actuamos diferentemente, pero son muchas de esas diferencias las que más admiro en ustedes. Sigan siendo una fuente de admiración para mí y sus familias.

La familia que la vida me ha obsequiado es muy grande, y así de grande es el amor y cariño que ellos siempre nos han expresado. Lo siento por no mencionar a cada uno de ustedes en estos momentos, pero puedo asegurarles que el nombre de cada uno viene a mi mente, especialmente de aquellos pocos que ya nos han dejado. Gracias por ser ese lazo que conecta el futuro con el pasado.

Desde que era un niño soñaba con ser científico, no sé si obtener un doctorado sea suficiente para serlo, pero estoy seguro que es un paso en la dirección correcta. Deseo agradecer a mí director, Prof. Moussa Naït-Abdelaziz, no solo por ayudarme a dar este paso de forma ideal sino especialmente por el apoyo y la confianza que en todo momento me ha brindado.

Siempre he creído que el tiempo avanza rápidamente cuando compartimos los momentos con personas que enriquecen nuestra forma de ser o que nos ayudan a adoptar una nueva perspectiva ante los problemas. Una de esas personas es mi amigo y co-director, Prof. Fahmi Zaïri. Gracias por las interesantes discusiones en torno a un café.

Deseo agradecer a los miembros del comité, Prof. Raphael Estevez, Prof. Lucien Laiarinandrasana y Prof. Nourredine Aït-Hocine por su indudable apoyo en el duro trabajo de corrección. Gracias, al igual, por sus brillantes comentarios y sugerencias respecto a mi trabajo de investigación y por permitir que mi defensa fuese un momento agradable.

Nuestra vida en Francia no hubiera sido tan gratificante sin nuestras diferentes familias adoptivas y amigos; especialmente, por el amor que siempre le han manifestado a mis dos amores. Indudablemente ustedes han llenado nuestras vidas de esperanzas y alegrías. Infinitamente gracias...

Qué duda cabe, los amigos son una extensión de la familia. Tengo tantos amigos a quienes agradecerles las palabras, momentos, risas y tristezas compartidas; honestamente, no sabría bien con quién empezar... Ustedes son parte de este sueño. Gracias por estar pendientes de este camino y mi familia, a pesar de la distancia.

REMERCIEMENTS

Sans toi, ma chère épouse, Leidy Cristina Velásquez, ce chemin semé d'embûches aurait manqué d'amour et de beauté. Tu m'as soutenu avec un amour infaillible en faisant parfois passer mes rêves avant les tiens, tu as rempli de joie ce chemin difficile à parcourir. Je remercie de tout cœur ton soutien immense et je remercie le destin de me permettre de t'avoir à mes côtés.

Toi, ma princesse Susan Valeria, tu as rempli nos cœurs de bonheur et de moments magnifiques. Tout comme ta maman, sans toi ce chemin n'aurait été pas plus qu'un sentier fait de mauvaises herbes et de cailloux. J'espère que cette expérience t'incitera à faire tous les efforts possibles pour réaliser tes rêves, peu importe si ils semblent inaccessibles.

Nous n'avons pas encore vu ton visage mais déjà nous en rêvons et nous t'aimons de tout notre coeur. Tu es une raison de plus que nous a donnée la vie pour continuer à nous fixer de nouveaux objectifs et pour être encore plus heureux. Tu seras bientôt à nos côtés pour remplir nos vies de joie.

Depuis tout petit mes parents, Wuilian Ruiz et María Luisa Rodas, ont guidé mes pas et aujourd'hui, en tant qu'adulte, leurs conseils m'enrichissent. Merci pour tout votre amour et votre soutien, malgré la distance qui nous sépare, vous avez toujours été à nos côtés. Le souvenir des moments que la vie nous a permis de passer ensemble fait toujours naitre un sourire sur mon visage.

Nous avons suivi des voies différentes, mais le fait de savoir que, tout comme moi, mes frères, Adolfo et Carlos Ovalle, ont trouvé le chemin du bonheur et de l'épanouissement, me remplit de joie. Nous sommes et nous agissons différemment, mais ce sont justement ces différences que j'admire en vous. Vous serez toujours une source d'admiration pour moi et pour toute la famille.

La famille que la vie m'a donné est très grande, aussi grande que l'amour et la tendresse que cette famille nous a toujours témoigné. Je regrette de ne pouvoir mentionner chacun d'entre vous mais je peux vous assurer que chacun de vos noms me vient à l'esprit, et notamment le nom de ceux qui ne sont plus de ce monde. Merci pour être le lien qui relie le futur au passé.

Depuis tout petit, je rêvais d'être un scientifique, je ne sais pas si obtenir un doctorat est suffisant pour en être un, mais je suis sûr que c'est un pas dans la bonne direction. Je souhaite remercier mon directeur, le Professeur Moussa Naït-Abdelaziz, pas seulement pour me guider dans la bonne voie, mais surtout pour le soutien et la confiance qu'il m'a accordé à chaque instant.

J'ai toujours pensé que le temps passait plus vite quand on le partage avec des personnes qui enrichissent notre manière d'être ou qui nous aident à envisager les problèmes sous une autre perspective. Une de ces personnes est mon ami et co-directeur, le Professeur Fahmi Zaïri. Merci pour toutes ces discussions intéressantes autour d'un café.

Je souhaite remercier les membres du comité, le Professeur Raphael Estevez, le Professeur Lucien Laiarinandrasana et le Professeur Nourredine Aït-Hocine pour leur indubitable soutien dans le dur travail de correction. Merci également pour leurs brillants commentaires et suggestions en ce qui concerne mon travail d'investigation et pour avoir fait de ma soutenance un moment agréable.

Notre vie en France n'aurait pas été aussi gratifiante sans les différentes familles d'adoption et les amis que nous avons, ici en France; et surtout grâce à l'amour que vous avez toujours témoigné à mes deux amours. Indéniablement, vous avez rempli nos vies d'espoir et de joie. Je vous remercie infiniment…

Sans aucun doute, les amis sont un prolongement de la famille. Tant d'amis que je souhaiterais remercier pour avoir eu un mot gentil, pour avoir partagé avec nous des moments de joie, des rires et parfois des peines. Honnêtement, je ne saurais même pas par qui commencer…. Vous faites partie de ce rêve. Merci d'avoir été présents pour moi et ma famille tout au long de ce chemin, et ce malgré la distance qui nous séparait.

INTRODUCTION

The present PhD dissertation deals with the coupled thermo-mechanical behavior of filled rubbers. In many common industrial applications, a filled rubber is submitted to cyclic deformations of significant magnitude and frequency to generate a considerable amount of heat and, depending on the rate of heat removal, a significant heat build-up. The order of magnitude of the heat build-up is related with the strain rate, the maximum strain, the geometry of the specimen, and the filler volume fraction. On the other hand, the physical consequences of a higher temperature include the degradation of the ultimate and abrasion resistances, decrease of the static and elastic module and smaller loss factor. Moreover, as a result of the effect of the increase of the temperature due to hysteresis, some rubber compounds that can be highly hysteretic at room temperature can be moderately hysteretic at the stabilized operating temperature. Since the material behavior depends both on the filler volume fraction and on the temperature of the studied specimen, the development of a physically-based thermo-mechanical model capable to explicitly take into account both characteristics, as well as to describe the temperature evolution under fatigue loadings in parallel with the well-known non-linear elastic behavior when submitted to large strains, is an open issue to be addressed.

This work is divided into three main parts. The first part (*Chapter 1*) brings a brief review about the necessary contents to understand the following chapters. The second part (*Chapter 2*) highlights the effect of both the filler volume fraction and the temperature over the thermo-mechanical response of filled rubbers. The third part (*Chapters 3* and *4*) is focused on the material heat build-up over a wide range of strain rates, stretch levels and filler volume fractions.

Chapter 1 is a succinct summary of classic knowledge which can be found in specialized works and that have been selected for their relevancy in the present study for the reader convenience. The industrial applications and the research history are briefly reported. Moreover, in order to understand the rubber behavior at the macroscopic scale from their microscopic architecture, the chemical characterization is presented. Then, the thermo-mechanical behavior of filled rubbers will be drawn. In the last section, the well known continuum mechanics theory as well as the laws of the thermodynamics are recalled. Finally, some notions about hyperelastic models of rubber-type materials are presented.

In *Chapter 2* a physically-based model to describe the large strain relaxed response of filled rubbers over a wide range of temperatures is developed. The non-linear mechanical behavior is described via a Langevin formalism in which the temperature and filler effects are, respectively, included by a network thermal kinetics and an amplification of the first strain invariant. Experimental observations on the relaxed state of styrene-butadiene rubber hourglass-shaped specimens with a given carbon-black content are reported at different temperatures. A hybrid experimental-numerical method is proposed to determine simultaneously the local thermo-mechanical response and the model parameters. Furthermore, the predictive capability of the proposed constitutive thermo-mechanical model is checked by comparisons with results issued from micromechanical simulations containing different arrangements of the microstructure. The results show that the proposed model offers a satisfactory way to predict the relaxed response of filled rubbers at different temperatures.

A thermo-visco-hyperelastic constitutive model, in accordance with the second thermodynamics principle, to describe the heat build-up in rubber materials under cyclic loading is formulated in *Chapter 3*. The mechanical part of the model is based upon a Zener rheological representation in which the specific free energy potential is dependent on an added internal variable, allowing the description of the time-dependent mechanical response. The large strain mechanical behavior is described

using a Langevin spring, while the continuous stress-softening under cyclic loading is taken into account by means of a network alteration kinetics. The thermo-mechanical coupling is defined by postulating the existence of a dissipation pseudo-potential, function of the viscous dilatation tensor. The proposed model is fully three-dimensional and was implemented into a finite element code. The model parameters are identified using experimental data obtained on a styrene-butadiene rubber under a given strain rate for different strain conditions. Predicted evolutions given by the model for other strain rates are found in good agreement with experimental data.

Finally, in *Chapter 4*, the proposed thermo-mechanical model presented in *Chapter 3* is modified to take explicitly into account the filler volume fraction effect over the heat build-up. Moreover, the stress-free thermal-dilatation is also taken into account. The model parameters are identified using experimental data obtained on a styrene-butadiene rubber with a fixed amount of carbon-black, 25 phr (part per hundred of rubber in weight), under a given strain rate for different strain conditions. Predicted evolutions given by the model for other strain rates and amounts of carbon-black, 15 and 43 phr, are found in good agreement with experimental data. The capability of the model to predict the heat build-up of cylindrical samples during fatigue as well as its effect on the rubber lifetime is discussed.

General conclusions and *Research perspectives* are presented at the end of the document.

CHAPTER 1

Elements of structure, mechanics and thermodynamics of elastomers

This chapter is intended to offer a conceptual frame of reference that allows the reader to deep into the posterior contents with a major sensation of comfort.

In the *generalities* section the application and the polymers research history, giving relative emphasis to the rubber materials, is briefly reported. Later, the definitions of concepts related with the chemistry that characterize the different polymers and that allow to understand their behavior in the macroscopic scale from their microscopic architecture are presented. From this characterization, it is possible to go more deeply into the particular characteristics of the elastomers and, especially, into the studied material: styrene-butadiene rubber filled with carbon-black particles.

The thermo-mechanical behavior of the elastomers as a result of different test conditions will be drawn in the section dedicated to the *filled elastomers thermo-mechanical behavior*. At the same time, the effects in the thermo-mechanical behavior of elastomers by the incorporation of carbon-black fillers are described in this section.

In the last section, *elements of continuum mechanics and thermodynamics*, the classic knowledge of finite strain mechanics of continuum medium as well as the thermodynamics laws that describe the material behavior in a coherent way regarding the physical laws is exposed. Finally, some notions concerning statistical and phenomenological models to describe the large strain elastic behavior of rubber-type materials are presented.

1. Generalities

1.1 Historical background[1]

In 1496, after his second voyage to America, Christopher Columbus brought back to Europe crude rubber balls after having seen the Haitian natives playing with rubber balls. The natives in Haiti made these by cutting into bark of the rubber tree, smearing the latex which exuded onto the pointed end of a wooden stick and then drying it near a fire. In fact, it is well established that ancient American cultures as the Olmec, the Aztecs, the Mayas and the Incas already used the latex to manufacture common objects like boots, containers, covered tiles and, especially, balls, as they used to play with them an ancient game representing an important aspect of their cosmogony (Ximenez, 1715). Although there was much interest in Europe in this material little progress was made concerning its use: the latex would coagulate on its long voyage from the New to the Old World and coagulated latex was hard to work with.

The South America exploration by the Frenchman Charles-Marie de La Condamine, in 1736, brought again the potential of rubber to the attention of the Europeans. He gallicizes the word 'cao tchu', meaning *tree that cries* in the native language, to *caoutchouc* and bring back some samples to the French Guyana. The first scientific studies are attributed to the French engineer François Fresneau who has impregnated his boots of latex to waterproof them. Unfortunately, the rubber is sensitive to the temperature (i.e., it rigidifies at low temperatures and becomes viscous at high temperatures) so its application remained very limited. In 1791, the British manufacturer Samuel Peal got a patent of the first industrial application of rubber related with the fabric waterproofing by means of a rubber - oil of turpentine solution. Around 1818, Charles Macintosh discovered another way to waterproof fabrics: he adhered two fabric sheets together using a rubber – coal-tar naphtha solution. The waterproof property is obtained when the solvent is evaporated. In 1835, the chloride of vinyl polymerization was accidentally discovered by Henri Victor Regnault. A great advance in rubber application was the discovery by Charles Goodyear in 1838 that natural rubber containing sulfur turned elastic after heat treatment (i.e., vulcanization). In 1862, Alexander

[1] The text is based on the natural rubber history section from Baranwal and Stephens (2001); however, additional references have been added.

Parks made a material named Parkesine modifying cellulose with nitric acid to form cellulose nitrate and mixing this polymer with a plasticizer. This discovery is the base of the modern plastic industry. The growth of rubber products was increasing and, in 1888, John Dunlop developed a pneumatic rubber tire for bicycles hereby initiating the *tire age*.

The 20th century marks the beginning of significant studies related with the behavior and properties of polymers and, specially, the development of synthetic polymers. In 1905, Leo Baekeland made the Bakelite, the first wholly synthetic polymer from phenol and formaldehyde. It can be said that the polymer science began in the 20s with the formulation of the macromolecular concept by Hermann Staudinger. In the 1930s, Werner Kuhn, Eugene Guth and Herman Mark proposed the statistical mechanical theory for rubber elasticity; besides, they found evidence that polymer chains in solution were flexible and that the viscosity in a solution was related to the molar mass of the polymer. Around 1933, the styrene-butadiene rubber was made in Germany; meantime, Wallace Carothers synthesize the first aliphatic polyester, and later and more importantly, the polychloroprene and the polyamide 6.6 (Nylon). The epoxy resins, the silicone rubbers and the polytetrafluoroethylene (Teflon®) were made, respectively, by Pierre Castan, Eugene Rochow and Roy Plunkett in the second half of the 30s. The thermodynamics theory for polymer solutions was presented, independently, in 1942 by Paul Flory and Maurice Huggins. The low-density polyethylene and the glass-fiber reinforced polyester were made during this decade. It is possible to say that since 1920 to 1950 a first generation of polymers was developed. Between 1950 and 1965 polymers of second generation were proposed. Karl Ziegler and Guilio Natta work led to the development of linear polyethylene and isotactic polypropylene. Theories for liquid crystals of rod-like polymers were proposed by Lars Onsager in 1949 and by Paul Flory in 1956. In this same year Michael Szwarc discovered living anionic polymerization - Kraton® is prepared by this method. The polyoxymethyle (Delrin®) and the aromatic polyamide (Nomex®) were made by DuPont in the first half of the 60s. Finally, a third generation of polymers, introduced since 1965, consisting mainly of polymers with a more complex chemical structure was developed. These polymers were characterized by high thermal and chemical stability and high strength. Meanwhile, existing polymers such as polyethylene have undergone significant improvement. In 1971, Pierre-Gilles de Gennes presented the reptation model to describe the diffusion of chain molecules

in a matrix of similar chain molecules. The first melt-processable polymer (Xydar®) was reported by Steven Cottis in 1972. Theories for the crystallization of polymers were introduced by John Hoffman and coworkers in the mid-70s. Paul Morgan and Stefanie Kwolek reported, in 1977, that solutions of poly(phenylene terephthalamide) could be spun to super-strong and stiff fibers (Kevlar®). In 1977, the first electrically conductive polymer was prepared by Alan MacDiarmid, Alan Heeger and Hideka Shirikawa. Nowadays, considering the nearby end of petroleum the industry of polymers contemplates, again, the use of natural rubber and searches substitutes to petroleum products by means of the synthesis of vegetal-based polymers.

1.2 Polymers

A polymer is a substance composed of molecules of high relative molecular mass, in which the structure essentially consists in the multiple repetition of units derived from molecules of low relative molecular mass connected between them in sufficient quantity to provide a set of properties that not varies significantly with the addition of one or few repetition units (Jones, 2008).

The polymer architecture, the shape of a single polymer molecule, is constituted by the chemical composition of the monomer (repetition unit), the atoms disposition and links, the sequence order and the topologic aspects. Common polymer architectures are presented in **Fig. 1.1**. The molecular architecture is important to describe many properties:

- Short-chain branching tends to reduce crystallinity,
- Long-chain branching tends to have a profound effects on rheological properties,
- Hyperbranched polymers consist of molecules with an approximately spherical shape, and
- Cross-linked polymers do not melt.

Considering the number of repeating units, a homopolymer consists of only one type of repeating unit whereas, on the other hand, a copolymer consists of two or more repeating units.

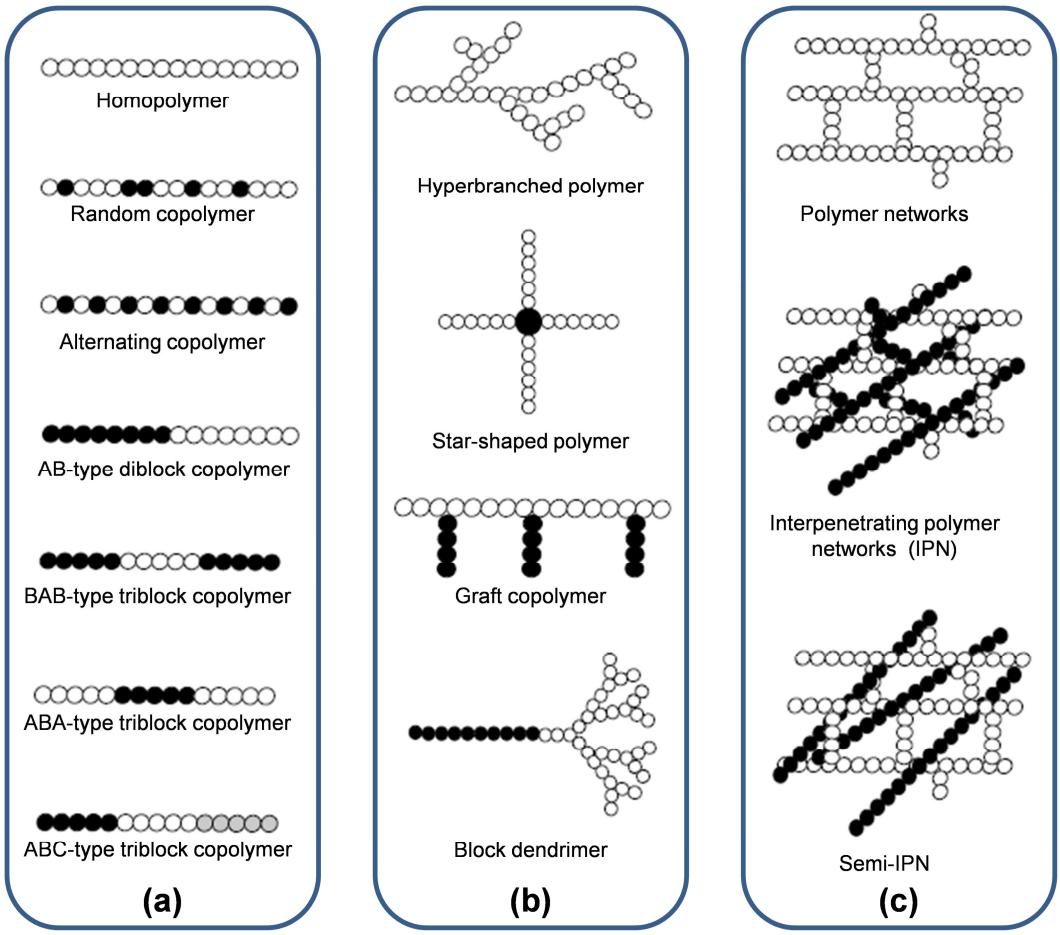

Fig. 1.1 Polymer architectures: (a) linear polymers, (b) branched polymers, and (c) cross-linked polymers (Qiu and Bae, 2006).

In general, the polymers are constituted by nine chemical elements: the carbon, the hydrogen, the sulfur, the oxygen, the fluorine, the silicon, the phosphor, the nitrogen and the chlorine (Kausch et al., 2001). The chain framework is constituted principally of carbon atoms linked by covalent bonds where the dissociation energy is in the order of E_C = 300 kJ/mol. Other types of atoms or molecules can be linked to the framework by polar or by van der Waals bonds where the dissociation energy is in the order of E_P = 10 kJ/mol, see **Fig. 1.2**. The large difference in dissociation energy between different molecules is of great importance for polymer properties. A polymer preserves its configuration, 'permanent' stereostructure of a polymer, until it reacts chemically. The configuration is defined by the polymerization method - chemical reaction that converts monomers to a polymer.

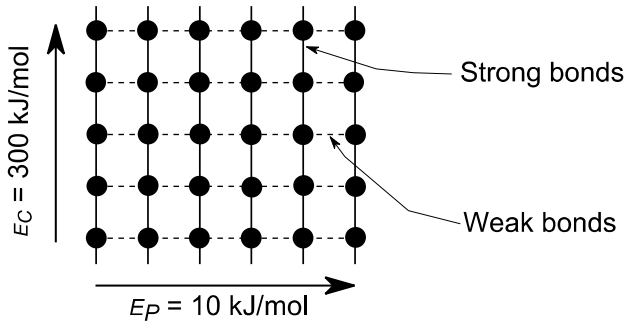

Fig. 1.2 Schematic representation of a polymer crystal illustrating the bonds type.

The polymerization method can be divided into step-growth and chain-growth polymerization. In the step-growth process the kinetics of polymerization is not affected by the size of the reacting parts. The number of reacting groups decreases with increasing length of the molecules. At any given moment, the system will consist of a mixture of growing chains and water. Chain-growth polymerization involves several consecutives stages: initiation, propagation and termination. Each chain is individually initiated and grows very rapidly to a high molar mass, until its growth is terminated. At a given time, there are essentially only two types of molecules present: monomer and polymer. The number of growing chains is always very low.

1.2.1 Amorphous and semi-crystalline polymers

The flexibility of the molecules allows different kinds of organization that presents an order less regular than within the metallic crystals. In fully amorphous polymers the chains are randomly arranged in the scale of a set of molecules but with certain order at a smaller scale (**Fig. 1.3**). In spite of the random arrangement, the amorphous polymers are isotropic and frequently transparent in the macroscopic scale.

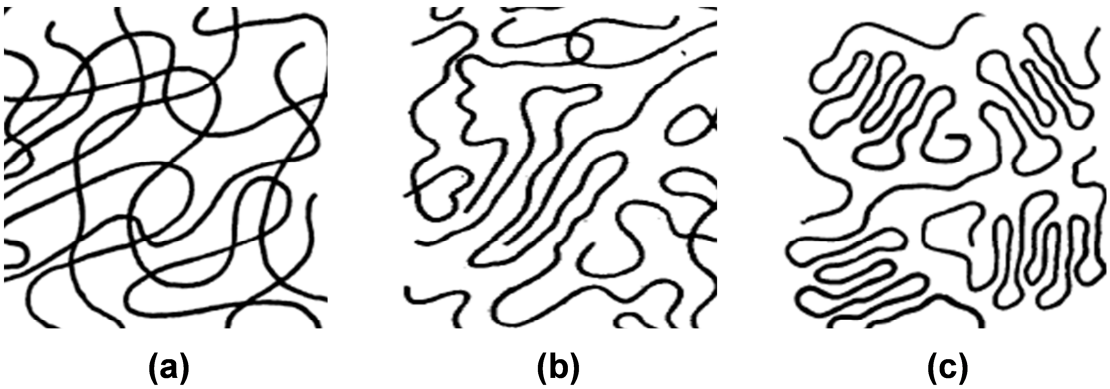

Fig. 1.3 Structural representation of an amorphous polymer: (a) (Flory, 1953), (b) (Privalko and Lipatov, 1974), and (c) (Yeh, 1980).

A polymer is called semi-crystalline when the molecules of long chains tend to be arranged in packages to form crystallites separated by amorphous regions (**Fig. 1.4**). In order that a polymer crystallizes it is necessary that its macromolecular chain has a strong regularity and also that its crystallization kinetics is not relatively slow. The crystallizable polymers will have a regular configuration and a regular global conformation, planar or helical zigzag in the thermoplastic polymers (Haudin, 1995). However, the macromolecular chains are not rigorously regular and the minimal irregularity, the enchainment of composing monomers or the presence of a ramification into the chain, will modify, limit, or avoid the crystallization. From the crystallization, the regular macromolecular chains, that can measure some micrometers of length, are organized and fold to form lamellae. The lamella crystallites form a superstructure with an average mesh size of 1 μm. They represent zones more resistant than the amorphous zones even that they contain an imperfect organization. The thickness and the regularity of the lamellae depend on the crystallization conditions and on the chains rigidity, ramifications, and the entanglements faults. These imperfections favor the connection between lamellae, where they are linked by means of chunks of macromolecular chains (link chains) that belongs to other lamellae. The partially crystalline polymers are translucent and opaque, although the individual crystallites are far too small to scatter visible light individually.

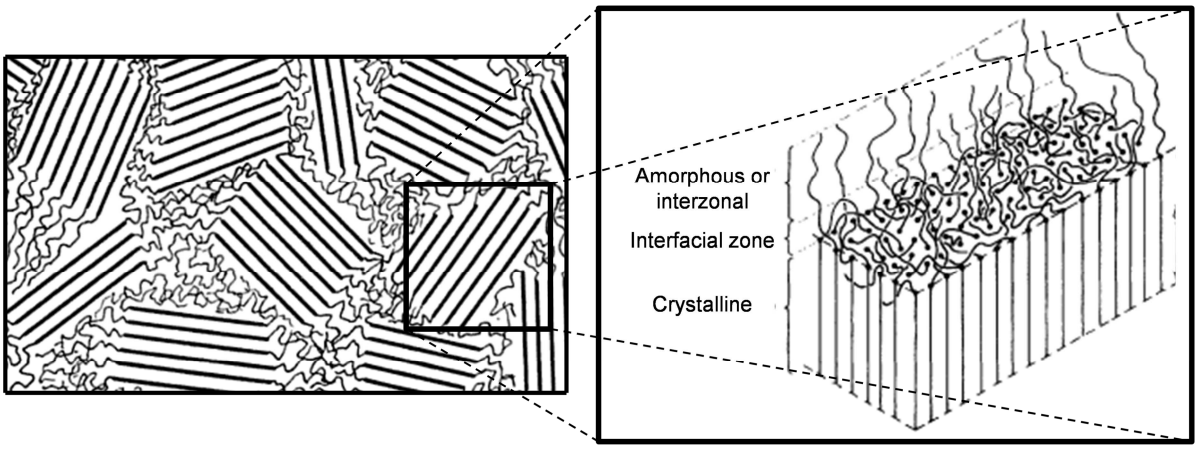

Fig. 1.4 Structural representation of a semi-crystalline polymer.

A third recently developed group of polymers is the liquid-crystalline polymers, showing orientational order but not positional order. They are thus intermediates between the amorphous and the crystalline polymers. The nematic is the most probable liquid-crystalline phase to be formed directly from an isotropic melt, see **Fig. 1.5**.

Fig. 1.5 Structural representation of a liquid-crystalline polymer.

The differences in crystallinity can lead to differences in physical properties. A polymer can appear in four different states, as a function of the temperature, which corresponds to a temperature-function growth of the intermolecular free volume and a decrease of the link forces, e.g. analyzing the curve of the density or of the elasticity modulus as a function of temperature, different polymer states can be observed (**Fig. 1.6**).

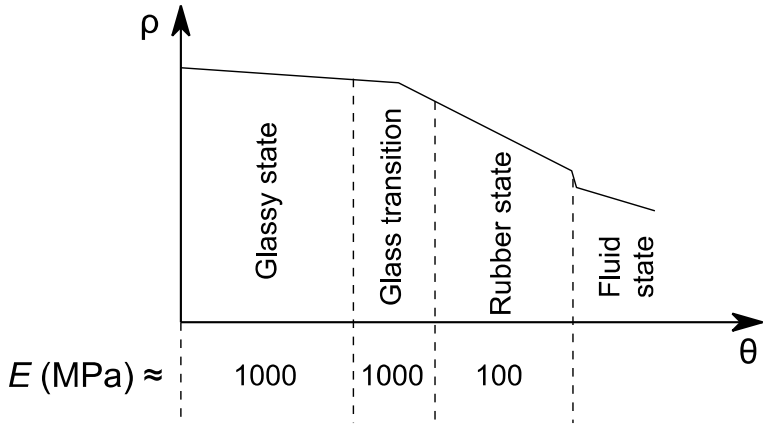

Fig. 1.6 Polymer states.

According to the polymer, the environment temperature can be found into one of the four zones. At the glass transition region a fully amorphous polymer shows an important drop in modulus. The material state is glassy at temperatures below the glass transition temperature, θ_g. Under these conditions the organic glasses admits uniquely weak deformations predominantly due to stretching of secondary bonds and bond angle deformation. The glass transition region shows many kinetic peculiarities (e.g., damping behavior) and it is not a true thermodynamic phase transition like crystal melting. In this region, the linear

thermoplastic and cross-linked polymers where the chemical decomposition occurs before fusion are found. At temperatures above θ_g, the materials are rubber-like with a weak modulus. In the rubber state region, large groups of atoms can change their conformation, e.g. cross-linked polymers show elastic properties due to the high rate at which the conformational changes occurs that the strain response to a step stress is instantaneous. On the other hand, the pronounced drop in modulus occurring at higher temperatures in uncross-linked polymers is due to the melting of the crystalline component.

1.2.2 Polymer categories

One suitable way to categorize the polymers is in terms of their mechanical and thermal behavior as:

- **Thermoplastics** are composed of long chains produced by a chain-growth polymerization; they typically behave in a plastic-ductile manner. The chains may or may not have branches. Individual chains are intertwined. There are relatively weak van der Waals bonds between atoms of different chains. This is somewhat similar to a few trees that are tangled up together. The trees may or may not have branches, each tree is on its own and not connected to another. The chains in the thermoplastics can be untangled by application of a tensile stress. Thermoplastics can be amorphous or crystalline. Upon heating, thermoplastics soften and melt. They are processed into shapes by heating to elevated temperatures. Thermoplastics are easily recycled.
- **Thermosetting polymers** are composed of long chains (linear or branched) of molecules that are strongly cross-linked to one another to form three-dimensional network structures. Network of thermosetting polymers are like a bunch of strings that are knotted to one another in several places and not just tangled up. Each string may have other side strings attached to it. Thermosets are generally stronger, but more brittle, than thermoplastics. Thermosets do not melt upon heating but begin to decompose. They cannot easily be reprocessed after cross-linking reaction has occurred and hence recycling is difficult.
- **Elastomers** may be thermoplastics or lightly cross-linked thermosets. The polymer chains consist of coil-like molecules that can reversible stretch by applying a force. They can be stretched easily to high extensions and rapidly recover their original dimensions. They are commonly known as rubbers.

1.3 Elastomers

1.3.1 Processes to obtain synthetic elastomers

The synthetic elastomers are obtained by means of polymerization, polycondensation or copolymerization reactions that consist on the creation of chemical bonds between molecules to develop other molecules of higher dimensions.

The polymerization confronts the monomer with activation elements into a reactor[2]. The polymerization takes place in several stages:

- **Activation**: this reaction aims to create active centers, A* and B* (**Fig. 1.7**), if R is the monomer.
- **Propagation**: the active center (ion or radical) is placed at an extremity of the chain and reacts little by little with the monomer.
- **Chain transfer and ending**: the active center can be preserved or destroyed during the ending stage.

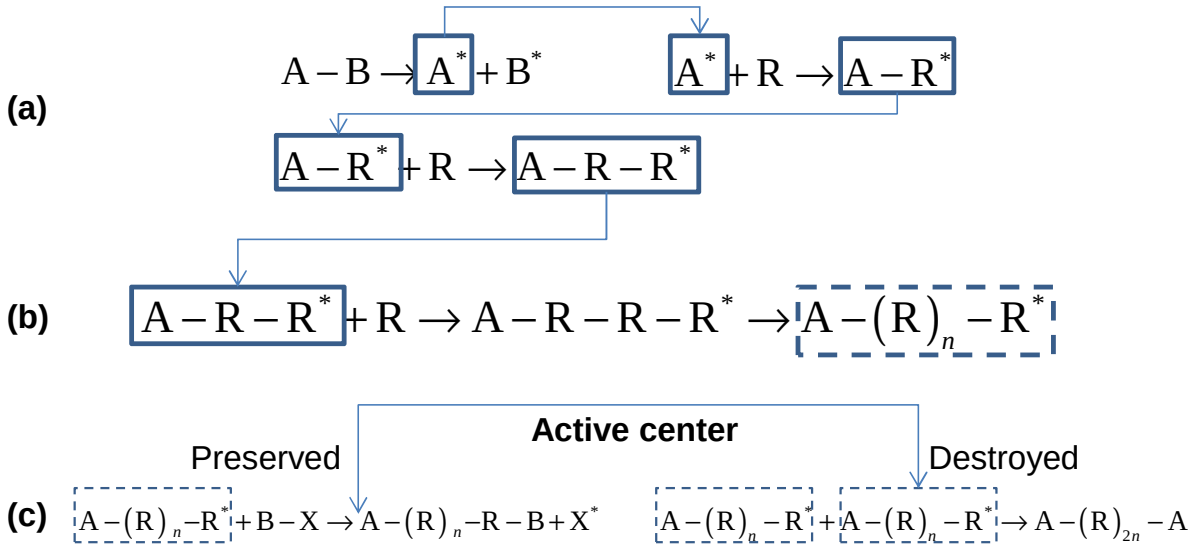

Fig. 1.7 Polymerization reaction: (a) activation, (b) propagation, and (c) chain transfer and ending.

On the other hand, during the polycondensation the macromolecule is produced by the reaction of molecules having different chemical nature. Finally, the copolymerization

[2] The chemical reactors offer the ideal conditions in terms of temperature, pH, solvents, pressure, etc. to obtain a certain type of elastomer.

consists of associate different types of monomers in order to improve the properties of the final material. There are three types of copolymers: alternating copolymer, statistical copolymer and block copolymer (**Fig. 1.1**).

1.3.2 Formulation of elastomers

Seven categories of ingredients in the composition of an elastomer are distinguished:

A. **Elastomeric matrix**: The most important ingredient in rubber formulation. The elastomers can have natural or synthetic origin. Diverse elastomer grades exist differentiating, for example, the molecular distribution, the chain-length, the link rate, the monomer rate – copolymers and terpolymers[3] – and the oil or carbon-black presence. Specific elastomers are selected for desired compound properties. An elastomeric matrix can be used alone or associated with one or several elastomeric matrices.

B. **Fillers**: They are particles used to reinforce or enhance properties of elastomers while reducing cost of the compound. Their ability to interact with the elastomeric matrix confers a, more or less, reinforcing character to the final mixture. Evidently, the reinforcing character depends on the filler-matrix chemical compatibility. Usually, the used mixtures have a load-rate that place them near the percolation limit, e.g., for a mixture containing 100 g of elastomer (ρ_e = 1000 kg /m^3) and 50 g of filler (ρ_f = 2000 kg /m^3), the volumetric fraction, φ_{filler}, is 0.2, whereas the limit is 0.3. The average particle size of the filler is the most important parameter concerning the capability to impart reinforcement to elastomers – reinforcement is obtained with sizes smaller than 100 nm.

   There are two types of fillers commonly used by the rubber industry: Carbon-black and white fillers. High-resolution electron microscopy has shown (Leblanc, 2002) that carbon-black is built up of complex arrangements of spherical entities (colloidal black) whose diameter ranges from 10 to 90 nm (**Fig. 1.8**). In general, the smaller the particle size, the more reinforcing the carbon-black, i.e. improvement in tensile, modulus, hardness and abrasion strength. The colloidal blacks are spheres made-up of broken quasi-graphitic layers whose stacking gives edges with a steps-like structure; depending on the manufacturing process, they exist in various forms of aggregation. The aggregates – smallest dispersible entity – form complex tri-dimensional objects (structure) which are

[3] Polymer consisting of three distinct monomers.

associated into agglomerates. In a rubber compound, the void spaces within the aggregates are filled with rubber. This rubber – occluded rubber – is partly shielded from deformation and thus acts as part of the filler rather than as part of the rubber matrix (Medalia, 1970).

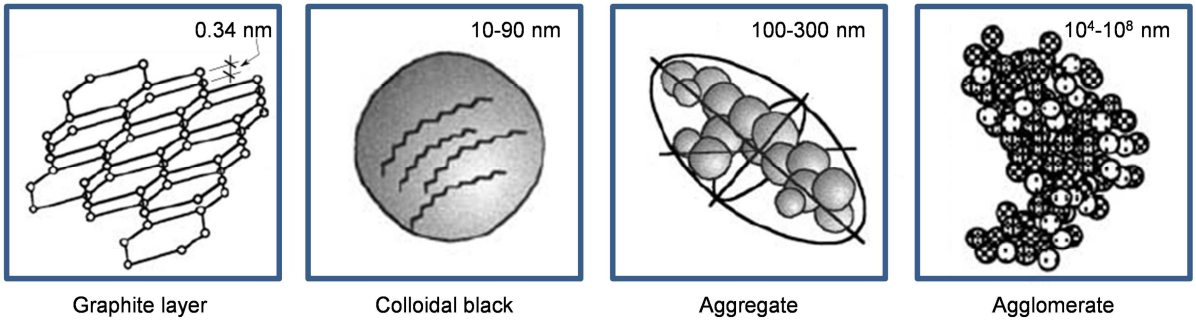

Fig. 1.8 Relevant dimensions concerning the filler structure.

On the other hand, the non-black fillers contribution to the compound properties depends exclusively on the surface area. The first fillers used in rubber products were minerals that were naturally available: zinc oxide, clay, mica and asbestos. As in the carbon-black fillers, they were added to reduce tack, increase hardness and reduce the cost of the compound. It must be taken into account that the fillers increase up to 10° the glass transition temperature.

C. **Processing aids**: They aim to improve the mixing operation of the different constituents of the material and to facilitate the calendering, extrusion and molding of the final product having increased the mobility of the polymer chains diminishing, therefore, the viscosity of the mixture. They act – without a chemical reaction – upon the mechanical properties of the final mixture and especially upon the viscoelastic properties – inverse relation between the chains mobility and the glass transition temperature. Additionally, they are used as dilution component of the elastomeric matrix in order to obtain a more economic mixture and to preserve satisfactory mechanical properties with higher filler molecules.

   Hydrocarbon oils are the most commonly used processing aids. Other processing aids used in rubber compounds are fatty acids, waxes, organic esters and low molecular weight polymers.

D. **Deterioration inhibitors**: The deterioration inhibitors or antidegradants are chemical products used to protect rubber both in uncured and cured states. The time, the

temperature, the ozone and the light evolve the material structure (i.e., aging). These environment phenomena break in depth the double links within the material; as a consequence, a mechanical properties evolution can be seen. Evidently, good aging properties of rubber compounds are essential for providing acceptable service life. In general, the more saturated the main chain of the elastomer matrix, the better are the aging properties.

E. **Vulcanizing agents**: They are chemical products that, upon heating, crosslink elastomer molecules to provide harder, more thermally stable elastic products. The most common vulcanizing agent is sulfur. During curing (vulcanization) a three-dimensional crosslinked network which imparts properties to compounds is formed. In fact, upon the vulcanization the rubber is changed from essentially a plastic material to either elastic or hard material (**Fig. 1.9**).

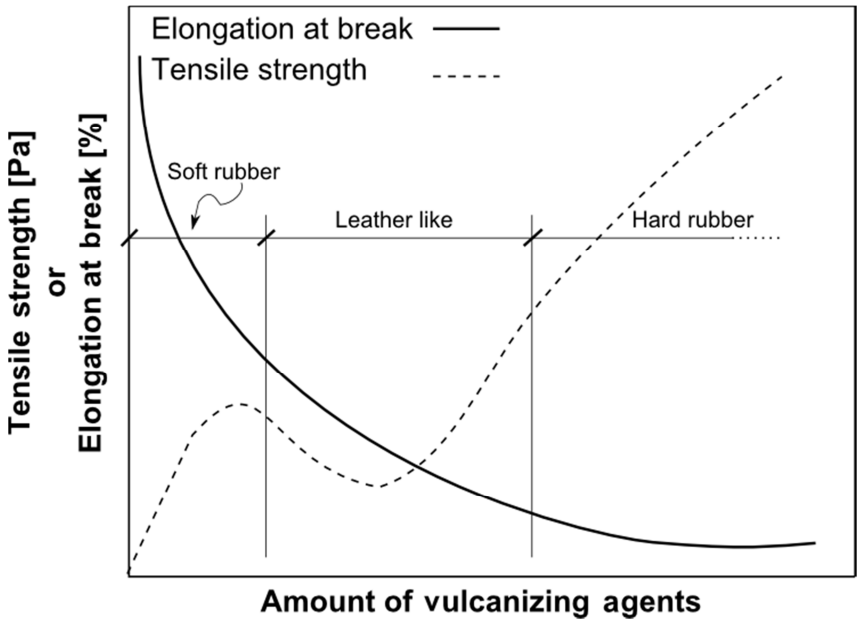

Fig. 1.9 Influence of the amount of vulcanizing agents on common mechanical properties of natural rubber.

In general, crosslink density, which is a measure of the extent of vulcanization, increases with cure time. Crosslink density and type of crosslinks (polysulfidic or monosulfidic) both affect compound properties. In **Fig. 1.10** it can be seen the cross-link density effect on properties. In relation to the type of crosslinks, the polysulfidic crosslink gives poor aging properties and poorer long-term flex life. On the other hand, mono- or di-sulfidic crosslinks provide poor fatigue life.

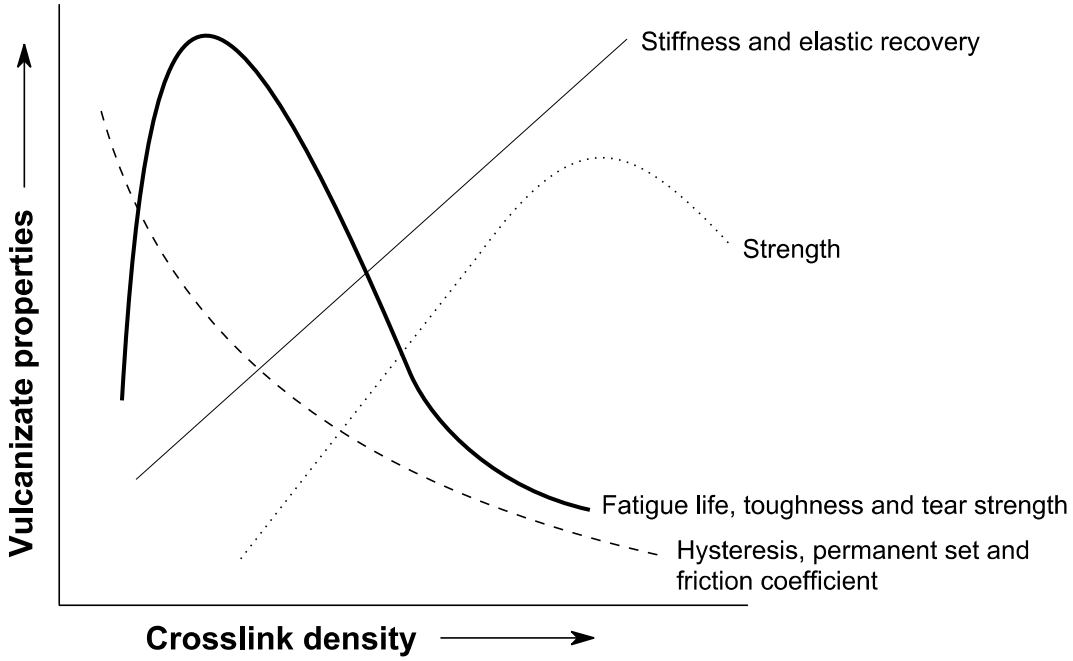

Fig. 1.10 Effect of cross-link density on common properties of natural rubber.

F. **Accelerators**: The chemical accelerators help raise the vulcanization speed by increasing the rate of crosslinking reactions. As sulfur alone takes a commercially prohibitive length of time to cure a rubber compound then chemical accelerators to speed up the curing rate are used.

G. **Activators**: Chemical products used to form complexes with accelerators and further activate the curing process. Most commonly used activators are zinc oxide and stearic acid.

1.3.3 Carbon-black in rubber

Carbon-black has been known and produced since antiquity but its discovery is attributed to S.C. Mote who came upon this in 1904. When it was discovered that carbon-black improves the mechanical properties of rubber compounds, it was extensively manufactured and used.

The *carbon-black* term refers to a group of industrial products consisting of:

- **Furnace black**: Furnace-made by the partial combustion of hydrocarbons.
- **Thermal black**: Produced by the thermal decomposition of natural gas.
- **Channel black**: Produced by the impingement of natural gas flames on channel irons.
- **Lampblack**: Made by burning hydrocarbons in open, shallow pans.

The most important characteristic of carbon-black, as rubber filler, is its specific surface area (total exposed surface per unit mass); it directly impacts the amount of interfacial contact area with the rubber. As its measurement involves molecular adsorption – phenomenon influenced by the carbon-black surface energy and activity (inhomogeneous across the surface) – the measurements of the specific surface area become a physicochemical characteristic as well as a geometrical characteristic. The second characteristic is the volume of the carbon-black aggregate.

Carbon-black is commonly incorporated into rubber by shear forces practiced in an open mill. The carbon-black agglomerates become encapsulated by polymer during the first stage of incorporation, but the interstices between agglomerates and aggregates are still filled with air. Then, the rubber is forced through the channels between agglomerates and aggregates to form a reinforced rubber compound.

The properties of uncured rubber are greatly influenced by the incorporation of carbon-black fillers: they change significantly the flow and viscosity. Contrary to unfilled compounds, carbon-black filled compounds have highly non-Newtonian flow and high viscosity – when the compound is forced to flow the hydrodynamic effect from the filler reduces the volume fraction of the flow medium causing shear strain amplification.

1.3.4 Styrene-butadiene rubber

Styrene and butadiene are co-monomers used in the manufacture of ESBR (emulsion) and SSBR (solution) by a chemical reaction (**Fig. 1.11**).

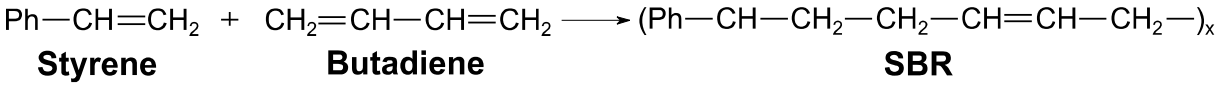

Fig. 1.11 Styrene-butadiene rubber chemical reactions.

SBR compounding is similar to that of natural rubber (NR). It requires reinforcing fillers, as natural rubber, to acquire the necessary modulus and strength. The SBR does not change viscosity as much as natural rubber during mixing, extrusion and remilling. As in NR compounds, other ingredients such as plasticizers, activators and accelerators are used in SBR compounds as well. Compared to NR, SBR requires additional acceleration and less sulfur during vulcanization. Additionally, as it takes longer to cure, increasing the primary accelerator or adding a second one the required cure rate for the compound is accomplished.

Whereas sulfur and accelerators are optimized for rapid cure rate, fillers and processing aids need to be balanced to attain a smooth extrusion.

SBR has a higher heat build-up behavior than a comparable NR compound. This is not a significant factor in many applications so, additional to their intrinsic advantages, the SBR is the preferably selected material. SBR is commonly blended with NR or low-cis polybutadiene to get optimum balance of properties for some applications. The major applications and uses of SBR are listed in **Table 1.1**.

Product categories	Usage, % of total
Tires and related products	65
Belt and Hose	10
Footwear	5
Foamed products	5
Mechanical goods	5
High Impact Polystyrene	–

Table 1.1 Major applications and uses of SBR by category.

2. Filled elastomers thermo-mechanical behavior

2.1 Thermo-mechanical behavior of elastomers

2.1.1 Finite deformation rubber elasticity

An unvulcanized elastomer flows easily under applied loads since the interactions between the chains are weak – these having great movement freedom under the influence of thermal agitation. On the other hand, the vulcanization turns solid the links among macromolecules – by means of sulfur and oxygen bridges – then the movements between chains are limited but the structure preserves, generally, an enormous flexibility. As a consequence, the elastomers behavior is directly related to the possibility of movement between the polymeric chains. Besides, this architecture is responsible of the different macroscopic behaviors under variable deformation.

The stress-strain curve obtained from a uniaxial traction test can be divided into two domains: linear and, predominantly, non-linear elasticity (**Fig. 1.12**). Under small deformations, the stress-strain relation is linear, exhibiting a Young's modulus in the order of

1 MPa. This behavior is strongly related with the filler network created into the elastomeric matrix: the occluded rubber inside the carbon-black network or carbon-black agglomerates does not take part in the deformation – the volumetric fraction of the active elastomeric matrix is smaller than expected. If the deformation is superior to 1 or 10% then the filler network is fractured and the initially occluded rubber is activated. Above this limit, the resistance of the mixture increases slowly under higher deformations. Besides, the secondary structures of the volume fraction of non-occluded rubber, entanglements between macromolecules, are loaded. At high deformation the high increase in stress is due largely, if not entirely, to strain-induced crystallization (Mark, 1982). Finally, the deformation strength grows highly up to break: the chains have attained their extensibility limit – the maximum extensibility for NR usually falls within the range 500-1000%.

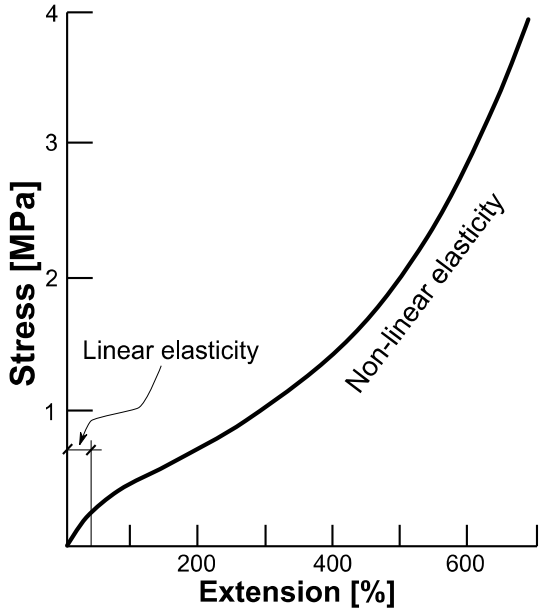

Fig. 1.12 Common stress-extension curve of a vulcanized rubber.

2.1.2 Thermoelastic effects and temperature-dependent mechanical behavior

In 1805, James Gough published his results concerning the thermal behavior of natural rubber (Gough, 1805) evidencing the following observations:

- Rubber self-heats under stretching loads.
- Rubber held in a stretched state, under a constant load, contracts on heating.

These conclusions were confirmed for vulcanized rubber by Joule (1859). Since then both effects are known as the Gough-Joule effects. The rubber heat build-up effect depends on

two different phenomena. First, the extension work is transformed into heat and, inversely, heat is absorbed pending relaxation. Second, if the elongation is considerable, the stretching induces the formation of a crystalline phase in the rubber matrix accompanied by the evolution of the latent heat of crystallization (Ehrbar and Boissonas, 1955). Concerning the second observation, the consequences are given in more detail.

The experiments of Meyer and Ferri (1935) demonstrate that the stretching force, for a given state of strain, is proportional to the absolute temperature (**Fig. 1.13**). Such proportionality is related with the modification of the conformations of a system of long-chain molecules – associated uniquely with changes in the configurational entropy of the system – in passing from the unstrained to the strained state. However, under lower strains, the thermo-mechanical behavior is inversed, i.e. the force decreases as the temperature raises (**Fig. 1.14**). It can be seen that the inversion point occurs at an extension of about 10% – the thermoelastic inversion point.

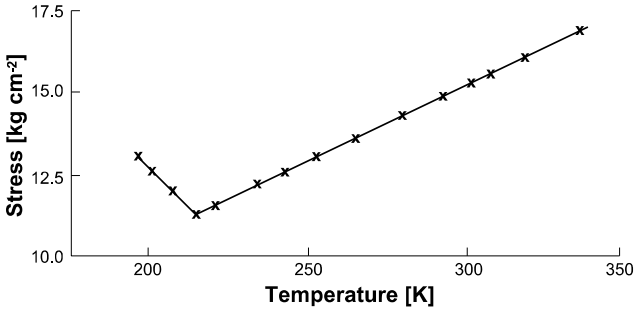

Fig. 1.13 Stress at constant length, extension 350%, as function of the absolute temperature of a vulcanized rubber-sulfur compound (Meyer and Ferri, 1935).

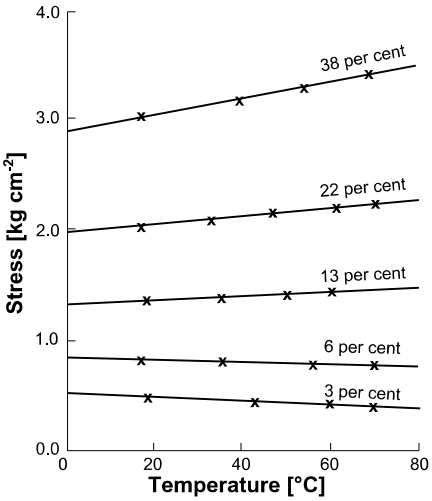

Fig. 1.14 Stress-temperature curves obtained for elongations ranging from 3% to 38% from a vulcanized rubber (Anthony et al., 1943).

The negatives slopes at small extensions and the existence of an inversion point are due to the volume thermal expansion which is present in both the stretched and the unstretched states of rubber, i.e. even that the rubber samples were held at constant length it does not mean that they were held at constant elongation – at each temperature the unstressed length will have a different value. Therefore, even though the force at a given strain increases with the temperature, this increase is counterbalanced by the associated reduction in strain. Then, if the strain is calculated on the basis of the unstrained length at a given temperature, all stress curves pass through a single origin and the stress value is proportional to the absolute temperature, **Fig. 1.15**.

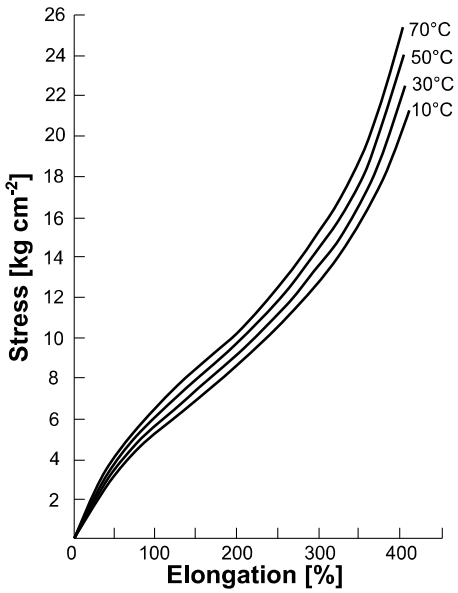

Fig. 1.15 Stress-elongation curves obtained at various temperatures from a vulcanized rubber (Anthony et al., 1943).

2.1.3 Time effects

The elastomers exhibit a strong time-dependent mechanical behavior: response of the material under creep and stress-relaxation tests. A creep test consists on following the time evolution of the deformation of a test sample under a constant stress σ_0 during a sufficiently long time interval t before suppressing it. An elastic deformation (segment *AB*) appears instantaneously after the application of the stress (**Fig. 1.16**). The viscoelastic behavior is seen under the form of a delayed deformation (segment *BC*) and a continuous evolution of the deformation (segment CD). Posterior to unloading the test sample there is an instantaneous recovery of the elastic deformation (segment *DE*) and, later, a total recovery of the delayed

deformation (segment *EF*). From point *F* the test sample presents a residual deformation that is recovered after long periods of time.

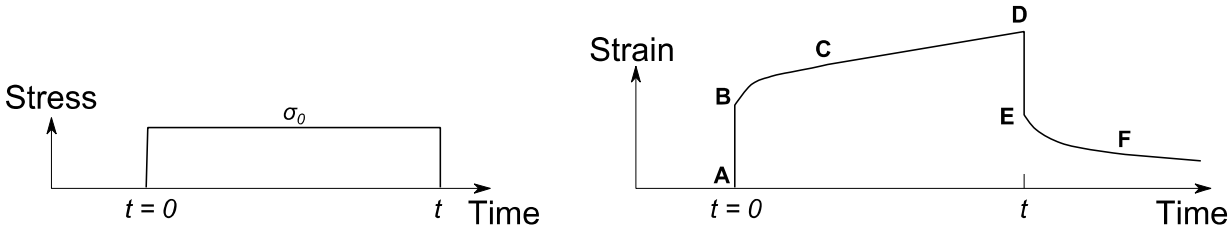

Fig. 1.16 Creep behavior.

A stress-relaxation test consists on following the time evolution of the stress of a test sample under a constant deformation ε_0. An elastic stress (segment *AB*) appears instantaneously after the application of the deformation (**Fig. 1.17**). The viscoelastic behavior is seen under the form of a progressive decrease of the stress (segment *BC*) up to a constant not-null value (from point *C*).

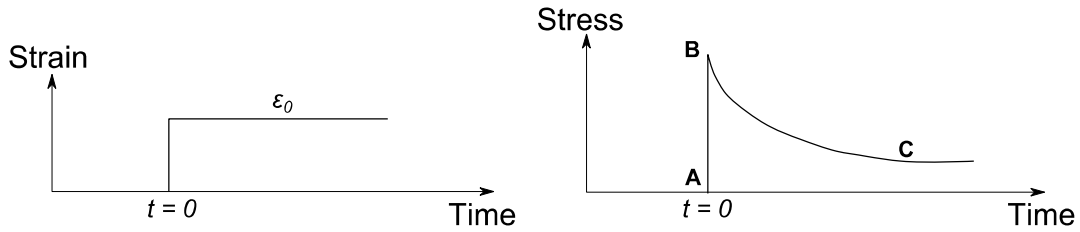

Fig. 1.17 Stress-relaxation behavior.

The results of these tests demonstrate that to establish a relationship between the stress σ and the strain ε it is necessary to account for this time-dependence.

2.1.4 Dynamic properties and hysteretic behavior

Elastomers exhibit a complex mechanical behavior including both the behavior of a solid characterized by an instantaneous response and the viscous behavior of a liquid characterized by a delayed response and a loss of energy at each cycle. The response of an elastomer under dynamic loads is better visualized in terms of a specimen undergoing uniform sinusoidal deformation as shown in **Fig. 1.18.** The stress response is nearly sinusoidal but out of phase with the strain. The total stress response can be resolved into two components: one in-phase response (elastic stress) and one out-of-phase response (viscous stress), so at any time the measured stress is the algebraic sum of its two components. The phase is expressed by defining a cycle as a circle. Dividing the stress amplitudes by the strain

amplitude gives the modulus components: storage modulus G' (related with elastic response) and the loss modulus G'' (related with viscous response)[4]. The storage modulus is related with the stored energy that will be recovered during the deformation process compensating partially or completely the, previously obtained, deformation of the structure. The loss modulus is related with the dissipated energy responsible of the heating-up of the test material – another part may be lost in the form of heat to the surrounding environment.

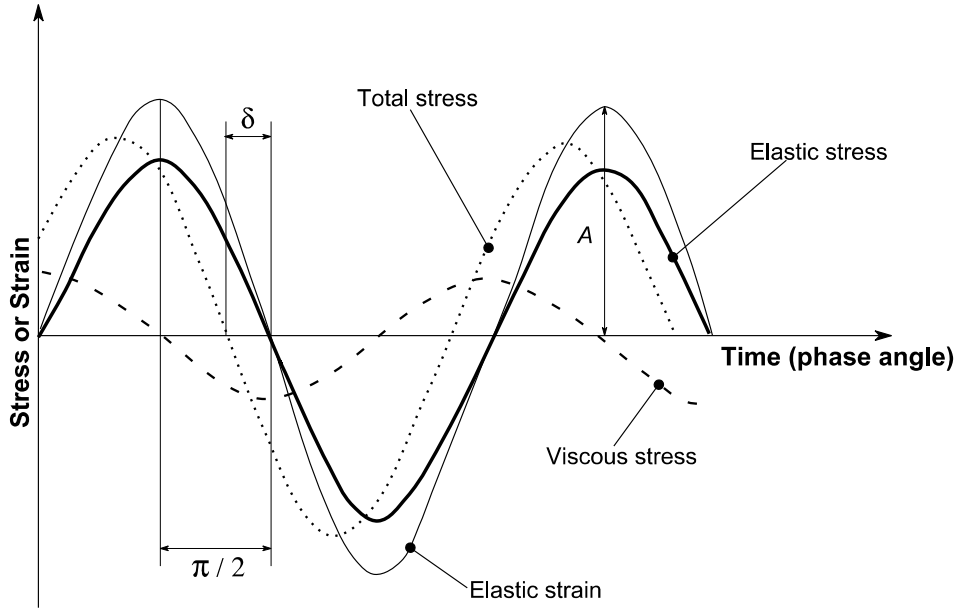

Fig. 1.18 Stress components of an elastomer under dynamic loads.

The complex modulus G^* can be calculated as:

$$G^* = G' + iG'' \tag{1.1}$$

and the absolute value of the complex modulus can be calculated by:

$$\left|G^*\right| = \sqrt{G'^2 + G''^2} \tag{1.2}$$

where $\left|G^*\right|$ is simply called the dynamic modulus. Finally, the loss factor (or damping factor)

$$\tan\delta = \frac{G''}{G'} \tag{1.3}$$

is a measure of the loss energy from internal friction of the material.

If the stress is plotted against strain, for a single cycle, a hysteresis loop is seen (**Fig. 1.19**). The area inside the hysteresis loop represents the mechanical energy which is not recovered

[4] *G* or *E* letters denote the shear and longitudinal modulus, respectively.

during a cycle but instead is converted into heat. The isolating nature of rubbers can retain this heat and generate a thermal gradient (heat build-up). The mechanical energy loss or heat generated per cycle in compression-extension tests is the hysteresis (Medalia, 1991):

$$H = \frac{\pi}{4}\frac{2A}{100}E' \tan\delta \tag{1.4}$$

where A is the strain amplitude (see **Fig. 1.18**).

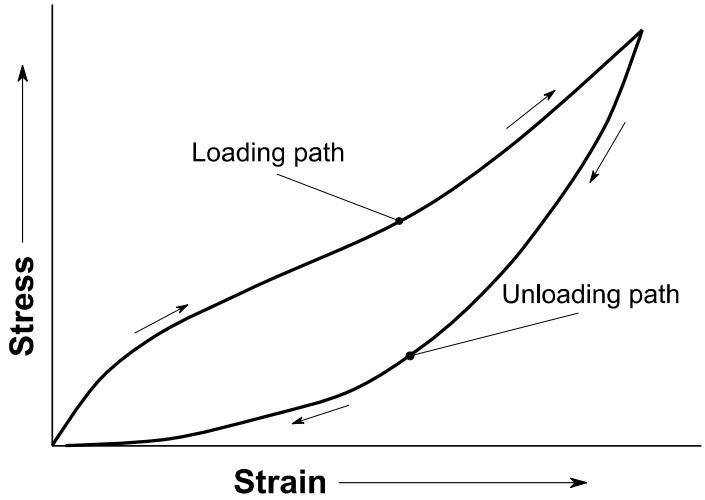

Fig. 1.19 Hysteresis loop.

2.1.5 Mullins effect

The Mullins effect consists in an appreciable change of the mechanical properties of filled and non-filled rubber-type materials resulting from the first extension. This change is made evident as a stress-softening – lower resulting stress for the same applied strain – after the first load which increases progressively with the increasing maximum stretch (**Fig. 1.20**). After a few cycles the material responses coincide during the following ones. This property was firstly observed by Bouasse and Carrière (1903) and intensively investigated by Mullins and his co-workers (Mullins, 1948, 1969; Mullins and Tobin, 1957, 1965). The principal phenomenological observations described by Mullins and co-workers can be summarized as follows:

- The softening is uniquely observed under higher elongations than the preceding ones in the loading history.
- An induced anisotropy as a consequence of the softening.
- The softening increases with an increasing volume of the initial fraction of filler.

- The complete recovery of the initial stiffness is never reached.
- The softening behavior is seen also from non-dilating load conditions, i.e. compression and shearing tests.

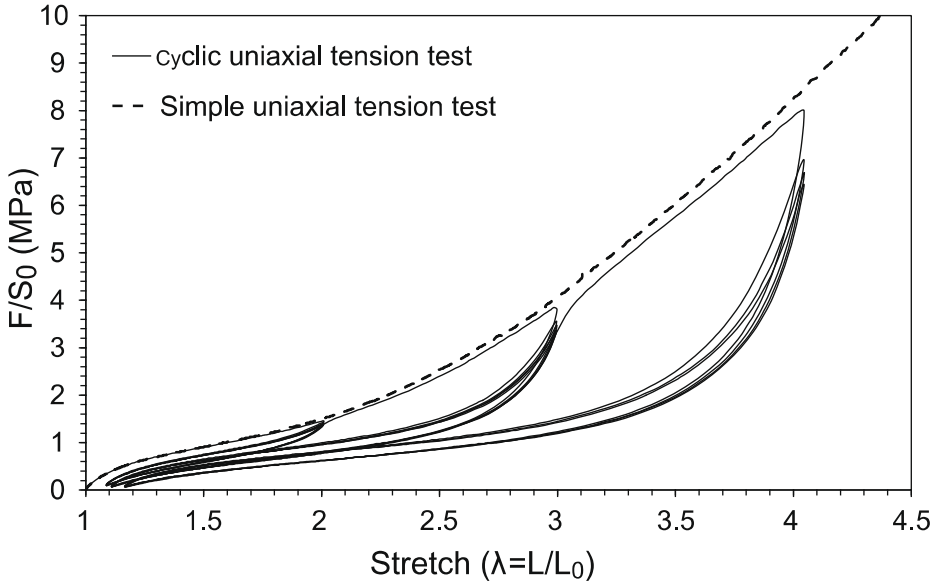

Fig. 1.20 Stress-strain response of a filled SBR submitted to a simple uniaxial tension test and to a cyclic uniaxial tension test with increasing maximum stretch every 5 cycles (Diani et al., 2009).

Several physical interpretations have been proposed in order to explain the Mullins effect (**Fig. 1.21**). The numerous interpretations proposed for the Mullins effect evidence that there is still no general agreement on the microscopic or mesoscopic origin of this effect. Blanchard and Parkinson (1952) related the first pre-strain softening with the rupture of the weaker bonds (physical bonds) at the rubber-particle interface while a further pre-strain would break the stronger bonds (chemical bonds). Bueche (1960) interpreted the Mullins effect in a similar way as Blanchard and Parkinson (1952); however, he has added to his interpretation an explanation of the softening in unfilled rubbers considering that the junctions arrange so as not to over-stretch the shorter chains. Simo (1987) and Govindjee and Simo (1991), pursuing the model proposed by Bueche (1960), estimated that the deformation induced by the relative movement between the fillers and the elastomeric matrix was the origin of the stress-softening.

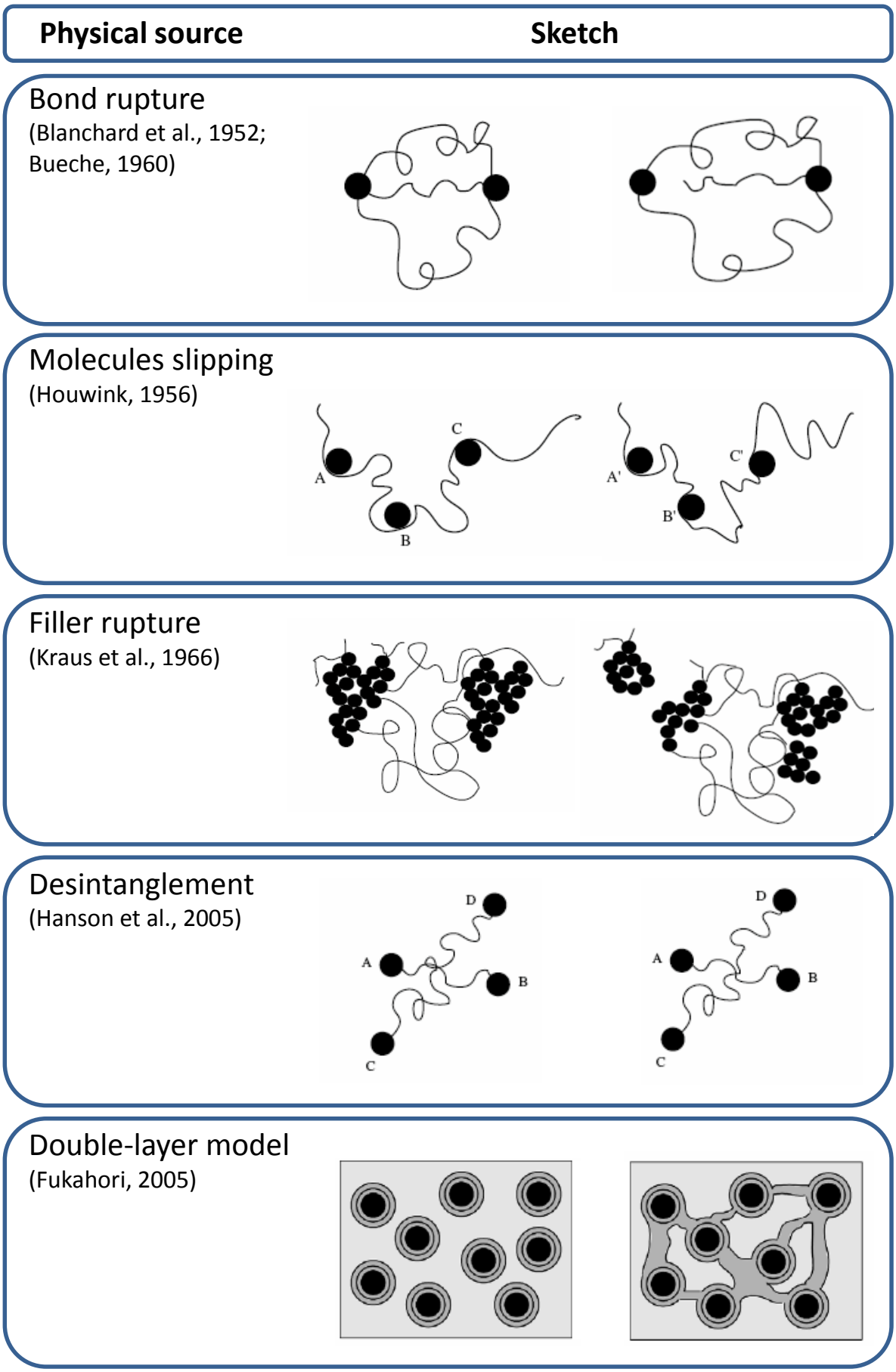

Fig. 1.21 Physical interpretations of the Mullins effect (Diani et al., 2009).

Houwink (1956) argued that the Mullins effect was related with the molecules slip over the surface of the fillers, considering the slow recovery of the stress-softening which could not be explained by the bond rupture source because, otherwise, this behavior would be permanent. During the first extension new bonds are instantaneously created, at different places of the original ones, along the rubber molecules. After measuring no significant change in the crosslink density of stretched networks – no reversible part of the Mullins effect results in bond breakage – Dannenberg and Brennan (1965) adhered to Houwink model (Houwink, 1956). Admitting that bond ruptures happen and vacuoles form in the material during the first strain, Kraus et al. (1966) have proposed to attribute the main source of the Mullins effect to the rupture of the carbon-black structure. Pursuing the interpretation proposed by Kraus et al. (1966), Klüppel and Schramm (2000) developed a macromolecular model which uses a strain amplification factor – the filler seen as a local strain amplifier – that decreases with an increasing maximum strain. Hanson et al. (2005), adopting Hamed and Hatfield (1989) configuration of chain entanglements between particles, proposed a new interpretation of the Mullins effect which takes into account the induced anisotropy. Finally, Fukahori (2005) proposed an interface model – the material is represented by particle aggregates surrounded by a double-layer structure of bound rubber embedded in a crosslinked rubbery matrix – to explain the mechanics and mechanisms of reinforcement and softening.

2.1.6 Cyclic stress-softening

Additional to the first pre-strain softening (Mullins effect), the effect of repeated deformation leads the rubber to approach asymptotically a steady state with a constant – equilibrium – stress response (**Fig. 1.22**). Softening occurs in both filled and non-filled rubber-type materials. Numerous authors (Bouasse and Carrière, 1903; Shedd and Ingersol, 1904; Schwartz, 1907) published data demonstrating that stretching resulted in a softening of rubber; however, Holt (1931) was the first to describe the effects of repeated stretching and stretching-speed on the stress-strain properties of rubber compounds. Together with the progressive softening during repeated deformation, Holt also showed that stretching to a series of increasing strains resulted in a progressive increase in the observed softening at low strains, as can be deducted from **Fig. 1.20**.

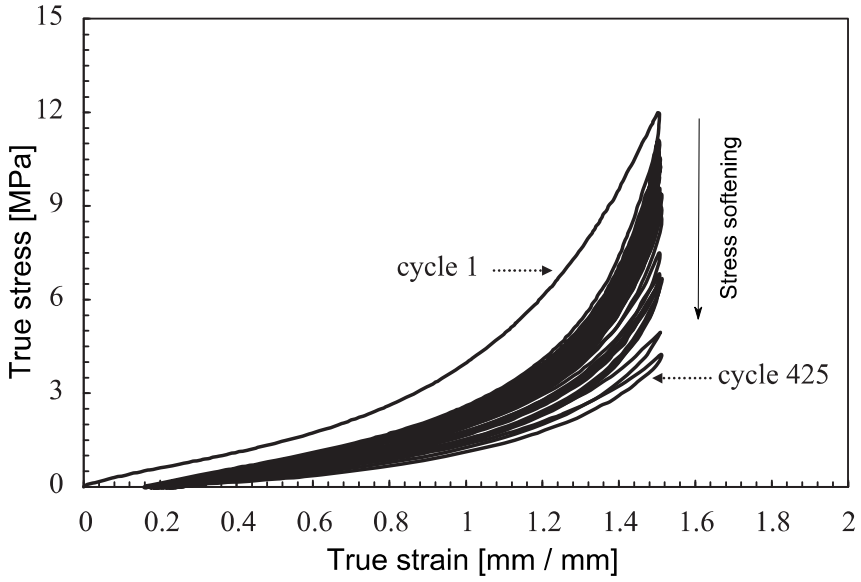

Fig. 1.22 Stress-strain curves of SBR submitted to a cyclic tension test: from the first cycle up to 425 cycles (Ayoub et al., 2011a).

In both unfilled and filled rubbers, most of the softening appears to be due to configurational changes of the rubber molecular network due to displacement of network junctions and entanglements during deformation and incomplete recovery to their original positions. The remaining and minor part of the softening in filled rubbers can be related to break-down or slippage of filler-filler and filler-rubber linkages – any linkage broken and reformed while the rubber is deformed also contribute to softening and incomplete recovery after deformation.

2.1.7 Fatigue lifetime of rubber materials

The rubber lifetime can be seen as the result of three successive phenomena (Legorjujago and Bathias, 2002; Mars and Fatemi, 2003; Aït Hocine et al., 2011):

1. Crack nucleation
2. Crack propagation, and
3. Total failure.

In general, it is considered that the crack precursors are flaws that originally exist in the virgin material (Mars and Fatemi, 2006; Naït-Abdelaziz et al., 2012). Besides, the lifetime under fatigue depends on many parameters such as the microstructure, the fatigue-induced crystallinity, the specimen geometry, the loading conditions, etc.

In order to account for the lifetime of rubber components under multi-axial loading conditions, Ayoub et al. (2012) have proposed a model based on the continuum damage mechanics approach, see **Fig. 1.23**. The proposed model was able to unify the multi-axial experimental data (tension-torsion) for two specimen geometries (AE2 and AE42), but it fails to unify the data regarding the specimen geometry. The divergence was attributed to the material heat build-up, as during a fatigue test, the two specimens do not reach the same surface stabilized temperature[5].

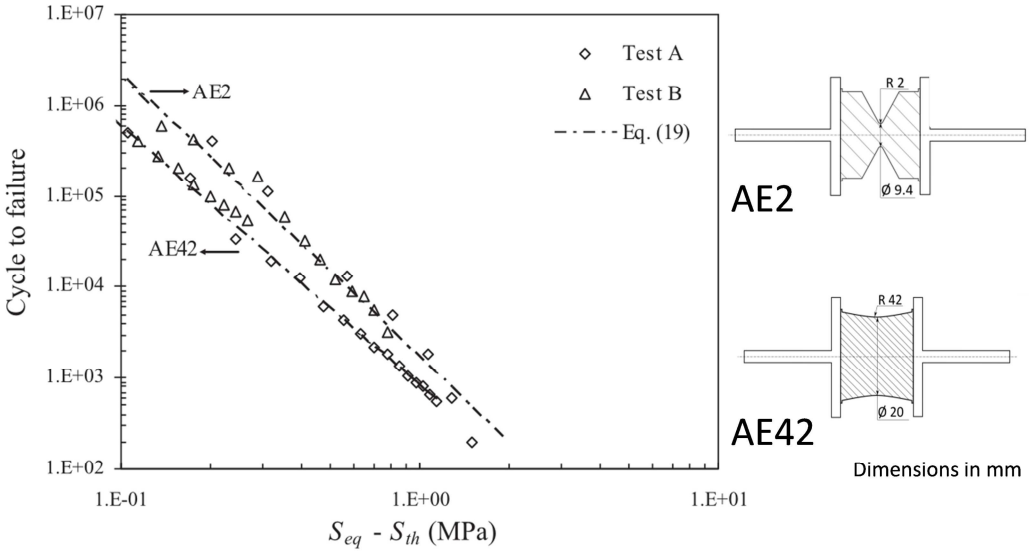

Fig. 1.23 Fatigue lifetime of a SBR as a function of a multiaxial fatigue predictor S_{eq} and a threshold damage stress S_{th} (Ayoub et al., 2012).

2.2 Carbon-black effects on the rubber properties

2.2.1 Carbon-black effect on rubber elastic behavior

It is well known that adding small amounts of filler particles to a rubber can significantly improve both the stiffness and the strength of the rubber compound. Numerous authors (Smallwood, 1944; Guth, 1945; Vand, 1948; Mooney, 1951) have investigated the influence of filler particles on the stiffness of rubbers compounds. The filler volume has an increasing effect on the stress-strain behavior of NR vulcanizates (**Fig. 1.24**). Independently of the filler concentration, all curves have a linear behavior from the origin up to strains of about 0.02. At

[5] The divergence in both temperatures is related with the difference in the volume of material implied in the fatigue process.

higher strains all curves showed the characteristic sigmoid shape of rubber-type materials with an upward sweep of the curve at strains greater than 1. The mechanism by which the stiffness increase occurs is still a subject of debate; it has been considered to result from two contributions:

- Continuum level: the stiffness of a rubber compound will be the weighted combination of the stiffnesses of the individual constituent materials, depending on the exact microstructure (Bueche, 1960).
- Molecular level: the filler acts both to effectively increase the crosslink density of the material – providing additional crosslinking sites at the particle-matrix interface – and to reduce the segmental mobility close to the filler particles (Kraus, 1978).

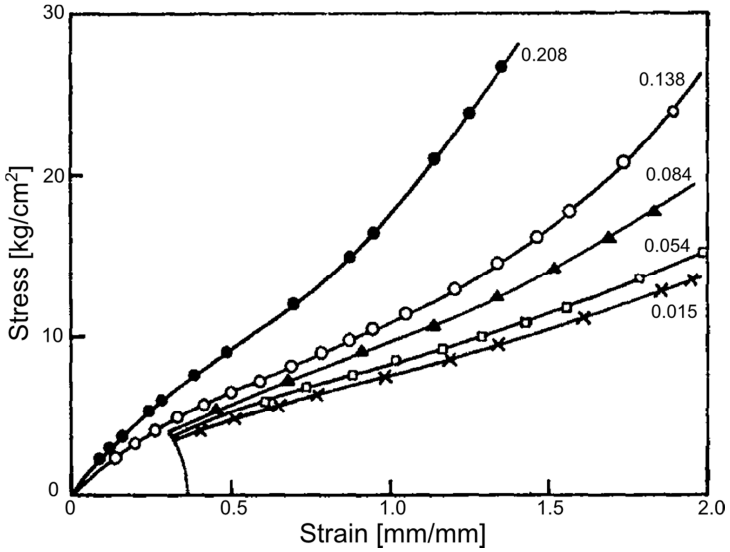

Fig. 1.24 Stress-strain curves of NR containing different volumes of carbon-black (Mullins and Tobin, 1965).

In addition to the volume fraction of filler particles, a number of state variable were supposed to influence the stiffness increase magnitude: the size, type and shape of the fillers (Mullins, 1950), the filler aggregate structure (Smallwood, 1944) and the rubber-filler interface area (Medalia and Kraus, 2013). In spite of the diverse number of contributions, Smallwood (1944) demonstrated that the main influence is found by changing the aggregate structure. The filler effect on the elastic behavior of filled rubbers has been extensively modeled (see **Fig. 1.25**). One approach consists on taking into account the increase in viscosity of a viscous fluid – rubber matrix – caused by a suspension of colloidal particles –

carbon-black. Using this concept Smallwood (1944) predicted the small-strain Young's modulus of particle-filled solids:

$$E = E_m\left(1+2.5v_f\right) \tag{1.5}$$

where E_m is the Young's modulus of the rubber matrix and v_f is the filler volume fraction; however, this estimate is valid uniquely for very low filler concentrations. Attempting to incorporate interactions between neighboring particles – allowing predictions for higher volume fractions – Guth and Gold (1938) have added one more term to the polynomial series expansion of the amplification factor:

$$E = E_m\left(1+2.5v_f+14.1v_f^2\right) \tag{1.6}$$

Using an experimental crowding factor k to incorporate particle-particle interactions, Mooney (1951) proposed a different method:

$$E = E_m \exp\left(\frac{2.5v_f}{1-kv_f}\right) \tag{1.7}$$

Guth (1945) have developed a model that accounts for rod-like shapes other than spherical-shape particles (as the aforementioned models). The shape is characterized by the ratio of the length to the width of the particles or the filler aggregate structures, g_f:

$$E = E_m\left(1+0.67g_fv_f+1.62g_f^2v_f^2\right) \tag{1.8}$$

This model attempts to account for the rapid increase with concentration in the viscosity of suspensions of rod-like particles, in contrast to the slower increase for spherical particles.

Govindjee and Simo (1991) have developed another approach based on the concept of amplified strain which, for the case of rigid particles in a neo-Hookean matrix, can be written as

$$E = E_m\frac{1-\frac{v_f}{2}}{1-v_f} \tag{1.9}$$

In addition to these models specifically developed for filled rubbers, a number of general composite theory model have been developed (Hashin and Shtrikman, 1963; Budiansky, 1965; Ponte Castañeda, 1989; Bergström and Boyce, 1999).

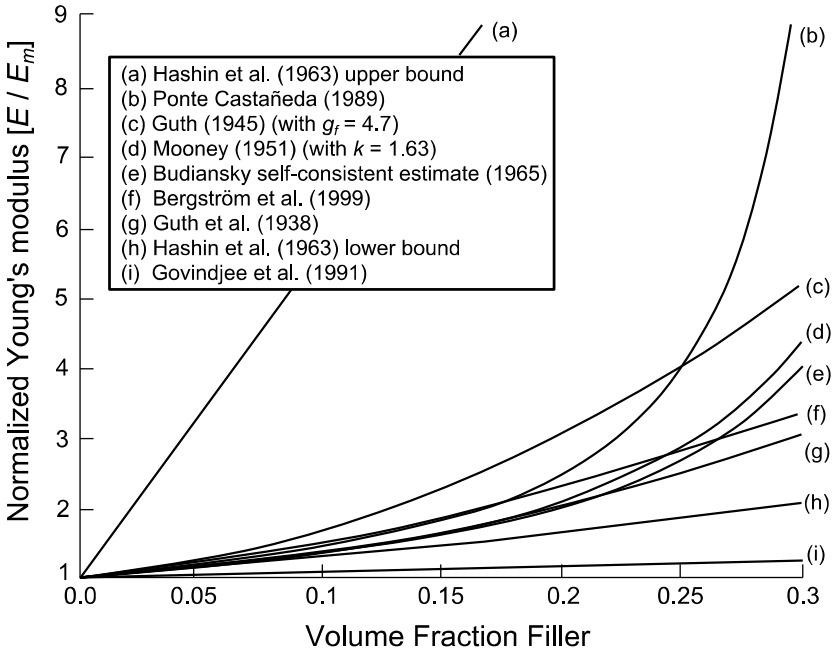

Fig. 1.25 Theoretical predictions of the normalized Young's modulus, $E_{filler} = 100E_m$.

2.2.2 Carbon-black effect on dynamic[6] elastic modulus

Dynamic measurements demonstrate the significant difference between dynamic and static properties, e.g. the dynamic elastic modulus E' is greater than the static modulus E. This effect is considerably greater with black-filled than with gum compounds (Dillon et al., 1944). Under a shear dynamic test, pure rubber shows a linear behavior of the storage modulus G' in the domain of deformations below 100 %. The adding of fillers drives the compound to a non-linear behavior. **Fig. 1.26** shows the diminution of the storage modulus as a function of impose deformation amplitude. The values of G' remained constant up to about 0.1 to 0.5% double strain amplitude (DSA) and thereafter decreased tending to an apparent constant minimal value G'_∞ – this value is superior to the unfilled rubber modulus. This phenomenon is known as the Payne effect (Payne, 1960).

In Payne's experiments the value of G' at low amplitudes was constant, called G'_0, over a range of more than a decade (e.g., 0.05 to 0.5% DSA); however, Voet and Cook (1967) and Sircar and Lamond (1975a; 1975b) have shown, using an apparatus slightly modified from that of Payne, G' increasing from a low value at 0.01% DSA to a maximum at about 0.1% DSA. At high amplitudes the carbon network structure is broken down – regardless of the

[6] The term dynamic, as applied to rubber-type materials, refers to the response – after reaching a pseudo-equilibrium state – to periodic or transient forces which do not cause failure.

loading or interaggregate bond strength – and the storage modulus is governed by the individual carbon-black aggregates. Similarly, in a well-dispersed compound at low loadings, where the individual aggregates are well separated, the amplitude effect is very small and the storage modulus is governed uniquely by the individual aggregates. Under these conditions the effect of carbon-black is essentially equivalent to the hydrodynamic effect of isolated spheres on the modulus of rubber, corresponding to the effect of perturbation of flow behavior on the viscosity of liquids. The contribution of carbon-black to the storage modulus under these conditions depends on structure or bulkiness and is independent of surface area (Medalia, 1973; Ulmer et al., 1973; Kraus, 1978). At amplitudes between G_0' and G_∞', the storage modulus is the sum of G_∞' and the contribution $\Delta G'$ related with the augmentation made by still unbroken agglomerates of varying dimensions, e.g. a relatively small amount of strain-work would be required to reduce the agglomerate size by a factor of 2 and more work is then required to reduce each of the residues by another factor of 2, and so on.

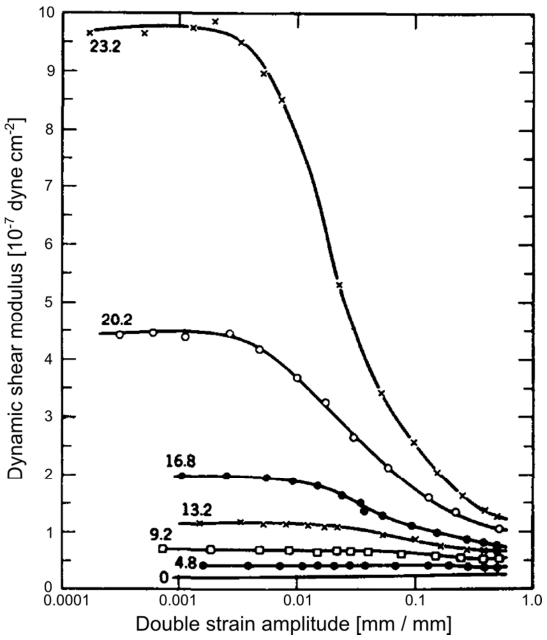

Fig. 1.26 Storage modulus-strain amplitude relation for a rubber compound with different volumes of carbon-black (Payne, 1963a).

The increase of G' is greatly affected by loading characteristics, i.e. at high loadings the low-amplitude modulus is dominated by the surface area of the carbon-black (Payne, 1963b) while at low loadings it is dominated by the carbon-black structure (Medalia, 1973; Ulmer et al., 1973). From a practical point of view, the dependence of G' on both structure and surface

area can cause that the modulus-amplitude curve of a high structure-low area black intersects the one of a low structure-high area black.

2.2.3 Carbon-black effect on loss parameters and hysteresis

Along with the amplitude dependence of the storage modulus there is a significant amplitude dependence of the loss factor and the loss modulus which is more pronounced as the loading is increased (**Fig. 1.27** and **Fig. 1.28**). The loss factor at low amplitudes rises to a maximum at around 5 to 15% DSA in shear, and then decreases at still higher amplitudes; however, it generally remains higher than its value at very low amplitudes. The loss modulus passes through a maximum, as an amplitude function, which is reached at the amplitude at which the storage modulus changes most rapidly – the inflection point.

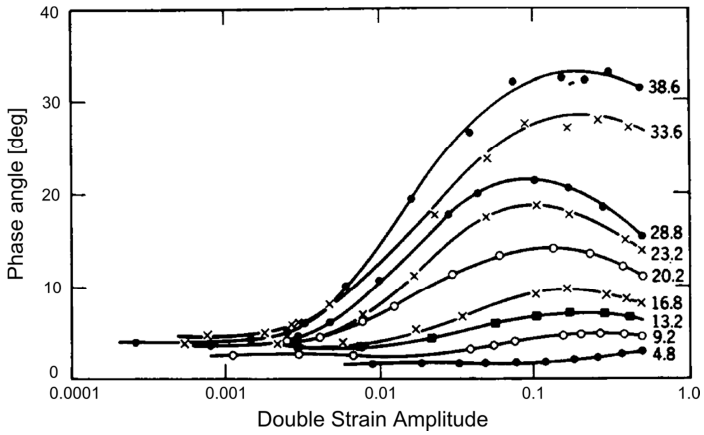

Fig. 1.27 Phase angle-strain amplitude relation for a rubber compound with different volumes of carbon-black (Payne, 1963a).

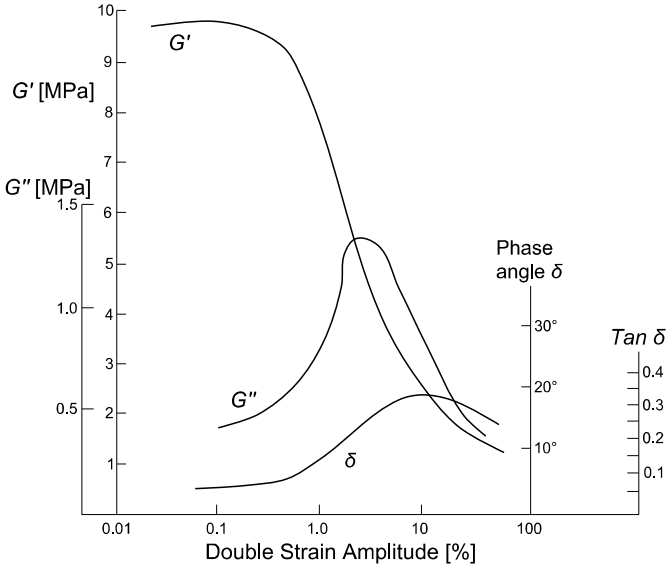

Fig. 1.28 Dynamic parameters-strain amplitude relation for a rubber compound with 23.2 volume % of carbon-black (**Fig. 1.26** and **Fig. 1.27**).

As for the storage modulus, the amplitude dependence of the viscous parameters has been interpreted on the basis of the interaggregate interaction (Ulmer et al., 1998). It is assumed that hysteresis H results from breakdown and reformation of interaggregate bonds: at low amplitude there is little breakdown of bonds, therefore little hysteresis; at intermediate amplitudes considerable breakdown and reformation of bonds take place, thus hysteresis is high; and at high amplitudes both G' and $\tan\delta$ continue to decrease, thus their product, the loss modulus G'', can become quite low. Low values of G'' at high amplitudes have been interpreted on the basis that at high amplitude the structure destruction is complete and little energy needs to be expanded (Voet and Cook, 1967) – the decrease in loss factor at high amplitudes indicates that less reformation of interaggregate bonds takes place than at intermediate amplitudes. Note that in comparing different compounds, H is proportional to $\tan\delta$ when the compounds are cycled at the same energy input, H is proportional to G'' under equal strain conditions, while under equal stress conditions, H is approximately proportional to $\tan\delta/G'$ (Medalia, 2001).

2.2.4 Temperature effect in carbon-black rubber compounds

Dynamic properties of rubber compounds are important over a wide range of temperatures, especially in the so-called rubbery region of polymer behavior (**Fig. 1.6**). In this region, the storage modulus of carbon-black filled rubbers increases with lower temperature – entanglements and other physical crosslinks become more effective. The loss factor increases with lower temperature in the rubber region and passes through a maximum in the region where G' is changing most rapidly (transition to glassy state), while G'' reaches a maximum at somewhat lower temperature.

Fletcher and Gent (1957) showed, using carbon-black filled NR flat samples, that the values of G' were relatively high at high temperatures and the increase in G' on going to low temperature was less steep than for the gum. Over the temperature range examined (-62 to 81.5°C), $\tan\delta$ passed through a maximum which was much lower and less sharp for the filled vulcanizates that for the gum. Similar results were reported by Payne (1958). Using different carbon-blacks at 50 phr[7] loading vulcanizates, Medalia (1973) evidenced the decreasing of the elastic modulus with an increasing temperature. Payne (1963b)

[7] Parts per hundred of rubber.

experiments over carbon-black filled NR vulcanizates reported similar results (**Fig. 1.29**). Concerning pure gum thermo-mechanical behavior, Medalia (1978) shown the increasing of the elastic modulus with an increasing temperature, as later reported by Treloar (2005). The temperature dependence of the dynamic parameters has been interpreted on the basis of the loading characteristics, e.g., at low temperatures the low-amplitude modulus is dominated by the surface area of the black, while at high temperature it is dominated by carbon-black structure.

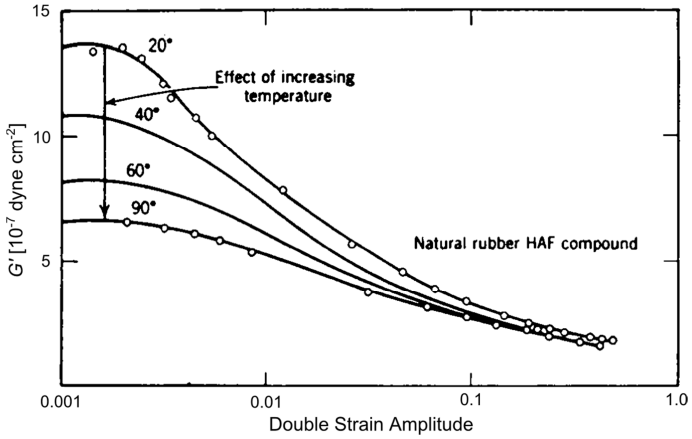

Fig. 1.29 Effect of temperature on strain amplitude dependence of G' (Payne, 1963a).

2.2.5 Carbon-black rubber interactions effect

The carbon-black effect on the dynamic properties of rubbers differs quantitatively from one rubber to another and also depends upon various procedures which are known to alter interaction of the polymer with the carbon-black. The carbon-black dispersion affected by both the size and number of agglomerates and the distance of interaggregate separation is the most sensible interaction, e.g. reduction in hysteresis after increasing time of mixing or heat treatment, attributed to reduction in carbon-carbon frictional losses as the dispersion was improved (Dannenberg, 1952). Boonstra and Medalia (1963) found that large agglomerates are responsible for the poor ultimate properties of short-time mixes, interaggregate occlusion of a large amount of rubber, high Mooney viscosity and high vulcanizates modulus at low strain. As mixing proceeds the large agglomerates virtually disappear and the now existing small agglomerates are gradually dispersed. During the later stages of mixing there was a significant decrease in torsional hysteresis and heat buildup. These changes were related to the disappearance of the small agglomerates and the separation of the aggregates from each other. Numerous authors (Payne, 1965; Medalia, 1973;

Sommer and Meyer, 1974) have confirmed the positive effect of improved dispersion on dynamic properties of rubber compounds. It is well known that an undercured rubber is related with high hysteresis (Baranwal and Stephens, 2001). In pure rubber vulcanizates this has been generally attributed to the slow response of untrapped entanglements and dangling chain ends (Ferry, 1980); however, recent studies have related hysteresis to trapped entanglements (Cohen et al., 1977) and questioned the importance of dangling chain ends (Sullivan et al., 1978). Payne et al. (1972) shown that the loss factor of pure rubber vulcanizates decreased progressively with increasing cure, and this was reflected in the filled compounds. On the other hand, comparing NR compounds at three curative levels, Sommer and Meyer (1974) reported increasing values of G' and G'' with increasing cure time – increasing level of crosslinking. Similar results were found by Medalia (1978) – the author suggests that "the viscoelastic behavior of the rubber immobilized by the carbon-black could somehow be responsible for this effect". In an interesting study by Sircar and Lamond (1975a; 1975b) dynamic parameters of ten elastomers were evaluated (**Fig. 1.30**); however, microscopic measurement of dispersion did not help to give a simple explanation of the order. There are wide differences in G', having the nitrile-butadiene rubber (NBR) the highest value. The maximum values of $\tan\delta$, for only seven of these compounds, were found at close to 10% DSA (in shear). The $\tan\delta$ values were in somewhat the same order of G'. Payne (1964) reported the same rubber-type dependence; however, the values were not in the same order – different compounding and curing systems were used for each polymer.

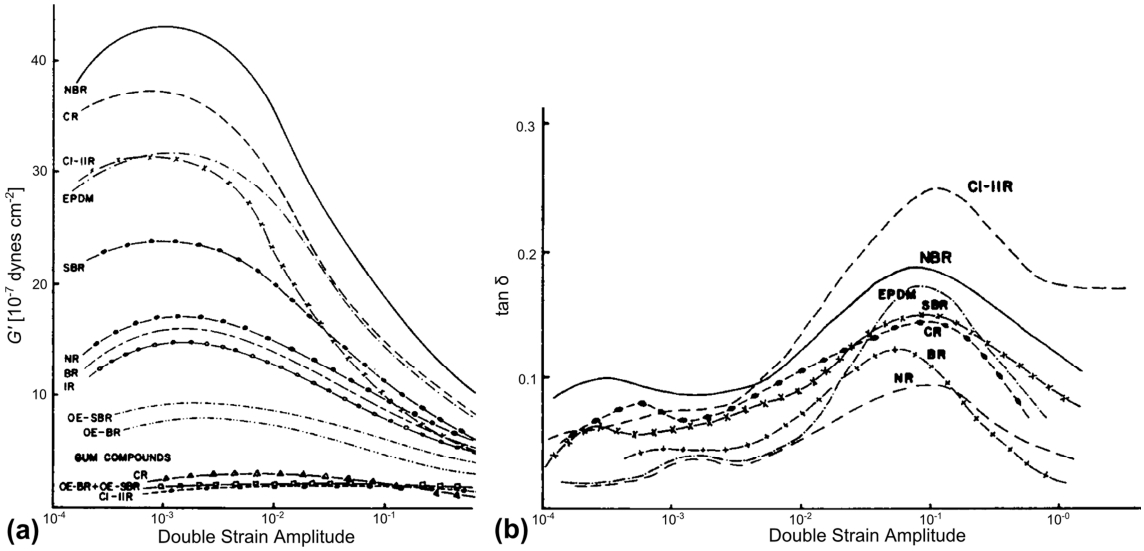

Fig. 1.30 Effect of the elastomer type: (a) on the storage modulus G', and (b) on the loss factor $\tan\delta$ (Sircar and Lamond, 1975a).

3. Elements of continuum mechanics and thermodynamics

The continuum medium is an infinite set of particles (region or part of a solid, fluid or gas) that can be studied macroscopically without considering the possible existing discontinuities in the microscopic level – atomic or molecular level. In consequence, the mathematical description of this medium and of his properties can be developed by means of continuous functions.

The continuum medium configuration Ω_t is the geometric place of the positions that the material points – particles – of the continuum medium occupy in the space at a certain time *t*. The configuration at a given time $t = t_0$ of the time interval of analysis is named initial, material or reference configuration Ω_0 (**Fig. 1.31**). In the reference configuration, the position vector **X** of a particle that occupies a point *P* in the space is given by:

$$\mathbf{X} = X_i \hat{\mathbf{e}}_i \tag{1.10}$$

where X_i are the material coordinates of the particle and $\hat{\mathbf{e}}_i$ is a unit vector of orthonormal basis. In the current configuration Ω_t, the particle, originally situated in the material point *P*, occupies the spatial point *P'* and his position vector x is given by:

$$\mathbf{x} = x_i \hat{\mathbf{e}}_i \tag{1.11}$$

where x_i are the spatial coordinates of the particle in the time instant *t*.

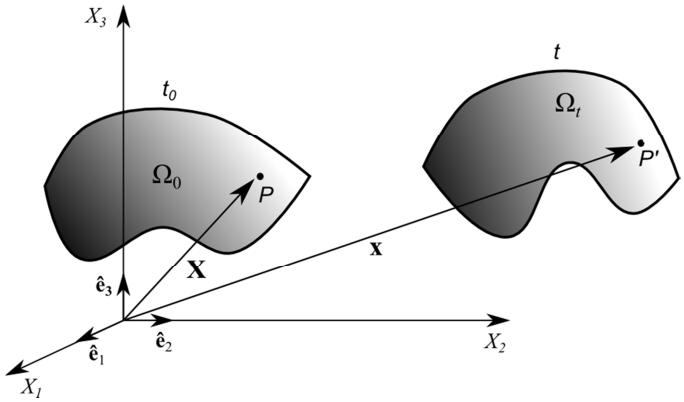

Fig. 1.31 Configuration of the continuum medium.

Finally, the mathematical description of the properties of the particles can be done by means of two alternative ways according to the configuration: the Lagrangian description (reference configuration) and the Eulerian description (current configuration)

3.1 Finite deformation and stress

3.1.1 Description of the deformation

A key quantity to describe finite deformation in the continuum mechanics framework is the deformation gradient tensor **F** defined as:

$$\mathbf{F} = \frac{\partial \mathbf{x}}{\partial \mathbf{X}} \tag{1.12}$$

The deformation gradient tensor contains the information relative to the movement, throughout time, of all the material particles in the differential neighborhood of a given one. The determinant of **F**, denoted *J* (for Jacobian), represents the local variation of volume and it is always positive because of the principle of non-interpenetration of the material: $J = \det \mathbf{F} > 0$. On the other hand, the displacement of a particle *P* at a given time is defined by the vector **u** which joins the position *P* of the particle in the reference configuration and its actual position *P'* (**Fig. 1.32**). The displacement of all the particles of the medium defines the displacement field vector:

$$\mathbf{u}(\mathbf{x},t) = \mathbf{x} - \mathbf{X}(x,t) \tag{1.13}$$

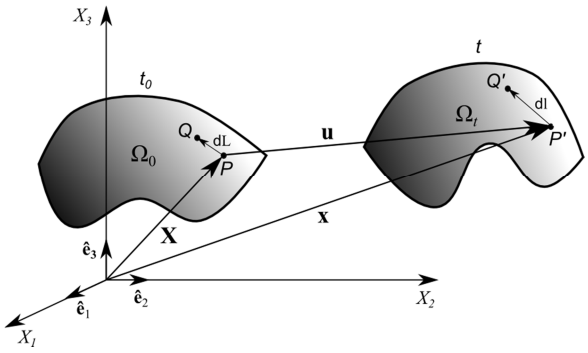

Fig. 1.32 Displacement vector.

The relative movement in the neighborhood of a particle through the deformation process (characterized by **F**) can be understood as the composition (**Fig. 1.33**) of a rotation and a deformation – polar decomposition theorem – as:

$$d\mathbf{x} = \mathbf{F}d\mathbf{X} = \mathbf{V}\mathbf{R}d\mathbf{X} = \mathbf{V}(\mathbf{R}d\mathbf{X}) \tag{1.14}$$

in which $\mathbf{F} = \mathbf{V}\mathbf{R}$ is the right polar decomposition, **V** is the right stretch tensor and **R** is the orthogonal rotation tensor, and

$$d\mathbf{x} = \mathbf{F}d\mathbf{X} = \mathbf{R}\mathbf{U}d\mathbf{X} = \mathbf{R}(\mathbf{U}d\mathbf{X}) \tag{1.15}$$

and $\mathbf{F}=\mathbf{RU}$ is the left polar decomposition and **U** is the left stretch tensor.

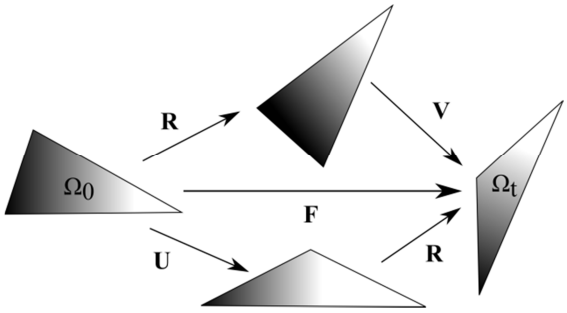

Fig. 1.33 Polar decomposition.

The time-dependent deformation is described by means of the velocity gradient tensor:

$$\mathbf{L}=\dot{\mathbf{F}}\mathbf{F}^{-1}=\mathbf{D}+\mathbf{W} \tag{1.16}$$

where **D** is the stretching rate (symmetric tensor) and **W** is the spin rate (non-symmetric tensor). The stretching rate tensor gives the rate of stretching of line elements while the spin rate tensor indicates the rate of rotation or vorticity of the motion.

Let us consider now a particle situated in *P* in the reference configuration, and a second one situated in his differential neighboring *Q* separated from the previous one by the segment d**X** (length $dL=\sqrt{d\mathbf{X}d\mathbf{X}}$). The segment d**x** (length $dl=\sqrt{d\mathbf{x}d\mathbf{x}}$) is its counterpart in the current configuration (**Fig. 1.31**), from which some quantities can be defined:

$$\begin{aligned}\left(dl\right)^2&=d\mathbf{x}d\mathbf{x}=\left[\mathbf{F}d\mathbf{X}\right]\left[\mathbf{F}d\mathbf{X}\right]=d\mathbf{X}\mathbf{F}^T\mathbf{F}d\mathbf{X}=d\mathbf{X}\mathbf{C}d\mathbf{X}\\ \left(dL\right)^2&=d\mathbf{X}d\mathbf{X}=\left[\mathbf{F}^{-1}d\mathbf{x}\right]\left[\mathbf{F}^{-1}d\mathbf{x}\right]=d\mathbf{x}\mathbf{F}^{-1}\mathbf{F}^{-T}d\mathbf{x}=d\mathbf{x}\mathbf{B}^{-1}d\mathbf{x}\end{aligned} \tag{1.17}$$

where $\mathbf{C}=\mathbf{F}^T\mathbf{F}$ and $\mathbf{B}=\mathbf{F}\mathbf{F}^T$ are the right and left Cauchy-Green strain tensors, respectively.

Subtracting both expressions of Eq. (1.14) between them we have:

$$\begin{aligned}\left(dl\right)^2-\left(dL\right)^2&=d\mathbf{X}\mathbf{C}d\mathbf{X}-d\mathbf{X}d\mathbf{X}=2d\mathbf{X}\mathbf{E}d\mathbf{X}\\ \left(dl\right)^2-\left(dL\right)^2&=d\mathbf{x}d\mathbf{x}-d\mathbf{x}\mathbf{B}^{-1}d\mathbf{x}=2d\mathbf{x}\mathbf{e}d\mathbf{x}\end{aligned} \tag{1.18}$$

where

$$\mathbf{E}=\frac{1}{2}\left(\mathbf{C}-\mathbf{I}\right) \tag{1.19}$$

is the Green-Lagrange finite strain tensor,

$$\mathbf{e}=\frac{1}{2}\left(\mathbf{I}-\mathbf{B}^{-1}\right) \tag{1.20}$$

is the Euler-Almasi finite strain tensor and **I** is the unit vector.

Finally, since each previously defined strain tensor is symmetrical and positive then six independent components must be defined to characterize the current configuration of a body; however, another way consists on defining the corresponding principal strain invariants I_1, I_2 and I_3. Invariants of **C** and **B** are often used in the expressions for strain energy density functions. The principal strain invariants, considering **B**, are defined as:

$$I_1 = \mathrm{tr}\mathbf{B} = B_1 + B_2 + B_3 = \lambda_1^2 + \lambda_2^2 + \lambda_3^2 \tag{1.21}$$

$$I_2 = \frac{1}{2}\left[\left(\mathrm{tr}\mathbf{B}\right)^2 - \mathrm{tr}\mathbf{B}^2\right] = B_1B_2 + B_2B_3 + B_1B_3 = \lambda_1^2\lambda_2^2 + \lambda_2^2\lambda_3^2 + \lambda_1^2\lambda_3^2 \tag{1.22}$$

$$I_3 = \det\mathbf{B} = B_1B_2B_3 = \lambda_1^2\lambda_2^2\lambda_3^2 = J^2 \tag{1.23}$$

where λ_i are stretch ratios of the unit fibers that are initially oriented along the directions of the orthonormal axis in the coordinate system.

3.1.2 Description of the stress

The stress at a given point is defined as the resultant of the internal forces through a surface element, relative to a certain configuration (**Fig. 1.34**). As for the deformations, it is possible to use a eulerian or lagrangian description, or even a mixed formulation.

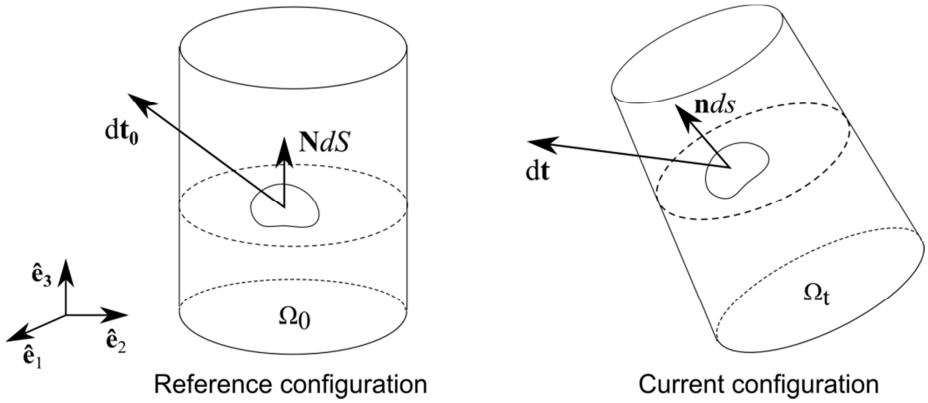

Fig. 1.34 Stress vectors in the reference and current configuration.

In the eulerian description, the inner forces d**t** in the current configuration applied by a solid region over another one through a deformed surface element **n***ds* are considered. This definition drives us to the Cauchy stress tensor expression:

$$d\mathbf{t} = \mathbf{T}\mathbf{n}ds \tag{1.24}$$

where $\mathbf{T}$ is the Cauchy stress tensor. However, it can be useful to describe the stress field in the reference configuration, e.g., the application of the boundary conditions. The transport of the deformed surface element $\mathbf{n}ds$ to the reference configuration returns:

$$d\mathbf{t} = \boldsymbol{\pi}\mathbf{N}dS \tag{1.25}$$

where $\boldsymbol{\pi} = J\mathbf{T}\mathbf{F}^{-T}$ is the first Piola-Kirchhoff stress tensor (non-symmetric). This stress describes the real cohesion forces applied through a deformed surface element per unit of non-deformed surface. The description of the stress field under a total lagrangian formulation needs the transport of the real force $d\mathbf{t}$ to the reference configuration:

$$d\mathbf{t}_0 = \mathbf{S}\mathbf{N}dS \tag{1.26}$$

where $\mathbf{S} = J\mathbf{F}^{-1}\mathbf{T}\mathbf{F}^{-T} = \mathbf{F}^{-1}\boldsymbol{\pi}$ is the second Piola-Kirchhoff stress tensor (symmetric).

3.1.3 Equilibrium equations

The continuum mechanics is based upon a series of general postulates or principles that are supposed valid, independently of the type of material and of the range of displacements or of deformations. Among them we can find the so-called Conservation-Balance postulates: Conservation of momentum, Conservation of mass and Energy Balance postulates.

The application of the momentum conservation postulate – in a closed system the total momentum is constant – in the current configuration (**Fig. 1.35**) of a solid sub-domain d gives:

$$\int_{\partial\delta} \mathbf{t}ds + \int_{\delta} \rho\mathbf{b}dv = 0 \tag{1.27}$$

where $\mathbf{t}$ is the cohesion forces tensor acting over the surface $\partial\delta$, ρ is the mass density per unit volume in the current configuration and $\mathbf{b}$ is the force density tensor acting over the volume δ.

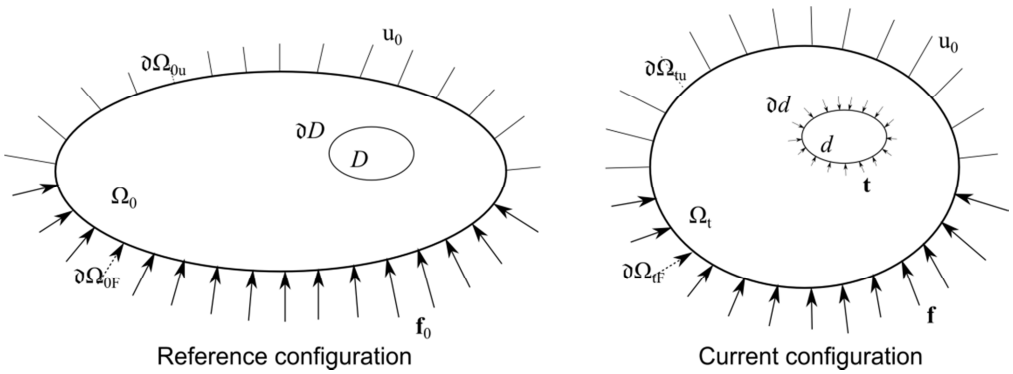

Fig. 1.35 Boundary conditions in the reference and current configuration.

From the divergence theorem[8], Eq. (1.24) and considering the boundary conditions, it is possible to establish the equilibrium equations for the current configuration:

$$\begin{aligned} &\nabla_x \mathbf{T} + \rho \mathbf{b} = 0 && \text{over } \Omega_t \\ &\mathbf{T}\mathbf{n} = \mathbf{f} && \text{over } \Omega_{tF} \\ &\mathbf{u} = \mathbf{u_0} && \text{over } \Omega_{tu} \end{aligned} \tag{1.28}$$

On the other hand, if Eq. (1.27) is modified to take into account the sub-domain *D* then it is possible to establish the equilibrium equations for the reference configuration:

$$\begin{aligned} &\nabla_X \boldsymbol{\pi} + \rho_0 \mathbf{b} = 0 && \text{over } \Omega_0 \\ &\boldsymbol{\pi}\mathbf{N} = \mathbf{f}_0 && \text{over } \Omega_{0F} \\ &\mathbf{u} = \mathbf{u_0} && \text{over } \Omega_{0u} \end{aligned} \tag{1.29}$$

where

$$\rho_0 = J\rho \tag{1.30}$$

is the mass density per unit volume in the reference configuration, as the mass conservation postulate – the mass of a closed system must remain constant over time – must be considered.

3.2 Elements of thermodynamics

3.2.1 Fundamental principles of the thermodynamics

If we consider a solid in a certain configuration Ω_t (respectively Ω_0) then there is a state function E, internal energy of the system, such that its variation per unit time is equal to the sum of the inner mechanical power P and the amount of heat supplied to the system Q:

$$\dot{E} = P + Q \tag{1.31}$$

It is possible to express each term of Eq. (1.31) in the current or reference configuration, e.g. the internal energy of the system is given by:

$$E = \int_{\Omega_t} \rho e dv = \int_{\Omega_0} \rho_0 e dV \tag{1.32}$$

where *e* is the specific internal energy. The inner mechanical power is deducted from the principle of virtual powers – the virtual power of an acceleration quantity is equal to the sum

[8] The outward flux of a vector field through a closed surface is equal to the volume integral of the divergence over the region inside the surface.

of the virtual power of the internal and external forces – and it is equal to the product of a kinematic variable with its corresponding stress:

$$-\mathsf{P} = \int_{\Omega_t} \mathbf{T} : \mathbf{D} dv = \int_{\Omega_0} \mathbf{S} : \dot{\mathbf{E}} dV = \int_{\Omega_0} \boldsymbol{\pi} : \dot{\mathbf{F}} dV \tag{1.33}$$

Finally, the amount of heat supplied to the system can be decomposed into an energy source per unit mass r and a heat flux loss $\mathbf{q}$ (respectively $\mathbf{q}_0$) in the surface border $\partial\Omega_t$ (respectively $\partial\Omega_0$):

$$\mathsf{Q} = \int_{\Omega_t} r dv - \int_{\partial\Omega_t} \mathbf{q}\mathbf{n} ds = \int_{\Omega_0} r dV - \int_{\partial\Omega_0} \mathbf{q}_0 \mathbf{N} dS \tag{1.34}$$

where $\mathbf{q}\mathbf{n}ds = \mathbf{q}_0\mathbf{N}dS$ is the heat flux lagrangian expression. Then, the energy conservation expression – first law of thermodynamics – can be defined, in a Eulerian formulation, as

$$\rho \dot{e} = \mathbf{T} : \mathbf{D} + r - \nabla_x \mathbf{q} \tag{1.35}$$

in Lagrangian formulation as

$$\rho_0 \dot{e} = \mathbf{S} : \dot{\mathbf{E}} + r - \nabla_X \mathbf{q}_0 \tag{1.36}$$

and, in a mixed formulation as

$$\rho_0 \dot{e} = \boldsymbol{\pi} : \dot{\mathbf{F}} + r - \nabla_X \mathbf{q}_0 \tag{1.37}$$

It is necessary to add a restriction to the energy balance equation introduced by the second principle of the thermodynamics. The second law establishes the following postulates:

1) There is a state function called absolute temperature $\theta(\mathbf{x}, t)$ which is strictly positive, i.e. $\theta > 0$.
2) There is a state function called entropy S with the following characteristics:
   a) It is an extensive variable, i.e. there is a specific entropy η such that:

$$S = \int_{\Omega_t} \rho \eta dv = \int_{\Omega_0} \rho_0 \eta dV \tag{1.38}$$

   b) The following inequality is fulfilled:

$$\frac{dS}{dt} \geq \mathsf{Q}_{ext} \tag{1.39}$$

   where $\mathsf{Q}_{ext} = \mathsf{Q}/\theta$ is the heat rate supplied to the system divided by the absolute temperature.

If $\frac{dS}{dt} = Q_{ext}$ the process is called reversible – it is possible to return from the final thermodynamic state *B* to the initial thermodynamic state *A* by the same way – and if $\frac{dS}{dt} > Q_{ext}$ the process is called irreversible – it is not possible to return from the final thermodynamic state *B* to the initial thermodynamic state *A* by the same way, even if it is possible to return by a different way. Introducing the corresponding expression of Eqs. (1.34) and (1.38) into Eq. (1.39), the abovementioned inequality can be formulated, in the current configuration, as

$$\rho\dot{\eta} - \frac{r}{\theta} + \mathbf{q}\nabla_x \frac{1}{\theta} \geq 0 \tag{1.40}$$

or in the reference configuration

$$\rho_0\dot{\eta} - \frac{r}{\theta} + \mathbf{q}_0\nabla_X \frac{1}{\theta} \geq 0 \tag{1.41}$$

Furthermore, substituting *r* from Eq. (1.35) into Eq. (1.40) or *r* from Eqs. (1.36) and (1.37) into Eq. (1.41), three new expressions for the second law of thermodynamics are defined:

$$-\rho\left(\dot{e} - \theta\dot{\eta}\right) + \mathbf{T}:\mathbf{D} - \frac{1}{\theta}\mathbf{q}\nabla_x\theta \geq 0 \tag{1.42}$$

in the Eulerian formulation,

$$-\rho_0\left(\dot{e} - \theta\dot{\eta}\right) + \mathbf{S}:\dot{\mathbf{E}} - \frac{1}{\theta}\mathbf{q}_0\nabla_X\theta \geq 0 \tag{1.43}$$

in the Lagrangian formulation, and

$$-\rho_0\left(\dot{e} - \theta\dot{\eta}\right) + \boldsymbol{\pi}:\dot{\mathbf{F}} - \frac{1}{\theta}\mathbf{q}_0\nabla_X\theta \geq 0 \tag{1.44}$$

in the mixed formulation.

Introducing a new variable, the specific free energy:

$$\psi = e - \theta\eta \tag{1.45}$$

it is possible to define the Clausius-Duhem inequality – common way to express the second law of thermodynamics – in the mixed formulation, as:

$$-\rho_0\left(\dot{\psi} + \eta\dot{\theta}\right) + \boldsymbol{\pi}:\dot{\mathbf{F}} - \frac{1}{\theta}\mathbf{q}_0\nabla_X\theta \geq 0 \tag{1.46}$$

3.2.2 Thermodynamics of local state

The local state method postulates that the thermodynamic state of a point in a continuum medium at a given time is completely defined by the values of a certain number of variables that depend uniquely on the given material point. The time derivatives of these variables are not required to define the thermodynamic state, i.e. any time evolution could be considered as a succession of equilibrium states. It is by the choice of the nature and the number of state variables that a physical phenomenon can be described. Two types of state variables can be distinguished:

- The **observable variables** are related with directly measurable properties of the continuum. The mechanics and thermodynamics formalism impose the deformation-temperature variables $(\mathbf{F},\theta)$.
- The **internal variables** are introduced to describe the dissipative phenomena, e.g. the viscosity or the plasticity, or to describe the inner state of the material, e.g. dislocation density, microcracks configuration or cavities, without the possibility to measure the aforementioned properties in a direct way. There is not an objective method to choose the nature of the internal variables. Depending on the complexity of the phenomenon, the internal variables could be scalar $(V_1,V_2,\dots V_k)$ or tensorial $(\mathbf{V}_1,\mathbf{V}_2,\dots \mathbf{V}_k)$.

Once that the state variables are defined, the existence of a thermodynamic potential – specific free energy potential – from which the state laws are derived can now be postulated. This function allows checking the conditions of thermodynamic stability imposed by the inequalities that can be deduced from the second thermodynamic principle. Then, the specific free energy potential, for *k* tensorial internal variables, can be defined as:

$$\psi = \psi\left(\mathbf{F},\theta,\mathbf{V}_k\right) \tag{1.47}$$

and the specific free energy potential rate as:

$$\dot{\psi} = \frac{\partial \psi}{\partial \mathbf{F}} : \dot{\mathbf{F}} + \frac{\partial \psi}{\partial \theta}\dot{\theta} + \frac{\partial \psi}{\partial \mathbf{V}_k} : \dot{\mathbf{V}}_k \tag{1.48}$$

From Eq. (1.48) the thermodynamic force associated with the internal variable $\mathbf{V}_k$ is defined as follows:

$$\mathbf{A}_k = \rho \frac{\partial \psi}{\partial \mathbf{V}_k} \tag{1.49}$$

The thermodynamic potential allows writing the state relations between the observable variables and its associate variables; however, for the internal variables, it only allows the definition of its associate variables. The description of the evolution of the internal variables is carried out by means of a complementary formalism: the dissipation potential. The dissipation potential (or dissipation pseudo-potential) is expressed as a continuous function in which the state variables are introduced as parameters:

$$\varphi = \varphi\left(\dot{\mathbf{F}}, \dot{\mathbf{V}}_k, \mathbf{q}/\theta\right) \tag{1.50}$$

Then, considering that the thermodynamic forces are the components of the $\nabla\varphi$ vector, the complementary law can be expressed as:

$$\boldsymbol{\pi} = \frac{\partial\varphi}{\partial\dot{\mathbf{F}}} \quad \mathbf{A}_k = -\frac{\partial\varphi}{\partial\dot{\mathbf{V}}_k} \quad \nabla\theta = -\frac{\partial\varphi}{\partial\left(\mathbf{q}/\theta\right)} \tag{1.51}$$

Finally, the Clausius-Duhem inequality can be reduced to a dissipation expression as:

$$\gamma = \Phi_m + \Phi_T \geq 0 \tag{1.52}$$

where γ is the dissipation,

$$\Phi_m = \boldsymbol{\pi} : \dot{\mathbf{F}} - \mathbf{A}_k : \mathbf{V}_k \tag{1.53}$$

is the intrinsic dissipation (or mechanical dissipation), and

$$\Phi_T = -\frac{1}{\theta}\mathbf{q}_0 \nabla_X \theta \tag{1.54}$$

is the heat flux.

3.2.3 Heat transfer

The heat transfer by conduction is a way of inner heat propagation, independent of the movement, associated with the thermal gradient inside the continuum medium which is characterized by Fourier's Law:

$$\mathbf{q}_0 = -\mathbf{K}_X \nabla\theta_X \tag{1.55}$$

where

$$\mathbf{K}_X = \mathbf{F}^{-1}\mathbf{K}\mathbf{F}^{-T} \tag{1.56}$$

is the conductivity tensor in the initial configuration, and $\mathbf{K}$ is the Euler conductivity tensor. In the isotropic case, this one reduces to $\mathbf{K} = \kappa\mathbf{I}$, where κ is the material conductivity factor.

Inserting the specific internal energy rate expressed in mixed formulation, after a series of straightforward derivations using Eqs. (1.45) and (1.47), as:

$$\dot{e} = \frac{1}{\rho_0}\boldsymbol{\pi} : \dot{\mathbf{F}} + \frac{1}{\rho_0}\mathbf{A}_k : \mathbf{V}_k - \theta\frac{1}{\rho_0}\left(\frac{\partial \boldsymbol{\pi}}{\partial \theta} : \dot{\mathbf{F}} + \frac{\partial \mathbf{A}_k}{\partial \theta} : \dot{\mathbf{V}}_k\right) - \theta\frac{\partial^2 \psi}{\partial \theta^2}\dot{\theta} \tag{1.57}$$

into the standard formulation of the first thermodynamics law, Eq. (1.37), leads to the heat equation:

$$\rho_0 C\dot{\theta} = -\mathbf{A}_k : \dot{\mathbf{V}}_k + \theta\left[\frac{\partial \boldsymbol{\pi}}{\partial \theta} : \dot{\mathbf{F}} + \frac{\partial \mathbf{A}_k}{\partial \theta} : \dot{\mathbf{V}}_k\right] + r + \mathbf{K}_X \nabla \theta_X \tag{1.58}$$

where C is the specific heat per unit mass:

$$C\left(\mathbf{F}, \theta, \mathbf{V}_k\right) = -\theta\frac{\partial^2 \psi}{\partial \theta^2} \tag{1.59}$$

3.3 Hyperelastic models

The hyperelasticity is the capability of a material to experience large elastic strains due to small forces – nonlinear behavior – without losing its original properties. An elastic material is hyperelastic if there is a scalar function – denoted by W and called strain energy function – such that:

$$\mathbf{T} = 2\frac{\partial W}{\partial \mathbf{B}} \tag{1.60}$$

in the current configuration,

$$\mathbf{S} = 2\frac{\partial W}{\partial \mathbf{C}} \tag{1.61}$$

in the reference configuration, and

$$\boldsymbol{\pi} = \frac{\partial W}{\partial \mathbf{F}} \tag{1.62}$$

in the mixed configuration.

3.3.1 Statistical mechanics treatments

The statistical mechanics approach begins by assuming a structure of randomly-oriented long molecular chains. In the Gaussian treatment, when deformation is applied, the chain structure stretches and its configurational entropy decreases. If one considers the deformation of an assembly of n chains by a principal stretch state $\left(\lambda_1, \lambda_2, \lambda_3\right)$ and the

deformation is such that the chain length *r* does not approach its fully extended length *Nl*, *N* being the number of connected rigid-links in a chain and *l* the length of each link, then the elastic strain energy function can be derived from the change in configurational entropy:

$$W = \frac{1}{2} nk\theta \left(\lambda_1^2 + \lambda_2^2 + \lambda_3^2 - 3 \right) \tag{1.63}$$

where *k* is Boltzmann's constant. At large deformations where *r* begins to approach *Nl*, the non-Gaussian nature of the chain stretch must be taken into account. Kuhn and Grün (1942) accounted for the finite extensibility of chain stretch using Langevin chain statistics which account for the effect of the relative chain length on the configuration available to the chain. The resulting non-Gaussian force-extension relationship for a chain is given by:

$$f = \frac{k\theta}{l} \mathcal{L}^{-1}\left(\frac{r}{Nl} \right) = \frac{k\theta}{l} \mathcal{L}^{-1}\left(\frac{\lambda}{\sqrt{N}} \right) \tag{1.64}$$

where $\mathcal{L}^{-1}$ is the inverse of the Langevin function given by:

$$\mathcal{L}^{-1}(\beta) = \coth(\beta) - 1/\beta \tag{1.65}$$

Assuming a representative network structure (**Fig. 1.36**), to link the chain stretch of individual chains to the applied deformation, it is possible to incorporate the non-Gaussian relationship into a constitutive framework. The models differ in how the chains deformation is related to the deformation of the unit cell.

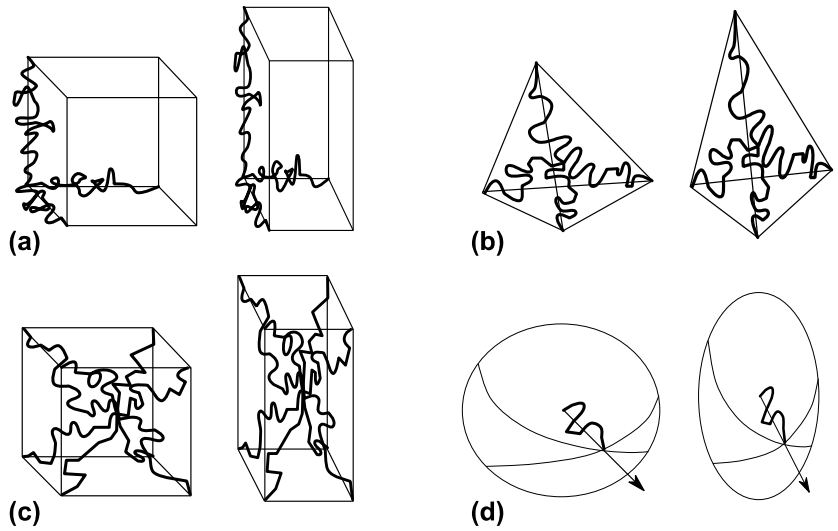

Fig. 1.36 Non-Gaussian networks: (a) 3-chain model, (b) 4-chain model, (c) 8-chain model, and (d) full network model. Each model is depicted in its undeformed and deformed state.

In the 3-chain model (James and Guth, 1943), the chains deform with the cell and the stretch on each chain will then correspond to a principal stretch value. The resulting strain energy function is given by:

$$W = \frac{nk\theta}{3}\sqrt{N}\sum_{i=1}^{3}\left(\lambda_i\beta_i + \sqrt{N}\ln\left(\frac{\beta_i}{\sinh\beta_i}\right)\right) \tag{1.66}$$

where $\beta_i = \mathcal{L}^{-1}\left(\lambda_i/\sqrt{N}\right)$. In the 4-chain model (Flory and Rehner, 1943), the tetrahedron deforms according to the imposed deformation and the chains deform accordingly with the interior junction point displacing in a non-affine manner such that the equilibrium is satisfaid. This model provides a more cooperative network deformation than the 3-chain model as the chains stretch and rotate with deformation; however, the individual chain stretch-applied stretch relationship is obtained by iterative methods. In the 8-chain model (Arruda and Boyce, 1993), the chains undergo tensile stretching for all imposed deformations and also rotate towards the principal axis of stretch mimicking, in an average sense, what would be expected in the cooperative deformation of a real network. Due to the symmetry of the chain structure the interior junction point remains centrally located throughout the deformation and the resulting strain energy function is given by:

$$W = nk\theta\sqrt{N}\left[\beta_{ch}\lambda_{ch} + \sqrt{N}\ln\left(\frac{\beta_{ch}}{\sinh\beta_{ch}}\right)\right] \tag{1.67}$$

where $\beta_{ch} = \mathcal{L}^{-1}\left(\lambda_{ch}/\sqrt{N}\right)$ and

$$\lambda_{ch} = \left[\frac{1}{3}\left(\lambda_1^2 + \lambda_2^2 + \lambda_3^2\right)\right]^{1/2} \tag{1.68}$$

is the stretch on each chain in the structure. In the full-network model (Wu and van der Giessen, 1993), the chains are assumed to be randomly distributed in space and to deform in an affine manner. The strain energy function is found by integrating over the stress-stretch response of all chains.

3.3.2 Invariant-based and stretch-based continuum mechanics treatments

The continuum mechanics treatment of rubber elasticity is based upon dependence between the strain energy density and stretch via one or more of the three invariants of the stretch tensor, Eqs. (1.21), (1.22) and (1.23). The elastomer is often approximated to be

incompressible, thus $I_3 = 1$ and does not contribute to the strain energy. Considering out this dependence relation, Rivlin (1948) proposed one general representation of *W* given by

$$W = \sum_{i,j=0}^{\infty} C_{ij} \left(I_1 - 3\right)^i \left(I_2 - 3\right)^j \tag{1.69}$$

where C_{ij} are material parameters. By keeping only the first term of the Rivlin expression, it returns,

$$W = C_{10} \left(I_1 - 3\right) \tag{1.70}$$

which is often called the Neo-Hookean model – note that Eq. (1.70) is the continuum mechanics equivalent to the Gaussian model, Eq. (1.63), where $C_{10} = nk\theta/2$. The often referred to as Mooney-Rivlin model is obtained by keeping the second term of the Rivlin expression:

$$W = C_{10} \left(I_1 - 3\right) + C_{01} \left(I_2 - 3\right) \tag{1.71}$$

This equation was first derived by Mooney (1940) by determining an expression for the strain energy that would provide a constant modulus in shear, i.e. a modulus that did not depend on the shear strain. The apparent success in capturing deviations from the Gaussian/Neo-Hookean model in uniaxial tension is, perhaps, the responsible of the popularity of the Mooney-Rivlin model. Several researchers have used higher order terms in I_1 and, in some cases, I_2, to account for the departure from neo-Hookean/Gaussian behavior at large stretches – as for the Gaussian model, at large deformation, the real stress-stretch behavior departs significantly from that predicted by the neo-Hookean model. Using higher order I_1 terms, Yeoh (1993) proposed a strain energy function,

$$W = C_{10} \left(I_1 - 3\right) + C_{20} \left(I_1 - 3\right)^2 + C_{30} \left(I_1 - 3\right)^3 \tag{1.72}$$

that has been shown to work well in capturing different deformation state from moderate to large deformations. An alternate high order I_1 model has been proposed by Gent (1996):

$$W = -\frac{E}{6} \ln\left(1 - \frac{J_1}{J_\infty}\right) \tag{1.73}$$

where *E* is the small-strain tensile modulus, $J_1 = (I_1 - 3)$ and J_∞ denotes a maximum value for J_1 accounting for the limiting extensibility. The natural logarithm term can be expanded to yield to the following formulation:

$$W = \frac{E}{6}\left[\sum_{n=0}^{\infty} \frac{1}{(n+1)J_\infty^n}(I_1 - 3)^{n+1}\right] \tag{1.74}$$

which is a form of the Rivlin expression, with all coefficients, C_{i0}, now related to the two material parameters *E* and J_∞. Considering that the aforementioned 8-chain model (Arruda and Boyce, 1993), is I_1-based since it is a function of chain stretch λ_{ch}, which is equivalent to $\sqrt{I_1/3}$, then a invariant-based form can be formulated:

$$W = \sum_{i=1}^{n} C_i \left(I_1^i - 3_i\right) \tag{1.75}$$

where the C_i are all determined a priori as functions of the material properties *n* and *N*. The success of the higher order I_1 continuum mechanics models is due to their mimicking the physics of successful non-Gaussian statistics models thus providing the connection between the higher order continuum models and the statistical mechanics models – similar to the neo-Hooken model being equivalent to the Gaussian model. One caution regarding the use of phenomenological higher order I_1 continuum mechanics models is that the constants chosen must result in physically realistic and stable constitutive responses in all deformation states – one judicious choice would be to choose all coefficients to be positive-valued.

Strain energy density functions based on the principal stretches, as opposed to the stretch invariants, have also been proposed by several investigators. Valanis and Landel (1967) proposed a strain energy function related with the principal stretches:

$$W = \sum_{i=1}^{3} w(\lambda_i) \tag{1.76}$$

The functions $w(\lambda_i)$ are experimentally obtained. Following a similar approach, Ogden (1972) proposed a strain energy function in terms of principal stretches:

$$W = \sum_n \frac{\mu_n}{\alpha_n}\left(\lambda_1^{\alpha_n} + \lambda_2^{\alpha_n} + \lambda_3^{\alpha_n} - 3\right) \tag{1.77}$$

where μ_n and α_n are data-fit constants.

Statistical mechanics models which account for the non-Gaussian nature of the molecular chain stretch together with and effective or representative network structure provide the most predictive model of the larger strain behavior under different states of deformations. Furthermore, the physically based foundation of the non-Gaussian statistical mechanics network models provides a constitutive law that requires only two material properties – the network chain density *n*, which is determined from the small strain behavior, and the limiting chain extensibility $\sqrt{N}$, which is determined from the behavior at large strain. Besides, the continuum mechanics invariant-based constitutive models are equivalent phenomenological representations of the microstructurally based statistical mechanics models – the first invariant I_1 is correlated with the average chain stretch in the network model. Strain energy expressions which contain a polynomial series in I_1 including higher order I_1 terms capture the non-Gaussian nature of the network stretch behavior while, on the other hand, strain energy expressions which contain the second invariant of stretch I_2 should be used with caution – results are stiffer in certain types of deformation.

CHAPTER 2

Temperature and filler effects on the relaxed response of filled rubbers[9]

Heat build-up of filled rubbers under cyclic loading at environmental conditions is well known. This increase in temperature seriously affects the constitutive stress-strain behavior by producing a thermal softening of the rubber compound. Although this feature is well-recognized and considered as important to account for, few constitutive thermo-mechanical models attempt to quantify the stress-temperature relationship. In this chapter, a physically-based model is developed to describe the large strain relaxed response of filled rubbers over a wide range of temperatures. The non-linear mechanical behavior is described via a Langevin formalism in which the temperature and filler effects are, respectively, included by a network thermal kinetics and an amplification of the first strain invariant. Experimental observations on the relaxed state of styrene-butadiene rubber hourglass-shaped specimens with a given carbon-black content are reported at different temperatures. A hybrid experimental-numerical method is proposed to determine simultaneously the local thermo-mechanical response and the model parameters. In addition, the predictive capability of the proposed constitutive thermo-mechanical model is checked by comparisons with results issued from micromechanical simulations containing different arrangements of the microstructure. The results show that the model offers a satisfactory way to predict the relaxed response of filled rubbers at different temperatures.

[9] This chapter is based on the following paper: Ovalle Rodas, C., Zaïri, F., Naït-Abdelaziz, M., Charrier, P., 2015. Temperature and filler effects on the relaxed response of filled rubbers: Experimental observations on a carbon-filled SBR and constitutive modeling. *International Journal of Solids and Structures*, in press.

1. Introduction

In the automotive and aeronautical industries, filled rubbers are commonly used as damping components which are, under typical operating conditions, submitted to cyclic loading. Due to the thermo-mechanical coupling, in connection with the viscous-related behavior, the material heats up (Gough, 1805). The order of magnitude of the heat build-up is related with the strain rate, the maximum strain and the geometry of the specimen (Ayoub et al, 2012; Ovalle Rodas et al., 2013, 2014). Since the material properties depend on temperature the heat build-up evidently influences the stress-strain response. On the other hand, adding fillers (e.g. carbon-black particles) to reinforce the mechanical properties of the rubber compound is a common industrial practice. Both, the filler-rubber gum and filler-filler interactions have a strong effect on the thermal behavior and vice versa. Since the material behavior depends both on the filler volume fraction and on the temperature of the studied specimen, the development of a physically-based thermo-mechanical model capable to explicitly take into account both characteristics, in parallel with the well-known non-linear elastic behavior when submitted to large strains, is an open issue to be addressed.

The basic features of the rubber stress-strain behavior, generally described by large strain elastic models, are based upon two approaches. The first approach, issued from statistical mechanics developments, considers the change in the configuration entropy of randomly-oriented long molecular chains. Several models proposed under this framework (Kuhn and Grün, 1942; Flory and Rehner, 1943; James and Guth, 1943; Treloar, 1944; Arruda and Boyce, 1993; Wu and van der Giessen, 1993) appear to provide a good predictive tool of the large strain elastic behavior with a minimal number of physical-related material parameters. The second approach is phenomenological and is issued from invariant-based and stretch-based continuum mechanics framework. This phenomenological approach has been successfully used to model the large strain elastic response of unfilled and filled rubbers (Mooney, 1940; Rivlin, 1948; Ogden, 1972; Yeoh, 1993; Gent, 1996).

Furthermore, some efforts have been made to include explicitly the filler effect on the mechanical properties (Guth and Gold, 1938; Smallwood, 1944; Guth, 1945; Mooney, 1951; Ponte Castañeda, 1989; Govindjee and Simo, 1991; Bergström and Boyce, 1999; Bouchart et al., 2008). On the other hand, thermo-mechanical models that include the temperature effect on the mechanical properties of filled rubbers, without the filler effect, have been already proposed (Lion, 1997a; Drozdov and Christiansen, 2009; Li et al., 2011; Rey et al., 2013). While Drozdov and Christiansen (2009) and Li et al. (2011) have shown a stress-softening with increasing temperature, an inverse behavior, i.e. stress-hardening with increasing temperature, was reported by Lion (1997a) and Rey et al. (2013) highlighting the complex thermo-mechanical behavior of filled rubbers. Among the aforementioned models, only Li et al. (2011) proposed a volumetric thermal expansion model in connection with the rubber network parameters. Although it offers a numerical tool to describe the macroscopic experimental observations, i.e. temperature-related stress-softening of filled rubbers, it will be demonstrated further that this model is not physically consistent.

In this chapter, a large strain thermo-mechanical model is developed to capture the relaxed response of filled rubbers. The thermo-mechanical behavior is described by two components acting in series: A thermal resistance linked with the stress-free thermal-dilatation and a mechanical resistance linked with the finite relaxed response. In the mechanical resistance, the explicit effect of the fillers is included by the amplification of the first strain invariant whereas the explicit effect of the temperature is included by a linear evolution of the chain-scale mechanical properties. Experimental observations on the relaxed response of carbon-black-filled styrene-butadiene rubber are reported at different temperatures. The proposed model is implemented into a finite element (FE) code, and hourglass-shaped specimens, using the same thermo-mechanical conditions as those of the experimental protocol, are simulated. In order to extract the local thermo-mechanical response as well as the model parameters, a hybrid experimental-numerical method is proposed. A set of micromechanical simulations with different volumes of fillers is

designed and used to check the predictive capability of the proposed thermo-mechanical constitutive model.

The chapter is organized as follows: in Section 2, the experimental procedure and results are presented. In Section 3, the formulation of the constitutive thermo-mechanical model is detailed. In Section 4, the identification procedure and verification of the proposed model regarding experimental-numerical data are presented. Finally, concluding remarks are given in Section 5.

2. Experimental procedure and observations

2.1 Studied material

The material used in this paper is a sulfur-vulcanized styrene-butadiene rubber (SBR), provided by the Trelleborg Vibracoustic group. The details on material characteristics, provided by the manufacturer, are given in **Table 2.1**. The studied SBR is filled with 34 phr of carbon-black.

2.2 Sample geometry and experimental method

Cylindrical hourglass-shaped specimens with a curvature radius equal to 2 mm (referred to as AE2) were used; details about the geometry are given in **Fig. 2.1**. The specimens were obtained by directly bonding the SBR compound to metal plates during the vulcanization process. In contrast to flat samples, the cylindrical ones allow the measurement of the compression force induced by the thermal expansion of the material and, therefore, facilitate determining the axial thermal-dilatation of the specimen, i.e. the stress-free thermally equilibrated state of the specimen.

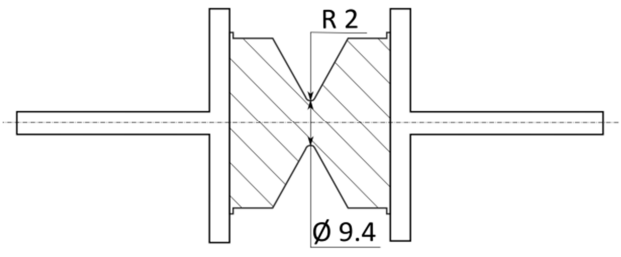

Fig. 2.1. AE2 sample geometry (dimensions in mm).

Ingredients	Value [phr]
SBR	100
Zinc oxide	10
Processing oil	0
Carbon-black	34
Sulfur	3
Stearic acid	3
Antioxidant	5
Accelerators	4.3

Table 2.1. SBR material formulation.

Tests were performed to quantify the relaxed temperature-dependent stress-strain response. The constant-temperature mechanical tests were carried out on an electro-mechanical testing device (Instron-5800) provided with a high temperature environmental chamber (Instron-3119). A displacement-control function was imposed for the loading-unloading condition, load and displacement versus time being recorded during the tests. The tests were performed under temperatures ranging from 293 up to 353 K. The temperature levels above 288 K (room temperature) were attained by forced convection (high speed circulation fan) from a surrounding air operating atmosphere.

Lion (1997a) proposed a time of about 20 minutes to attain a homogenous temperature distribution in cylindrical samples of carbon-black filled rubber. The author validates the homogeneity hypothesis by comparing the temperature evolution in the core and on the specimen surface measured by inserting a thermocouple into a hole drilled in the center and by placing a second one on the specimen surface, respectively. Even that the aforementioned method provides a reasonable way to establish the necessary time to attain a homogenous temperature distribution, it modifies the geometry and boundary conditions of the sample. So, it is not possible to assume that the measured temperature in the core corresponds with

the true temperature into a non-drilled specimen. In this contribution, the homogeneity of the temperature distribution was checked by the stabilization of the compression force induced by the thermal expansion (see **Fig. 2.2a**) and verified by a thermal-dilatation simulation model, as explained below.

The data and simulations have shown that the temperature distribution is constant after about 25 minutes. Therefore, the mechanical tests were carried out 25 minutes after exposure of the sample in the environmental chamber. Likewise, prior to the mechanical test, the specimen was lead to an axial stress-free equilibrated configuration (Anthony et al., 1943). In order to get rid of the Mullins effect (Mullins and Tobin, 1965), the sample was submitted to two loading-unloading cycles up to the maximum stretch $\lambda_{1_{MAX}} = 2$ with a cross-head speed of 1 mm/s.

Multi-relaxation tests were performed to determine the relaxed response of the SBR material. During the loading-unloading condition, the test was interrupted at prescribed levels of displacement x_{R_i} for a given holding time t_R. During this holding time, the load evolution was stored. Both the number of displacement levels and the holding time were defined to be sufficiently low, i.e. $x_R = [2,4,7]\,\text{mm}$ and $t_R = 1\,\text{min}$, in order to avoid the degradation of the mechanical properties of the SBR material due to thermal aging (Tobolsky et al., 1944; South et al., 2003; Mostafa et al. 2009). To assess repeatability of observations, tests were carried out on five different specimens.

2.3 Experimental results

The thermal dilatation in the loading direction (called axial dilatation) X_i due to the temperature increasing is shown in **Fig. 2.2b**. As usually observed for filled rubbers (Thiele and Cohen, 1980), the SBR material exhibits an increasing thermal expansion strain for increasing temperature. From the axial dilatation-absolute temperature slope and the initial axial length of the sample, L_0 = 30 mm, the thermal expansion coefficient of the SBR material can be derived:

$\alpha = (1/L_0)(dL/d\theta) = 3.6\times10^{-4}$ K^{-1}. Similar results, for different rubber materials, were observed (Kraus and Gruver, 1970; Thiele and Cohen, 1980; Holzapfel and Simo, 1996; Lion, 1997a; Lion et al., 2014) [10]. It should be noted that the "pre-test" axial force due to thermal dilatation is composed of both a viscous component and a relaxed component. Thus, the relaxed axial force due to the thermal-dilatation is smaller than the total one. Therefore, the axial displacement to attain an axial stress-free configuration should be smaller. Moreover, during the procedure to attain the axial stress-free configuration, a variation of the temperature into the specimen should appear due to the thermo-mechanical coupling (Medalia, 1991; Luo et al., 2010). Both phenomena slightly decrease the dilatation-absolute temperature slope and, accordingly, the coefficient of thermal expansion; however, the relaxed "pre-test" force is found to be approximately equal to the total force, **Fig. 2.3a**, and the temperature evolution for a SBR material under small stretching is almost imperceptible (Ovalle Rodas et al., 2014).

The mechanical response of the studied material, in terms of load-displacement curves, is illustrated in **Fig. 2.3**. In **Fig. 2.3a**, the relaxed curves derived from a multi-relaxation test are plotted for two temperatures (293 K and 333 K). The SBR material exhibits a well-known non-linear response followed by a severe hardening under large displacements. During the holding time, relaxation (i.e. load decrease versus time) is observed during the loading phase while inverse-relaxation (i.e. load increase versus time) can be seen during unloading. Note that both evolve towards an equilibrium state whose envelope gives the relaxed response. Furthermore, this relaxed response seems to increase asymptotically as it approaches a given displacement E_∞ depending on the temperature. As a matter of fact, during holding phases, the load decrease (loading phase) is more significant under large displacements while the load increase is more significant under small displacements

[10] The linear thermal expansion coefficient was found of the order of $\alpha = [2.0-6.0]\times10^{-4}\,\mathrm{K}^{-1}$.

(unloading phase). In **Fig. 2.3b**, the relaxed response for different temperatures ranging from 293 to 353 K are reported. These curves point out the non-linear decrease of the material stiffness with temperature.

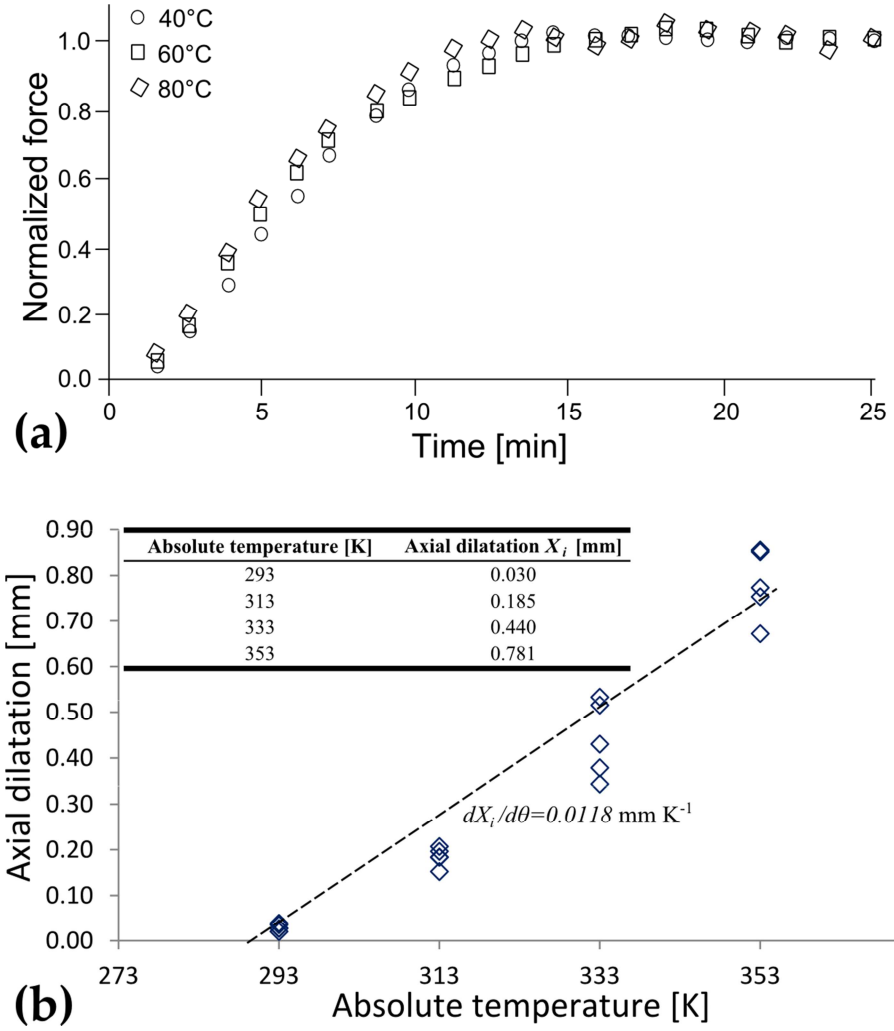

Fig. 2.2. Experimental procedure: (a) Normalized force induced by the thermal expansion, (b) axial thermal-dilatation of the AE2 sample.

In what follows, to capture and to predict the observed behavior a constitutive model is proposed.

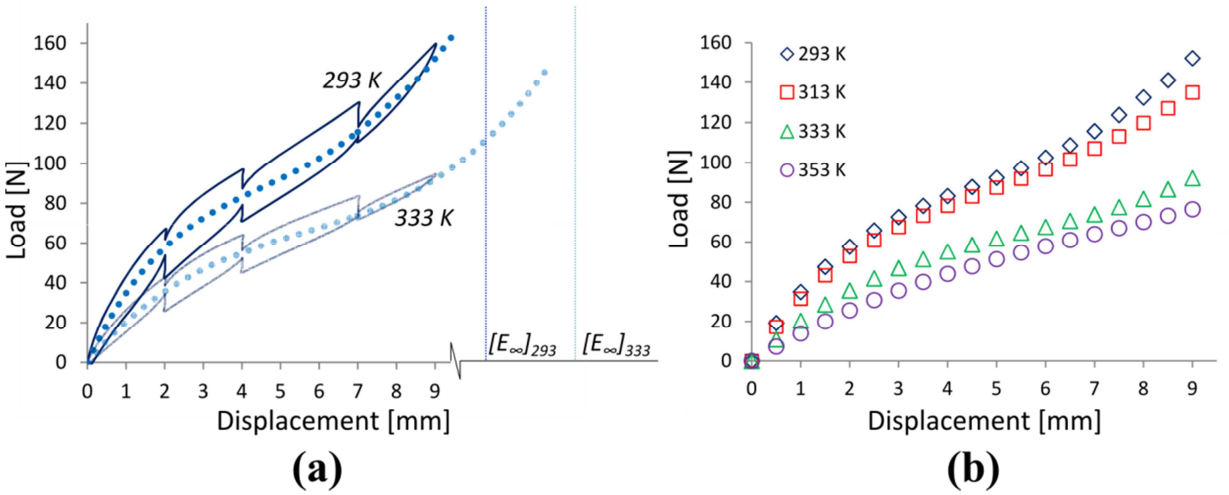

Fig. 2.3. Load-displacement curves of the AE2 sample: (a) Multi-relaxation responses, (b) temperature-dependent relaxed responses.

3. Constitutive model

The constitutive model considers the large strain thermo-elastic response of filled rubbers. The schematic representation of the model is shown in **Fig. 2.4a**. To account for the temperature-dependent mechanical behavior, the thermo-mechanical model is composed of a thermal resistance (temperature-dependent element) acting in series with a mechanical resistance (non-linear elastic spring) linked to the stress-free thermal-dilatation and to the large strain rubber elastic behavior, respectively.

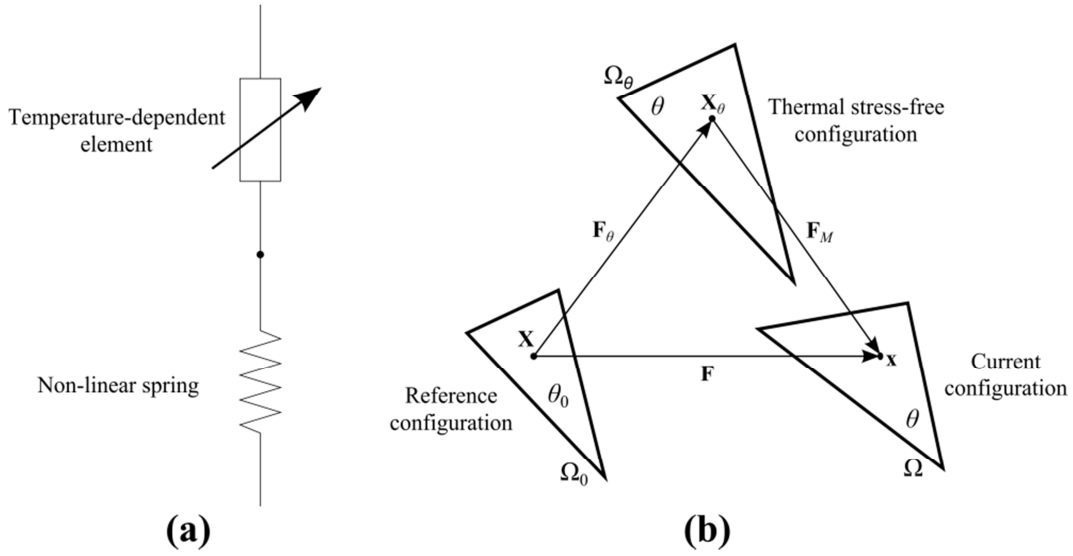

Fig. 2.4. Thermo-elastic model: (a) Schematic representation, (b) multiplicative decomposition of the thermo-mechanical deformation.

3.1 Thermo-elastic kinematics

Let us first consider a continuum body with the reference configuration Ω_0 and an actual configuration Ω, see **Fig. 2.4b**. For the sake of simplicity, Ω_0 is assumed to be stress-free and subjected to a uniform absolute temperature θ_0 taken as a reference. The mapping of a given material point with the position **X** in the reference configuration to the position **x** in the actual configuration is given by the deformation gradient: $\mathbf{F} \equiv \partial \mathbf{x} / \partial \mathbf{X}$[11].

In order to take thermal deformation effects in combination with the mechanical behavior of the continuum body into account, the deformation gradient can be written using a multiplicative form and decomposed into a thermal part $\mathbf{F}_\theta$ and a mechanical part $\mathbf{F}_M$ (Lee and Liu, 1967; Lu and Pister, 1975; Miehe, 1995; Holzapfel and Simo, 1996):

$$\mathbf{F} = \mathbf{F}_\theta \mathbf{F}_M \tag{2.1}$$

The local deformation is then decomposed into two successive arrangements. The first one, related with the stress-free thermal dilatation of the continuum body, is characterized by the thermal deformation gradient tensor:

$$\mathbf{F}_\theta \equiv \frac{\partial \mathbf{X}_\theta}{\partial \mathbf{X}} \tag{2.2}$$

where $\mathbf{X}_\theta$ is the position of a given point in the thermal stress-free configuration but at a homogeneous absolute temperature $\theta \neq \theta_0$. The second one, related with the isothermal mechanical behavior of the continuum body, is characterized by the mechanical deformation gradient tensor:

$$\mathbf{F}_M \equiv \frac{\partial \mathbf{x}}{\partial \mathbf{X}_\theta} \tag{2.3}$$

[11] In all that follows, variables in italics indicate scalar quantities; variables in lower case bold indicate vector quantities; variables in upper case bold indicate second-order tensors, and any exception will be specifically noted.

For thermally isotropic materials, the thermal deformation gradient tensor can be written as:

$$\mathbf{F}_\theta = \exp\left[\int_{\theta_0}^{\theta} \alpha(\theta)\, d\theta\right]\mathbf{I} \tag{2.4}$$

where $\alpha(\theta)$ is the temperature-dependent coefficient of the thermal expansion and $\mathbf{I}$ is the unit tensor. In Eq. (2.4), the exponential expression is a temperature function representing the intrinsic thermal dilatation characteristics of the continuum body (Lu and Pister, 1975; Holzapfel and Simo, 1996).

In view of the local transformations expressed through Eqs. (2.3) and (2.4), the volume change *J* is defined as:

$$J = J_\theta J_M \tag{2.5}$$

where

$$J_\theta = \det \mathbf{F}_\theta = \exp\left[\int_{\theta_0}^{\theta} 3\alpha(\theta)\, d\theta\right] \tag{2.6}$$

is the thermal volume change, and

$$J_M = \det \mathbf{F}_M = \lambda_1\lambda_2\lambda_3 \tag{2.7}$$

is the mechanical volume change. In Eq. (2.7), $\lambda_{i=1,2,3}$ are the three (real and positive) eigenvalues of $\mathbf{F}_M$ related with the isothermal mechanical stretches of the continuum body.

3.2 Constitutive equations

To ensure the consistence of the thermo-mechanical coupling, the constitutive equations must fulfill the second law of thermodynamics. The Clausius-Duhem inequality, stating that the dissipation is always positive and commonly used for this purpose, could be written in a mixed description:

$$\gamma = -\rho\left(\dot{\psi} + \dot{\theta}\eta\right) + \boldsymbol{\pi} : \dot{\mathbf{F}} - \frac{1}{\theta}\mathbf{q}\cdot\nabla_X\theta \geq 0 \tag{2.8}$$

where γ is the dissipation, ρ is the mass density for a unit reference volume, η is the specific entropy, $\boldsymbol{\pi} = \partial\psi/\partial\mathbf{F} = J\mathbf{T}\mathbf{F}^{-T}$ is the first Piola-Kirchhoff stress tensor and $\mathbf{T}$ is the Cauchy stress tensor, $\dot{\mathbf{F}}$ is the deformation gradient tensor rate, $\mathbf{q}$ is the Piola-Kirchhoff heat flow, $\nabla_X\theta$ is the temperature gradient and ψ is the Helmholtz free energy potential.

To derive the constitutive equations, the existence of a free energy function for a unit reference volume (a special form of the Helmholtz free energy potential) is postulated:

$$\psi = \psi_\theta + \psi_M \tag{2.9}$$

where ψ_θ is the thermal contribution of the temperature-dependent resistance (Holzapfel and Simo, 1996):

$$\psi_\theta = -\int_{\theta_0}^{\theta} c_v(u)(\theta - u)\frac{du}{u} \tag{2.10}$$

and ψ_M is the mechanical contribution of the non-linear resistance which can be defined by any, phenomenologically-based or statistically-based, strain energy density function. By contrast to phenomenological functions, the material constants of statistical ones are related to the rubbery structure. A number of non-Gaussian statistics theories, based on the prior work of Kuhn and Grun (1942), which introduce the extensibility limit of molecular chain network were proposed: James and Guth (1943) three-chain, Flory and Rehner (1943) four-chain, Treloar and Riding (1979) full-network, Arruda and Boyce (1993) eight-chain and Wu and van der Giessen (1993) approximate full-network functions. In this work, the Arruda-Boyce (1993) model, considering the mechanical contribution as the resistance to deformation energy of an eight-chain non-Gaussian network, is chosen. The strain energy density function is expressed in its compressible version as a function of both the first stretch invariant $I_1 = \mathrm{tr}\left(\mathbf{F}_M\mathbf{F}_M^T\right)$ and the third stretch invariant $I_3 = J_M = \det\mathbf{F}_M$ (Bischoff et al., 2001):

$$\psi_M\left(I_1\right)=nk\theta\sqrt{N}\left(\beta\sqrt{\frac{I_1}{3}}+\sqrt{N}\ln\frac{\beta}{\sinh\beta}-\frac{\beta_0}{3}\ln J_M\right)+\frac{K}{2}\left(J_M-1\right)^2 \tag{2.11}$$

The thermo-mechanical free energy function, defined by Eqs. (2.10) and (2.11), introduces four material constants: the specific heat capacity at constant volume $c_v(\theta)$, the average number of chains per unit volume n, the number of connected rigid-links in a chain N and the temperature-dependent bulk modulus K which, for rubbers, is significantly higher than the shear modulus, e.g. $K\approx 500nk\theta$ in which k is the Boltzmann constant. In Eq. (2.11), the terms β and β_0 correspond to the inverse of the Langevin function $\mathcal{L}^{-1}$ in the current and reference configurations, respectively:

$$\beta=\mathcal{L}^{-1}\left(\sqrt{\frac{I_1}{3N}}\right) \tag{2.12}$$

$$\beta_0=\mathcal{L}^{-1}\left(\sqrt{\frac{1}{N}}\right) \tag{2.13}$$

The inverse of the Langevin function $\mathcal{L}^{-1}(u)=\coth(u)-1/u$ may be estimated through the Padé approximation (Cohen, 1991): $\mathcal{L}^{-1}(u)=u\left(3-u^2\right)/\left(1-u^2\right)$.

Although this model coherently describes the thermo-mechanical behavior of filled rubbers, the filler effect is not explicitly taken into account in any of the material constants. Moreover, the Arruda-Boyce model cannot characterize the large strain elastic response of a rubber at different temperatures with a unified group of parameters as the temperature effect is not explicitly accounted for.

3.2.1 Effect of fillers

The effect of fillers may be explicitly addressed by considering that at any given strain, the presence of the particles acts to locally amplify the strain and stress in the rubber compound over that of a corresponding unfilled rubber at the same macroscopic applied strain (Trabelsi et al., 2003). Firstly introduced by Mullins and Tobin (1965), the amplified strain notion, in the case of uniaxial loading, is quantified as:

$$\Lambda = 1 + \chi(\lambda - 1) \tag{2.14}$$

where Λ is the amplified stretch and λ is the applied axial stretch. The χ constant is an amplification factor depending on the filler volume fraction. The exact form of χ is not clear; however, a general empirical form was proposed by Guth (1945):

$$\chi = 1 + 0.67 c v_f + 1.62 c^2 v_f^2 \tag{2.15}$$

where $c \geq 1$ is a shape factor that considers the filler agglomeration and the reinforcing effect of the filler and v_f is the filler volume fraction. Applying this amplification correction to the first invariant of the stretch, an explicit model that accounts for the filler effect can be defined:

$$\psi_M = (1 - v_f)\psi_M\left(\langle I_1 \rangle_m\right) \tag{2.16}$$

in which $\langle I_1 \rangle_m = \chi(I_1 - 3) + 3$ is the amplified first invariant.

3.2.2 Effect of temperature

The temperature effect on the mechanical behavior of filled rubbers has been addressed in recent thermo-mechanical models (Lion, 1997a; Drozdov and Christiansen, 2009; Li et al., 2011; Rey et al., 2013). A stress-hardening with increasing temperature was shown by Lion (1997a) and Rey et al. (2013), while an inverse behavior, i.e. stress-softening with increasing temperature, was evidenced by Drozdov and Christiansen (2009) and Li et al. (2011) highlighting the complex thermo-mechanical behavior of filled rubbers. Among the aforementioned models, only Li et al. (2011) proposed a thermo-mechanical model related with the rubber network parameters.

- *Li et al. (2011) thermo-mechanical model*

Using a modified version of the Arruda-Boyce (1993) model, Li et al. (2011) describe the temperature effect on the mechanical behavior of rubbers by means of the volumetric thermal expansion of the eight-chain non-Gaussian network.

Considering that the total number of chains n_T in a specimen remains invariable, the average number of chains per unit volume can be calculated as:

$$n = \frac{n_T}{V} = \frac{n_0}{\left[1+\alpha\left(\theta-\theta_0\right)\right]^3} \tag{2.17}$$

where $V = V_0\left[1+\alpha\left(\theta-\theta_0\right)\right]^3$ accounts for the volumetric thermal expansion of a reference volume V_0, α is the thermal expansion coefficient, θ_0 is the reference absolute temperature and n_0 is the reference average number of chains per unit volume. Introducing the term $nk\theta = \left(\theta/\theta_0\right)nk\theta_0$, the temperature explicit-dependence of C_r was defined:

$$C_r = \frac{\theta}{\theta_0\left[1+\alpha\left(\theta-\theta_0\right)\right]^3} C_{r_0} \tag{2.18}$$

where $C_{r_0} = n_0 k\theta_0$ is the rubbery modulus at the reference temperature. Using the Taylor series expansion and assuming that $\left(\theta-\theta_0\right)/\theta_0 < 1$ and $\alpha\left(\theta-\theta_0\right) \ll 1$, Li et al. (2011) propose to rewrite Eq. (2.18) as:

$$C_r = \left[1 + c_1\left(\frac{\theta-\theta_0}{\theta_0}\right) + c_2\left(\frac{\theta-\theta_0}{\theta_0}\right)^2\right] C_{r_0} \tag{2.19}$$

where c_1 and c_2 are unknown parameters. Using Eq. (2.19), the temperature effect on the mechanical response of four tire rubbers was modeled by Li et al. (2011).

Note that in Eq. (2.18) there is only one physical parameter that accounts for the material thermal expansion whereas in Eq. (2.19) there are two parameters which are not clearly related to a physical property. Besides, equating Eqs. (2.18) and (2.19) the corresponding values of α can be determined. The implicit values of α are reported in **Table 2.2**. Several authors (Kraus and Gruver, 1970; Thiele and Cohen, 1980; Holzapfel and Simo, 1996; Lion, 1997a; Lion et al., 2014) have shown that the linear thermal expansion coefficient of rubber materials is of the order of $\alpha = \left[6.0-2.0\right]\times 10^{-4}\,\mathrm{K}^{-1}$. As a consequence, it can be seen that the implicit values of α

used in the thermo-mechanical model proposed by Li et al. (2011) are overestimated. As a matter of fact, the implicit values are, at least, six times higher than the real values.

	Eq. (2.19) (Li et al., 2011)		Eq. (2.18)
Tire rubbers code	c_1	c_2	α [$10^{-4}K^{-1}$]
EBF	-1.7508	2.4123	31
BSP	-2.2242	2.6529	36
KCF	-2.8515	4.6364	45
IHF	-3.3031	4.0972	52

Table 2.2. Material parameters and corresponding thermal expansion coefficient of four tire rubbers extracted from Li et al (2011).

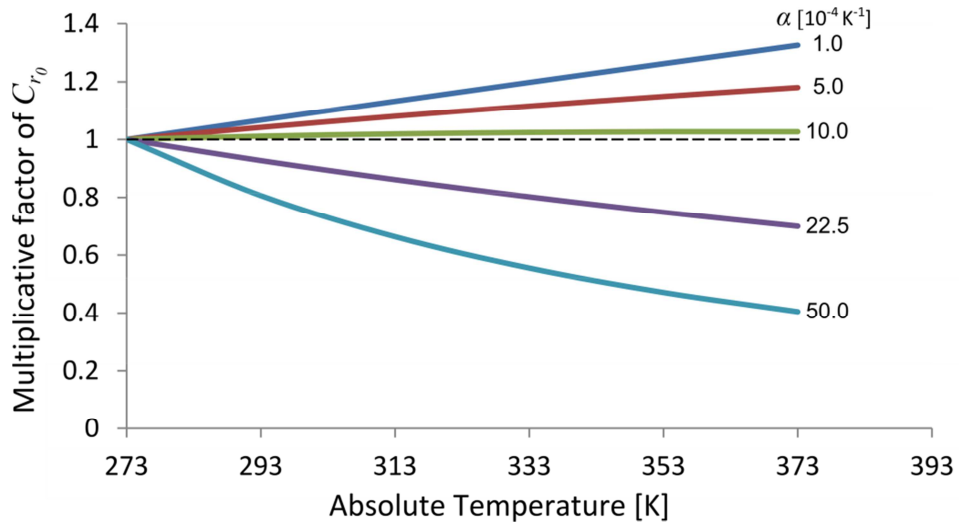

Fig. 2.5. Relation between the absolute temperature and the multiplicative factor of C_{r_0}, Eq. (2.18), for different coefficients of thermal expansion.

In **Fig. 2.5,** the effect of the magnitude of the thermal expansion coefficient over the multiplicative factor of C_{r_0} in Eq. (2.18) can be deduced: for higher values than $10^{-3}K^{-1}$, approximately, the multiplicative factor decreases and, as a consequence, the stress decreases as the temperature increases. Furthermore, using lower values than $10^{-3}K^{-1}$, the linear stress-temperature dependence of rubber materials, as shown by

Meyer and Ferri (1935), is achieved, i.e., an increasing linear relationship between the stress and temperature. Besides, it has been shown (Kraus and Gruver, 1970; Thiele and Cohen, 1980) that the addition of fillers impedes the segmental mobility of polymeric chains in a rubber compound and, as consequence, decreases the coefficient of thermal expansion. It can be then concluded that even the thermo-mechanical model proposed by Li et al. (2011) offers a numerical way to explain the thermal-induced stress-softening of filled rubbers, it is not physically consistent.

- *A network thermal kinetics*

In opposition to the volumetric thermal expansion model proposed by Li et al. (2011) and in accordance with the physical behavior of rubber materials, the effect of temperature on the mechanical response is accounted by the thermal evolution of the chain-scale material parameters n and N. In agreement with previous experimental results (Medalia, 1978; Drozdov and Christiansen, 2009; Li et al., 2011) on carbon-black filled rubbers, we propose a linear phenomenological model for the temperature dependence of the chain density:

$$n_\theta = n_0 + n_{,\theta}\,\theta \tag{2.20}$$

where $n_{,\theta}$ is a material constant accounting for the chain density temperature-rate. As a matter of fact (Boyce, 1986; Arruda et al., 1995; Zaïri et al., 2010), the decrease in chain density n_θ, with increasing temperature, results in an increase in the number of connected rigid-links in a chain N_θ according to the following relationship:

$$n_\theta N_\theta = n_0 N_0 = \text{constant} \tag{2.21}$$

where N_0 is the reference number of connected rigid-links in a chain. The consistent representation of the thermal evolution of the material properties, Eq. (2.21), is ensured by the mass conservation law.

4. Constitutive model identification and verification

4.1 Simulation model

In order to identify the model parameters and define the local stress-strain mechanical response of the SBR material, a simulation model accounting for the geometry of the sample and the boundary conditions concerning the experimental protocol has been developed. By means of a user subroutine, the model has been implemented into an advanced non-linear FE software, MSC.Marc (MSC.Marc, 2004a). This subroutine allows definition of the strain energy function (MSC.Marc, 2004b) taking into account the material compressibility behavior.

The FE model was designed according to the dimensions of the sample (**Fig. 2.1**) and to the axial symmetry of the thermal and mechanical loads of the experimental protocol using 4-node axisymmetric elements. To simulate the thermal dilatation, a constant temperature $\theta = \theta_\infty$ was applied at both ends of the sample (**Fig. 2.6a**). The remaining external surface was subjected to a convection heat transfer condition:

$$\mathbf{q} = -h\left(\theta - \theta_\infty\right)\mathbf{n} \tag{2.22}$$

where h is the convection coefficient, θ_∞ is the environmental temperature inside the chamber, taken as a constant, and $\mathbf{n}$ is the normal vector to the surface of the mesh element. In the remaining boundary, i.e. the symmetry axis, a heat flux normal to the axis $q_r = 0$ was assigned.

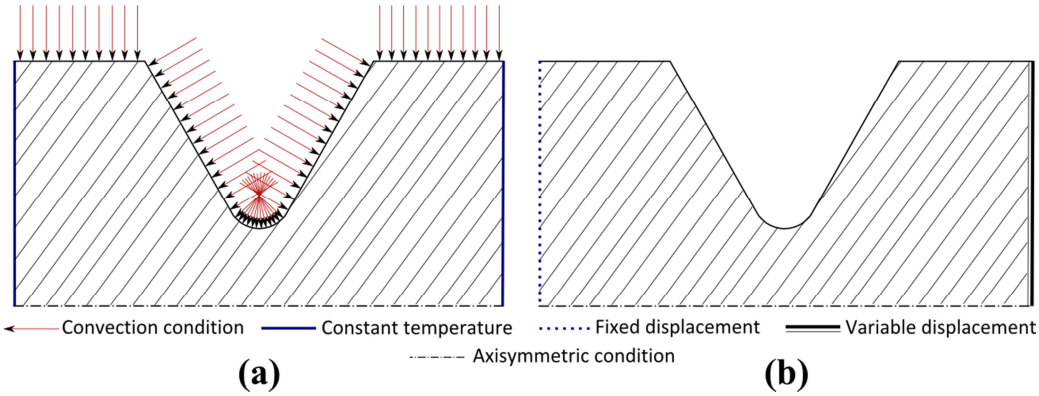

Fig. 2.6. Simulation model of the AE2 sample: (a) thermal and (b) mechanical boundary conditions.

The low initial radius of the AE2 sample induces a multi-axial stress state in the median cross-section. The multi-axial stress state can be quantified using a multi-axiality ratio defined as the ratio between the mean true stress $\mathrm{trace}(\mathbf{T})$ and the axial true stress T_{11}. In **Fig. 2.7**, the multi-axiality ratio evolution, for five equidistant points in the median cross-section of the sample, as a function of the axial displacement is plotted. The multi-axial stress state is clearly pointed out. Except at the surface, the curves evidence a strong multi-axial state at the beginning of the test which softens as the strain increases, converging towards a uniaxial tension state.

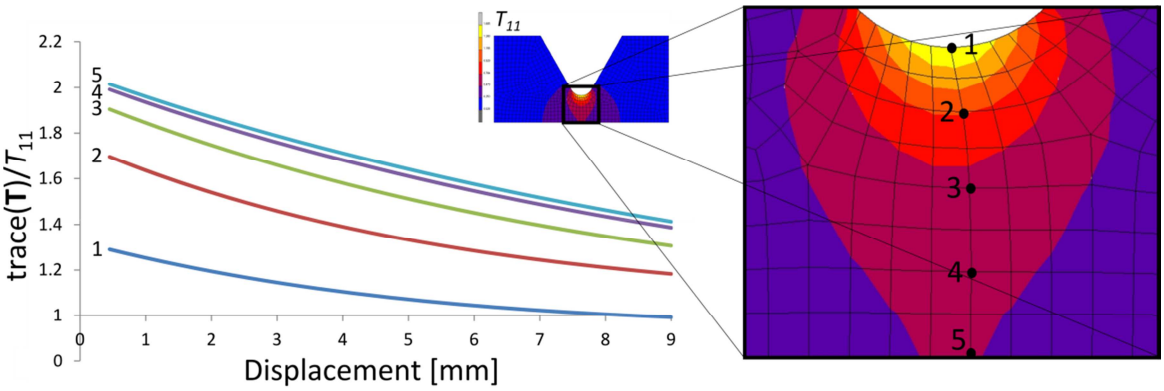

Fig. 2.7. Multi-axiality ratio in the median cross-section of the AE2 sample.

The methodology used in this work takes into consideration the multi-axiality of the AE2 sample, and its consequence on the effective mechanical response. **Fig. 2.8** compares the SBR uniaxial response[12] with the effective mechanical response of the AE2 sample[13]. It can be observed that the stress level is higher for the investigated specimen. By increasing the initial radius of the sample, it is possible to converge towards a uniaxial state. For example, taking a cylindrical hourglass-shaped specimen with a curvature radius equal to 42 mm (referred to as AE42) (as used in

[12] The uniaxial response $\mathrm{trace}(\mathbf{T})/T_{11} = 1$ has been determined from the numerical simulation of a straight cross-section sample.

[13] The true axial stress, T_{11}, was calculated from $T_{11} = F/A$, where F is the current load, and $A = A_0/\lambda_{11}$ is the current section area, A_0 is the initial section area and λ_{11} is the axial stretch. Also, the true axial strain, E_{11}, was calculated from $E_{11} = \ln(\lambda_{11})$. Note that the true axial stress and the true axial strain were calculated from the minimum diameter of the deformed specimen.

Ayoub et al., 2011a, b, 2014) a multi-axiality ratio close to 1.0 is obtained. In **Fig. 2.9**, the multi-axiality ratio evolution, for five equidistant points in the median cross-section of the AE42 sample as a function of the axial displacement is plotted. The curves evidence a weak multi-axiality, i.e. quasi-uniaxial condition, at the beginning of the test which decreases for large stretches. This observation is confirmed at the macroscopic scale in **Fig. 2.8** for which the uniaxial behavior of the AE42 sample is pointed out. The multi-axiality ratio involved in the median cross-section of the AE2 sample leads potentially to a cavitational process (Aït-Hocine et al., 2011; Zaïri et al., 2011a) which can interact with the thermal behavior. For the sake of simplicity, the cavitation is disregarded.

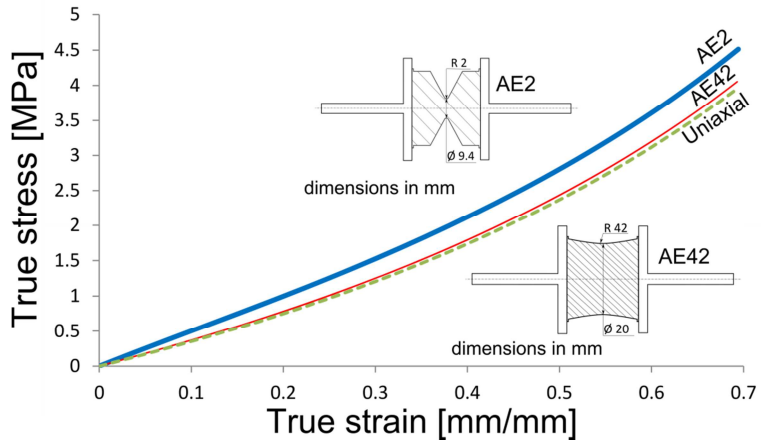

Fig. 2.8. Effective stress-strain responses of the AE2 and AE42 samples, in comparison with the uniaxial path.

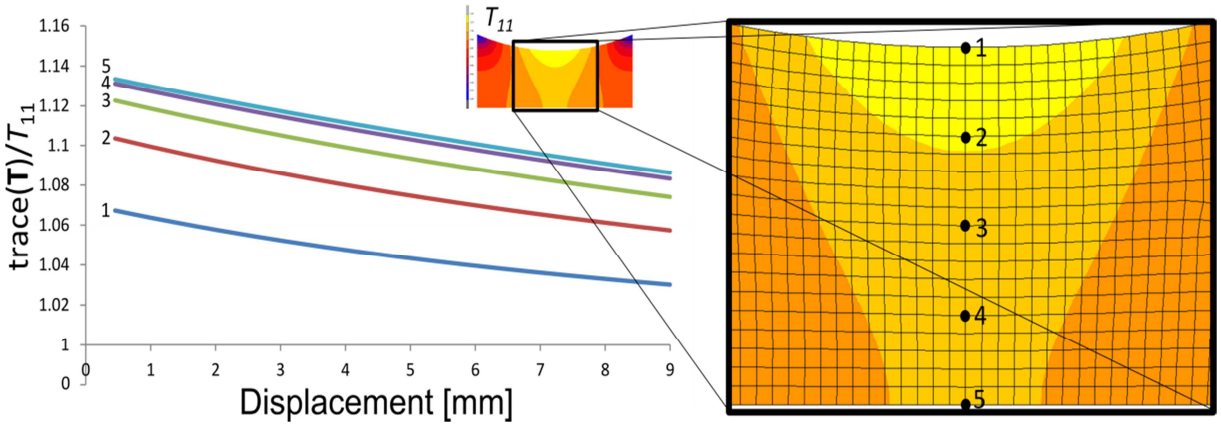

Fig. 2.9. Multi-axiality ratio in the median cross-section of the AE42 sample.

4.2 Parameter identification algorithm

Note that before running the thermal simulation, the mechanical properties of the material, for one environmental temperature, must be defined, i.e. the average number of chains per unit volume n_θ and the number of connected rigid-links in a chain N_θ. As the first group of mechanical parameters not necessarily accounts for the material response or boundary conditions, a recursive algorithm to identify the model parameters has been developed (**Fig. 2.10**). During a step, a set of mechanical properties must be defined - the values being updated at the end of the step. Once the thermal simulation is launched, the mean axial dilatation $\bar{X}_{NODES}$ is then validated with regard the experimental axial dilatation X_i and the new geometry, accounting for the thermal dilatation, is remeshed following the initial mesh distribution (rezone mesh).

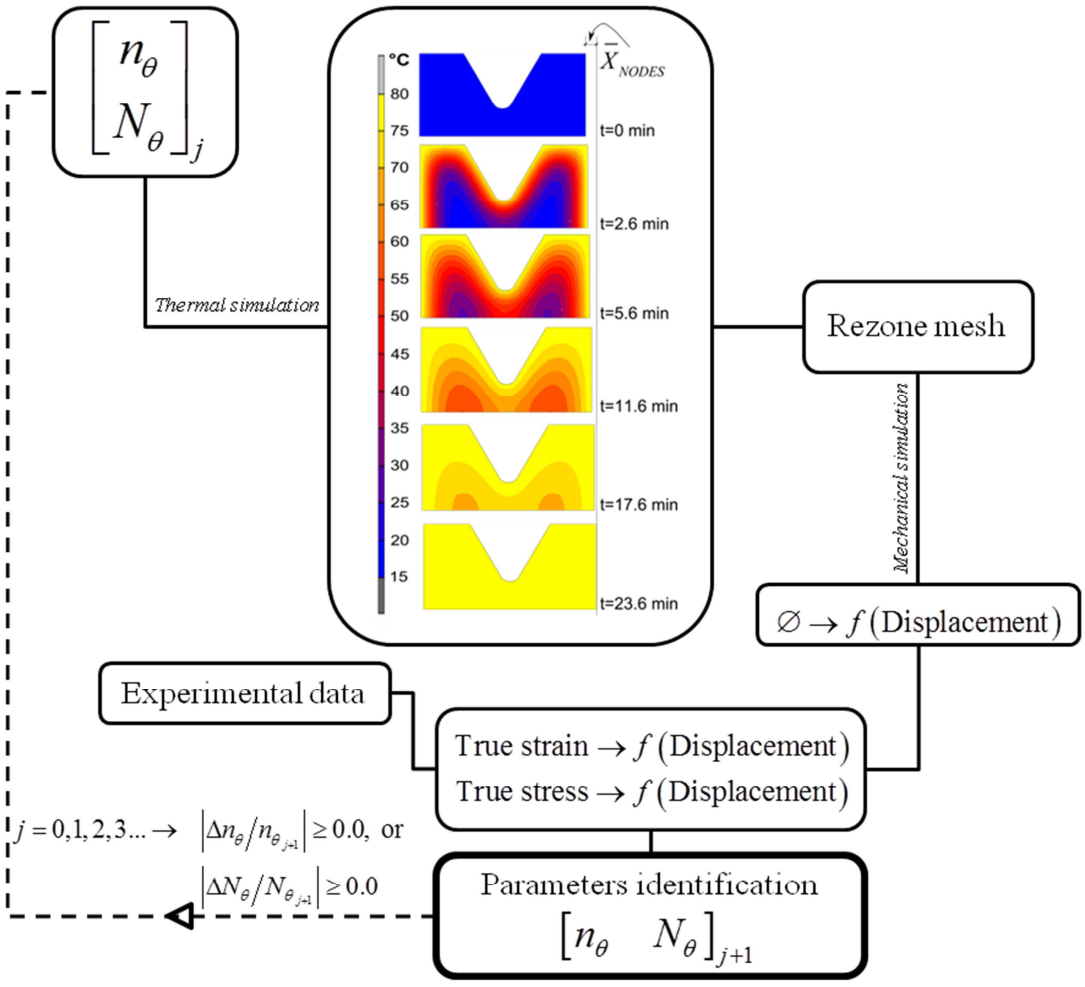

Fig. 2.10. Parameter identification algorithm.

To simulate the mechanical loading, one end of the remeshed geometry was fixed, $u_{x1}=0$, the other end being subjected to a displacement, $u_{x2}=9\ \text{mm}$, as shown in **Fig. 2.6b**. Considering the strong non-linearity of the model response, the displacement variable should be applied step by step as a linear function of time, i.e. $u_{x2}\rightarrow u(t)$. A fixed displacement normal to the axis $u_y=0$ was assigned to the symmetry axis. Note that the number of time steps have been selected in a way that the relative difference between the simulations results of two different time steps is less than 0.01. From the mechanical simulation, a function that describes the minimum diameter evolution as regards the axial displacement, $\varnothing\rightarrow f(\text{Displacement})$, can be deducted. This procedure has been validated by comparing the minimum diameter evolution of a sample at room temperature with the prediction of a simulation model with the same boundary conditions. Using the diameter evolution function in parallel with the experimental data, the experimental true strain and true stress in the median cross-section of the sample is calculated. Through the adjustment of the best response by means of trial and error for the experimental stress-strain curve, a new set of mechanical parameters can be identified. A recursive condition on the result accuracy is defined at the end of the algorithm. Note that the algorithm must be handled in this way for only two environmental temperatures[14], but for the second one Eq. (2.21) must be satisfied. From this set of mechanical parameters for two temperatures, the linear model accounting for the temperature-dependence of the chain density can be defined according to Eq. (2.20). The algorithm is then used to identify the local experimental stress-strain curves for the other temperatures. As a matter of fact, no more than three steps are required to attain the recursive condition. Besides, it should be pointed out that the values of the mechanical parameters have few effects on the function that describes the minimum diameter evolution.

[14] In this work, the model parameters were identified using the results obtained at 293 and 353 K.

4.2.1 Material parameters

The described algorithm allows estimating the thermo-mechanical variables values for the SBR material, which are reported in **Table 2.3**. The material conductivity factor κ and the convection coefficient h have been taken from the literature (Bérardi et al., 1996; Holzapfel and Simo, 1996). Although it would be desirable to get samples with different filler volumes, such samples were not available. The volume fraction[15] v_f of carbon-black for the studied SBR material is approximately 0.19.

Mechanical model parameters		**Thermal properties**	
n_{293} [m^{-3}]	1.548×10^{14}	κ [W m^{-1} K^{-1}]	0.127
N_{293}	39.6	h [J m^{-1} K^{-1}]	17.0
$n_{,\theta}$ [m^{-3} K^{-1}]	-1.607×10^{12}	α [K^{-1}]	3.6×10^{-4}
c	4.0		

Table 2.3. Mechanical model parameters and thermal properties.

4.2.2 Experimental vs. numerical load-displacement responses

A quantitative comparison between the experimental and simulated load-displacement curves for four environmental temperatures is presented in **Fig. 2.11**. It can be observed that the FE model is able to predict in a satisfactory extent the thermo-mechanical behavior of the sample. The difference between experimental and simulated curves, under large displacement, for $\theta = 333$ K can be explained by the non-linear temperature response of the SBR material whereas the proposed model considers a linear evolution of the mechanical properties. Nonetheless, the obtained results confirm the FE model capabilities.

---

[15] The filler volume fraction is calculated from: $v_f = phr\left[\rho_f \left(100/\rho_{matrix} + phr/\rho_f\right)\right]^{-1}$ where $\rho_f = 1.8\times10^3$ kg m^{-3} (Abe et al., 2003) is the carbon-black density, $\rho_{matrix} = 1.21\times10^3$ kg m^{-3} (Wood et al., 1943) is the matrix density and $phr = 34$.

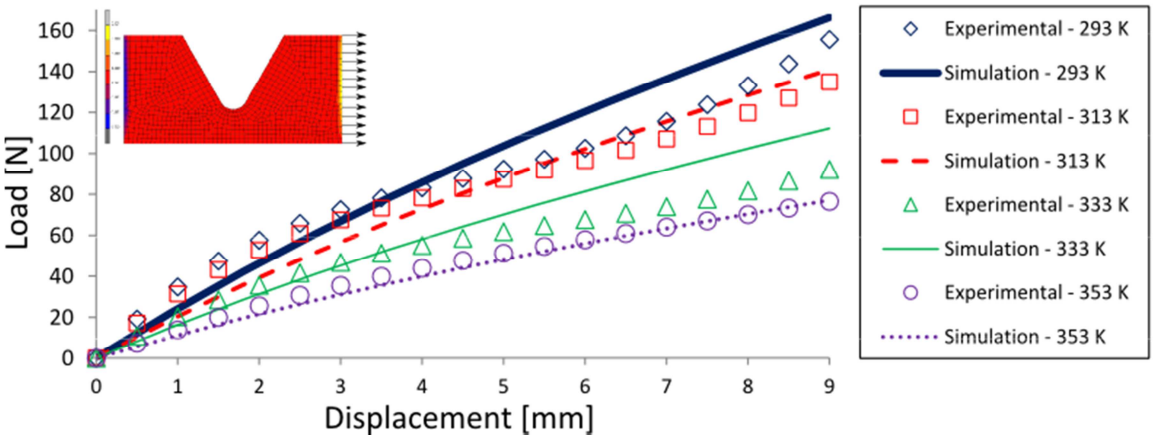

Fig. 2.11. Experimental and simulation results.

4.3 Local thermo-mechanical response

Results of the relaxed stress-strain behavior of the SBR material for different environmental temperatures ranging from 293 to 353 K are plotted in **Fig. 2.12a**. Contrary to the observed trend on pure-rubber materials (Meyer and Ferri, 1935), these curves point out that for a given strain value the stress decreases when increasing the temperature. The decrease in stiffness with temperature is attributed to reduction in the effective number of chains per unit volume (Fischer and Henderson, 1967). Indeed, this phenomenon is associated with the mobility enhancement of the chains at higher temperatures. **Fig. 2.12b** draws attention to the non-linear decrease of the stiffness which seems to stabilize at high temperatures. On the other hand, the shape of the stress-strain curve is temperature-dependent, e.g. when increasing temperature, the inflexion point gradually moves towards increasing strain. Similar results have been reported by Drozdov and Christiansen (2009) for carbon-black reinforced thermoplastic elastomers, and by Li et al. (2011) for four different kinds of filled rubbers. In contrast to pure-rubber materials, in which the thermo-mechanical response is explained uniquely by the contribution of the entropy-related energy (Treloar, 2005), the thermo-mechanical response of filled rubbers can be explained, in addition, by the contribution of an enthalpy-related energy (Clément et al., 2001). The amount of the enthalpy contribution can be linked with the filler-elastomer and filler-filler interactions, as well as with the filler fraction.

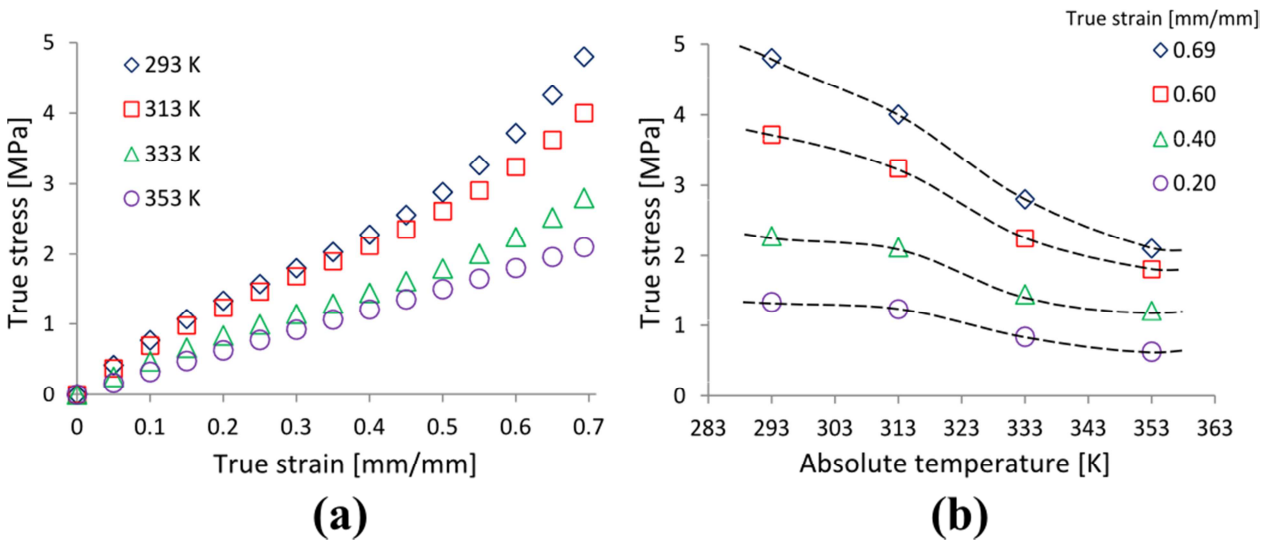

Fig. 2.12. Experimental results: (a) Relaxed response at different absolute temperatures, (b) true stress at constant true strain as a function of temperature.

To summarize, the experimental observations on the constitutive response lead to the following remarks: (1) The relaxed response of the filled SBR material is dependent on the temperature; and (2) the temperature-dependent response decreases in a non-linear way.

4.4 Micromechanical modeling

In order to verify the model capability to include explicitly the filler volume fraction effect on the large strain stress-strain response of the SBR compound, a set of FE micromechanical models containing different arrangements of the microstructure with different volumes of carbon-black particles has been achieved.

4.4.1 Micromechanical model characteristics

The FE micromechanical representations were designed using second-order 8-node, plane strain and arbitrarily quadrilateral elements. In the simulations, the matrix is modeled using the mechanical properties identified for the virgin material (see **Table 2.3**) and the carbon-black particles are modeled as a linear elastic medium with $E_{CB} = 200$ MPa and Poisson's ratio $\nu_{CB} = 0.3$ (Bergström and Boyce, 1999). The simulations were performed for different filler volume fractions ranging from 0.14 up to 0.24.

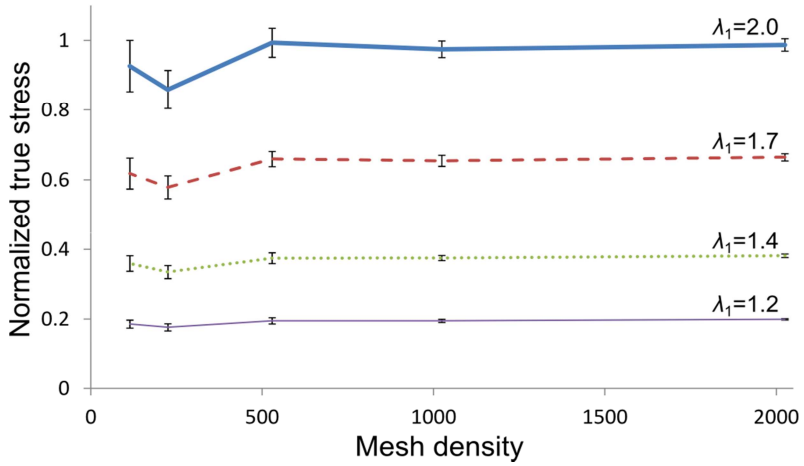

Fig. 2.13. Normalized true stress as a function of mesh density for different stretch levels, $v_f = 0.19$.

The representativity of the micromechanical model is an important issue, for the linear response as well as for the non-linear response (Khdir et al., 2013, 2014). The mesh density effect on the mechanical response of a given microstructure arrangement was investigated. An example with $v_f = 0.19$ and different stretch levels is shown in **Fig. 2.13**. It can be seen that the mesh size has not a significant effect on the mean mechanical response. However, a larger number of random distributions, for small mesh densities, will be needed to attain a desired accuracy level. On the other hand, a higher mesh density leads to a higher precision but implies a higher computational time. So, a balance between required accuracy and computational time is required. In order to attain an optimal equilibrium, one filler volume fraction was selected and up to 10 different random distributions with a mesh density of 1024 elements were designed. **Fig. 2.14** presents an example of a carbon-black distribution with $v_f = 0.19$. In the carbon-black distribution, no agglomerate was defined purposely.

4.4.2 Micromechanical model validation

The ability of the micromechanical simulation to describe the temperature-dependent stress-strain response of the SBR compound for $v_f = 0.19$ is shown in **Fig. 2.14**. The error bars represent the standard deviation in the predicted data. Except for

$\theta = 333$ K under large displacement, a good agreement between the predicted and experimental data is highlighted. We can then conclude that the micromechanical model offers a satisfactory way to take into account the filler volume effect and to predict the SBR compound response for filler volumes other than v_f = 0.19. Details about the results of the micromechanical simulations for v_f = 0.14 and v_f = 0.24 will be given further.

The interactions between filler and rubber or between filler particles are clearly important in filled rubbers, and can also have significant impact on the effective response. The local fields in the micromechanical model may evidence such interactions. **Fig. 2.15** presents for one microstructure arrangement the local first strain invariant in different paths (A-A', B-B', C-C' and D-D'). As expected, it can be observed that the presence of the particles acts to amplify the local first strain invariant in the rubber compound over that of a corresponding unfilled rubber at the same applied strain. Moreover, the local first strain invariant grows significantly in the regions where the SBR matrix is constrained by filler particles.

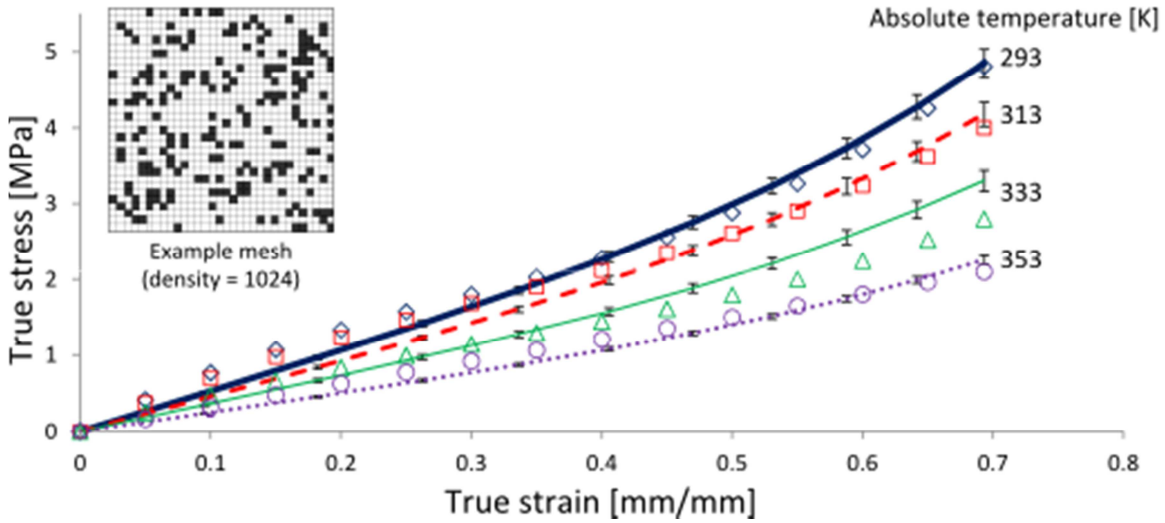

Fig. 2.14. Experimental (symbols) and micromechanical simulation (lines) stress-strain curves at different temperatures, v_f = 0.19.

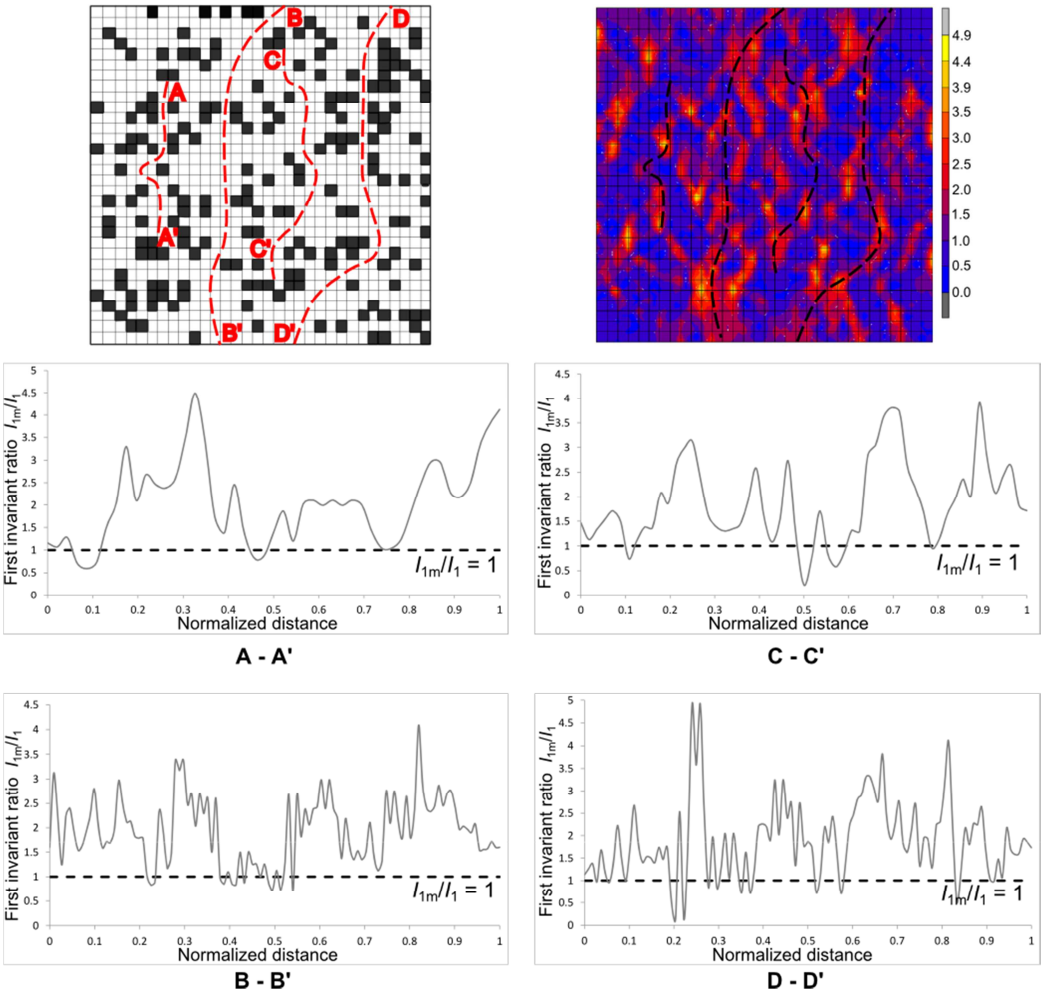

Fig. 2.15. Effect of filler fraction on the local first stretch invariant for $v_f = 0.19$.

4.5 Model verification

The proposed constitutive model presented in Section 3 can now be compared with the experimental and FE micromechanical simulations results of Section 4.3 and Section 4.4, respectively.

In **Fig. 2.16** the experimental results and model predictions of the temperature-dependent relaxed response of the SBR compound for $v_f = 0.19$ are presented. A good agreement between the experimental and predicted curves is evidenced in **Fig. 2.16a**. Likewise, in **Fig. 2.16b** the model capability to take into consideration the temperature-dependence of the SBR is highlighted. Indeed, it can be seen that, despite the strong non-linear dependence with regard to the temperature evidenced by the SBR compound, the proposed linearly-evolving model offers a satisfactory way to describe the thermo-mechanical evolution. The scope of the model can be

expanded by considering a non-linear evolution of the chain-scale parameters, as a temperature-hardening can be attained for temperatures higher than 353 K.

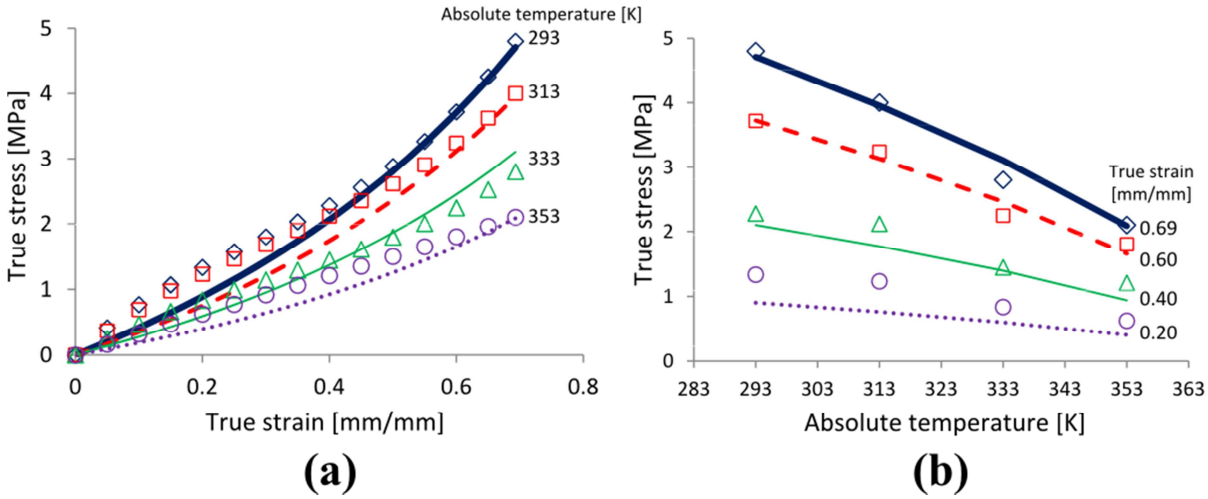

Fig. 2.16. Experimental (symbols) and model (lines) results: (a) Stress-strain curves at different temperatures, (b) Stress-temperature curves at different constant true strains, $v_f = 0.19$.

The capability of the constitutive model to take into account explicitly the filler volume effect for two volume fractions, $v_f = 0.14$ and $v_f = 0.24$, is shown in **Fig. 2.17a** and **Fig. 2.17b**, respectively. Although the obtained results confirm the good agreement between the predictions of the FE micromechanical model and the constitutive model, a small difference can be seen for $v_f = 0.24$. This difference could be related with the formation of aggregates in rubber compounds exhibiting high volume fraction of filler, as the existence of aggregates contributes increasing even more the value of the amplified strain (see **Fig. 2.15**).

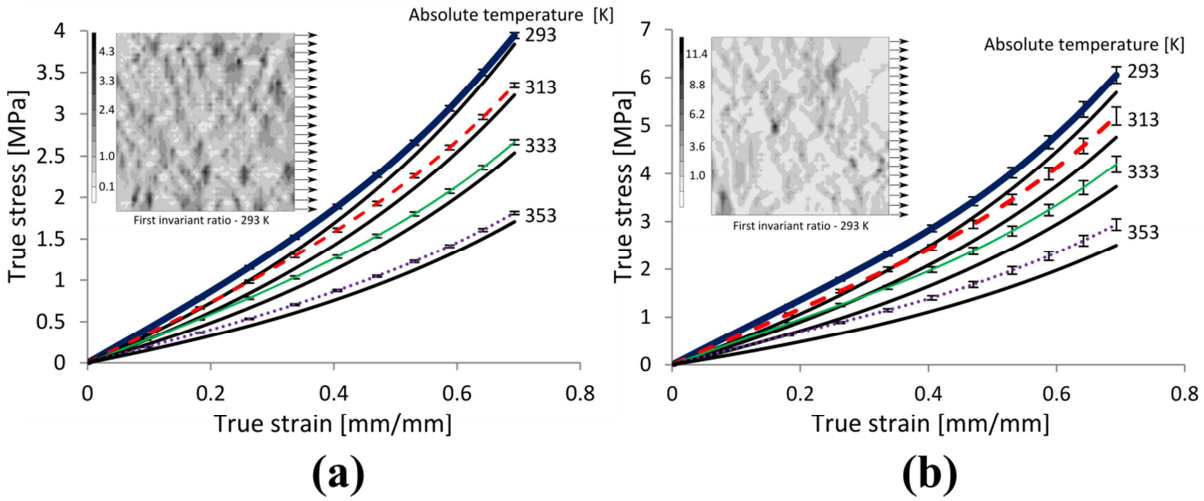

Fig. 2.17. Stress-strain curves at different temperatures of the micromechanical simulation (lines with error bars) and the proposed model (lines without error bars) for different filler volume fractions: (a) $v_f = 0.14$, (b) $v_f = 0.24$.

5. Partial conclusions

A combined approach including experimental investigation, constitutive modeling and micromechanical FE simulations has been followed in this contribution to study the temperature-dependent relaxed response of a carbon-black filled SBR. Based on experimental observations, a network kinetics has been introduced into a large strain mechanical model to account for the thermal effects. Micromechanical simulations have shown that the strain amplification introduced into the thermo-mechanical model is an adequate method to take into consideration the presence of fillers.

The thermo-mechanical model, implemented into a FE code by means of a strain energy function subroutine, has been validated by comparing the simulation and experimental load-displacement curves obtained on hourglass-shaped specimens. By this way, a hybrid experimental-numerical method has been proposed to determine simultaneously the thermo-mechanical response in the median cross-section of the hourglass-shaped specimen and the model parameters. The decreasing temperature-dependence of the relaxed response of the SBR material has been well reproduced by the proposed thermo-mechanical model.

The next chapter deals with the heat build-up of the SBR during fatigue via a thermo-mechanical model in accordance with the second thermodynamics principle. In order to avoid the evolution of the mechanical properties due to heat build-up of the SBR, flat samples with a fixed amount of carbon-black were used.

CHAPTER 3

A finite strain thermo-viscoelastic constitutive model to describe the heat build-up of rubbers during low-cycle fatigue[16]

In this chapter, a thermo-visco-hyperelastic constitutive model, in accordance with the second thermodynamics principle, is formulated to describe the heat build-up evolution in rubbers under cyclic loading. The mechanical part of the model is based upon a Zener rheological representation in which the specific free energy potential is dependent on an added internal variable, allowing the description of the time-dependent mechanical response. The large strain mechanical behavior is described using a Langevin spring, while the continuous stress-softening under cyclic loading is taken into account by means of a network alteration kinetics. The thermo-mechanical coupling is defined by postulating the existence of a dissipation pseudo-potential, function of the viscous dilatation tensor. The proposed model is fully three-dimensional and is implemented into a finite element code. The model parameters are identified using experimental data obtained on a SBR material under a given strain rate for different strain conditions. Predicted evolutions given by the model for other strain rates are found in good agreement with the experimental data.

[16] This chapter is based on the following paper: Ovalle Rodas, C., Zaïri, F., Naït-Abdelaziz, M., 2014. A finite strain thermo-viscoelastic constitutive model to describe the self-heating in elastomeric materials during low-cycle fatigue. *Journal of the Mechanics and Physics of Solids* 64, 396-410.

1. Introduction

Rubbers are often submitted to cyclic loading conditions in the automotive and aeronautical industries. During cyclic loading and depending on the boundary conditions, the temperature evolves as a consequence of the viscous properties of the material. The heat build-up is a phenomenon that depends on the strain rate (Lion, 1997a), on the maximum strain (La Rosa and Risitano, 2000) and, obviously, on the geometry of the test sample (Ayoub et al., 2012).

Since the material behavior depends on the temperature of the sample, the development of a thermo-mechanical constitutive model able to describe the temperature evolution under fatigue loadings is necessary. The model must take into consideration not only the properties associated with the mechanical behavior of the material, namely:

- Non-linear elastic behavior when it is submitted to large strains,
- strain rate dependence,
- relaxation to an equilibrium state for a given strain, and
- stress-softening,

but also the aforementioned parameters (strain rate, maximum strain,...).

Recently, different approaches describing the thermo-mechanical behavior of different kinds of materials submitted to a cyclic loading have been proposed. The thermo-mechanical coupling description is generally based upon three approaches. The first approach is purely phenomenological. Following this framework, the stored energy quantity of cold work (Kamlah and Haupt, 1998), the fatigue limit of materials related to a sudden self-heating (La Rosa and Risitano, 2000; Fargione et al., 2002; Le Saux et al., 2010), and the temperature evolution as a function of the number of cycles (Doudard and Calloch, 2009) have been described. The second approach is based upon the numerical solution of the problem by means of analytical or finite element (FE) methods. This approach has been used to describe the heat build-up and the mechanical parameters evolution with the temperature in polymers

submitted to compressive cyclic loading (Molinari, 1996; Rittel, 2000; Rittel and Rabin, 2000). Hakannson et al. (2005) have proposed a large strain thermo-plastic model, in which the kinematic and isotropic hardenings have been taken into account, leading to satisfactory results when compared to experimental data. Recently, neglecting the thermo-mechanical coupling, the description of the self-heating behavior in polymers under cyclic loading has been achieved using simulation algorithms, implemented into a FE code (de Cazenove et al., 2012; Pichon et al., 2012). The third approach is based on a variational formulation of the thermo-mechanical problem. This approach offers an alternative solution to describe the thermo-visco-plastic behavior of metallic materials (Yang et al., 2006; Stainier and Ortiz, 2010), and the predictions in terms of self-heating rate due to the dissipation were found accurate. Using a variational model similar to that developed by Stainer and Ortiz (2010), Canadija and Mosler (2011) solve the variational problem by means of a completely implicit time integration scheme. In the case of elastomeric materials, Boukamel et al. (2001) have proposed to solve the thermo-mechanical problem by means of a variational formulation applied to the rheological model of Poynting-Thomson. Its solution was numerically obtained after implementation into a FE code (Meo et al., 2002).

Thermo-mechanical constitutive models in accordance with the dissipation principle have been already proposed (Lion, 1997a, 1997b; Boukamel et al., 2001; Hakannson et al., 2005; Yang et al., 2006; Stainier and Ortiz, 2010); however, except (Lion, 1997b) and (Boukamel et al., 2001), these models generally deal with metallic materials, thus restricting their application fields. Even the thermo-mechanical model proposed by Lion was reported in several papers (Lion, 1996, 1997a, 1997b), its application to the heat build-up is restricted to a demonstration of the existence of a dissipative self-heating phenomenon due to inelastic deformations. Similarly, the model proposed by Boukamel et al. (2001) is limited to describe the heat build-up of

an elastomeric piece submitted to shear loading, without validating it for other loading paths.

In this chapter, a large strain thermo-viscoelastic constitutive model is developed to describe the heat build-up in elastomeric materials during low-cycle fatigue loading. A Zener type rheological model is used to describe the mechanical behavior of elastomeric materials, the strain response being decomposed into two components:

- An equilibrium component that reflects the long time material behavior,
- a viscous component that describes the non-linear time-dependent deviation from the equilibrium response.

The stress-softening phenomenon is taken into account by means of a network alteration kinetics as proposed by Ayoub et al. (2011a, 2014). In the thermodynamic scheme, the specific free energy potential is defined by introducing, in addition to the usual observable variables ($\boldsymbol{F}$, θ), the viscous dilatation tensor related to the time-dependent deviation from the equilibrium. The existence of a dissipation pseudo-potential, function of the viscous dilatation tensor, is postulated. The associate specific free energy is defined using a Langevin formulation. The proposed model is implemented into a FE code, and the same mechanical and boundary conditions regarding the experimental tests were simulated. Finally, when comparing the predicted results with the experimental data for different strain rate and strain conditions, a good agreement is observed.

The chapter is organized as follows: in Section 2, the formulation of the constitutive model including the thermo-mechanical coupling is presented. The experimental methods and results are presented in Section 3. In Section 4, the parameters identification procedure is highlighted. In Section 5, the implementation of the model algorithm is described in a general way. The validation of the model regarding the experimental data is presented in Section 6. Finally, the concluding remarks are given in Section 7.

2. Model formulation

The proposed model deals with the non-linear time-dependent behavior of rubber materials. Following a Zener rheological representation, the constitutive model considers the stress-strain response as resulting of two polymer networks acting in parallel. The schematic representation of the model is shown in **Fig. 3.1a** in which it is considered that the overall resistance to deformation is the sum of an equilibrium response *A* (non-linear elastic spring) and a time-dependent deviation with regard to the equilibrium state *B* (non-linear elastic spring in series with a viscous dashpot).

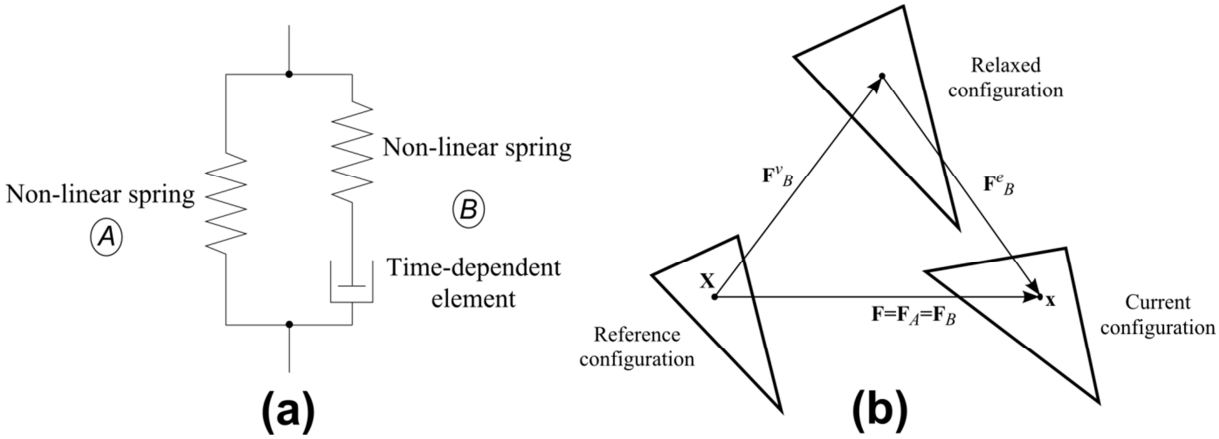

Fig. 3.1. Visco-elastic model: (a) Schematic representation, (b) multiplicative decomposition of the mechanical deformation.

2.1 Visco-elastic kinematics

The model is based upon continuum mechanics and developed using the finite strain kinematic framework. As already introduced in *Chapter 2*, a key quantity in this kinematic framework is the deformation gradient defined as: $\mathbf{F} \equiv \partial \mathbf{x} / \partial \mathbf{X}$, $\mathbf{x}$ being the position in the current configuration and $\mathbf{X}$ the position in the reference configuration of a given material point. Since a parallel scheme is used, the mathematical representation of the constitutive model is based upon the additive partition of the overall resistance into an equilibrium network (resistance *A*) and a

time-dependent network (resistance *B*), both $\mathbf{F}_A$ and $\mathbf{F}_B$ are equal to the total deformation gradient $\mathbf{F}$[17]:

$$\mathbf{F} = \mathbf{F}_A = \mathbf{F}_B \tag{3.1}$$

According to the approach proposed by Lee (1969), the deformation gradient of the network *B* can be written using a multiplicative form, and decomposed into an equilibrium part, $\mathbf{F}_B^e$, and a viscous part, $\mathbf{F}_B^v$:

$$\mathbf{F}_B = \mathbf{F}_B^e \mathbf{F}_B^v \tag{3.2}$$

where the viscous deformation gradient represents the obtained configuration during a spontaneous virtual elastic unloading of the network *B* to a free stress state as schematically illustrated in **Fig. 3.1b**. In this case, the viscous deformation of the viscous dashpot does not change during the unloading step and remains frozen.

The elastic deformation gradient, $\mathbf{F}_B^e$, and the viscous deformation gradient, $\mathbf{F}_B^v$, can be in turn decomposed into stretching and rotation components:

$$\mathbf{F}_B^e = \mathbf{V}_B^e \mathbf{R}_B^e \tag{3.3}$$

$$\mathbf{F}_B^v = \mathbf{V}_B^v \mathbf{R}_B^v \tag{3.4}$$

The corresponding kinematic rate for the resistance *B* can be written as:

$$\mathbf{L}_B = \dot{\mathbf{F}}_B \mathbf{F}_B^{-1} \tag{3.5}$$

Introducing the elastic and viscous parts of this quantity leads to:

$$\mathbf{L}_B = \dot{\mathbf{F}}_B^e \mathbf{F}_B^{e-1} + \mathbf{F}_B^e \dot{\mathbf{F}}_B^v \mathbf{F}_B^{v-1} \mathbf{F}_B^{e-1} = \mathbf{L}_B^e + \mathbf{L}_B^v \tag{3.6}$$

where

[17] In order to facilitate the lecture and understanding of the model formulation, some equations from the previous chapter have been repeated.

$$\mathbf{L}_B^v = \mathbf{D}_B^v + \mathbf{W}_B^v \tag{3.7}$$

$\mathbf{D}_B^v$ is the viscous stretching rate and $\mathbf{W}_B^v$ is the viscous spin rate. Details about the definition of these two quantities will be given further.

2.2 Constitutive equations

To formulate a consistent model with the thermo-mechanical properties of the material, the physical theory must respect the thermodynamics principles, since the mere assumption of temperature dependent parameters is not sufficient. This assures the non-negative property of the dissipation and allows the correct representation of the thermo-mechanical coupling.

As in *Chapter 2*, the Clausius-Duhem inequality, written in a mixed description, is invoked to make the developed formulation obey to the second principle of thermodynamics:

$$\gamma = -\rho\left(\dot{\psi} + \dot{\theta}\eta\right) + \boldsymbol{\pi} : \dot{\mathbf{F}} - \frac{1}{\theta}\mathbf{q}\cdot\nabla_X\theta \geq 0 \tag{3.8}$$

where

$$\psi = e - \theta\eta \tag{3.9}$$

γ is the dissipation, ρ is the mass density for a unit reference volume, ψ is the specific free energy, η is the specific entropy, $\boldsymbol{\pi}$ is the first Piola-Kirchhoff stress tensor, $\dot{\mathbf{F}}$ is the deformation gradient tensor rate, $\mathbf{q}$ is the Piola-Kirchhoff heat flow, $\nabla_X\theta$ is the temperature gradient, θ is the absolute temperature and e is the specific internal energy.

To derive the constitutive equations, the existence of the special form of the Helmholtz free energy potential for a unit reference volume is postulated:

$$\psi = \psi\left(\mathbf{F}, \theta, \mathbf{C}_v\right) \tag{3.10}$$

where

$$\mathbf{C}_v = \mathbf{F}_B^{vT}\mathbf{F}_B^v \tag{3.11}$$

is the viscous dilatation tensor introduced as an internal variable which is related to the time-dependent deviation from the equilibrium. Note that, since the free energy potential ψ is an isotropic function which depends on the viscous dilatation tensor $\mathbf{C}_v$, the free energy itself and all constitutive equations are independent on inelastic rotations (Haupt, 2002). Consequently, the viscous spin rate $\mathbf{W}_B^v$ drops out in Eq. (3.7).

From the Coleman relations, the first Piola-Kirchhoff stress tensor $\boldsymbol{\pi}$ in the rubber material is given by:

$$\boldsymbol{\pi} = \frac{\partial \psi}{\partial \mathbf{F}}\left(\mathbf{F}, \theta, \mathbf{C}_v\right) \tag{3.12}$$

Note that the Cauchy stress tensor $\mathbf{T} = J^{-1}\boldsymbol{\pi}\mathbf{F}^T$ can be calculated from Eq. (3.12).

The free energy is defined as:

$$\psi = \psi_A + \psi_B \tag{3.13}$$

Considering the parallel scheme adopted in the model, the total stress tensor $\mathbf{T}$ in the material is given by the sum of the equilibrium network stress $\mathbf{T}_A$ and the time-dependent network stress $\mathbf{T}_B$:

$$\mathbf{T} = \mathbf{T}_A + \mathbf{T}_B \tag{3.14}$$

2.2.1 Viscous dilatation tensor

If the Clausius-Duhem inequality (3.8) is defined by means of the specific free energy rate:

$$\dot{\psi} = \frac{\partial \psi}{\partial \mathbf{F}} : \dot{\mathbf{F}} + \frac{\partial \psi}{\partial \theta}\dot{\theta} + \frac{\partial \psi}{\partial \mathbf{C}_v} : \dot{\mathbf{C}}_v \tag{3.15}$$

then

$$\left(\boldsymbol{\pi} - \rho\frac{\partial \psi}{\partial \mathbf{F}}\right) : \dot{\mathbf{F}} - \rho\left(\eta + \frac{\partial \psi}{\partial \theta}\right)\dot{\theta} - \rho\frac{\partial \psi}{\partial \mathbf{C}_v} : \dot{\mathbf{C}}_v - \frac{1}{\theta}\mathbf{q}\cdot\nabla_X\theta \geq 0 \tag{3.16}$$

The thermodynamic force, associated with the internal variable A_v, is derived as follows:

$$A_v = \rho \frac{\partial \psi}{\partial \mathbf{C}_v} \tag{3.17}$$

Considering that the volumetric effect adds a supplementary difficult factor (Zaïri et al., 2011a), the deformation is assumed to occur without volume change. The incompressibility assumption is taken into account by means of:

$$\det(\mathbf{C}) = 1 \tag{3.18}$$

$$\dot{\mathbf{C}}_v : \mathbf{C}_v^{-1} = 0 \tag{3.19}$$

where $\mathbf{C} = \mathbf{F}^T\mathbf{F}$ is the right Cauchy-Green strain tensor.

On the other hand, to get the complementary laws associated with the dissipative processes, the existence of a dissipation pseudo-potential, φ, is postulated such that:

$$A_v = -\frac{\partial \varphi}{\partial \dot{\mathbf{C}}_v} \tag{3.20}$$

It is then assumed that the dissipation pseudo-potential depends solely on the internal variable. According to Sidoroff (1974), the dissipation pseudo-potential could adopt the following quadratic form:

$$\varphi\left(\dot{\mathbf{C}}_v\right) = \begin{cases} 1/2\,\mu\left(\dot{\mathbf{C}}_v : \dot{\mathbf{C}}_v\right) & \text{if} \quad \dot{\mathbf{C}}_v : \mathbf{C}_v^{-1} = 0 \\ \infty & \text{otherwise} \end{cases} \tag{3.21}$$

where μ is a viscosity parameter (Boukamel et al., 2001; Meo et al., 2002).

Equating Eqs. (3.17) and (3.20) leads to:

$$\rho \frac{\partial \psi}{\partial \mathbf{C}_v} = -\frac{\partial \varphi}{\partial \dot{\mathbf{C}}_v} \tag{3.22}$$

Due to the incompressibility assumption, a hydrostatic term multiple of $\mathbf{C}_v^{-1}$ must be introduced in the above expression (Boukamel et al., 2001):

$$\rho\frac{\partial\psi}{\partial\mathbf{C}_v}+a\mathbf{C}_v^{-1}=-\frac{\partial\varphi}{\partial\dot{\mathbf{C}}_v} \tag{3.23}$$

where a is a Lagrange multiplier which controls the incompressibility restriction.

Substituting (3.10) and (3.21) in (3.23), it is possible to obtain, after a series of lengthy but straightforward derivations, the following complementary expression for thermodynamically reversible and isothermal processes:

$$-\rho\mathbf{C}_v^{-1}\mathbf{C}\mathbf{C}_v^{-1}\left[\left(\frac{\partial\psi}{\partial I_1}+\frac{\partial\psi}{\partial I_2}I_1\right)\mathbf{I}-\frac{\partial\psi}{\partial I_2}\mathbf{C}\mathbf{C}_v^{-1}\right]+\mu\dot{\mathbf{C}}_v+a\mathbf{C}_v^{-1}=0 \tag{3.24}$$

where $I_1=\mathrm{tr}\mathbf{B}$ and $I_2=\mathrm{tr}\mathbf{B}^2$ are the first and second stretch invariants, respectively, $\mathbf{B}=\mathbf{F}\mathbf{F}^T$ being the left Cauchy-Green strain tensor.

In order to get rid of the $a\mathbf{C}_v^{-1}$ term, Eq. (3.24) can be simplified if multiplying it by $\mathbf{C}_v$ and considering only its deviatoric part. That leads to the following expression:

$$-\rho\left[\mathbf{C}\mathbf{C}_v^{-1}\left[\left(\frac{\partial\psi}{\partial I_1}+I_1\frac{\partial\psi}{\partial I_2}\right)\mathbf{I}-\frac{\partial\psi}{\partial I_2}\mathbf{C}\mathbf{C}_v^{-1}\right]\right]'+\left[\mu\mathbf{C}_v\dot{\mathbf{C}}_v\right]'=0 \tag{3.25}$$

which can be written in the following general form:

$$\dot{\mathbf{C}}_v=\dot{\mathbf{C}}_v\left(\mathbf{F},\theta,\mathbf{C}_v\right) \tag{3.26}$$

2.2.2 Thermo-mechanical dissipation potential

Inserting the specific internal energy rate, $\dot{e}$, expressed, after a series of straightforward derivations using Eqs. (3.9) and (3.15), as[18]:

$$\dot{e}=\frac{1}{\rho}\boldsymbol{\pi}:\dot{\mathbf{F}}+\frac{1}{\rho}\mathbf{A}_v:\dot{\mathbf{C}}_v-\theta\frac{1}{\rho}\left(\frac{\partial\boldsymbol{\pi}}{\partial\theta}:\dot{\mathbf{F}}+\frac{\partial\mathbf{A}_v}{\partial\theta}:\dot{\mathbf{C}}_v\right)-\theta\frac{\partial^2\psi}{\partial\theta^2}\dot{\theta} \tag{3.27}$$

into the standard formulation of the first thermodynamics law[19], i.e $\rho\dot{e}=\boldsymbol{\pi}:\dot{\mathbf{F}}-\mathrm{div}\left[\mathbf{q}\right]$, leads to the following relation

[18] Details about are given in Annex A.

$$\rho C\dot{\theta} = -\mathbf{A}_v : \dot{\mathbf{C}}_v + \theta\left[\frac{\partial \boldsymbol{\pi}}{\partial \theta} : \dot{\mathbf{F}} + \frac{\partial \mathbf{A}_v}{\partial \theta} : \dot{\mathbf{C}}_v\right] - \mathrm{div}[\mathbf{q}] \tag{3.28}$$

where C is the specific heat per unit mass:

$$C(\mathbf{F}, \theta, \mathbf{C}_v) = -\theta \frac{\partial^2 \psi}{\partial \theta^2} \tag{3.29}$$

In Eq. (3.28), the term

$$\Phi_m = -\mathbf{A}_v : \dot{\mathbf{C}}_v + \rho\theta\left[\frac{\partial \boldsymbol{\pi}}{\partial \theta} : \dot{\mathbf{F}} + \frac{\partial \mathbf{A}_v}{\partial \theta} : \dot{\mathbf{C}}_v\right] \tag{3.30}$$

is the mechanical dissipation and

$$\Phi_T = -\mathrm{div}[\mathbf{q}] \tag{3.31}$$

is the divergence of the heat flux vector. The first term of the mechanical dissipation is the dissipation capacity due to the viscous behavior of the material, while the second term corresponds to the dissipation due to the mechanical properties dependence on the temperature.

Since the temperature evolution during a numerical step is imperceptible (as shown below, see **Fig. 3.10**), it is reasonable, in a first approximation, to neglect the mechanical properties dependence on the temperature; therefore, under such an assumption, the mechanical dissipation reduces to

$$\Phi_m \approx -\mathbf{A}_v : \dot{\mathbf{C}}_v = \frac{\partial \varphi}{\partial \dot{\mathbf{C}}_v} : \dot{\mathbf{C}}_v \tag{3.32}$$

Furthermore, in Eq. (3.31), $\mathbf{q}$ is the Piola-Kirchhoff heat flux given by the Fourier law:

$$\mathbf{q} = -\mathbf{K}_X \cdot \nabla_X \theta \tag{3.33}$$

[19] The term related with the heat supply per unit mass has been omitted since it is neglected in the present study.

where

$$\mathbf{K}_X = \mathbf{F}^{-1}\mathbf{K}\mathbf{F}^{-T} \tag{3.34}$$

is the conductivity tensor in the reference configuration, and $\mathbf{K}$ is the Euler conductivity tensor in the actual configuration. In the isotropic case, this one reduces to $\mathbf{K} = \kappa\mathbf{I}$, where κ is the material conductivity factor.

2.3 Model particularization

The large strain mechanical behavior of the material is described using the Arruda-Boyce (Arruda and Boyce, 1993, Bischoff et al., 2001) eight-chain strain energy density function which is expressed for the two networks as follows:

$$\psi_{A,B} = C_{rA,B}\sqrt{N_{A,B}}\left(\beta\sqrt{\frac{I_1}{3}} + \sqrt{N_{A,B}}\ln\frac{\beta}{\sinh\beta} - \frac{\beta_0}{3}\ln J\right) + \frac{K}{2}(J-1)^2 \tag{3.35}$$

with

$$\beta = \mathcal{L}^{-1}\left(\sqrt{\frac{I_1}{3N_{A,B}}}\right) \quad \text{and} \quad \beta_0 = \mathcal{L}^{-1}\left(\sqrt{\frac{1}{N_{A,B}}}\right) \tag{3.36}$$

In Eq. (3.35), $C_{rA,B} = n_{A,B}k\theta$ is the rubbery modulus (where $n_{A,B}$ is the average number of chains per unit volume, k is the Boltzmann constant and θ is the absolute temperature), $N_{A,B}$ is the number of connected rigid-links in a chain, I_1 is the first stretch invariant defined by $I_1 = \mathrm{tr}\mathbf{B}$ and $I_1 = \mathrm{tr}\mathbf{B}^e$ for the networks A and B, respectively, $J = \det\mathbf{F}_{A,B}$ is the volume change, K is the temperature-dependent bulk modulus which, for rubbers, is significantly higher than the shear modulus, e.g. $K \approx 500 n_{A,B}k\theta$, and $\mathcal{L}^{-1}$ is the inverse of the Langevin function given by: $\mathcal{L}^{-1}(u) = \coth(u) - 1/u$ which can be estimated through the Padé approximation (Cohen, 1991):

$$\mathcal{L}^{-1}(u) = u\frac{3-u^2}{1-u^2} \tag{3.37}$$

Note that $C_{rA} = n_A k\theta$ corresponds to the slope of the stress-strain curve during the strain-hardening, $C_{rB} = n_B k\theta$ corresponds to the slope of the stress-strain curve during the unloading stage once the equilibrium response has been subtracted from the overall response (Bergström and Boyce, 1998), the term $\sqrt{N_A}$ corresponds to the chain extensibility limit and $J = 1$ as it is assumed that the deformation occurs without volume change.

On the other hand, to account for the network rearrangement during the cyclic stress-softening, the following kinetics may be adopted[20]:

$$n_{A,B} = n_{A,B}(D) \tag{3.38}$$

$$N_{A,B} = N_{A,B}(D) \tag{3.39}$$

where

$$D = \frac{N_c}{N_f} \tag{3.40}$$

is a damage parameter regarded as a life fraction, $0 \leq D \leq 1$, N_c is the current cycle number and N_f is the number of cycles at failure.

As a consequence of the mass conservation law, it is possible to assume that

$$n_{A,B} N_{A,B} = n_0 N_0 = \text{constant} \tag{3.41}$$

where n_0 and N_0 are, respectively, the chain density and the number of connected rigid-links in a chain for the virgin material.

The fatigue mechanism is described by means of the following exponential form (Ayoub et al., 2011a):

[20] Since the definition of the stress-softening remains unchanged from that initially proposed by (Ayoub et al., 2011a) only a summary of the main equations are presented. The details can be found in the aforementioned paper.

$$N_{A,B} = \begin{cases} N_0 + \alpha\left(1-\exp\left(-\beta D\right)\right) & 0 \le D \le D_c \\ N_0 + \alpha\left(1-\exp\left(-\beta D_c\right)\right) + \gamma\left(\exp\left(\delta D\right) - \exp\left(\delta D_c\right)\right) & D_c \le D \le 1 \end{cases} \tag{3.42}$$

where α, β, γ and δ are material constants and D_c corresponds to the D value where a fast decrease before complete failure of the specimen is observed. **Fig. 3.2** illustrates an example of the network evolution kinetics during fatigue loading[21] as a function of the normalized cycle number taken as the variable D. This evolution may be correlated to the macroscopic stress-softening generally observed during fatigue loading. This macroscopic softening is a consequence of both a decrease of the average number of chains per unit volume $n_{A,B}$ conjugated to an increase of the number of connected rigid-links in a chain $N_{A,B}$.

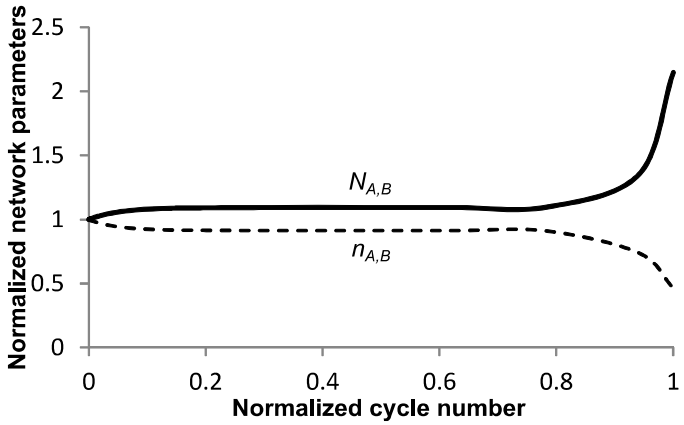

Fig. 3.2. Evolution of the two physical material parameters affected by the network alteration during fatigue loading.

When now considering the time-dependent network, the elastic deformation gradient is determined from Eqs. (3.2), (3.6) and (3.7) knowing that the viscous stretching rate must be specified. It is defined as:

$$\mathbf{D}_B^v = \dot{\gamma}_B \mathbf{N}_B \tag{3.43}$$

where $\mathbf{N}_B$ is the normalized deviatoric part of the stress acting on network B:

[21] The material constants of Eq. (3.42), used to plot **Fig. 3.2**, were taken from (Ayoub et al., 2011a). They were identified on experimental data obtained from a SBR in the form of hourglass-shaped samples.

$$\mathbf{N}_B = \frac{1}{\sqrt{2}\tau_B}\mathbf{T}_B' \tag{3.44}$$

$$\tau_B = \left[\frac{1}{2}\mathrm{trace}\left(\mathbf{T}_B'\mathbf{T}_B'\right)\right]^{1/2} \tag{3.45}$$

According to (Boyce et al., 2000) the flow rate, $\dot{\gamma}_B$, could be written in the following form:

$$\dot{\gamma}_B = c\left(\frac{1}{\lambda_B^v - 1}\right)\tau_B \tag{3.46}$$

where

$$\lambda_B^v = \left(\frac{1}{3}\mathrm{trace}\left(\mathbf{B}_B^v\right)\right)^{1/2} \tag{3.47}$$

$\mathbf{B}_B^v = \mathbf{F}_B^v\mathbf{F}_B^{vT}$ and c is a positive material constant to be identified.

3. Experimental procedure and observations

3.1 Studied material

The studied material is the same SBR as the one studied in the last chapter. It contains 34 phr of carbon-black. Different mechanical tests were performed to quantify the heat build-up due to the thermo-mechanical coupling.

3.2 Sample geometry and experimental method

Flat samples which geometry is shown in **Fig. 3.3** were cut from 2 mm thickness plates. The reduced section in the center of the sample allows locating the highest increase of temperature in this region. Moreover, its weak thickness allows avoiding a high temperature gradient in the transverse direction.

The mechanical tests were carried out on an electro-pulse mechanical set up (Instron 5500). The temperature was measured using an infrared camera (Flir SC300) interfaced with a computer which allows the storage of the thermal images during

the test. The stored images can be post processed to determine the temperature increase in the analyzed region. The tests were carried out at room temperature.

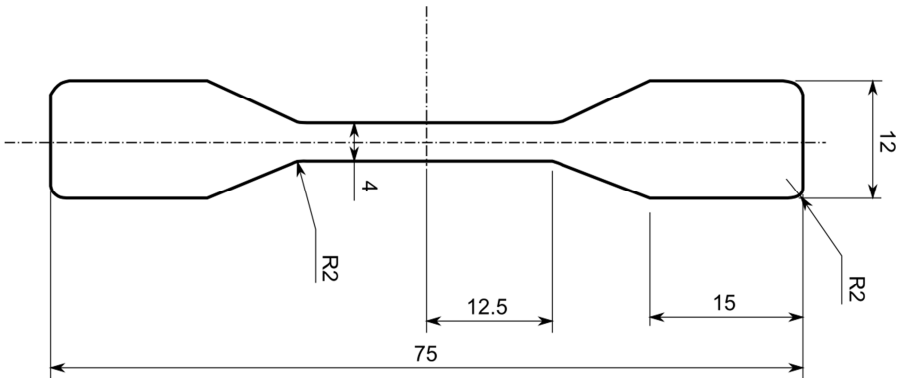

Fig. 3.3. Schematic representation of the sample.

In the parameter identification process and the analysis of the thermo-mechanical coupling, three types of tests were performed:

- Multi-relaxation tests in order to determine the parameters of the material equilibrium response: during this test, the sample is initially deformed up to a prescribed strain under a given strain rate; then the local strain is maintained constant for at least one hour; during this holding time, the stress evolution is stored. Note that the Mullins effect (Mullins and Tobin, 1965) was previously cancelled by submitting the sample to two loading-unloading cycles up to the maximum stretch under the same strain rate.
- Single cycle tests were performed in order to determine the parameters of the time-dependent mechanical behavior. It consists in loading the sample up to a strain value (taken equal to the maximum strain prescribed in the multi-relaxation tests) under a constant strain rate and, then, unloading it down to its initial position. The loading-unloading cycle has been repeated three times and, as in the multi-relaxation test, only the results obtained for the third cycle were taken into consideration (because of the Mullins effect).
- Fatigue tests were also done in order to determine the viscosity parameter, μ, and to describe the sample self-heating evolution under different strains.

Previous to the tests, 15 loading-unloading cycles up to a stretch $\lambda_{11} = 2.0$ were carried out in order to eliminate the surface flake that appears in the sample, which can alter the infrared camera data measurements because of the variation of the surface emissivity. The sample was shut in, then, using an open box allowing the infrared camera measurements, but reducing the surrounding radiation. The camera was located at a distance lower than 0.5 m in order to reduce the reflected radiation influenced by the surrounding humidity. In order to determine the surrounding temperature 50 images were taken and stored previous to the tests. During the test, the required number of images to reach the stabilization temperature of the sample was stored. The images correspond to the same condition of strain level of the sample.

3.3 Experimental results

The stress-strain mechanical response of the studied material is illustrated in **Fig. 3.4**. Results of the uniaxial tension tests are plotted for different strain rates ranging from 0.01 /s to 1.0 /s in **Fig. 3.4a**. The non-linear response of the material is clearly pointed out. As usually observed for rubbers, the SBR material exhibits a non-linear behavior which is accompanied by a drastic strain hardening for large strains (see **Fig. 3.4b**). Moreover, this non-linear response is strain-rate dependent. Indeed, for a given strain value the stress increases when increasing the strain rate. In **Fig. 3.4b**, when considering the relaxation stages, a stress decrease versus time is observed during the loading phase while an increase is pointed out during unloading. The stress relaxation during loading as well as during unloading evolves towards an equilibrium value whose envelop gives the equilibrium response. Note that this equilibrium stress tends to increase significantly as it approaches a given deformation (E_∞). Similar results have been observed by Lion (1996) and Bergström and Boyce (1998). The information also provides a quantitative estimate of the hysteresis that occurs during the unloading stage and, by the way, of the energy consumed during a cycle.

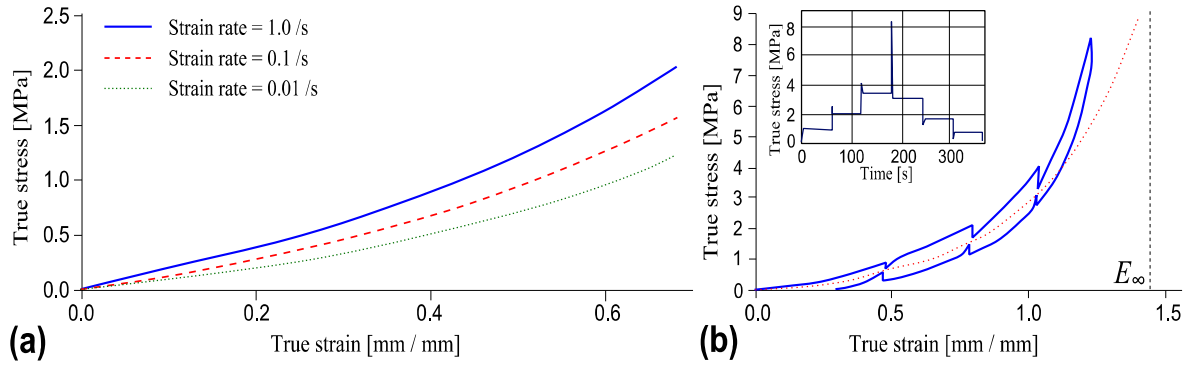

Fig. 3.4. Time-dependence of the SBR material: (a) Uniaxial tension response at different strain rates, (b) multi-relaxation response for a strain rate of 1.0 /s.

The continuous stress-softening during fatigue tests for two maximum applied strains is illustrated in **Fig. 3.5**. The results show that the stress-softening is very weak.

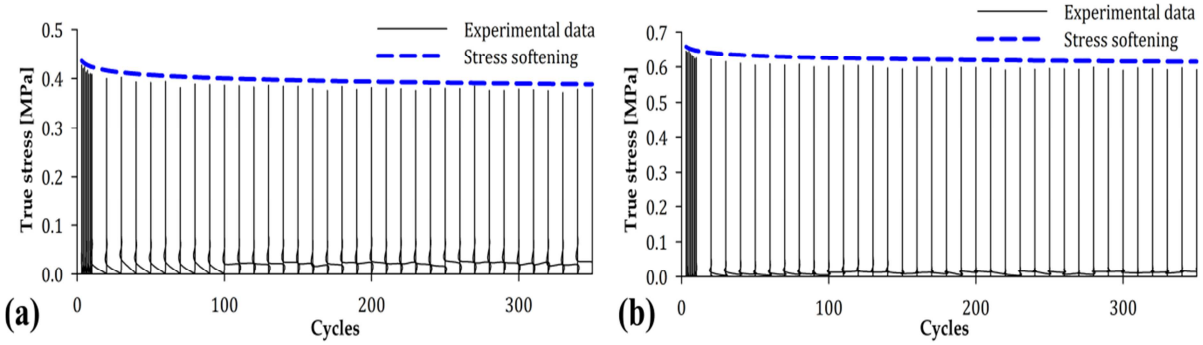

Fig. 3.5. Stress-softening for a strain rate of 1.0 /s: (a) $\lambda_{11} = 1.2$, (b) $\lambda_{11} = 1.4$.

The heat build-up in the central zone of the specimen is highlighted in **Fig. 3.6** which shows the temperature evolution of a material point in this zone for the two above mentioned test conditions. This evolution is quite linear in the beginning but followed by a non-linear stage which tends to a stabilized value, depending on the strain rate and on the maximum applied strain. The increase of the temperature due to self-heating with the strain rate is also pointed out. Similar results have been observed by Lion (1997a). The temperature increase with the strain rate is related with the rise of the hysteresis loop, the dissipation being strain rate dependent (Tomita et al., 2008; Luo et al., 2010). This phenomenon is explained by the disability of the vacant sites (free volume of the elastomer) to migrate to other points inside the

material to the same speed that the chain segments displaced by the deformation (Medalia, 1991). As a consequence the mechanical movement is transformed into a random thermal movement.

The increase of the heat build-up with the strain level can be also clearly observed in this figure. We can argue that, similarly to the previous observations on the strain rate dependence, the temperature increase with the maximum strain can be due to the hysteresis loop which increases with the applied strain (Luo et al., 2010); nevertheless, for λ_{11} = 1.4 a mesoscopic phenomenon turns relevant: the breakdown and reformation of the network aggregates (carbon-black). During each cycle, the aggregates bonds are broken during the loading path initiating with the weakest bonds and progressing towards the stronger ones. As the specimen is distorted, the aggregates form new bonds in other locations and the cycle is repeated in a successive way. For λ_{11} > 1.2 the break and reformation of interaggregates bonds is the major responsible of the heat generation (Medalia, 1991).

The stabilized temperature is related with the stabilization of the hysteresis loop with the number of cycles (Bartolomé et al., 2013), i.e. the mean temperature of a material point becomes constant when the dissipated inelastic energy per loading cycle is equal to the amount of energy which is consumed by heat transfer to its environment.

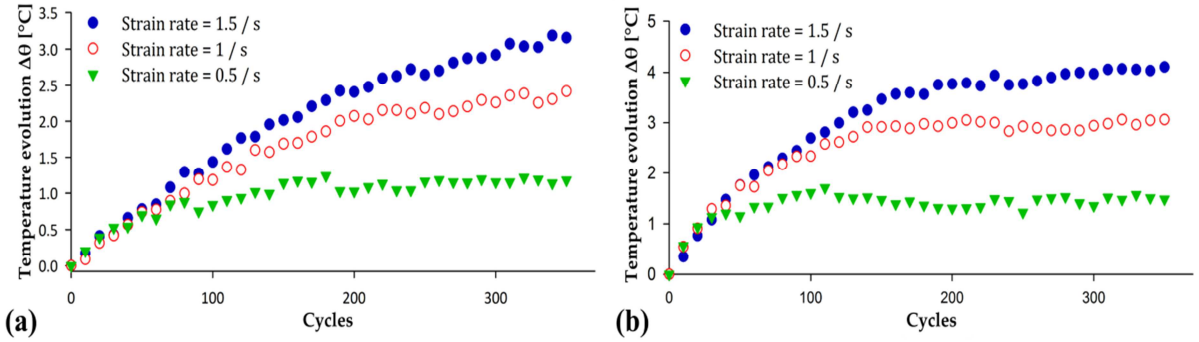

Fig. 3.6. Heat build-up at different strain rates: (a) λ_{11} = 1.2, (b) λ_{11} = 1.4.

To summarize, the experimental results have shown that: (1) The SBR material response is dependent on the strain rate; (2) under relaxation periods both in loading

and in unloading conditions the stress tends to the same equilibrium stress, function of the strain level; (3) the stress-softening is, in a first approximation, negligible; (4) the heat build-up, for the same strain level, is dependent on the strain rate; and finally, (5) the heat build-up, for the same strain rate, is dependent on the strain level.

4. Parameters identification

The required material properties for the constitutive model are: the network parameters[22] for the branch A [C_{rA},N_A] and the branch B [C_{rB},N_B], the time-dependent element parameter [c] and the viscosity parameter [μ]**.** The procedure that follows remains unchanged from those initially proposed by Bergström (1999) and Boyce et al. (2000).

4.1 Equilibrium response

The constants C_{rA} and N_A can be determined from the multi-relaxation tests. If λ_∞=exp(E_∞), see **Fig. 3.4b**, is the stretching for which the true stress increases in an exponential way, the value of N_A can be determined by considering that the denominator of the Padé approximation given by Eq. (3.37) is equal to zero:

$$N_A = \frac{1}{3}\left(\lambda_\infty^2 + \frac{2}{\lambda_\infty}\right) \tag{3.48}$$

Likewise, if (λ_i,T_{Ai}) is a point belonging to the equilibrium curve under small strain, the value of C_{rA} can be approximated by means of:

$$C_{rA} = \frac{T_{Ai}}{\lambda_i^2 - 1/\lambda_i}\sqrt{\frac{\lambda_i^2 + 2/\lambda_i}{3N_A}}\left(\mathcal{L}^{-1}\left[\sqrt{\frac{\lambda_i^2 + 2/\lambda_i}{3N_A}}\right]\right)^{-1} \tag{3.49}$$

[22] Since the maximum true stress does not vary significantly as a function of the number of cycles (see **Fig. 3.5**), the stress-softening characteristics for the present application have not been considered.

4.2 Time-dependent response

For simplicity, the constant N_B can be considered of equal magnitude than N_A. The constant C_{rB} can be determined from the instantaneous unloading slope of a single cycle uniaxial test, once the equilibrium response has been already subtracted:

$$C_{rB} = \frac{E_u}{3}\left(2\lambda_u^2 + \frac{1}{\lambda_u}\right)^{-1} - C_{rA} \tag{3.50}$$

where E_u is the tangent modulus of the instantaneous unloading and λ_u is the magnitude of the stretching in this condition.

The time-dependent property of the element B, c, is obtained through the adjustment of the best response by means of trial and error for a strain rate of 1 /s.

4.3 Viscosity parameter

The viscosity parameter, μ, for a given maximum strain, is obtained in the same way than c.

4.4 Material parameters

The described procedure allows estimating the mechanical variables values for the SBR material which are reported in **Table 3.1**. Elsewhere, the thermal parameters values have been taken from the literature (Bérardi et al., 1996).

	Mechanical model parameters			**Thermal properties**
	Equilibrium response A	Time-dependent response B		
$C_{rA,B}$ [MPa]	0.35	0.65	κ[W m^{-1} K^{-1}]	0.127
$N_{A,B}$	4.6	4.6	ρC [J m^{-3} K^{-1}]	0.7×10^6
c [(Pa s)$^{-1}$]		5.0×10^{-9}	h [W m^{-1} K^{-1}]	17.0

Table 3.1. Mechanical model parameters and thermal properties.

Finally, the viscosity parameter acquires the following values: $\mu(\lambda_{11}=1.2) = 0.70$ and $\mu(\lambda_{11}=1.4) = 0.28$.

The model does not account for the mechanical properties dependence on the temperature. This assumption, which greatly simplifies the model, is reasonable since in the experiments we have achieved, the temperature increase measured at the surface is relatively small.

5. Finite element implementation

The proposed constitutive model has been implemented by means of a mechanical user subroutine into an advanced non-linear FE software, MSC.Marc (MSC.Marc, 2004a). This subroutine allows the writing of a program from which the variables of a given element that will be written in the post-processing reading file are defined (MSC.Marc, 2004b). The heat build-up due to the thermo-mechanical coupling has been defined by means of the plastic heat generation option and a state variable user subroutine. This subroutine allows the definition of the generated internal heat due to the inelastic energy dissipation (MSC.Marc, 2004b).

During a numerical step, the mechanical subroutine is called at the beginning of each increment. In this subroutine the stress components and, later, the total stress tensor (3.14) are calculated. Moreover, the viscous deformation rate tensor $\dot{\mathbf{F}}_B^v$ and the viscous deformation tensor $\mathbf{F}_B^v$ of the element B for the next increment are calculated from Eqs. (3.6) and (3.7). The viscous deformation tensor for each element is stored, at the end of the increment, in an arrangement that accounts for the number of elements, the nodes per element and the number of variables per node; later, at the beginning of the next increment, reading of the calculated values of the previous increment is therefore available.

Finally, the mechanical dissipation given in Eq. (3.32) is calculated for each element and the value is shared by means of a common block with the state variable subroutine at the end of each increment. Then, the new temperature is calculated, from the solution of the first thermodynamics principle and the boundary conditions of the studied case. The algorithm is outlined in **Fig. 3.7a**.

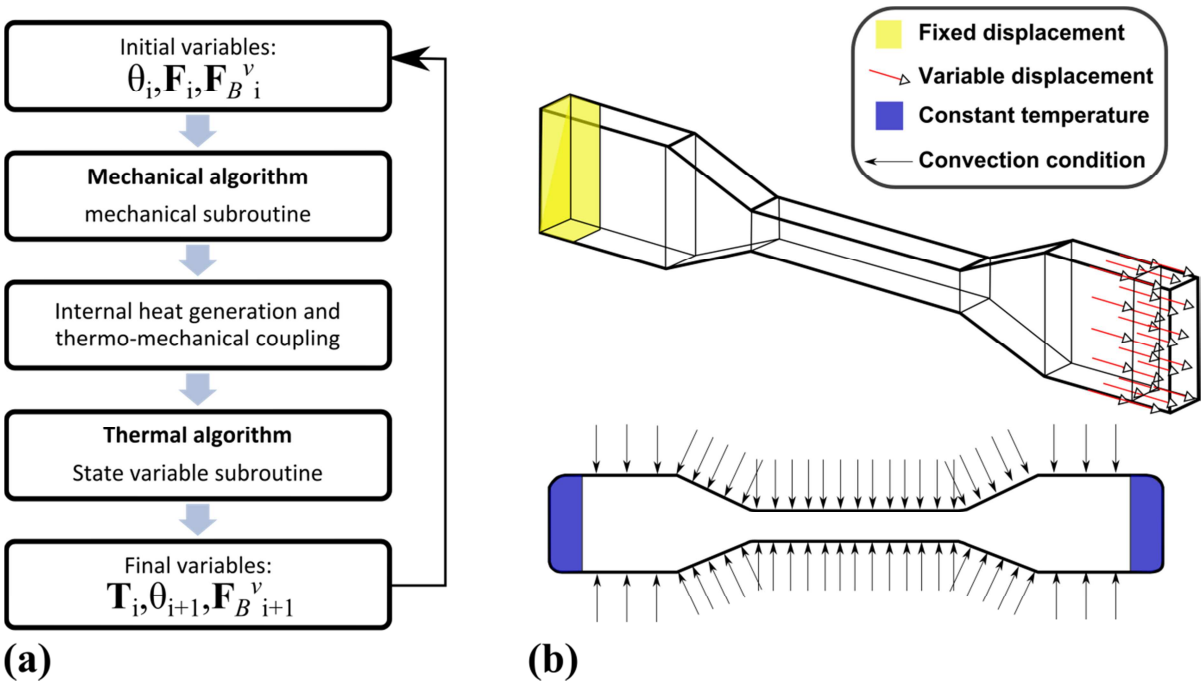

Fig. 3.7. Finite element implementation: (a) algorithm block-diagram, (b) simulation model and boundary conditions.

The FE model was designed according to the dimensions of the test sample (**Fig. 3.3**) using 8-node meshing elements, isoparametric and arbitrarily hexahedrics. The incompressibility condition was introduced by means of an updated Lagrange frame of reference. To simulate the test conditions, one end of the sample was fixed $u_{x1}=0$ the other end being subjected to an increasing displacement $u_{x2}=u(t)$ as shown in **Fig. 3.7b**. The strain rate was controlled by the time function $u_{x2}=u(t)$.

The cyclic loading condition has been simulated by repeating n times a single loading-unloading test under a constant strain rate, n being the total number of cycles.

Concerning the thermal boundary conditions of the test, a constant temperature $\theta=\theta_0$ was applied, at the ends of the sample and a convection heat transfer condition, $\mathbf{q}=\mathbf{q}_s$, in the remaining frontiers:

$$\mathbf{q} = -h\left(\theta - \theta_\infty\right)\vec{n} \tag{3.51}$$

where h is the convection coefficient, θ_∞ is the ambient temperature, taken as a constant, and $\vec{n}$ is the normal vector to the surface of the element.

6. Model verification

The constitutive model presented in Section 2 can be now compared with the experimental results of Section 3.3. Concerning the stress-strain response this comparison is shown in **Fig. 3.8**. A good agreement is pointed out whatever the strain rate.

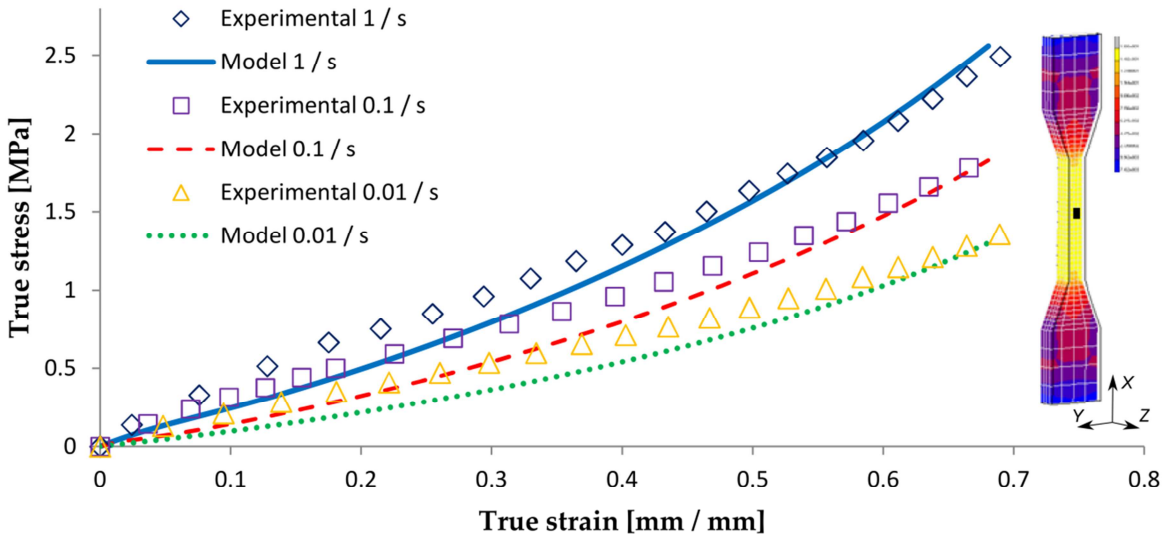

Fig. 3.8. Experimental and simulated stress-strain curves at different strain rates.

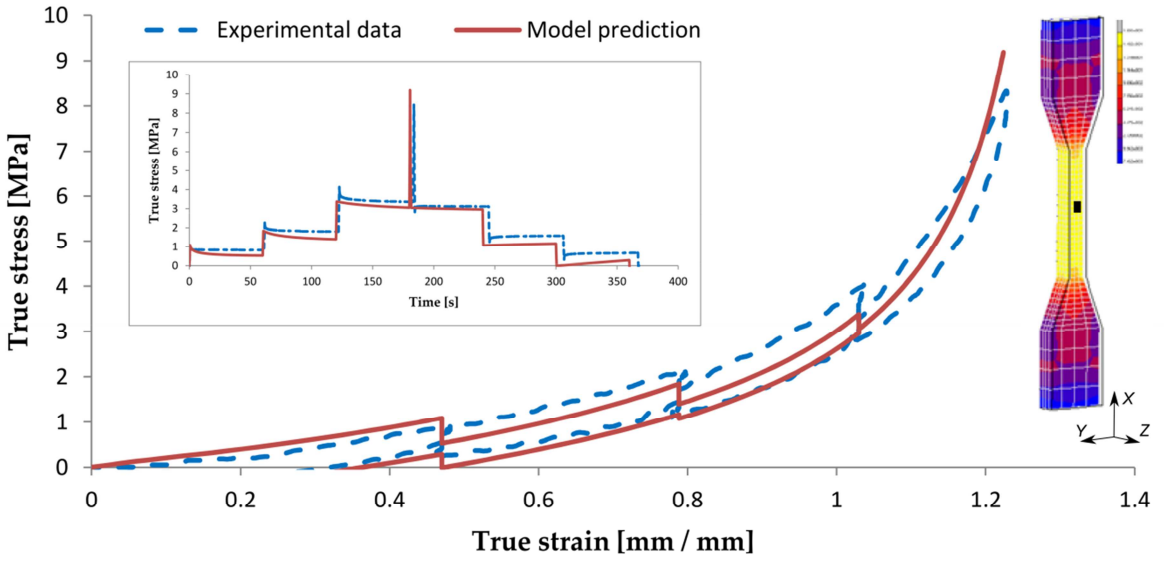

Fig. 3.9. Experimental and simulated multi-relaxation curves, 60 s relaxation time, for a strain rate of 1.0 /s.

The ability of the model to capture the evolution observed during a relaxation test for a strain rate of 1.0 /s and a relaxation time t_{relax} = 60 s, is shown in **Fig. 3.9**. A good agreement between the predicted and experimental curves is highlighted, whether considering loading or unloading path. Indeed, the model takes into account the relaxation difference experimentally observed between the loading and unloading segments.

Fig. 3.10 presents the computed temperature evolution of a material point on the sample surface. Note that since $\dot{\mathbf{C}}_v$ is related to the viscous component of the total deformation gradient but also to the elastic component (see Eq. (3.25)), the mechanical dissipation is then also function of the instantaneous stretch. As a consequence, a material point has an oscillating temperature whose amplitude depends on both components of the stretch (elastic and viscous components). That can explain the thermo-viscoelastic origin of the model response. However, for simplicity reasons only the mean value of the temperature will be taken into account to contrast the simulation model results with the experimental data given in **Fig. 3.6**.

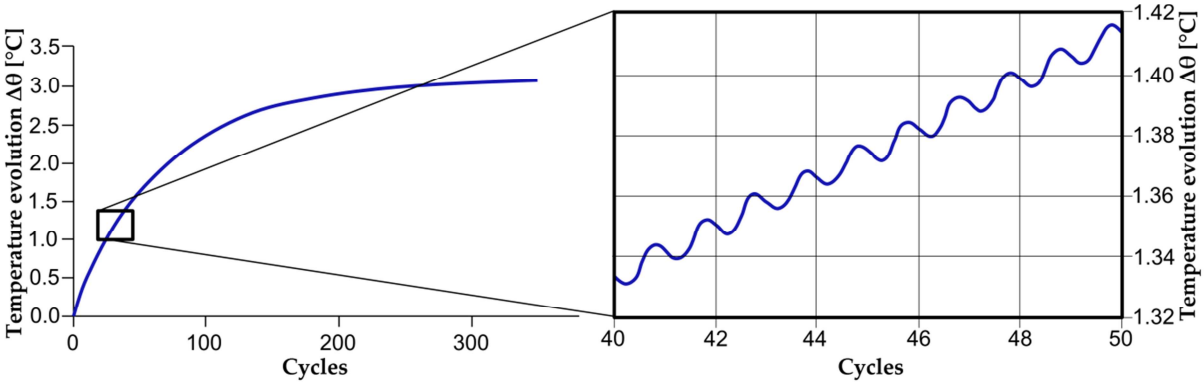

Fig. 3.10. Heat build-up predicted by the simulation model, λ_{11} = 1.2.

In **Figs. 3.11** and **3.12** the predicted temperature evolution due to self-heating for three strain rates and two stretch values (λ_{11} = 1.2 and λ_{11} = 1.4), respectively, is presented. The FE results are compared to the experimental data. The results show that the model captures in a satisfactory manner the temperature evolution due to

the self-heating of a rubber material under fatigue loading at different strain rates and strain levels.

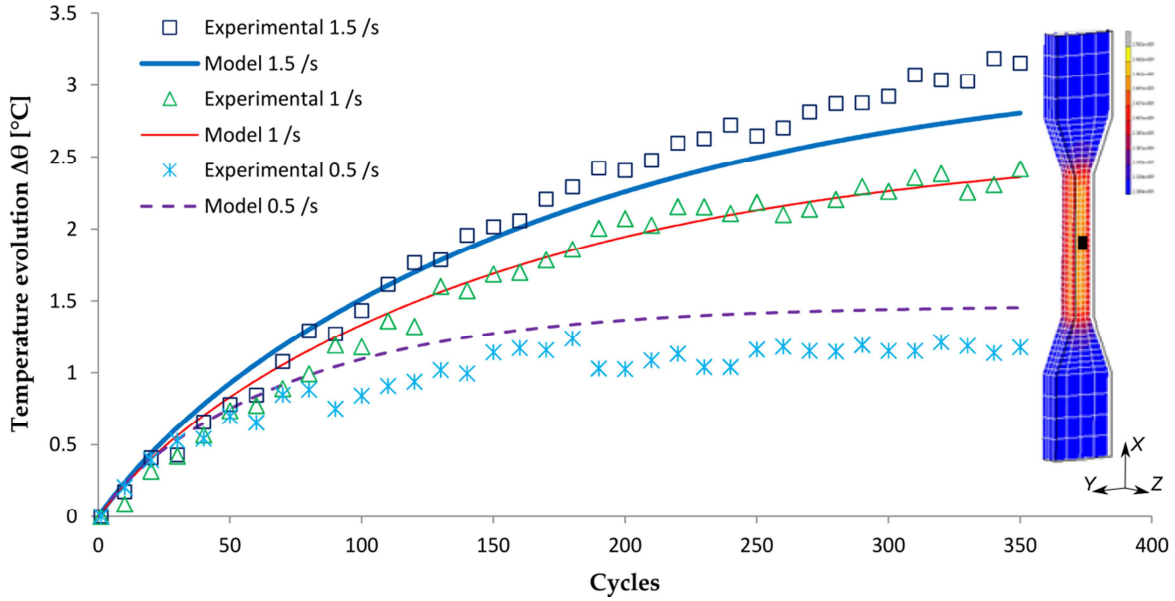

Fig. 3.11. Predicted and experimental heat build-up at different strain rates, $\lambda_{11} = 1.2$.

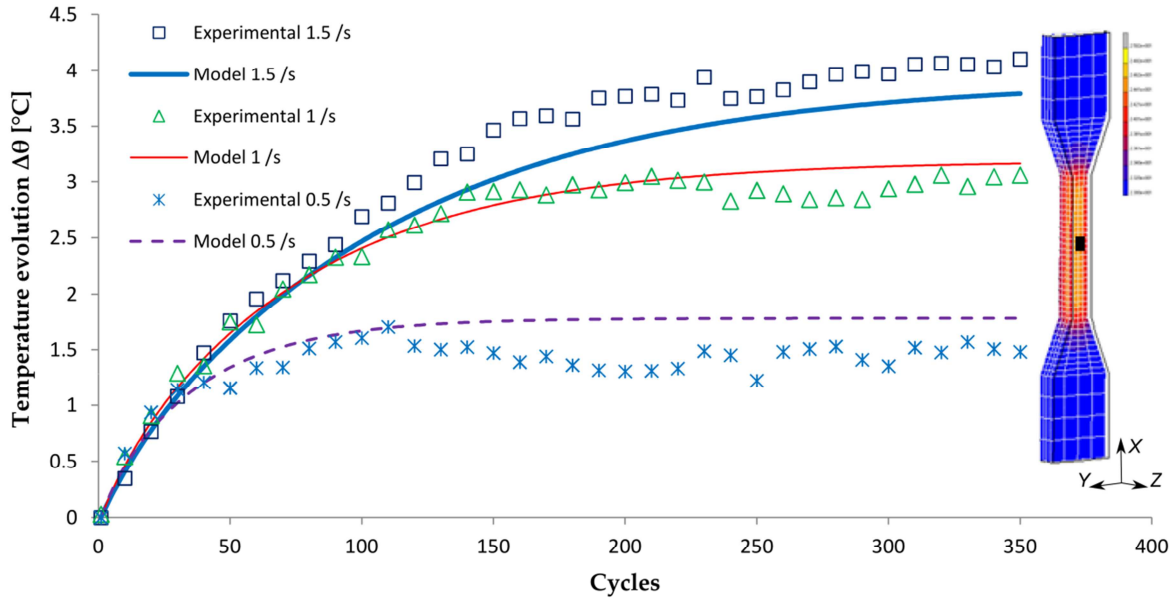

Fig. 3.12. Predicted and experimental heat build-up at different strain rates, $\lambda_{11} = 1.4$.

In order to assess and to confirm the model ability to describe the heat build-up evolution of the test sample, a qualitative and quantitative comparison between a temperature mapping given by the infrared camera and the corresponding FE output, when reaching the 350th cycle, is presented in **Fig. 3.13**. **Fig. 3.13c** also shows

the temperature evolution along the specimen in the loading direction. The obtained results confirm the nice agreement between the FE model and the experimental data.

Now let us consider the variation of the temperature in the thickness direction. In **Fig. 3.14,** the temperature evolution calculated at different locations of the cross-section, in the center and on the surface, is presented. The figure shows that, due to the low heat conduction property of the elastomeric material, the increase of the temperature in the center of the specimen is relatively more important than on the surface. Consequently, it is reasonable to assume that for a thicker specimen the temperature evolution in its center could be sufficiently important to modify the mechanical behavior of the material. As a perspective, defining mechanical variables as temperature dependent is intended (e.g. Zaïri et al., 2010).

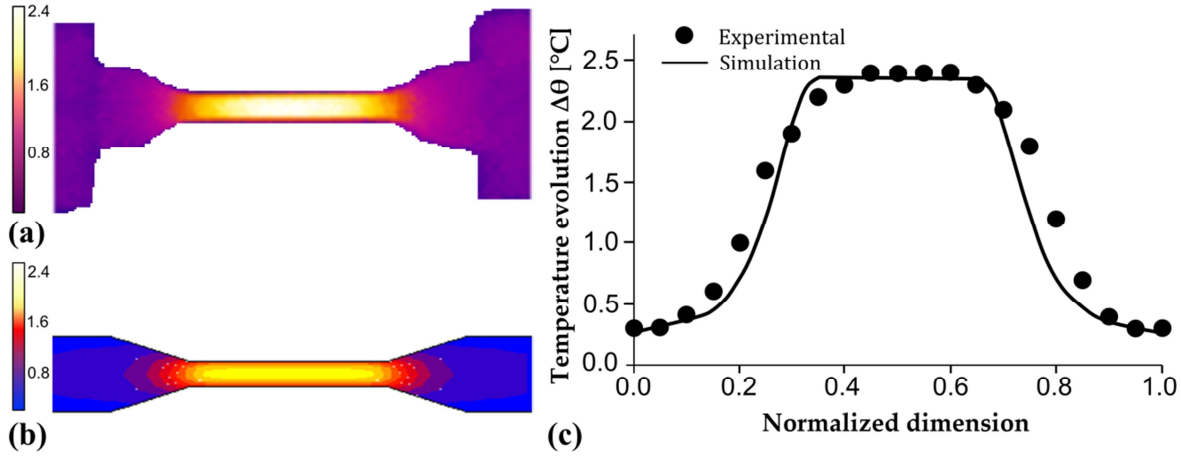

Fig. 3.13. Surface temperature distribution at the 350th cycle with a strain rate of 1.0 /s and $\lambda_{11} = 1.2$: (a) experimental thermal image, (b) numerical model thermal image, (c) experimental and predicted temperature in the sample surface.

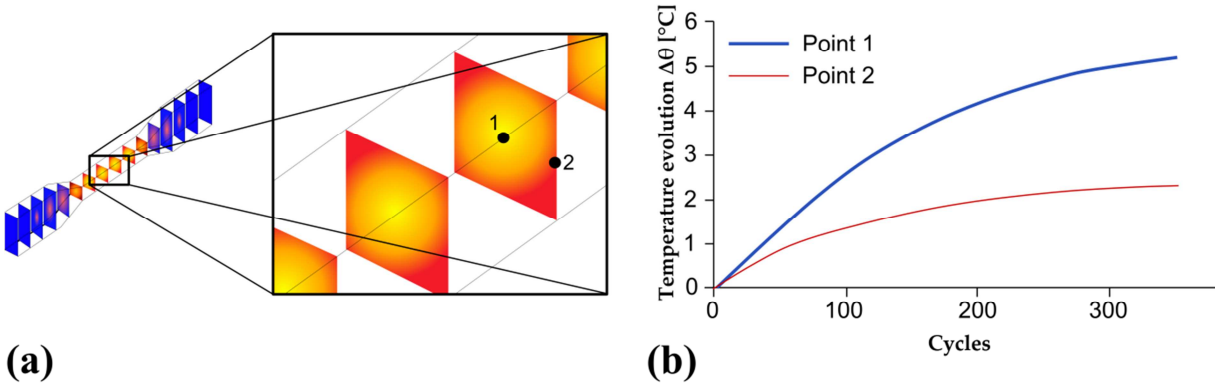

Fig. 3.14. Cross-section temperature distribution at the 350th cycle with a strain rate of 1.0 /s and λ_{11} = 1.2: (a) cross-section and analysis points, (b) temperature evolution at the center and at the surface of the sample.

7. Partial conclusions

A large strain thermo-viscoelastic constitutive model to describe the heat build-up of rubber materials during low-cycle fatigue response has been developed.

The model is based on the assumption that the mechanical behavior can be represented by the response of two networks acting in parallel: the first network captures the equilibrium state and the second one accounts for the time-dependent deviation with regard to the equilibrium response.

In the thermo-mechanical coupling, it is considered that the specific free energy potential is a function of the deformation gradient tensor, the instantaneous temperature, and the viscous dilation tensor, taken as an internal variable that is related with the time-dependent deviation from the equilibrium response. Since this free energy potential does not take into account the maximum strain to which the sample will be submitted, a strain-dependent viscosity parameter was included.

This model was implemented in a FE code and the numerical simulations which have been achieved, have been compared with experimental data for a styrene-butadiene rubber submitted to different loading conditions. It has been shown that the constitutive model offers satisfactory predictions of both the mechanical behavior and the heat build-up.

The thermo-mechanical model developed in the present chapter is extended in *Chapter 4* to account for the explicit effect of the filler volume fraction over the heat build-up of rubbers. In order to avoid the effect of the heat build-up on the mechanical response of the SBR material, flat samples with different amounts of carbon-black were used.

CHAPTER 4

A finite strain thermo-viscoelastic constitutive model to describe the heat build-up in filled rubbers during low-cycle fatigue[23]

In the previous chapter, a finite strain thermo-visco-elastic constitutive model, in accordance with the second thermodynamics principle, has been developed to predict the heat build-up field in rubbers during low-cycle fatigue. Using a viscous dilation tensor, related to the time-dependent response of the rubber material, as an internal variable of the specific free energy potential, both the mechanical behavior and the heat build-up have been predicted for different strain rates and stretches. In the present chapter, the finite strain thermo-mechanical constitutive model is extended by using a stretch amplification factor to account for the effect of carbon-black filler on the heat build-up. Experimental observations on the mechanical response and the heat build-up during fatigue tests of carbon-black filled styrene-butadiene rubber (SBR) containing different filler contents are reported at room temperature. The increasing effect of the filler fraction on the heat build-up is evidenced. The proposed constitutive model is implemented into a finite element code and the same thermo-mechanical boundary conditions regarding the experimental tests are simulated. The model parameters are identified using experimental data issued from SBR filled with a given carbon-black content under a given strain rate and different stretches. Predicted evolutions given by the proposed constitutive model for other strain rates and amounts of carbon-black are found in good agreement with the experimental data.

[23] This chapter is based on the following paper: Ovalle Rodas, C., Zaïri, F., Naït-Abdelaziz, M, Charrier, P. A thermo-visco-hyperelastic model for the heat build-up during low-cycle fatigue of filled rubbers: formulation, implementation and experimental verification. *International Journal of Plasticity*, in press.

1. Introduction

In many common applications, filled rubbers are subjected to cyclic loading with significant magnitude and frequency which may generate a significant quantity of heat and, depending on the heat removal rate, a significant temperature change (Medalia, 1991; Meo et al., 2002; Ovalle Rodas et al., 2013, 2014). The physical consequences of a higher temperature may include the degradation of the rubber mechanical properties. Moreover, as a result of the effect of the temperature increase due to hysteresis, some rubber compounds, which can be highly hysteretic at room temperature (Bergström and Boyce, 1998, 2000; Khan and Zhang, 2001; Laiarinandrasana et al., 2003; Amin et al., 2006; Tomita et al., 2008; Ayoub et al., 2010a; 2011c; Freund et al., 2011; Shim and Mohr, 2011), may be moderately hysteretic at an elevated temperature of operation (Lion, 1997a; Ovalle Rodas et al., 2015). That highlights the complex thermo-mechanical behavior of filled rubbers, besides other phenomena: Mullins effect (Mullins, 1948; Marckmann et al., 2002), continuous stress-softening (Ayoub et al., 2011a; Drozdov, 2012; Drozdov et al., 2013), failure (Mars and Fatemi, 2002; 2006; 2008; Ayoub et al., 2010b; 2011b; 2012).

In the previous chapter, a finite strain thermo-visco-elastic constitutive model that allows the heat build-up prediction in rubbers during low-cycle fatigue has been developed. It has been shown that using a viscous dilation tensor related with the time-dependent response of the rubber material, as an internal variable of the specific free energy potential, the proposed model offers a satisfactory way to predict both the mechanical behavior and the heat build-up for different strain rates and stretches. Although the proposed constitutive model focused on the thermo-mechanical coupling of filled rubbers, the effect of fillers (e.g. carbon-black) has not been explicitly taken into account in any of the material properties, i.e. the constitutive model can be used to predict the thermo-mechanical behavior of a rubber with different filler volume fractions, but experiments to determine the effective material constants for each rubber system of interest must be conducted. Besides, several

works (Medalia, 1991; Meinecke, 1991; Samaca Martinez et al., 2013) have evidenced the increasing effect of the filler fraction on the heat build-up in rubber compounds, highlighting the importance of the explicit inclusion of the filler fraction in the constitutive model.

In the present chapter, a finite strain thermo-visco-elastic constitutive model is developed to describe the heat build-up during low-cycle fatigue of filled rubbers. A Zener-type rheological model is used to describe the thermo-mechanical behavior of filled rubbers, the strain response being decomposed into two components:

- A thermal resistance linked to the stress-free thermal-dilatation, and
- a mechanical resistance linked to the large strain visco-elastic material behavior.

Moreover, the mechanical resistance is seen as the sum of a relaxed component that reflects the long-time material behavior and a viscous component that describes the non-linear time-dependent deviation regarding the relaxed state. In order to take explicitly the filler effect on the thermo-mechanical response, a stretch amplification factor is introduced in the model formulation. This amplification factor is introduced to consider that the presence of the filler acts to amplify the local stress/strain in the rubber compound over that of a corresponding unfilled rubber at the same macroscopic applied stretch. In the thermo-mechanical coupling, the viscous dilation tensor related with the time-dependent deviation from the relaxed response is taken as an internal variable of the specific free energy potential. The existence of a dissipation pseudo-potential, function of the viscous dilatation tensor, is postulated. The associate specific free energy is defined using a Langevin formulation.

Experimental observations on the mechanical response and the heat build-up during fatigue tests of carbon-black filled styrene-butadiene rubber (SBR) containing different filler contents are reported at room temperature.

The proposed constitutive model is implemented into a finite element (FE) code, by means of a strain energy function subroutine in parallel with an internal heat

generation subroutine, and the same thermo-mechanical boundary conditions regarding the experimental tests are simulated. The constitutive model parameters are identified using experimental data obtained on a SBR with a fixed amount of carbon-black, 25 phr (part per hundred of rubber in weight), under a given strain rate for different stretches. Predicted evolutions given by the constitutive model for other strain rates and amounts of carbon-black, 15 and 43 phr, are found in good agreement with the experimental data.

The chapter is organized as follows: in Section 2, the formulation of the coupled thermo-mechanical constitutive model is presented. Section 3 discusses the experimental data, whereas the parameters identification procedure is presented in Section 4. In Section 5, the implementation of the constitutive model into a FE code is briefly described. The constitutive model capability regarding the experimental data is presented in Section 6. In Section 7, a discussion about the predictive model potential is highlighted. Finally, Section 8 closes with the concluding remarks.

2. Model formulation

The proposed constitutive model considers the large strain thermo-visco-elastic behavior of filled rubbers. The schematic representation of the model is shown in **Fig. 4.1a**. To account for the thermo-mechanical behavior, it is considered that the overall resistance to deformation is composed of a thermal resistance (temperature-dependent element) acting in series with a mechanical network, linked to the stress-free thermal-dilatation and to the large strain visco-elastic behavior, respectively. The mechanical response is the sum of a relaxed response *A* (non-linear elastic spring) and a time-dependent deviation regarding the relaxed state *B* (non-linear elastic spring in series with a viscous dashpot).

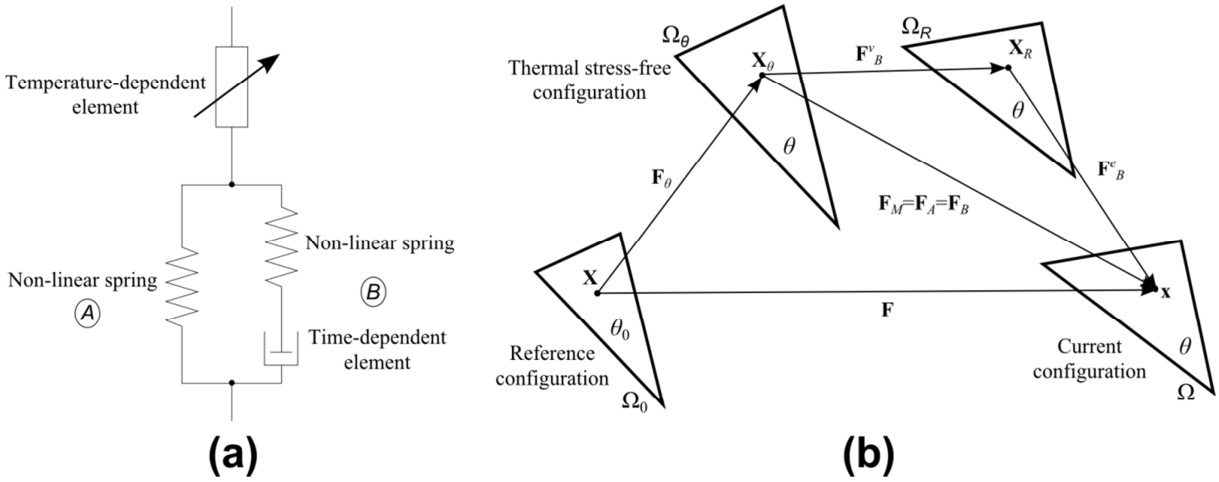

Fig. 4.1. Thermo-visco-elastic model: (a) Schematic representation, (b) multiplicative decomposition of the thermo-mechanical deformation.

2.1 Thermo-visco-elastic kinematics

Let us first consider a continuum body with the reference configuration Ω_0 and a current configuration Ω, see **Fig. 4.1b**. For the sake of simplicity, Ω_0 is assumed to be stress-free and with a uniform absolute temperature $\theta_0 > 0$ taken as a reference. The mapping of a given material point with the position $\mathbf{X}$ in the reference configuration to the position $\mathbf{x}$ in the current configuration is given by the deformation gradient[24]: $\mathbf{F} \equiv \partial \mathbf{x} / \partial \mathbf{X}$.

To account for the coupling between the thermal dilatation effects and the mechanical behavior of the continuum body, the thermo-mechanical response can be described as the multiplicative decomposition of the deformation gradient into a thermal part $\mathbf{F}_\theta$ and a mechanical part $\mathbf{F}_M$ as proposed by several authors (Lee and Liu, 1967; Sidoroff, 1974; Lu and Pister, 1975; Miehe, 1995; Holzapfel and Simo, 1996; Lion, 1997, 2000):

$$\mathbf{F} = \mathbf{F}_\theta \mathbf{F}_M \tag{4.1}$$

Note that in the mechanical part, the first resistance (resistance *A*) results in the static finite deformation elastic response whereas the second resistance (resistance *B*)

[24] In order to facilitate the lecture and understanding of the model formulation, some equations from previous chapters have been repeated.

results in the history-dependent deviation from the static state. Considering the parallel scheme of the mechanical network, both $\mathbf{F}_A$ and $\mathbf{F}_B$ are equal to the mechanical deformation gradient $\mathbf{F}_M$:

$$\mathbf{F}_M = \mathbf{F}_A = \mathbf{F}_B \tag{4.2}$$

The main multiplicative decomposition considers a conceptual sequence of stress-free configurations. The first one, i.e. the thermal stress-free configuration Ω_θ related to the thermal dilatation of the continuum body, is characterized by the thermal deformation gradient tensor:

$$\mathbf{F}_\theta = \exp\left[\int_{\theta_0}^{\theta} \alpha(u)\, du\right]\mathbf{I} \tag{4.3}$$

where α is the temperature-dependent coefficient of the thermal expansion and $\mathbf{I}$ is the unit tensor. In Eq. (4.3), the exponential expression is a temperature function representing the intrinsic thermal dilatation of the continuum body (Lu and Pister, 1975; Holzapfel and Simo, 1996). The second one, i.e. the relaxed configuration Ω_R related to the obtained configuration during a spontaneous virtual elastic unloading of the resistance *B*, is characterized by the time-dependent deformation gradient tensor $\mathbf{F}_B$:

$$\mathbf{F}_B = \mathbf{F}_B^e \mathbf{F}_B^v \tag{4.4}$$

where the time-dependent deformation gradient can be written using a multiplicative form and decomposed into an elastic $\mathbf{F}_B^e$ and a viscous component $\mathbf{F}_B^v$ (Lee, 1969). In this case, the viscous deformation of the viscous dashpot does not change during the unloading step and remains frozen.

The elastic deformation gradient $\mathbf{F}_B^e$ and the viscous deformation gradient $\mathbf{F}_B^v$ can be in turn decomposed into stretching and rotation components:

$$\mathbf{F}_B^e = \mathbf{V}_B^e \mathbf{R}_B^e \tag{4.5}$$

$$\mathbf{F}_B^v = \mathbf{V}_B^v \mathbf{R}_B^v \tag{4.6}$$

The corresponding kinematic rate for the resistance *B* can be written as:

$$\mathbf{L}_B = \dot{\mathbf{F}}_B \mathbf{F}_B^{-1} \tag{4.7}$$

Introducing the elastic and viscous parts of this quantity leads to:

$$\mathbf{L}_B = \dot{\mathbf{F}}_B^e \mathbf{F}_B^{e-1} + \mathbf{F}_B^e \dot{\mathbf{F}}_B^v \mathbf{F}_B^{v-1} \mathbf{F}_B^{e-1} = \mathbf{L}_B^e + \mathbf{L}_B^v \tag{4.8}$$

where

$$\mathbf{L}_B^v = \mathbf{D}_B^v + \mathbf{W}_B^v \tag{4.9}$$

in which $\mathbf{D}_B^v$ is the viscous stretching rate and $\mathbf{W}_B^v$ is the viscous spin rate. Details about the definition of these two rate tensors will be given further. In order to avoid the difficulties associated to the volumetric effects (Zaïri et al., 2008a, 2011a), we assume here that the mechanical deformation occurs without volume change, i.e. $\det \mathbf{F}_M = 1$.

2.2 Constitutive equations

To derive the constitutive equations, the existence of a free energy function is postulated:

$$\psi = \psi_\theta + \psi_M \tag{4.10}$$

and

$$\psi_M = \psi_A + \psi_B \tag{4.11}$$

In Eq. (4.10), ψ_θ is the thermal contribution of the temperature-dependent resistance (Holzapfel and Simo, 1996):

$$\psi_\theta = -\int_{\theta_0}^{\theta} C(u)(\theta - u)\frac{du}{u} \tag{4.12}$$

where $C(u)$ is the specific heat capacity at constant deformation (details will be given further) and, in Eq. (4.11), ψ_M is the mechanical contribution given by the sum of the relaxed-response resistance (non-linear elastic spring) and the time-dependent resistance (non-linear elastic spring in series with a viscous dashpot). In both cases, the non-linear springs can be defined by any, phenomenologically-based or statistically-based, strain energy density function. By contrast to phenomenological

functions, the material constants of statistical ones are related to the rubbery structure. A number of non-Gaussian statistics theories, based on the prior work of Kuhn and Grün (1942), which introduces the extensibility limit of molecular chain network were proposed: James and Guth (1943) three-chain, Flory and Rehner (1943) four-chain, Treloar and Riding (1979) full-network, Arruda and Boyce (1993) eight-chain and Wu and van der Giessen (1993) approximate full-network functions. Details about the definition of the strain energy density function will be given further.

On the other hand, the viscous dashpot is responsible for the loss of mechanical energy, i.e. it implies a dissipative phenomenon which is related with the strain rate. As a consequence, in addition to the common observable functions of state, the absolute temperature θ and the deformation gradient tensor $\mathbf{F}$, the mechanical contribution of the free energy can include an internal variable that accounts for the time-dependent deviation from the static response:

$$\psi_M = \psi_M\left(\theta, \mathbf{F}, \mathbf{C}_v\right) \tag{4.13}$$

where

$$\mathbf{C}_v = \mathbf{F}_B^{vT}\mathbf{F}_B^v \tag{4.14}$$

is the right Cauchy-Green strain tensor associated to the viscous deformation gradient $\mathbf{F}_B^v$, called viscous dilatation tensor. Note that, since the free energy potential ψ_M is an isotropic function which depends on the viscous dilatation tensor $\mathbf{C}_v$, the free energy itself and all constitutive equations are independent on inelastic rotations (Haupt, 2002). Consequently, the viscous spin rate $\mathbf{W}_B^v$ drops out in Eq. (4.9).

Once defined the functions of state, the process will be thermodynamically admissible if, at every instant, the Clausius-Duhem inequality is satisfied, written in a mixed description:

$$\gamma = -\rho\left(\dot{\psi} + \dot{\theta}\eta\right) + \boldsymbol{\pi} : \dot{\mathbf{F}} - \frac{1}{\theta}\mathbf{q}\cdot\nabla_X\theta \geq 0 \tag{4.15}$$

where

$$\psi = e - \theta\eta \tag{4.16}$$

γ is the dissipation, ρ is the mass density for a unit reference volume, $\eta = -\partial\psi/\partial\theta$ is the specific entropy, $\boldsymbol{\pi} = \partial\psi_M/\partial\mathbf{F}$ is the first Piola-Kirchhoff stress tensor, $\dot{\mathbf{F}}$ is the deformation gradient tensor rate, $\mathbf{q}$ is the Piola-Kirchhoff heat flux, $\nabla_X\theta$ is the temperature gradient and e is the specific internal energy.

Finally, the total Cauchy stress $\mathbf{T} = J^{-1}\boldsymbol{\pi}\mathbf{F}$ in the continuum material is the sum of the Cauchy stresses of the relaxed-response resistance $\mathbf{T}_A$ and the time-dependent resistance $\mathbf{T}_B$:

$$\mathbf{T} = \mathbf{T}_A + \mathbf{T}_B \tag{4.17}$$

2.2.1 Thermo-mechanical dissipation potential

In order to get the decoupling of the thermo-mechanical dissipation potential, let us first define the specific internal energy rate $\dot{e}$ by inserting the time rate of the specific free energy

$$\dot{\psi} = \frac{\partial\psi_M}{\partial\mathbf{F}} : \dot{\mathbf{F}} + \frac{\partial\psi_M}{\partial\mathbf{C}_v} : \dot{\mathbf{C}}_v + \frac{\partial\psi}{\partial\theta}\dot{\theta} \tag{4.18}$$

into Eq. (4.16), and after a series of straightforward derivations it returns:

$$\dot{e} = \frac{1}{\rho}\boldsymbol{\pi} : \dot{\mathbf{F}} + \frac{1}{\rho}\mathbf{A}_v : \dot{\mathbf{C}}_v - \theta\frac{1}{\rho}\left(\frac{\partial\boldsymbol{\pi}}{\partial\theta} : \dot{\mathbf{F}} + \frac{\partial\mathbf{A}_v}{\partial\theta} : \dot{\mathbf{C}}_v\right) - \theta\frac{\partial^2\psi}{\partial\theta^2}\dot{\theta} \tag{4.19}$$

where

$$A_v = \rho\frac{\partial\psi_M}{\partial\mathbf{C}_v} \tag{4.20}$$

is the thermodynamic force associated with the internal variable $\mathbf{C}_v$.

Inserting this expression for the time rate of the specific internal energy into the standard formulation of the first thermodynamics law, i.e. $\rho\dot{e} = \boldsymbol{\pi} : \dot{\mathbf{F}} - \mathrm{div}(\mathbf{q}) + \rho r$, leads to the following relation

$$\rho C\dot{\theta} = -\mathbf{A}_v : \dot{\mathbf{C}}_v + \theta\left(\frac{\partial\boldsymbol{\pi}}{\partial\theta} : \dot{\mathbf{F}} + \frac{\partial\mathbf{A}_v}{\partial\theta} : \dot{\mathbf{C}}_v\right) - \mathrm{div}(\mathbf{q}) + \rho r \tag{4.21}$$

where C is the specific heat at constant deformation per unit mass:

$$C\left(\mathbf{F},\theta,\mathbf{C}_v\right)=-\theta\frac{\partial^2\psi}{\partial\theta^2} \tag{4.22}$$

In Eq. (4.21), the terms Φ_M and Φ_θ are expressed as follows:

$$\Phi_M=-\mathbf{A}_v:\dot{\mathbf{C}}_v+\theta\left(\frac{\partial\boldsymbol{\pi}}{\partial\theta}:\dot{\mathbf{F}}+\frac{\partial\mathbf{A}_v}{\partial\theta}:\dot{\mathbf{C}}_v\right) \tag{4.23}$$

$$\Phi_T=-\mathrm{div}\left[\mathbf{q}\right]+\rho r \tag{4.24}$$

Eq. (4.23) corresponds to the intrinsic dissipation in which the first term is the dissipation potential due to the material visco-elastic behavior, while the second term is related to the dissipation due to the evolution of the material mechanical properties regarding the temperature. Besides, in Eq. (4.24), the first term corresponds to the divergence of the heat flux vector, while the second term corresponds to the material heat supply. Note that the heat supply per unit mass, r, can be omitted since it is neglected in the present study.

Since the temperature evolution during a numerical step is imperceptible, it is reasonable, in a first approximation, to neglect the evolution of the mechanical properties regarding the temperature; therefore, under such an assumption, the intrinsic dissipation reduces to

$$\Phi_m\approx-\mathbf{A}_v:\dot{\mathbf{C}}_v \tag{4.25}$$

Furthermore, in Eq. (4.24), the Piola-Kirchhoff heat flux $\mathbf{q}$ is given by the Fourier law:

$$\mathbf{q}=-\mathbf{K}_X\cdot\nabla_X\theta \tag{4.26}$$

where

$$\mathbf{K}_X=\mathbf{F}^{-1}\mathbf{K}\mathbf{F}^{-T} \tag{4.27}$$

is the conductivity tensor in the reference configuration, and $\mathbf{K}$ is the Euler conductivity tensor. In the isotropic case, this one reduces to $\mathbf{K}=\kappa\mathbf{I}$, where κ is the material conductivity factor.

In pursuance of the heat build-up associated with the thermo-mechanical boundary conditions of the continuum body, a procedure to calculate the time rate of the viscous dilatation tensor is necessary.

2.2.2 Time rate of the viscous dilatation tensor

The existence of a dissipation pseudo-potential, φ, associated with the internal variable $\mathbf{C}_v$ is postulated such that (Sidoroff, 1974):

$$\varphi\left(\dot{\mathbf{C}}_v\right)=\begin{cases}1/2\,\mu_f\left(\dot{\mathbf{C}}_v:\dot{\mathbf{C}}_v\right) & \text{if} \quad \dot{\mathbf{C}}_v:\mathbf{C}_v^{-1}=0\\ \infty & \text{otherwise}\end{cases} \tag{4.28}$$

where μ_f is a viscosity parameter (Boukamel et al., 2001) which is linked to the fraction of the intrinsic dissipation contributing with the heat build-up of the filled continuum body. In Eq. (4.28), considering that the volumetric effect adds an additional difficult factor (Zaïri et al, 2011a), the material incompressibility assumption is taken into account by means of:

$$\det\left(\mathbf{C}\right)=1 \tag{4.29}$$

$$\dot{\mathbf{C}}_v:\mathbf{C}_v^{-1}=0 \tag{4.30}$$

where $\mathbf{C}=\mathbf{F}^T\mathbf{F}$ is the right Cauchy-Green strain tensor.

Furthermore, if the reduction of the rubber content in the filled material is taken into account, the viscosity parameter will be reduced by the factor $\left(1-v_f\right)$ as:

$$\mu_f=\left(1-v_f\right)\mu_u \tag{4.31}$$

where v_f is the filler volume fraction and μ_u is the viscosity parameter of the unfilled continuum body. Furthermore, from the existence of the dissipation pseudo-potential, a complementary law related to the dissipation potential can be established:

$$A_v=-\frac{\partial\varphi}{\partial\dot{\mathbf{C}}_v} \tag{4.32}$$

Equating Eqs. (4.20) and (4.32) leads to:

$$\rho\frac{\partial\psi_M}{\partial\mathbf{C}_v}=-\frac{\partial\varphi}{\partial\dot{\mathbf{C}}_v} \tag{4.33}$$

Substituting Eqs. (4.13) and (4.28) in Eq. (4.33), it is possible to obtain, after a series of lengthy but straightforward derivations, the following complementary expression[25]:

$$-\rho \mathbf{C}_v^{-1}\mathbf{C}\mathbf{C}_v^{-1}\left[\left(\frac{\partial \psi_M}{\partial I_1}+\frac{\partial \psi_M}{\partial I_2}I_1\right)\mathbf{I}-\frac{\partial \psi_M}{\partial I_2}\mathbf{C}\mathbf{C}_v^{-1}\right]+\mu_f \dot{\mathbf{C}}_v=0 \tag{4.34}$$

where $\mathbf{C}=\mathbf{F}_M^T\mathbf{F}_M$ is the right Cauchy-Green strain tensor, $I_1=\mathrm{tr}\mathbf{B}_M$ and $I_2=\mathrm{tr}\mathbf{B}_M^2$ are the first and second stretch invariants, respectively, $\mathbf{B}_M=\mathbf{F}_M\mathbf{F}_M^T$ being the left Cauchy-Green strain tensor.

In the interest of simplicity, Eq. (4.34) can be reduced if multiplying it by $\mathbf{C}_v$. That leads to the following expression:

$$-\rho\left[\mathbf{C}\mathbf{C}_v^{-1}\left[\left(\frac{\partial \psi_M}{\partial I_1}+I_1\frac{\partial \psi_M}{\partial I_2}\right)\mathbf{I}-\frac{\partial \psi_M}{\partial I_2}\mathbf{C}\mathbf{C}_v^{-1}\right]\right]+\mu_f \mathbf{C}_v\dot{\mathbf{C}}_v=0 \tag{4.35}$$

which can be written in the following general form:

$$\dot{\mathbf{C}}_v=\dot{\mathbf{C}}_v\left(\mathbf{F},\theta,\mathbf{C}_v\right) \tag{4.36}$$

In Eqs. (4.35) and (4.36), the instantaneous time rate of the viscous dilatation tensor is related to the elastic and viscous components of the deformation gradient tensor. As a consequence, the magnitude of the intrinsic dissipation of a given material point depends on both components of the stretch (elastic and viscous components), i.e. the thermo-elastic effects are implicitly coupled with the thermo-viscous effects.

2.3 Model particularization

In this work, the eight-chain strain energy density function (Arruda and Boyce, 1993), which considers the mechanical contribution as the resistance to deformation energy of an eight-chain non-Gaussian network, is chosen. The strain energy density function is expressed in its compressible version as a function of the first stretch invariant I_1 and the mechanical volume change $J_M=\det\mathbf{F}_M$ (Bischoff et al., 2001):

[25] Details about the derivation can be found in Laiarinandrasana et al. (2003).

$$\psi_{M=A,B}\left(I_1\right)=n_{A,B}k\theta\sqrt{N_{A,B}}\left(\beta\sqrt{\frac{I_1}{3}}+\sqrt{N_{A,B}}\ln\frac{\beta}{\sinh\beta}-\frac{\beta_0}{3}\ln J_M\right)+\frac{K}{2}\left(J_M-1\right)^2 \quad (4.37)$$

where $n_{A,B}$ is the average number of chains per unit volume, k is the Boltzmann constant, $N_{A,B}$ is the number of connected rigid-links in a chain and K is the temperature-dependent bulk modulus which, for rubbers, is significantly higher than the shear modulus, e.g. $K\approx 500nk\theta$. In Eq. (4.37), the terms β and β_0 correspond to the inverse of the Langevin function $\mathcal{L}^{-1}$ in the current and reference configurations, respectively:

$$\beta=\mathcal{L}^{-1}\left(\sqrt{\frac{I_1}{3N}}\right) \quad (4.38)$$

$$\beta_0=\mathcal{L}^{-1}\left(\sqrt{\frac{1}{N}}\right) \quad (4.39)$$

The inverse of the Langevin function $\mathcal{L}^{-1}\left(u\right)=\coth\left(u\right)-1/u$ can be estimated through the Padé approximation (Cohen, 1991): $\mathcal{L}^{-1}\left(u\right)=u\left(3-u^2\right)/\left(1-u^2\right)$. The first stretch invariant I_1 corresponds to $I_1=\mathrm{tr}\mathbf{B}_M$ for the resistance A and $I_1=\mathrm{tr}\mathbf{B}_M^e$ for the resistance B. Besides, in Eq. (4.37), $n_Ak\theta$ correlates to the slope of the stress-strain curve during the strain-hardening, $n_Bk\theta$ correlates to the slope of the stress-strain curve during the unloading stage once the relaxed response has been subtracted from the overall response (Bergström and Boyce, 1998) and the term $\sqrt{N_{A,B}}$ corresponds to the chain extensibility limit.

Although the proposed strain energy density function can be used to model the mechanical response of filled rubbers, the filler effect is not explicitly taken into account in any of the material constants. Accordingly, the effect of fillers may be explicitly addressed by considering that at any given strain, the presence of the particles acts to locally amplify the strain and stress in the rubber compound over that of a corresponding unfilled rubber at the same macroscopic applied stretch (Trabelsi et al., 2003). First introduced by Mullins and Tobin (1965), the amplified stretch notion, in the case of uniaxial loading, is quantified as:

$$\Lambda = 1 + \chi(\lambda - 1) \tag{4.40}$$

where Λ is the amplified stretch and λ is the macroscopic applied axial stretch. The χ constant is an amplification factor related to the filler volume fraction and the distribution of the filler particles in the continuous matrix. The exact form of χ is not clear; however, a general empirical form was proposed by Guth (1945):

$$\chi = 1 + 0.67 c v_f + 1.62 c^2 v_f^2 \tag{4.41}$$

where $c \geq 1$ is a shape factor that considers the filler agglomeration and the reinforcing effect of the filler. Note that $c = 1$ is related to filler agglomerations in which the particles are seen as perfect spheres, whereas for $c > 1$ the particles are seen as elongated objects.

The stretch amplification factor approach is preferred to more sophisticated micromechanics-based approaches (Ponte Castañeda, 1989; Bouchart et al., 2008; Zaïri et al., 2008b, 2011b) for the sake of simplicity. Applying this amplification correction to the first invariant of the stretch, an explicit model that accounts for the filler effect can be defined:

$$\psi_M = (1 - v_f)\psi_M\left(\langle I_1 \rangle_m\right) \tag{4.42}$$

in which $\langle I_1 \rangle_m = \chi(I_1 - 3) + 3$ is the amplified first invariant.

When now considering the time-dependent network, the evolution of the elastic deformation gradient is determined from Eqs. (4.4), (4.8) and (4.9) knowing that the rate of the viscous stretching must be specified. It is defined as:

$$\mathbf{D}_B^v = \dot{\gamma}_B \frac{1}{\sqrt{2}\tau_B} \mathbf{T}_B^{'} \tag{4.43}$$

where $\mathbf{T}_B^{'}$ is deviator part of $\mathbf{T}_B$,

$$\tau_B = \left[\frac{1}{2}\operatorname{trace}\left(\mathbf{T}_B^{'}\mathbf{T}_B^{'}\right)\right]^{1/2} \tag{4.44}$$

is the effective stress acting on network *B*, and

$$\dot{\gamma}_B = \eta\left(\frac{1}{\lambda_B^v - 1 + \Delta}\right)\tau_B^m \tag{4.45}$$

is the flow rate (Bergström and Boyce, 1998) in which η and m are positive material constants to be identified and

$$\lambda_B^v = \left(\frac{1}{3} \text{trace}\left(\mathbf{F}_B^v \mathbf{F}_B^{vT} \right) \right)^{1/2} \tag{4.46}$$

In Eq. (4.45), the term $\Delta \approx 0.01$ is a parameter that eliminates the singularity nature of the $\lambda_B^v - 1$ expression.

3. Experimental procedure and observations

3.1 Experiments

3.1.1 Studied material

The materials used in this paper are sulfur-vulcanized styrene-butadiene rubber (SBR) filled with three different amounts of carbon-black: 15, 25 and 43 phr (part per hundred of rubber in weight), denoted SBR15, SBR25 and SBR43, respectively. The details about the material characteristics, provided by the manufacturer, are given in **Table 4.1**.

Ingredients	Value [phr]
SBR	100
Zinc oxide	5
Processing oil	37.5
Carbon-black	15, 25 and 43
Stearic acid	3
Antioxidant	5.5
Accelerators	4

Table 4.1. SBR material formulation.

3.1.2 Sample geometry and experimental method

Dumbbell flat samples were cut from 2 mm thickness sheets. Details about the geometry are given in **Fig. 4.2**. The reduced section in the center of the sample allows locating the highest strain in this region and, as a consequence, the highest increase of temperature. Furthermore, its weak thickness allows avoiding a high temperature gradient in the transverse direction.

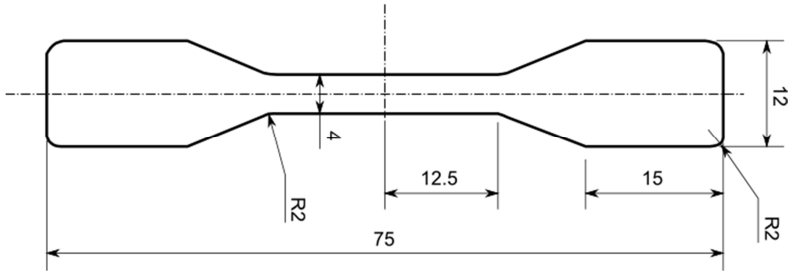

Fig. 4.2. Dumbbell flat sample geometry (dimensions in mm).

Different tests were performed to characterize the thermo-mechanical behavior and to quantify the surface heat build-up due to thermo-mechanical coupling. The constant-temperature mechanical tests were carried out on an electro-mechanical testing device (Instron-5800) provided with a high temperature environmental chamber (Instron-3119). The temperature levels above 288 K (room temperature) were attained by forced convection (high speed circulation fan) from a surrounding air operating atmosphere. The room temperature mechanical tests were carried out on an electro-pulse mechanical device (Instron-5500). A displacement-control function was imposed for the loading-unloading condition, load and displacement versus time being recorded during the tests. The temperature field was measured using an infrared camera (Flir SC300) interfaced with a computer which allows the storage of the thermal images during the test. The stored images can be post processed to determine the temperature evolution in the analyzed region. The temperature precision, noise-equivalent temperature difference, is equal to 100 mK for a temperature range of 273-353 K.

In the parameter identification process and the analysis of the thermo-mechanical coupling, four types of mechanical tests were performed:

- Constant-temperature tests were performed in order to determine the thermal expansion coefficient of the studied material. The axial dilatation X_i due to the temperature increasing was measured. The tests were developed under temperatures ranging from 293 up to 353 K.
- Multi-relaxation tests were performed in order to determine the parameters of the relaxed response of the SBR materials. During the loading-unloading

condition, the test was interrupted at prescribed levels of axial stretch, λ_{R_i}, for a given holding time, t_R. During this holding time, the load evolution was stored. Both the number of stretch levels and the holding time were defined to be sufficiently enough, i.e. λ_R = [1.25, 1.5, 1.75, 2.0] and t_R = 1 h, in order to attain which appears to be a stabilized relaxed-response. The multi-relaxation tests were made at a strain rate of $1.5s^{-1}$.

- Single cycle tests were performed in order to determine the parameters of the time-dependent response of the SBR materials. It consists in loading the sample up to a stretch value (taken equal to the maximum axial stretch prescribed in the multi-relaxation tests) under a constant strain rate and, then, unloading it down to its initial position.
- Fatigue tests were also performed in order to determine the viscosity parameter, μ_u, and to quantify the surface temperature evolution on the sample under different axial stretches. Previous to the tests, 15 loading-unloading cycles up to an axial stretch λ_{11} = 2.0 were carried out in order to eliminate the surface flake that appears in the sample, which can alter the infrared camera data measurements because of the variation of the surface emissivity. The external heat sources were reduced by using a black box surrounding the sample, featuring a small window for the camera to be able to observe the gauge zone on the sample. The camera was located at a distance lower than 0.5 m in order to reduce the reflected radiation due to surrounding humidity. In order to determine the initial surrounding temperature, 50 images were taken previous to the tests. During the test, the required number of images to reach the stabilization temperature of the sample was stored. The images correspond to the same strain level condition.

To assess repeatability of observations, tests were carried out on six different specimens for each condition.

3.1.3 Experimental results

In **Fig. 4.3** is shown the uniaxial stress-strain mechanical response of SBR materials with 15, 25 and 43 phr. The strain rate dependence during uniaxial tension is shown in **Figs. 4.3a**, **4.3b** and **4.3c**. The experiments show that the stress increases with increasing strain-rate and filler fraction. Similar results, for filled natural and chloroprene rubbers, have been observed by Bergström and Boyce (2000) and, for natural rubber and high damping rubber, by Amin et al. (2006). The data also exhibits the highly non-linear response of the material which is accompanied by a drastic strain hardening for large strains. The history-dependence of the SBR material can be also shown with multi-relaxation tests, as the one illustrated for the SBR25 in the inset of **Fig. 4.3d**. The results from the test show that the stress decreases during the holding time in the loading path while an increase is pointed out during the holding time in the unloading. Note that, during the holding time, the stress evolves towards a stabilized value whose envelop gives the relaxed-response. The graph indicates that this relaxed-stress tends to increase significantly as it approaches a given deformation (E_∞). The data also provides a quantitative estimate of the hysteresis (Medalia, 1991):

$$H = \frac{\pi}{4}\left(\frac{2\cdot CSA}{100}\right)^2 E'\tan\delta \tag{4.47}$$

that occurs during the unloading path and, by the way, of the amount of mechanical energy that is dissipated as heat energy during a cycle. The heat generation can drive, depending on the rate of heat removal, to heat build-up, i.e. a higher temperature of the rubber component. In Eq. (4.47), CSA is the Cycle Strain Amplitude in percentage of the undeformed dimension, E' is the elastic modulus and $\tan\delta = E''/E'$ is the loss tangent, E'' being the viscous modulus. Furthermore, the results have shown that the relaxed-response increases with increasing the filler fraction.

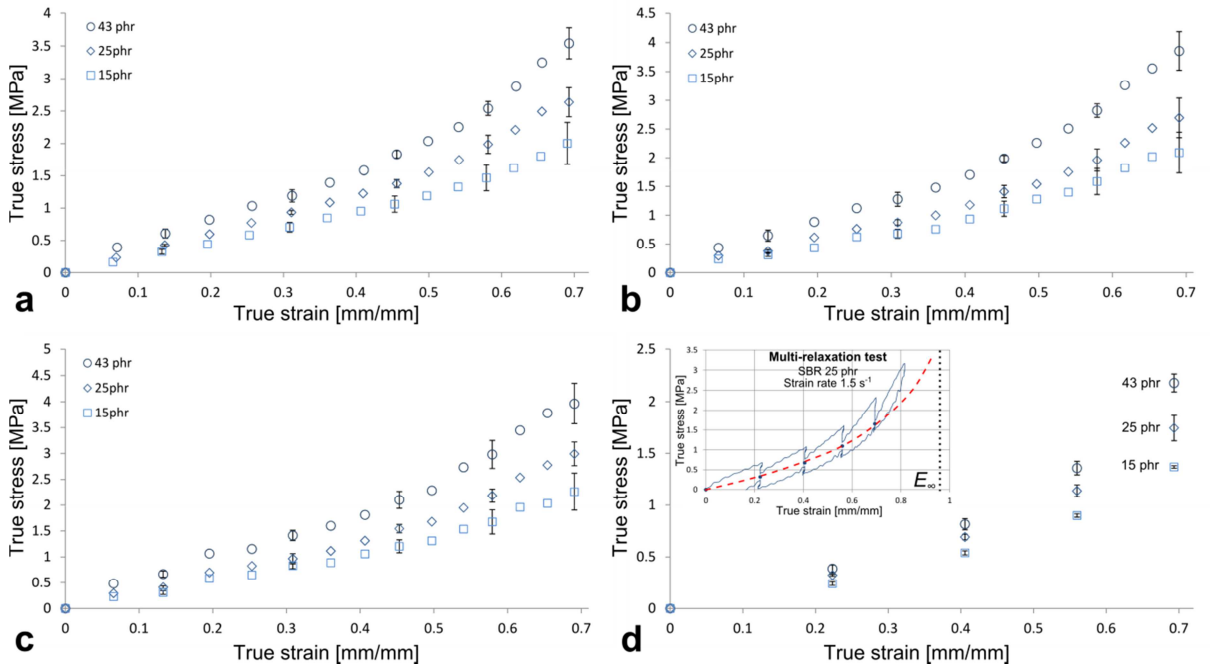

Fig. 4.3. Mechanical response of the SBR materials: Uniaxial response at different strain rates: (a) $1s^{-1}$; (b) $1.5s^{-1}$ and (c) $2s^{-1}$; and (d) Uniaxial relaxed response.

The continuous normalized stress-softening during fatigue tests for two applied stretches is illustrated in **Fig. 4.4**. It can be seen that the stress decreases with the number of cycles (Ayoub et al., 2011a). Furthermore, the experiments have shown that the normalized stress increases with increasing stretch (Ayoub et al. 2014). Moreover, the relation between the filler volume fraction and the normalized stress seems to be more complex, e.g. the normalized stress of the SBR43 seems to increase slowly with increasing stretch, while the normalized stress of the SBR15 increase significantly with increasing stretch. Then, it is possible to establish that a higher filler volume fraction is related to a quasi stretch-independent normalized stress, while a smaller filler volume fraction corresponds to a stretch-dependent normalized stress.

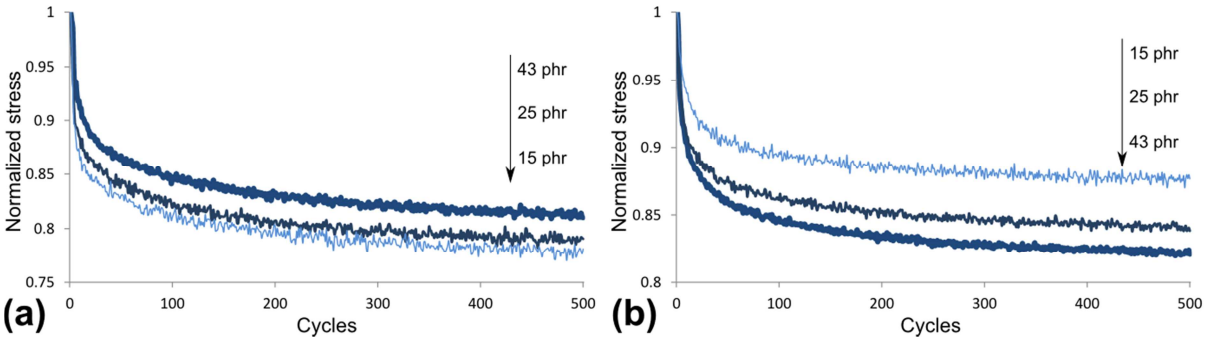

Fig. 4.4. Stress-softening for a strain rate of 1.5s^{-1}: (a) $\lambda_{11} = 1.25$, (b) $\lambda_{11} = 1.50$.

In **Figs. 4.5** and **4.6** is highlighted the surface temperature evolution due to material heat build-up in the gauge length of the SBR sample with 15, 25 and 43 phr. The heat build-up dependence regarding the strain rate, the filler fraction and the applied stretch-level during uniaxial tension is also evidenced. The experiments have shown that the temperature evolution is quite linear at the onset of the test then it evolves non-linearly towards a stabilized value which depends on the strain rate, the filler fraction and the maximum applied stretch. The stabilized temperature is linked to the stabilization of the hysteresis loop with the number of cycles (Bartolomé et al., 2013), i.e. the mean temperature of a material point becomes constant when the dissipated inelastic energy per loading cycle is equal to the amount of heat energy which is transferred to its environment. Furthermore, the data have shown that, independently of the filler fraction or the stretch level, the stabilized temperature increases with increasing strain rate (Lion, 1997a; Ovalle Rodas et al., 2014). The temperature-strain rate dependence is linked to the proportionality relation between the loss tangent and the strain rate, e.g. the loss tangent seems to increase with increasing strain rate (Medalia, 1978), and thus the hysteresis loop increases (Tomita et al., 2008; Luo et al., 2010). This phenomenon is due to friction at the molecular level: the stretch implicates a dragging of the polymeric chains, chain segments and crosslinks across the rubber compound. If the units are forced towards new sites faster than vacant sites (free volume of the rubber) are developed by thermal motion of the surrounding molecules, then the mechanical motion is turned into thermal random motion, i.e. heat energy. Note that, a smaller surrounding temperature has a

similar effect (Medalia, 1973), e.g. in the transition-zone the rubber starts becoming glassy; then it becomes impossible to drag units through it.

Besides, the experiments have shown that the heat build-up increases with the filler fraction (Medalia, 1991; Meinecke, 1991; Samaca Martinez et al., 2013). Due to the increase of the electrical conductivity with the carbon-black load, it has been evidenced that the filler in the rubber develops a network across the rubber compound (Pramanik et al., 1992), i.e. higher values of filler fraction are associated with an extensive network and a higher number of inter-aggregates links. As a consequence of the applied stretch, the inter-aggregates links are debonded, during each cycle, beginning with the weakest links (or those related with a higher local deformation) and progressing into the strongest ones. As the sample is deformed, the aggregates form new links in new positions, which are again broken and then reformed in other positions. Note that the reformation of inter-aggregates links is a hysteretic process which, in a typical filled rubber compound, is responsible of the major distribution of heat generation. On the other hand, the hysteresis increment with the carbon-black fraction can be explained by two phenomena:

- The addition of carbon-black is related to higher local strains, in the occluded rubber matrix, than the applied macroscopic strain (Trabelsi et al., 2003). As a consequence, the local hysteresis is different than the macroscopic hysteresis and, therefore, the heat generation at the local level can be higher in the points where the rubber is occluded.
- Explained by the breakdown and rebound of the links in the occluded rubber and in the rubber in a transition zone among the carbon-black and the occluded rubber, the addition of carbon-black increases the number of inter-aggregates interactions. A higher additional energy, than on bulk rubber, is dissipated with the breakdown and rebound of an inter-aggregate link, i.e. a higher carbon fraction is related to a higher number of interactions and, therefore, with a higher heat build-up (Kraus, 1984).

Furthermore, when rubber compounds with different carbon-black contents are compared, an extensive network is related with a higher loss tangent, i.e. a higher filler fraction is related to a higher heat generation.

Likewise, in **Figs. 4.5** and **4.6** is emphasized the effect of the stretch level on the heat build-up. The results have shown that the stabilized temperature increases with increasing stretch level. We can argue that, similarly to the previous observations on the strain rate and the filler fraction dependences, the temperature increase with the applied stretch can be due to the hysteresis loop which increases with the applied macroscopic stretch (Luo et al., 2010); nevertheless, for λ_{11} = 1.5 a mesoscopic phenomenon turns relevant: the breakdown and rebounding of the network aggregates, similar to the filler fraction dependence. Therefore, for λ_{11}> 1.25 the breakdown and reformation phenomenon of inter-aggregates bonds is the major mechanism responsible for the heat generation (Medalia, 1991).

To summarize, the experimental data have shown that: (1) The filled-SBR material response is dependent on the strain rate and the filler fraction; (2) under relaxation periods both in loading and in unloading conditions the stress tends to the same stabilized relaxed-stress, function of the stretch level; (3) the stress-softening is dependent on the stretch level and the filler fraction; (4) the heat build-up is dependent on the strain rate, the stretch level and the filler fraction.

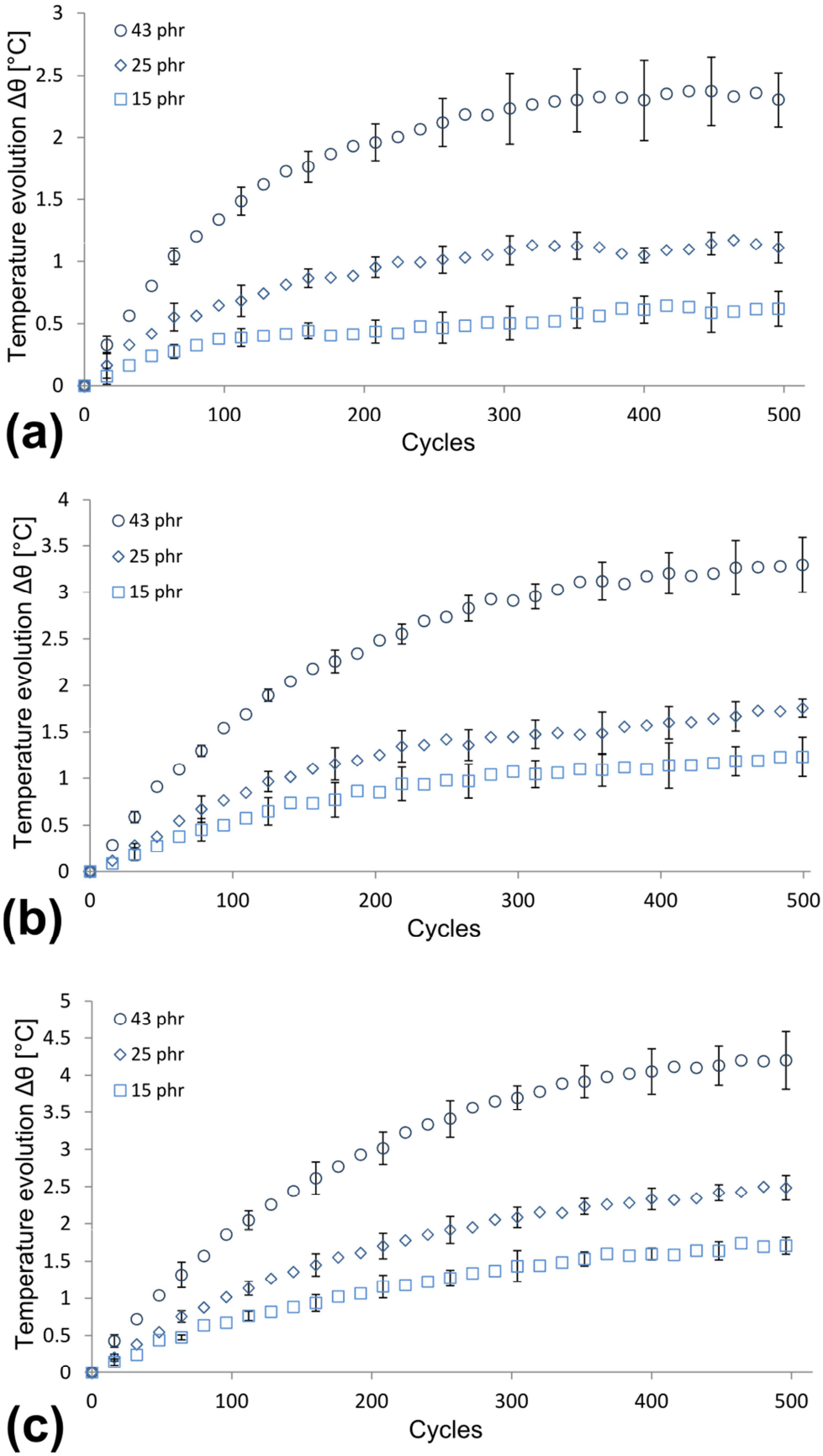

Fig. 4.5. Heat build-up at different strain rates, $\lambda_{11} = 1.25$: (a) $1s^{-1}$; (b) $1.5s^{-1}$ and (c) $2s^{-1}$.

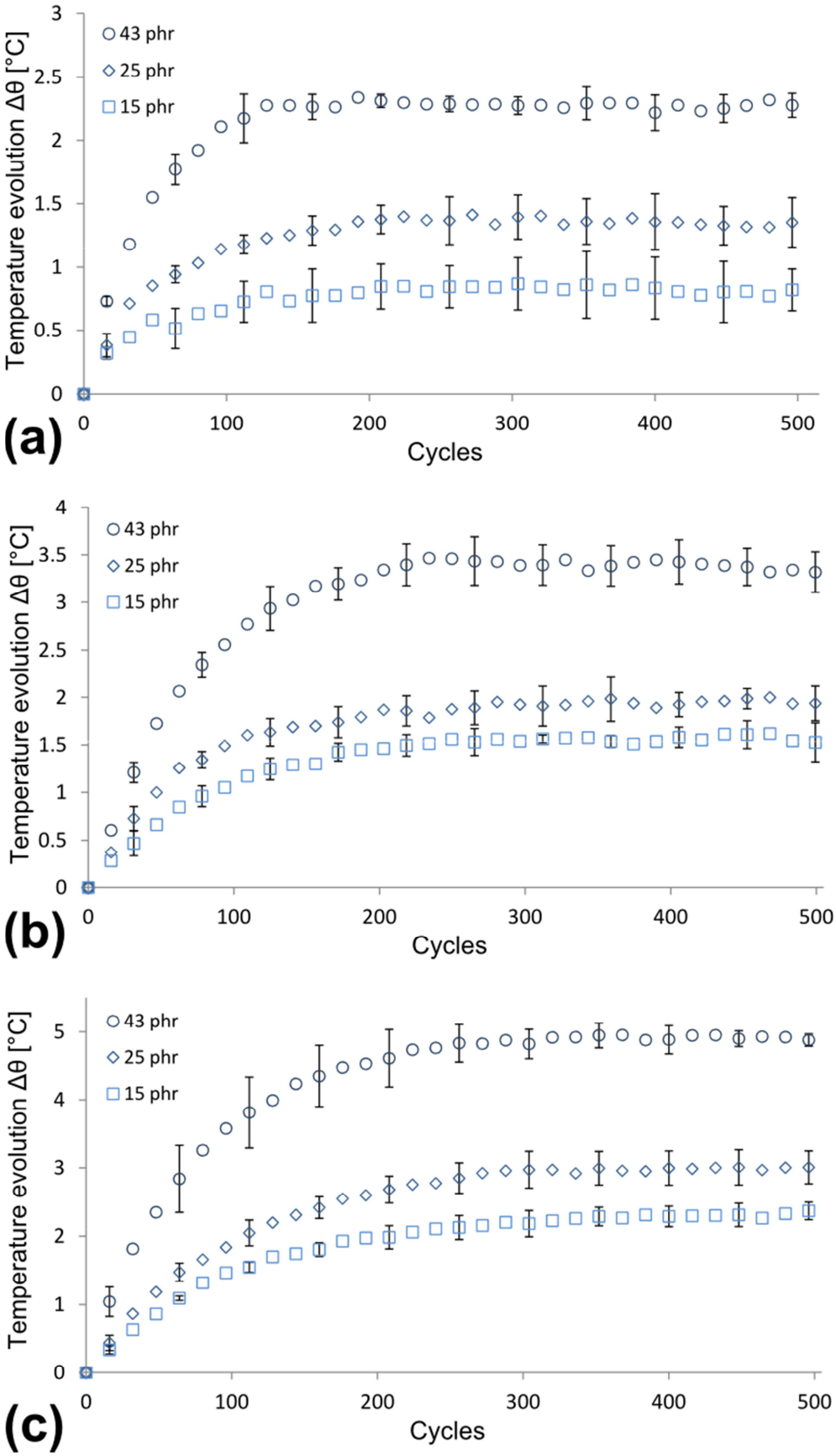

Fig. 4.6. Heat build-up at different strain rates, $\lambda_{11} = 1.50$: (a) $1s^{-1}$; (b) $1.5s^{-1}$ and (c) $2s^{-1}$.

4. Parameters identification

The needed material properties for the proposed thermo-mechanical model are: the dilatation element parameter [α], the network parameters for the branch A [C_{rA},N_A,c] and the branch B [C_{rB},N_B], the time-dependent element parameters [η,m] and the viscosity parameter [μ_u].

Since the definition of the network parameters [C_{rA},N_A,C_{rB},N_B] remains unchanged from that proposed in the last chapter (see also Ovalle Rodas et al., 2014) only a summary of the constant values are presented (see **Table 4.2**).

4.1 Thermal dilatation response

The thermal expansion coefficient of the SBR material can be calculated by means of:

$$\alpha = \left(\frac{1}{L_0}\right)\left(\frac{dL}{d\theta}\right) = 3.6\times10^{-4}\,\mathrm{K}^{-1} \tag{4.48}$$

where L_0 is the initial axial length of the sample[26] and $dL/d\theta$ is the axial dilatation-absolute temperature slope. Similar results, for rubber-type materials, were observed (Kraus and Gruver, 1970; Thiele and Cohen, 1980; Holzapfel and Simo, 1996; Lion, 1997; Lion et al., 2014).

4.2 Relaxed response

Besides, the filler shape factor, c, is obtained through the adjustment of the best response by means of trial and error from the multi-relaxation tests. Note that this factor acts as an amplifier of the filler effect over the mechanical response, e.g. a higher value of the shape factor is related with a bigger separation between stress-strain curves of two different filler fractions.

[26] The material constants of Eq. (4.48) were detailed in *Chapter 2*. They were identified on experimental data obtained from a styrene-butadiene rubber in the form of hourglass-shaped samples.

4.3 Time-dependent response

The time-dependent property of the element *B*, *m*, is obtained through the adjustment of the best response by means of trial and error for a strain rate of 1.5 s^{-1} and $v_f = 0.144$ (SBR25)[27]. By comparing the model predictions with experimental data from one additional single cycle test at a strain rate of 1 s^{-1}, the η parameter can be adjusted.

4.4 Viscosity parameter

The viscosity parameter, μ_u, for a given maximum strain, is obtained in the same way as *m*.

4.5 Material parameters

The described procedure allows estimating the thermo-mechanical variables values for the SBR material which are reported in **Table 4.2**. Elsewhere, the remaining thermal parameters $[h, \rho C]$ values have been taken from the literature (Bérardi et al., 1996).

	Mechanical model parameters		**Thermal properties**	
	Equilibrium response *A*	Time-dependent response *B*		
$C_{rA,B}$ [MPa]	0.265	0.795	α [K^{-1}]	3.6×10^{-4}
$N_{A,B}$	6.0	1.2	k [W m^{-1} K^{-1}]	0.127
c [$s^{-1}(MPa)^{-m}$]	2.0		ρC [J m^{-3} K^{-1}]	0.7×10^{6}
η [$(Pa\ s)^{-1}$]		1.65×10^{-6}	h [W m^{-1} K^{-1}]	17.0
m		2		

Table 4.2. Mechanical model parameters and thermal properties.

Finally, the viscosity parameter acquires the following values: $\mu_u(\lambda_{11}=1.25) = 0.063$ and $\mu_u(\lambda_{11}=1.5) = 0.037$.

[27] As already mentioned in *Chapter* 2, the filler volume fraction is calculated from: $v_f = phr\left[\rho_f \left(100/\rho_{matrix} + phr/\rho_f\right)\right]^{-1}$ where $\rho_f = 1.8 \times 10^3$ kg m^{-3} (Abe et al., 2003) is the carbon-black density, $\rho_{matrix} = 1.21 \times 10^3$ kg m^{-3} (Wood et al., 1943) is the matrix density and $phr = [15, 25, 43]$.

The constitutive model does not account for the mechanical properties dependence on the temperature. This assumption, which greatly simplifies the model, is reasonable since in the experiments we have achieved, the temperature increase measured at the surface is relatively small. Moreover, since the maximum true stress does not vary significantly as a function of the number of cycles (see **Fig. 4.4**); the stress-softening characteristics for the present application have not been considered.

5. Finite element implementation

The proposed constitutive model has been implemented by means of a coupled thermo-mechanical user subroutine into an advanced non-linear FE software, MSC.Marc (MSC.Marc, 2004a). In a previous work (Ovalle Rodas et al., 2014) a satisfactory visco-elastoplastic subroutine has been used; nevertheless, this subroutine has some limitations regarding the model formulation:

- The proposed model is a strain energy density function-based model whereas the subroutine requests the writing of all variables uniquely as tensors.
- The subroutine requests the increment of the tensor variables whereas the energy function offers a mean to calculate the instantaneous tensor variables.
- The plastic-related commands of the subroutine must be neglected, even if they must be defined at every mechanical step.

The effect of the limitations corresponds to a higher processing time. In order to reduce the simulation time, a visco-hyperelastic subroutine has been used. This subroutine allows the writing of an algorithm, by means of strain energy functions, from which the variables of a given element that will be written in the post-processing reading file are defined (MSC.Marc, 2004b). Moreover, the nearly incompressible behavior of filled rubbers is taken into account implicitly by the

visco-hyperelastic subroutine. On the other hand, the intrinsic dissipation due to the thermo-mechanical coupling has been defined by means of an internal heat generation subroutine (MSC.Marc, 2004b) which allows the definition of the heat build-up due to the inelastic energy dissipation.

The main steps of the FE calculation, in the form of a flowchart, are summarized in **Fig. 4.7a**. During a numerical step, the mechanical subroutine is called at the beginning of each increment. In order to provide the variables requested by the mechanical subroutine, the strain energy density function (4.42), and its first and second invariant derivatives are calculated. First of all, the deformation gradient tensor can be calculated by means of the numerical expression (Souza Neto et al., 2008):

$$\mathbf{F}_i = \exp\left(\mathrm{Ln}\left(\mathbf{F}_i\right)\right) = \sum_{j=0}^{\infty} \frac{1}{j!}\left(\mathrm{Ln}\left(\mathbf{F}_i\right)\right)^j \tag{4.49}$$

where $\mathrm{Ln}\left(\mathbf{F}_i\right)$ is the deformation tensor given by the numerical code at the beginning of the increment. On the other hand, the current elastic deformation gradient of the branch *B* can be calculated by means of the expression:

$$\mathbf{F}^e_{B\_i} = \mathbf{F}_i \left(\mathbf{F}^v_{B\_i}\right)^{-1} \tag{4.50}$$

where $\mathbf{F}^v_{B\_i}$ is the viscous deformation tensor that was saved at the end of the last increment and that can be called at the beginning of the current one. Furthermore, the viscous deformation rate tensor $\dot{\mathbf{F}}^v_{B\_i+1}$ and the viscous deformation tensor $\mathbf{F}^v_{B\_i+1}$ of the element *B* can be updated from Eqs. (4.8) and (4.9):

$$\dot{\mathbf{F}}^v_{B\_i+1} = \mathbf{F}^{e-1}_{B\_i}\mathbf{D}^v_{B\_i+1}\mathbf{F}_{B\_i} \tag{4.51}$$

$$\mathbf{F}^v_{B\_i+1} = \dot{\mathbf{F}}^v_{B\_i+1}\Delta t + \mathbf{F}^v_{B\_i} \tag{4.52}$$

where $\mathbf{D}^v_{B\_i+1}$ is the viscous stretching rate at the end of the increment and Δt is the time increment. The viscous deformation tensor at the end of the current increment has been stored by the user on a [*m*,*nn*,*x*] matrix where *m* is the element number, *nn* is the node and *x* is the tensor direction number; later, at the beginning of the next

increment, reading of the calculated values of the previous increment is therefore available.

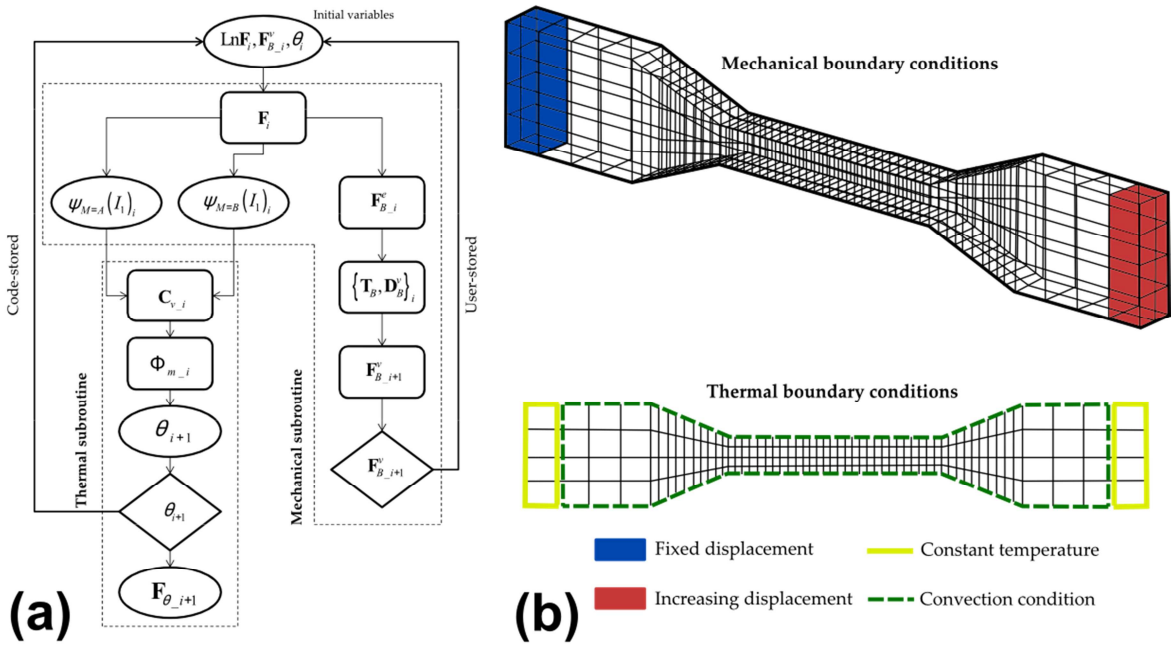

Fig. 4.7. FE implementation: (a) Flowchart of the thermo-mechanical algorithm, (b) simulation model[28] and boundary conditions.

The instantaneous time rate of the viscous dilatation tensor $\dot{\mathbf{C}}_{v\_i}$, given in Eqs. (4.35) and (4.36), can be calculated for each element by means of the strain energy density functions shared by means of a common block with the internal heat generation subroutine at the end of each increment. Next, the mechanical dissipation given in Eq. (4.25) is determined. Then, from the solution of the first thermodynamics principle and the boundary conditions of the studied case, the new temperature is calculated. The absolute temperature is a code-stored variable that is used to determine the thermal deformation gradient at the end of the current increment.

The FE model was designed according to the dimensions of the test sample (**Fig. 4.2**) using 3D 8-node meshing elements, isoparametric and arbitrarily hexahedrics.

[28] The simulation model was composed of 848 meshing elements corresponding to 1350 nodes.

To simulate the test conditions, one end of the sample was fixed, $u_{x1}=0$, the other end being subjected to an increasing displacement, $u_{x2}=u(t)$, as shown in **Fig. 4.7b**. The strain rate was controlled by the time function $u_{x2}=u(t)$. The cyclic loading condition has been simulated by repeating n times a single loading-unloading test under a constant strain rate, n being the total number of cycles. Concerning the thermal boundary conditions of the test, a constant temperature $\theta=\theta_0$ was applied, at both ends of the sample and a convection heat transfer condition, $\mathbf{q}=\mathbf{q}_s$, in the remaining frontiers:

$$\mathbf{q} = -h\left(\theta - \theta_\infty\right)\vec{n} \tag{4.53}$$

where h is the convection coefficient, θ_∞ is the room temperature, taken as a constant, and $\vec{n}$ is the normal vector to the surface of the element.

6. Model verification

The proposed constitutive model presented in Section 2 can be now compared with the experimental data of Section 3.1.3. In **Fig. 4.8** the stress-strain responses given by the proposed model and the experiments are shown for a material point taken on the gauge length of the sample surface. Note that, except the relaxed-response parameters, the model identification is performed using the SBR25 results obtained at a strain rate of 1.5 s^{-1}. A good agreement with the experimental data is pointed out and the model capabilities to predict the filler content and strain rate effects are highlighted.

The predicted temperature evolution due to heat build-up of the filled rubbers (SBR43, SBR25 and SBR15) for three strain rates is presented in **Figs. 4.9** and **4.10** for λ_{11}= 1.25 and λ_{11}= 1.5, respectively. The FE results are compared to the experimental data. Note that, for simplicity reasons, only the mean value of the temperature[29] is

[29]In a previous work (Ovalle Rodas et al. 2014) the capability of the thermo-mechanical model to describe the well-known oscillating temperature, depending on both components of the stretch (elastic and viscous components) during cyclic loading has been shown.

taken into account to contrast the simulation model results with the experimental data. The proposed model potential to take into account explicitly the filler fraction effect is highlighted. Note that, for λ_{11}= 1.25, the results show that the model captures in a satisfactory manner the temperature evolution due to heat build-up. However, for λ_{11}= 1.50 and higher filler fractions, a small difference between the experimental data and the simulation model predictions can be seen. This difference is related to the stiffer effect of high filler fractions on the model under large strains. Moreover, a higher filler fraction, up to v_f = 0.25, is linked to a higher heat conductivity (Frumkin and Dubinker, 1940) whereas, in the present work, a constant heat conductivy factor has been used. Note that, a higher heat conductivity factor corresponds to a higher capacity to extract heat energy, i.e. lower heat build-up, and vice-et-versa concerning the SBR15.

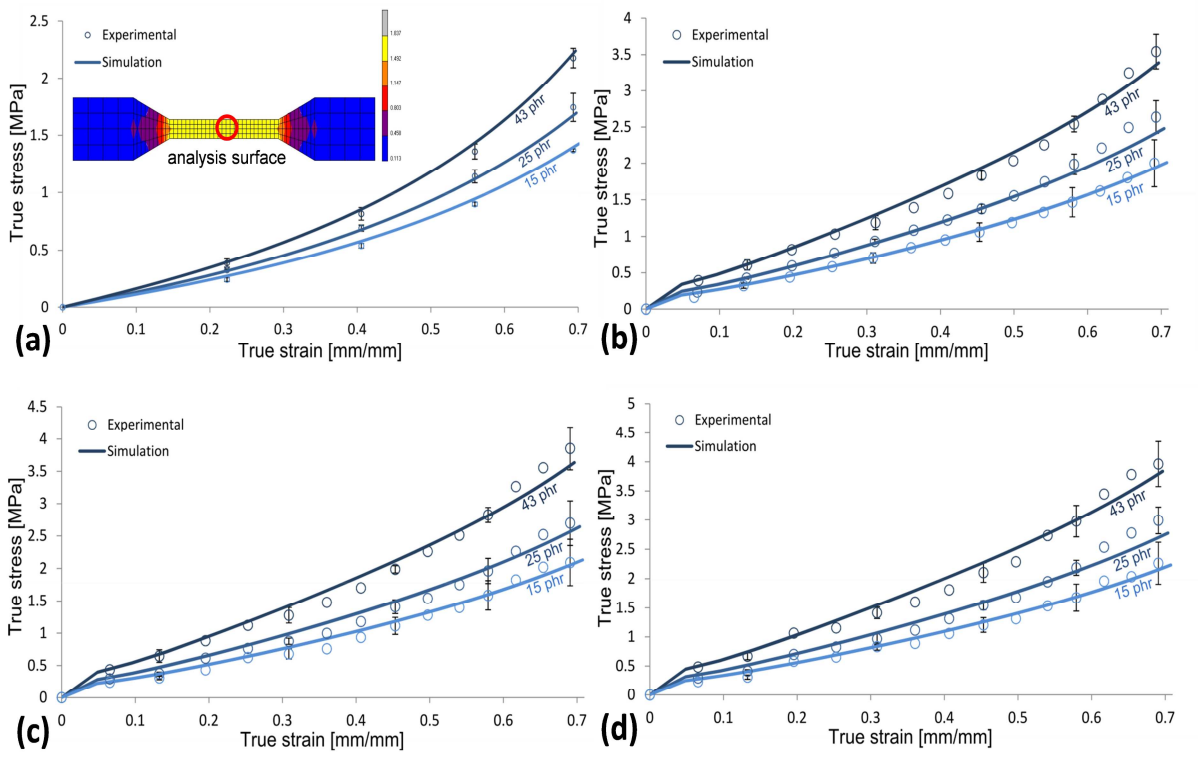

Fig. 4.8. Predicted and experimental mechanical response: (a) Uniaxial relaxed response; uniaxial response at different strain rates: (b) $1s^{-1}$; (c) $1.5s^{-1}$ and (d) $2s^{-1}$.

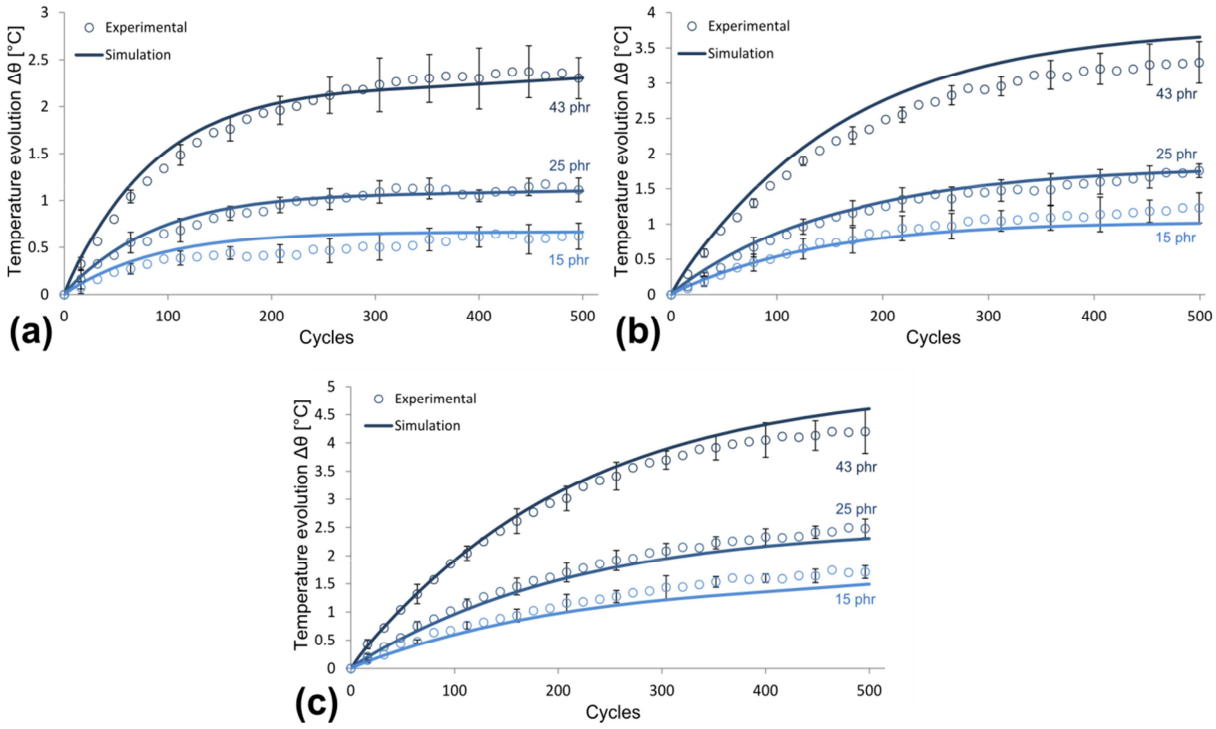

Fig. 4.9. Predicted and experimental heat build-up at different strain rates, λ = 1.25:

(a) $1s^{-1}$; (b) $1.5s^{-1}$ and (c) $2s^{-1}$

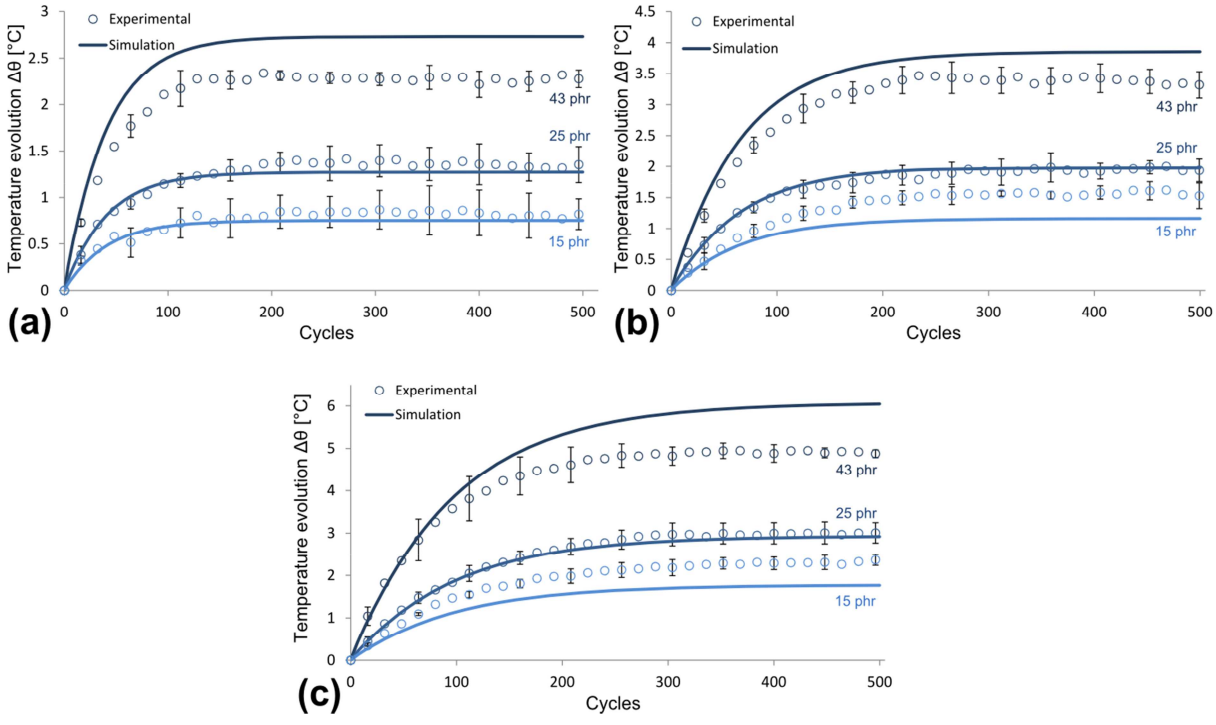

Fig. 4.10. Predicted and experimental heat build-up at different strain rates, λ = 1.50:

(a) $1s^{-1}$; (b) $1.5s^{-1}$ and (c) $2s^{-1}$

In **Fig. 4.11** the temperature field, due to heat build-up, inside the simulation model for different filler fractions is shown. The graph illustrates the temperature evolution predictions at different points, in the center and on the surface, of the cross-section. The results highlight a significant temperature gradient inside the sample, e.g. the temperature in the center is higher than the temperature on the surface. This time-stabilized gradient is related to the low heat conductivity property of filled rubbers. Thus, it is reasonable to assume that for a thicker specimen the heat build-up in its center could be sufficiently important to modify the mechanical behavior of the material (Johlitz et al., 2014). Besides, it has been shown (Gent and Hindi, 1988) that the higher temperature in the core is related with the internal blowout of cylindrical rubber specimens under repeated compression loads. As a perspective, defining mechanical variables as temperature-dependent is intended (e.g. Khan et al., 2006; Laiarinandrasana et al., 2009; Zaïri et al., 2010; Ovalle Rodas et al., 2015).

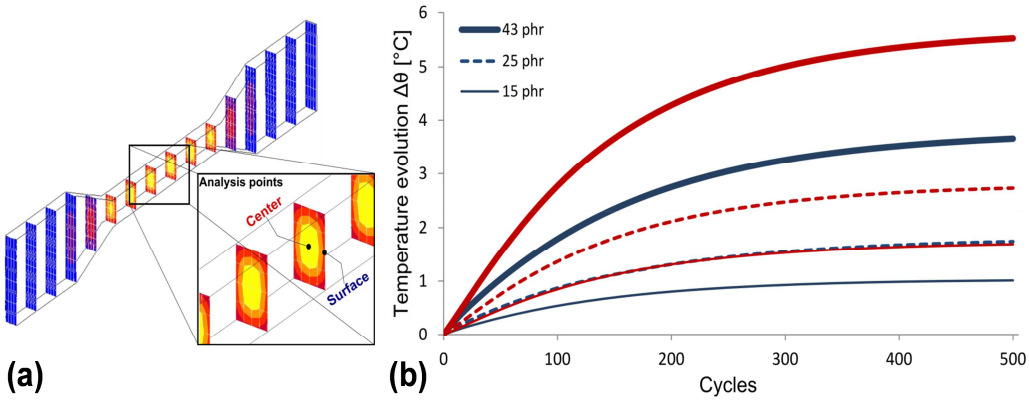

Fig. 4.11. Cross-section temperature distribution at the 500th cycle with a strain rate of 1.5 s^{-1} and $\lambda_{11} = 1.25$: (a) cross-section and analysis points, (b) temperature evolution at the center and at the surface of the sample.

7. Predictive capabilities of the thermo-mechanical model

The proposed constitutive model presented in Section 2 is now used to predict the heat build-up due to fatigue on the AE2 and AE42 samples. Note that the same

thermo-mechanical boundary conditions regarding the ones used to simulate the flat samples behavior were defined.

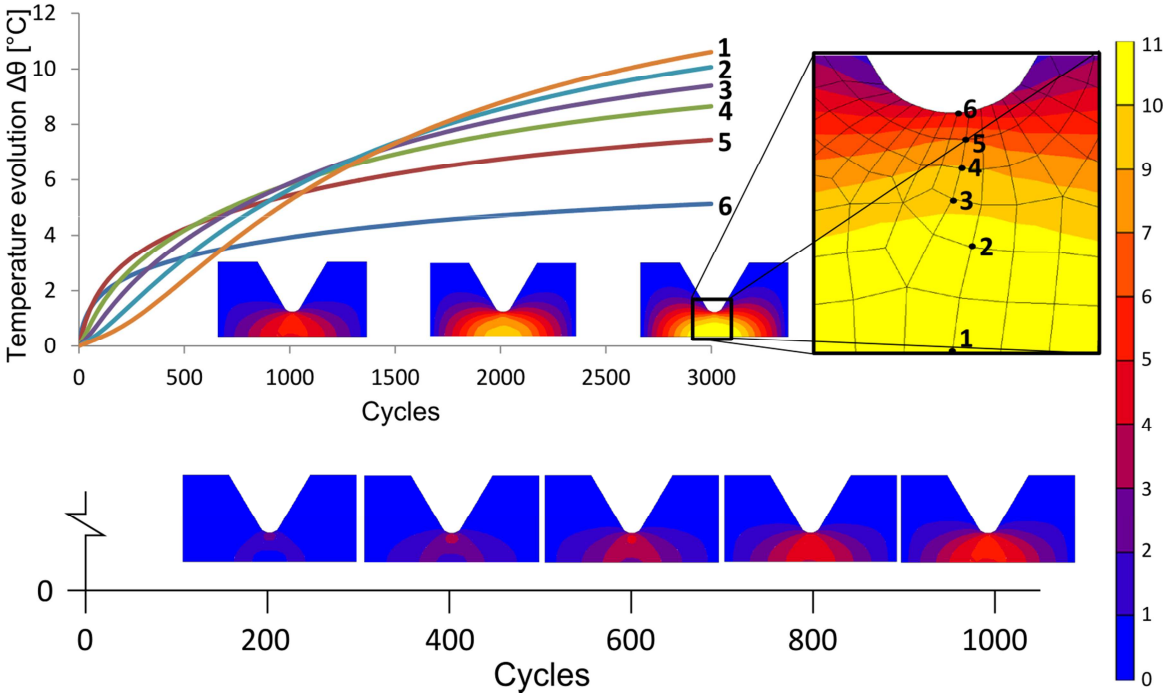

Fig. 4.12. Heat build-up in an AE2 test sample under simulated fatigue at a frequency of 5 Hz and $\lambda_{11}=1.1$.

The heat build-up due to fatigue on the AE2 and AE42 filled rubber samples are shown in **Figs. 4.12** and **4.13**, respectively. The computed temperature evolutions of material points along the minimum section of both test samples as well as the evolutions of the inner temperature fields are presented. The numerical results highlight a significant difference between the surface and center temperatures of the test samples. In the AE2 sample the temperature in the center is at least two times higher than the temperature on the surface whereas, in the AE42 sample, the temperature in the center is at least four times higher than the temperature on the surface. This difference could be linked with the different heat transfer mode acting in the sample. In the surface, the amount of heat transfer is related with the capacity of the material to dissipate heat to its surroundings by convection whereas, in the center, the heat transfer made by conduction and related with the ability of the material to conduct heat from one material point to another one. It is clear that the

amount of heat dissipated by convection is more important so that a temperature gradient appears in the bulk material.

On the other hand, the simulations results highlight a time-dependent temperature field, i.e. the position of the material point with the highest temperature in the sample depends on the cycle (e.g. at the 600th cycle the highest temperature is found between the surface and the center of the sample). This behavior could be explained by the dependence of the heat build-up with the maximum strain (Ovalle Rodas et al., 2014) as the local response is a position-dependent variable (see *Chapter 2*, Section 4.1). Besides, the position of the highest temperature in the center of the sample after a certain number of cycles could be explained by the quasi-adiabatic behavior of this region, i.e. the low heat conductivity capacity of rubber materials. The center area could be seen as a heat reservoir where the heat energy can be stored. Gent and Hindi (1988) have experimentally observed for cylindrical rubber specimens under repeated compression that the heat stored is related with an internal blowout due to the higher temperature in the core.

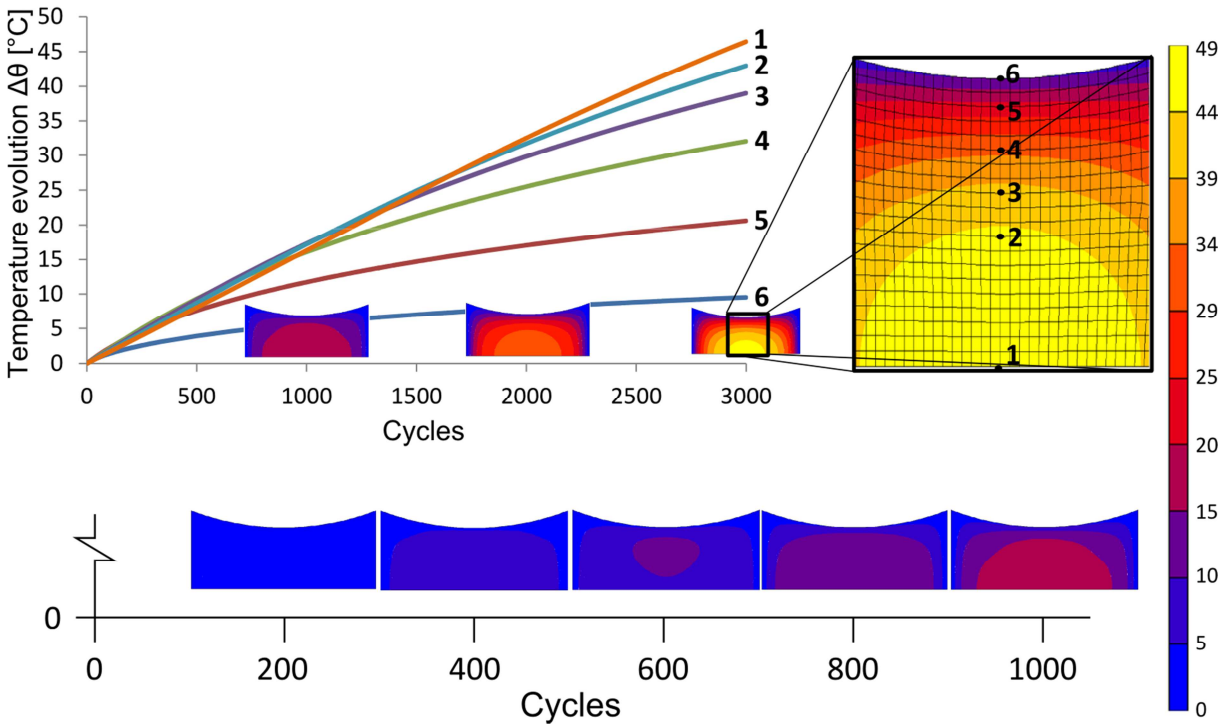

Fig. 4.13. Heat build-up in an AE42 test sample under simulated fatigue at a frequency of 5 Hz and λ_{11} =1.1.

In **Fig. 4.14** the temperature fields, due to heat build-up, inside the simulation models are shown. The graph illustrates the temperature evolution predictions at different points, in the center and on the surface, of the cross-sections. The predictions highlight a small difference between the temperature evolutions on the surface of both samples whereas, in the center, the difference is significant. As already explained, the high temperature in the center of the AE42 sample could be explained by the low heat conductivity factor of the SBR material in parallel with the dimensions of the sample.

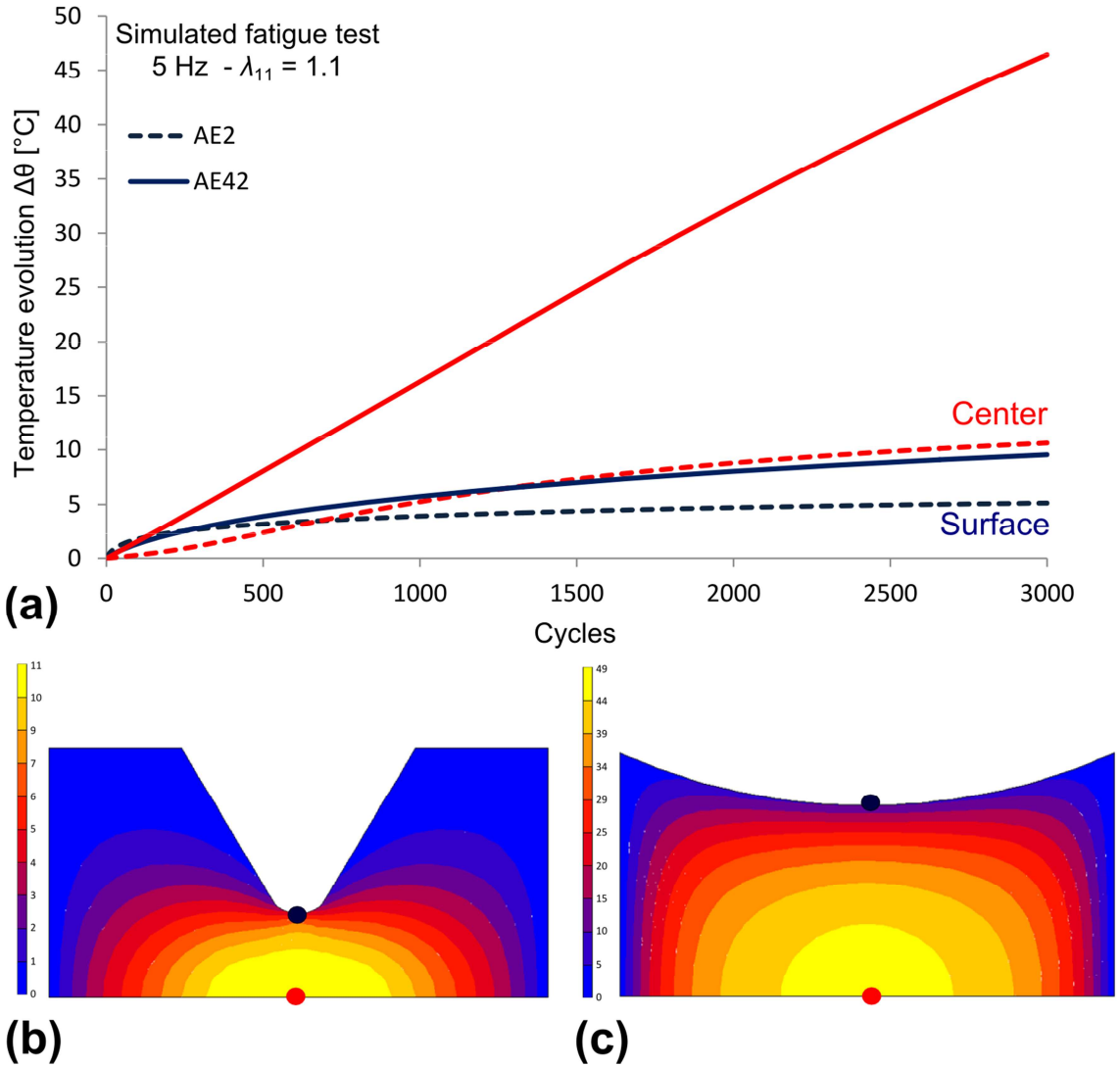

Fig. 4.14. Heat build-up evolution: (a) temperature evolution at the center and on the surface of the samples, (b) AE2 temperature field at the 3000th cycle and analysis points, (c) AE42 temperature field at the 3000th cycle and analysis points.

As shown in Section 2.1.7 of *Chapter 1*, the generalized continuum damage mechanics-based model proposed by Ayoub et al. (2012) to predict the rubber lifetime under multi-axial loading was unable to unify the experimental data issued from AE2 and AE42 samples. This was explained by the material heat build-up. As above evidenced, the operating temperature seems to be higher on the AE42 sample than on the AE2 sample (see **Fig. 4.14**), as a consequence a thermal degradation will have a higher effect on the lifetime under fatigue of the AE42 sample than on the AE2 sample, e.g. a lower lifetime of the AE42 sample for the same test conditions, see **Fig. 4.15**. Then, taking account of the heat build-up in the fatigue model is necessary. That could be done by, for example, using the time-temperature equivalence principle (Treloar, 1971).

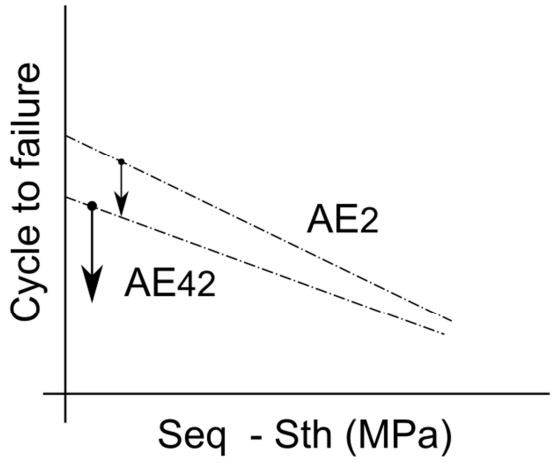

Fig. 4.15. Thermal effect on the generalized continuum damage mechanics-based model proposed by Ayoub et al. (2012).

8. Partial conclusions

In this chapter, a matrix-amplification inspired thermo-visco-hyperelastic constitutive model has been developed that allows for predictions of the heat build-up of filled rubbers during low-cycle fatigue. The model is based on the assumption that the thermo-mechanical behavior can be represented by the response of two networks acting in series: the first network captures the stress-free thermal-dilatation

state and the second one accounts for the large strain visco-elastic behavior, in which the mechanical response is the sum of a relaxed response and a time-dependent deviation regarding the relaxed response. Furthermore, the filler effect has been explicitly addressed by considering that at any given strain, the presence of the particles acts to locally amplify the strain and stress in the rubber compound over that of a corresponding unfilled rubber at the same macroscopic applied strain. On the other hand, in the thermo-mechanical coupling, the viscous dilation tensor related with the time-dependent deviation from the relaxed response is taken as an internal variable of the specific free energy potential. Since this free energy potential does not take into account the macroscopic maximum applied stretch to which the sample will be submitted, a stretch and filler volume fraction-dependent viscosity parameter was included.

The thermo-mechanical model, implemented into a FE code by means of a strain energy function subroutine in parallel with an internal heat generation subroutine, has been validated by comparing the simulations and experimental data of a SBR filled with different amounts of carbon-black submitted to different loading conditions.

It has been shown that the proposed model offers satisfactory predictions of both the mechanical behavior and the heat build-up.

Finally, the predictive model capability to describe the heat build-up of cylindrical samples during fatigue as well as its effect on the rubber lifetime has been highlighted.

GENERAL CONCLUSIONS

This PhD dissertation is a contribution to the thermo-mechanical coupling of filled rubbers. Both the stress-temperature relationship and the heat build-up due to thermo-mechanical coupling were investigated. The effect of the filler volume fraction over the thermo-mechanical response was explicitly taken into account.

In *Chapter 2*, a combined approach including experimental investigation, constitutive modeling and micromechanical FE simulations were developed to study the temperature-dependent relaxed response of a carbon-black filled SBR. Based on experimental observations, a network kinetics was introduced into a large strain mechanical model to account for the thermal effects. Micromechanical simulations have shown that the strain amplification introduced into the thermo-mechanical model is an adequate method to take into consideration the presence of fillers. The thermo-mechanical model, implemented into a FE code by means of a strain energy function subroutine, was validated by comparing the simulation and experimental load-displacement curves obtained on hourglass-shaped specimens. Besides, a hybrid experimental-numerical method was proposed to determine simultaneously the thermo-mechanical response in the median cross-section of the hourglass-shaped specimen and the model parameters. The decreasing temperature-dependence of the relaxed response of the SBR material was well reproduced by the proposed thermo-mechanical model.

In *Chapter 3*, a large strain thermo-viscoelastic constitutive model to describe the heat build-up of rubber materials during low-cycle fatigue response was highlighted. The model is based on the assumption that the mechanical behavior can be

represented by the response of two networks acting in parallel: the first network captures the relaxed state and the second one accounts for the time-dependence deviation with regard to the relaxed response. In the thermo-mechanical coupling, it was considered that the specific free energy potential was a function of the deformation gradient tensor, the instantaneous temperature, and the viscous dilation tensor, taken as an internal variable that is related with the time-dependent deviation from the equilibrium response. Since this free energy potential does not take into account the maximum strain to which the sample will be submitted, a strain-dependent viscosity parameter was included. This model was implemented in a FE code and the numerical simulation results were compared with experimental data for a SBR submitted to different loading conditions. Finally, it was shown that the constitutive model offers satisfactory predictions of both the mechanical behavior and the heat build-up.

Finally, in *Chapter 4*, the proposed thermo-mechanical model presented in *Chapter 3* was modified to take explicitly into account the filler volume fraction effect on the heat build-up. Moreover, the stress-free thermal-dilatation was also taken into account. The proposed model is fully three-dimensional and was implemented into a finite element code. The model parameters were identified using experimental data obtained on a SBR with a fixed amount of carbon-black, 25 phr, under a given strain rate for different strain conditions. Predicted evolutions given by the model for other strain rates and amounts of carbon-black, 15 and 43 phr, were found in good agreement with experimental data. The model capability to predict the heat build-up of cylindrical samples during fatigue as well as its effect on the rubber lifetime was discussed.

RESEARCH PERSPECTIVES

The results of the present work open the way to several perspectives: since it was observed the non-linear temperature-dependence of the chain-scale variables, the modification of the linear phenomenological model to a function which considers the slope change for higher temperatures and which takes into account explicitly the effect of the filler could expand the scope of the proposed model. Furthermore, the coupled effect of the temperature and the filler volume fraction on the time-dependent response of the material could enhance the capability of the model.

On the other hand, since it was observed that the heat build-up increases with the strain rate, the strain level or the filler volume fraction, the inclusion of the temperature-dependence of the chain-scale variables is suitable. Besides, notice that, a higher temperature is related with a smaller hysteresis loop. Likewise, the hysteresis loop characteristics depend upon the analysis material point, as a consequence of the inner temperature gradient. Thereafter, the experimental verification and study of an inner temperature field will bring light about the heterogeneous thermo-mechanical behavior of the material. Additionally, introducing the maximum strain as an internal variable in the formulation of the specific free energy potential could reasonably improve the scope of the model.

The model capability to describe and predict the heat build-up of filled rubbers during low-cycle fatigue for different loading conditions is a subject to be investigated.

In order to understand the thermo-mechanical origins of the material stress-softening due to cyclic loading, the study of the time-effect of the heat build-up on

the stress will bring some light about. Besides, the thermo-mechanical model scope could be improved by considering the heat build-up path from the reference configuration until failure. Then, the proposed model could be enhanced by adding the well known sudden heat build-up before failure.

Since the thermal degradation could play an important role as the sample mass, the strain rate, the strain level or the filler volume fraction is increased, the heat build-up effects on the material lifetime is an additional subjected to be investigated. Finally, the potential of the model to predict the material heat build-up due to crack initiation or crack growth is a subjected to be studied.

Finally, the generalized continuum damage mechanics-based model used to predict the rubber lifetime under multiaxial fatigue can be strengthened by including the thermal effects. In a first step, that could be done by using the time-temperature equivalence principle.

ANNEX A: THERMO-MECHANICAL DISSIPATION POTENTIAL

Let us define the specific internal energy e in terms of the specific entropy η, the absolute temperature θ and the specific free energy ψ, as follows (see Eq. (1.45)):

$$e = \psi + \theta\eta \tag{A.1}$$

where

$$\psi\left(\mathbf{F},\theta,\mathbf{C}_v\right) = \psi_M\left(\mathbf{F},\theta,\mathbf{C}_v\right) + \psi_\theta\left(\theta\right) \tag{A.2}$$

Then, substituting $\eta = -\partial\psi/\partial\theta$ into (A.1) returns

$$e = \psi - \theta\frac{\partial\psi}{\partial\theta} \tag{A.3}$$

Inserting the expression for the time rate of the specific free energy (see Eq. (1.48)), i.e.

$$\dot{\psi} = \frac{\partial\psi_M}{\partial\mathbf{F}} : \dot{\mathbf{F}} + \frac{\partial\psi_M}{\partial\mathbf{C}_v} : \dot{\mathbf{C}}_v + \frac{\partial\psi}{\partial\theta}\dot{\theta} \tag{A.4}$$

into the time rate of the specific internal energy:

$$\dot{e} = \dot{\psi} - \dot{\theta}\frac{\partial\psi}{\partial\theta} - \theta\frac{d}{dt}\left(\frac{\partial\psi}{\partial\theta}\right) \tag{A.5}$$

leads to the following relations:

$$\dot{e} = \frac{\partial\psi_M}{\partial\mathbf{F}} : \dot{\mathbf{F}} + \frac{\partial\psi_M}{\partial\mathbf{C}_v} : \dot{\mathbf{C}}_v + \frac{\partial\psi}{\partial\theta}\dot{\theta} - \dot{\theta}\frac{\partial\psi}{\partial\theta} - \theta\frac{d}{dt}\left(\frac{\partial\psi}{\partial\theta}\right) \tag{A.6}$$

$$\dot{e} = \frac{\partial\psi_M}{\partial\mathbf{F}} : \dot{\mathbf{F}} + \frac{\partial\psi_M}{\partial\mathbf{C}_v} : \dot{\mathbf{C}}_v - \theta\frac{d}{dt}\left(\frac{\partial\psi}{\partial\theta}\right) \tag{A.7}$$

Then, from the thermodynamics relations

$$\boldsymbol{\pi} = \rho\frac{\partial\psi_M}{\partial\mathbf{F}} \tag{A.8}$$

and

$$\mathbf{A}_v = \rho \frac{\partial \psi_M}{\partial \mathbf{C}_v} \tag{A.9}$$

Eq. (A.7) returns

$$\dot{e} = \frac{1}{\rho}\boldsymbol{\pi} : \dot{\mathbf{F}} + \frac{1}{\rho}\mathbf{A}_v : \dot{\mathbf{C}}_v - \theta \frac{d}{dt}\left(\frac{\partial \psi}{\partial \theta}\right) \tag{A.10}$$

$$\dot{e} = \frac{1}{\rho}\boldsymbol{\pi} : \dot{\mathbf{F}} + \frac{1}{\rho}\mathbf{A}_v : \dot{\mathbf{C}}_v - \theta\left[\frac{\partial^2 \psi}{\partial \mathbf{F}\partial\theta} : \dot{\mathbf{F}} + \frac{\partial^2 \psi}{\partial \mathbf{C}_v \partial\theta} : \dot{\mathbf{C}}_v + \frac{\partial^2 \psi}{\partial \theta^2}\dot{\theta}\right] \tag{A.11}$$

$$\dot{e} = \frac{1}{\rho}\boldsymbol{\pi} : \dot{\mathbf{F}} + \frac{1}{\rho}\mathbf{A}_v : \dot{\mathbf{C}}_v - \theta\frac{1}{\rho}\left[\frac{\partial \boldsymbol{\pi}}{\partial \theta} : \dot{\mathbf{F}} + \frac{\partial \mathbf{A}_v}{\partial \theta} : \dot{\mathbf{C}}_v\right] - \theta\frac{\partial^2 \psi}{\partial \theta^2}\dot{\theta} \tag{A.12}$$

Inserting this expression for the time rate of the internal energy into the standard formulation of the first law of thermodynamics, i.e.

$$\rho \dot{e} = \boldsymbol{\pi} : \dot{\mathbf{F}} - \operatorname{div}[\mathbf{q}] + \rho r \tag{A.13}$$

leads to the following relations:

$$\boldsymbol{\pi} : \dot{\mathbf{F}} + \mathbf{A}_v : \dot{\mathbf{C}}_v - \theta\left[\frac{\partial \boldsymbol{\pi}}{\partial \theta} : \dot{\mathbf{F}} + \frac{\partial \mathbf{A}_v}{\partial \theta} : \dot{\mathbf{C}}_v\right] - \rho\theta\frac{\partial^2 \psi}{\partial \theta^2}\dot{\theta} = \boldsymbol{\pi} : \dot{\mathbf{F}} - \operatorname{div}[\mathbf{q}] + \rho r \tag{A.14}$$

$$\mathbf{A}_v : \dot{\mathbf{C}}_v - \theta\left[\frac{\partial \boldsymbol{\pi}}{\partial \theta} : \dot{\mathbf{F}} + \frac{\partial \mathbf{A}_v}{\partial \theta} : \dot{\mathbf{C}}_v\right] - \rho\theta\frac{\partial^2 \psi}{\partial \theta^2}\dot{\theta} = -\operatorname{div}[\mathbf{q}] + \rho r \tag{A.15}$$

$$\rho C \dot{\theta} = -\mathbf{A}_v : \dot{\mathbf{C}}_v + \theta\left[\frac{\partial \boldsymbol{\pi}}{\partial \theta} : \dot{\mathbf{F}} + \frac{\partial \mathbf{A}_v}{\partial \theta} : \dot{\mathbf{C}}_v\right] - \operatorname{div}[\mathbf{q}] \tag{A.16}$$

In Eq. (A.16) the coefficient $C(\mathbf{F}, \theta, \mathbf{C}_v) = -\theta\frac{\partial^2 \psi}{\partial \theta^2}$ is the specific heat at constant deformation per unit mass and the heat supply per unit mass ρr is neglected.

REFERENCES

Abe, A., Dusek, K., Kobayashi, S., 2003. *Filler-Reinforced Elastomer - Scanning Force Microscopy*. Springer-Verlag Berlin Heidelber New York.

Aït Hocine, N., Hamdi, A., Naït-Abdelaziz, M., Heuillet, P., Zaïri, F., 2011. Experimental and finite element investigation of void nucleation in rubber-like materials. *International Journal of Solids and Structures* 48, 1248-1254.

Amin, A.F.M.S., Lion, A., Sekita, S., Okui, Y., 2006. Nonlinear dependence of viscosity in modeling the rate-dependent response of natural and high damping rubbers in compression and shear: Experimental identification and numerical verification. *International Journal of Plasticity* 22, 1610-1657.

Anthony, R., Caston, R., Guth, E., 1943. Equations of State for Natural and Synthetic Rubber-Like Materials. I Unaccelerated Natural Soft Rubber. *Rubber Chemistry and Technology* 16, 297-309.

Arruda, E., Boyce, M., 1993. A three-dimensional constitutive model for the large stretch behavior of rubber elastic materials. *Journal of the Mechanics and Physics of Solids* 41, 389-412.

Arruda, E., Boyce, M., Jayachandran, R., 1995. Effects of strain rate, temperature and thermomechanical coupling on the finite strain deformation of glassy polymers. *Mechanics of materials* 19, 193-212.

Ayoub, G., Zaïri, F., Naït-Abdelaziz, M., Gloaguen, J.M., 2010a. Modelling large deformation behaviour under loading-unloading of semicrystalline polymers: application to a high density polyethylene. *International Journal of Plasticity* 26, 329-347.

Ayoub, G., Naït-Abdelaziz, M., Zaïri, F., Gloaguen, J.M., 2010b. Multiaxial fatigue life prediction of rubber-like materials using the continuum damage mechanics approach. *Procedia Engineering* 2, 985-993.

Ayoub, G., Zaïri, F., Naït-Abdelaziz, M., J.M., Gloaguen, J.M., 2011a. Modeling the low-cycle fatigue behavior of visco-hyperelastic elastomeric materials using a new network alteration theory: Application to styrene-butadiene rubber. *Journal of the Mechanics and Physics of Solids* 59, 473-495.

Ayoub, G., Naït-Abdelaziz, M., Zaïri, F., Gloaguen, J.M., Charrier, P., 2011b. A continuum damage model for the high-cycle fatigue life prediction of styrene-butadiene rubber under multiaxial loading. *International Journal of Solids and Structures* 48, 2458-2466.

Ayoub, G., Zaïri, F., Fréderix, C., Gloaguen, J.M., Naït-Abdelaziz, M., Seguela, R., Lefebvre, J.M., 2011c. Effects of crystal content on the mechanical behaviour of polyethylene under finite strains: experiments and constitutive modelling. *International Journal of Plasticity* 27, 492-511.

Ayoub, G., Zaïri, F., Naït-Abdelaziz, M., J.M., Gloaguen, J.M., Charrier, P., 2012. Fatigue life prediction of rubber-like materials under multiaxial loading using a continuum damage mechanics approach: Effects of two-blocks loading and R ratio. *Mechanics of Materials* 52, 87-102.

Ayoub, G., Zaïri, F., Naït-Abdelaziz, M., Gloaguen, J.M., Kridli, G., 2014. A visco-hyperelastic damage model for cyclic stress-softening, hysteresis and permanent set in rubber using the network alteration theory. *International Journal of Plasticity* 54, 19-33.

Baranwal, K., Stephens, H., 2001. *Basic Elastomer Technology*. Rubber Division.

Bartolomé, L., Aurrekoetxea, J., Urchegui, M.A., Tato, W., 2013. The influences of deformation state and experimental conditions on inelastic behaviour of an extruded thermoplastic polyurethane elastomer. *Materials and Design* 49, 974-980.

Bérardi, G., Jaeger, M., Martin, R., Carpentier, C., 1996. Modelling of a thermo-viscoelastic coupling for large deformations through finite element analysis. *International Journal of Heat and Mass Transfer* 39, 3911-3924.

Bergström, J. S., 1999. *Large strain time-dependent behavior of elastomeric materials*. Thesis. Department of Mechanical Engineering, Massachusetts Institute of Technology, Cambridge, MA, United States.

Bergström, J. S., Boyce, M. C., 1998. Constitutive modeling of the large strain time-dependent behavior of elastomers. *Journal of the Mechanics and Physics of Solids* 46, 931-954.

Bergström, J., Boyce, M., 1999. Mechanical Behavior of Particle Filled Elastomers. *Rubber Chemistry and Technology* 72, 633-656.

Bergström, J., Boyce, M., 2000. Large strain time-dependent behavior of filled elastomers. *Mechanics of Materials* 32, 627-644.

Bischoff, J.E., Arruda, E.M., Grosh, K., 2001. A new constitutive model for the compressibility of elastomers at finite deformations. *Rubber Chemistry and Technology* 74, 541-559.

Blanchard, A., Parkinson, D., 1952. Breakage of carbon-rubber networks by applied stress. *Industrial Engineering Chemistry* 44, 799-812.

Boonstra, B., Medalia, A., 1963. Effect of Carbon Black Dispersion on the Mechanical Properties of Rubber Vulcanizates. *Rubber Chemistry and Technology* 36, 115-142.

Bouasse, H., Carrière, Z., 1903. Sur les courbes de traction du caoutchouc vulcanisé. *Annales de la faculté des sciences de Toulouse* 5, 257-283.

Bouchart, V., Brieu, M., Kondo, D., Naït-Abdelaziz, 2008. Implementation and numerical verification of a non-linear homogenization method applied to hyperelastic composites. *Computational Materials Science* 43, 670-680.

Boukamel, A., Méo, S., Débordes, O., Jaeger, M., 2001. A thermo-viscoelastic model for elastomeric behaviour and its numerical application. *Archive of Applied Mechanics* 71, 785-801.

Boyce, M., 1986. *Large inelastic deformation of glassy polymers.* Thesis. Department of Mechanical Engineering, Massachusetts Institute of Technology, Cambridge, MA, United States.

Boyce, M., Arruda, E., 2000. Constitutive models of rubber elasticity: A review. *Rubber Chemistry and Technology* 73, 504-523.

Boyce, M. C., Socrate, S., Llana, P. G., 2000. Constitutive model for the finite deformation stress-strain behavior of poly(ethylene terephthalate) above the glass transition. *Polymer* 41, 2183-2201.

Budiansky, B., 1965. On the elastic moduli of some heterogeneous materials. *Journal of the Mechanics and Physics of Solids* 13, 223-227.

Bueche, F., 1960. Molecular basis for the Mullins effect. *Journal of Applied Polymer Science* 4, 107-114.

Canadija, M., Mosler, J., 2011. On the thermomechanical coupling in finite strain plasticity theory with non-linear kinematic hardening by means of incremental energy minimization. *International Journal of Solids and Structures* 48, 1120-1129.

Clément, F., Bokobza, L., Monnerie, L., 2001. On the mullins effect in silica-filled polydimethylsiloxane networks. *Rubber Chemistry and Technology* 74, 847-870.

Cohen, A., 1991. A Padé approximant to the inverse Langevin function. *Rheologica Acta* 30, 270–273.

Cohen, R., Severson, S., Yu, C., Mark, J., 1977. Viscoelastic Properties of Polydimethylsiloxane Networks Prepared by Cross-Linking the Chains in Solution. *Macromolecules* 10, 663–667.

Dannenberg, E., 1952. Carbon Black Dispersion and Reinforcement. *Industrial, Engineering Chemistry* 44, 813–818.

Dannenberg, E., Brennan, J., 1965. Strain-energy as a criterion for stress softening in carbon-black-filled vulcanizates. *Rubber Chemistry and Technology* 39, 597-608.

de Cazenove, J., Rade, D.A., de Lima, A.M.G., Araújo, C.A., 2012. A numerical and experimental investigation on self-heating effects in visco elastic dampers. *Mechanical Systems and Signal Processing* 27, 433-445.

de Souza Neto, E.A., Peric, D., Owen, D.R.J., 2008. *Computational Methods for Plasticity: Theory and Applications*. John Wiley and Sons Publication.

Diani, J., Fayolle, B., Gilormini, P., 2009. A review on the Mullins effect. *European Polymer Journal* 45, 601-612.

Dillon, J., Prettyman, J., Hall, G., 1944. Hysteretic and Elastic Properties of Rubberlike Materials Under Dynamic Shear Stresses. *Journal of Applied Physics* 15, 309-323.

Doudard, C., Calloch, S., 2009. Influence of hardening type on self-heating of metallic materials under cyclic loadings at low amplitude. *European Journal of Mechanics A/Solids* 28, 233–240.

Drozdov, A.D., 2012. Stress and strain-controlled cyclic deformation of polypropylene. *Computational Materials Science* 64, 198-202.

Drozdov, A., Christiansen, J., 2009. Thermo-viscoplasticity of carbon black-reinforced thermoplastic elastomers. *International Journal of Solids and Structures* 46, 2298-2308.

Drozdov, A.D., Klitkou, R., Christiansen, J.C., 2013. Cyclic viscoplasticity of semicrystalline polymers with finite deformations. *Mechanics of Materials* 56, 53-64.

Ehrbar, J., Boissonas, C., 1955. The termal effect in the elongation and relaxation of rubber. *Rubber Chemistry and Technology* 28, 675-683.

Fargione, G., Geraci, A., La Rosa, G., Risitano, A., 2002. Rapid determination of the fatigue curve by the thermographic method. *International journal of fatigue* 24, 11-19.

Ferry, J., 1980. *Viscoelastic Properties of Polymers.* Wiley.

Fischer, E., Henderson, J., 1967. Effect of temperature on stress-optical properties of styrene butadiene block copolymers. *Rubber Chemistry and Technology* 40, 1373-1380.

Fletcher, W., Gent, A., 1957. Dynamic shear properties of some rubber-like materials. *British Journal of Applied Physics* 8, 194-201.

Flory, P., 1953. *Principles of polymer chemistry.* United States of America: Cornell University Press.

Flory, P., Rehner, J., 1943. Statistical mechanics of cross-linked polymer networks. *Journal of Chemistry and Physics* 11, 512-520.

Freund, M., Lorenz, H., Juhre, D., Ihlemann, J., Kluppel, M., 2011. Finite element implementation of a microstructure-based model for filled elastomers. *International Journal of Plasticity* 27, 902-919.

Frumkin, L., Dubinker, Y., 1940. The Heat Conductivity of Rubber. *Rubber Chemistry and Technology* 13, 361-374.

Fukahori, Y., 2005. New progress in the theory and model of carbon black reinforcement of elastomers. *Journal of Applied Polymer Science* 95, 60-67.

Gent, A., 1996. A New Constitutive Relation for Rubber. *Rubber Chemistry and Technology* 69, 59-61.

Gent, A., Hindi, M., 1988. Heat Build-Up and Blowout of Rubber Blocks. *Rubber Chemistry and Technolog* 61, 892-905.

Gough, J., 1805. A description of a property of Caoutchouc, or Indian rubber; with some reflections on the cause of the elasticity of this substance. In a letter to Dr. Holmf.. *Memoirs of the Literary and Philosophical Society of Manchester* 1, 288.

Govindjee, S., Simo, J., 1991. A micro-mechanically based continuum damage model for carbon black-filled rubbers incorporating Mullins' effect. *Journal of the Mechanics and Physics of Solids* 39, 87-112.

Guth, E., 1945. Theory of filler reinforcement. *Journal of Applied Physics* 16, 20-25.

Guth, E., Gold, O., 1938. On the hydrodynamical theory of the viscosity of suspensions. *Physical review* 53, 322.

Hakannson, P., Wallin, M., Ristinmaa, M., 2005. Comparison of isotropic hardening and kinematic hardening in thermoplasticity. *International Journal of Plasticity* 21, 1435–1460.

Hamed, G., Hatfield, S., 1989. On the role of bound rubber in carbon-black reinforcement. *Rubber Chemistry and Technology* 62, 143-156.

Hanson, D., Hawley, M., Houlton, R., Chitanvis, K., Rae, P., Orler, E.B., Wrobleski, D.A., 2005. Stress softening experiments in silica-filled polydimethysiloxane provide insight into a mechanism for the Mullins effect. *Polymer* 46, 10989-10995.

Hashin, Z., Shtrikman, S., 1963. A variational approach to the theory of the elastic behaviour of multiphase materials. *Journal of the Mechanics and Physics of Solids* 11, 127-140.

Haudin, J., 1995. *Introduction à la mécanique des polymères*. France: Institut National Polytechnique de Lorraine.

Haupt, P., 2002. *Continuum Mechanics and Theory of Materials*, 2nd ed. Springer-Verlag, Berlin Heidelberg GmbH.

Holt, W., 1931. Behaviour of Rubber under Repeated Stresses. *Industrial and Engineering Chemistry* 23, 1471–1475.

Holzapfel, G., Simo, J., 1996. Entropy elasticity of isotropic rubber-like solids at finite strains. *Computer Methods in Applied Mechanics and Engineering* 132, 17-44.

Houwink, R., 1956. Slipping of molecules during the deformation of reinforced rubber. *Rubber Chemistry and Technology* 29, 888-893.

James, H., Guth, E., 1943. Theory of the elastic properties of rubber. *Journal of Chemistry and Physics* 10, 455-481.

Johlitz, M., Diercks, N., Lion, A., 2014. Thermo-oxidative ageing of elastomers: A modelling approach based on a finite strain theory. *International Journal of Plasticity* 63, 138-151.

Jones, R., 2008. *Compendium of Polymer Terminology and Nomenclature*. United Kingdom: Royal Society of Chemistry.

Joule, J., 1859. On Some Thermo-Dynamic Properties of Solids. *Philosophical Transactions of the Royal Society of London* 149, 91-131.

Kamlah, M., Haupt, P., 1998. On the macroscopic description of stored energy and self heating during plastic deformation. *International Journal of Plasticity* 13, 893-911.

Kausch, H., Heymans, N., Plummer, C., Decroly, P., 2001. *Matériaux polymères : propiétés mécaniques et physiques*. France: Presses polytechniques et universitaires romandes.

Khan, A., Zhang, H., 2001. Finite deformation of a polymer: experiments and modeling. *International Journal of Plasticity* 17, 1167-1188.

Khan, A., Lopez-Pamies, O., Kazmi, R., 2006. Thermo-mechanical large deformation response and constitutive modeling of viscoelastic polymers over a wide range of strain rates and temperatures. *International Journal of Plasticity* 22, 581-601.

Khdir, Y.K., Kanit, T., Zaïri, F., Naït-Abdelaziz, M., 2013. Computational homogenization of elastic-plastic composites. *International Journal of Solids and Structures* 50, 2829-2835.

Khdir, Y.K., Kanit, T., Zaïri, F., Naït-Abdelaziz, M., 2014. Computational homogenization of plastic porous media with two populations of voids. *Materials Science and Engineering: A* 597, 324-330.

Klüppel, M., Schramm, M., 2000. A generalized tube model of rubber elasticity and stress softening of filler reinforced elastomer systems. *Macromolecular Theory and Simulations* 9, 742-754.

Kraus, G., 1978. Reinforcement of Elastomers by Carbon Black. *Rubber Chemistry and Technology* 51, 297-321.

Kraus, J., 1984. Mechanical losses in carbon black filled rubbers. *Journal of Applied Polymer science: Applied Polymer Symposia*.

Kraus, G., Childers, C., Rollman, K., 1966. Stress softening in carbon black reinforced vulcanizates. Strain rate and temperature effects. *Journal of Applied Polymer Science* 10, 229-240.

Kraus, G., Gruver, J., 1970. Thermal expansion, free volume, and molecular mobility in a carbon black-filled elastomer. *Journal of Polymer Science Part A-2: Polymer Physics* 8, 571–581.

Kuhn, W., Grün, F., 1942. Beziehungen zwischen elastischen Konstanten und Dehnungsdoppelbrechung hochelastischer Stoffe. *Kolloid-Zeitschrift* 101, 248-271.

La Rosa, G., Risitano, A., 2000. Thermographic methodology for rapid determination of the fatigue limit of materials and mechanical components. *International Journal of Fatigue* 22, 65-73.

Laiarinandrasana, L., Piques, R., Robisson, A., 2003. Visco-hyperelastic model with internal state variable coupled with discontinuous damage concept under total Lagrangian formulation. *International Journal of Plasticity* 19, 977-1000.

Laiarinandrasana, L., Besson, J., Lafarge, M., Hochstetter, C., 2009. Temperature dependent mechanical behaviour of PVDF: Experiments and numerical modelling. *International Journal of Plasticity* 25, 1301-1324.

Le Saux, V., Marco, Y., Calloch, S., Doudard, C., Charrier, P., 2010. Fast evaluation of the fatigue lifetime of rubber-like materials based on a heat build-up protocol and micro-tomography measurements. *International journal of fatigue* 32, 1582-1590.

Leblanc, J., 2002. Rubber-filler interactions and rheological properties in filled compounds. *Progress in Polymer Science* 27, 627-687.

Lee, E. H., 1969. Elastic–plastic deformation at finite strains. *Journal of Applied Mechanics* 36, 1-6.

Lee, E., Liu, D., 1967. Finite-strain elastic-plastic theory with application to plane-wave analysis. *Journal of Applied Physics* 38, 19-27.

Legorjujago, K., Bathias, C., 2002. Fatigue initiation and propagation in natural and synthetic rubbers. *International Journal of Fatigue* 24, 85-92.

Lion, A., 1996. A constitutive model for carbon black filled rubber: Experimental investigations and mathematical representation. *Continuum Mechanics and Thermodynamics* 8, 153-169.

Lion, A., 1997a. On the large deformation behaviour of reinforced rubber at different temperatures. *Journal of the Mechanics and Physics of Solids* 45, 1805-1834.

Lion, A., 1997b. A physically based method to represent the thermo-mechanical behaviour of elastomers. *Acta Mechanica* 123, 1-25.

Lion, A., 2000. Constitutive modelling in finite thermoviscoplasticity: a physical approach based on nonlinear rheological models. *International Journal of Plasticity* 16, 469-494.

Lion, A., Dippel, B., Liebl, C., 2014. Thermomechanical material modelling based on a hybrid free energy density depending on pressure, isochoric deformation and temperature. *International Journal of Solids and Structures* 51, 729-739.

Li, X., Dong, Y., Li, Z., Xia, Y., 2011. Experimental study on the temperature dependence of hyperelastic behavior of tire rubbers under moderate finite deformation. *Rubber Chemistry and Technology* 84, 215-228.

Luo, W., Hu, X., Wang, C., Li, Q., 2010. Frequency- and strain-amplitude-dependent dynamical mechanical properties and hysteresis loss of CB-filled vulcanized natural rubber. *International Journal of Mechanical Sciences* 52, 168–174.

Lu, S., Pister, K., 1975. Decomposition of deformation and representation of the free energy function for isotropic thermoelastic solids. *International Journal of Solids and Structures* 11, 927-934.

Mark, J., 1982. Rubber Elasticity. *Rubber Chemistry and Technology* 55, 1123-1136.

Marckmann, G., Verron, E., Gornet, L. Chagnon, G., Charrier, P., Fort, P., 2002. A theory of network alteration for the Mullins effect. *Journal of the Mechanics and Physics of Solids* 50, 2011-2028.

Mars, W.V., Fatemi, A., 2002. A literature survey on fatigue analysis approaches for rubber. *International Journal of Fatigue* 24, 949-961.

Mars, W.,V., Fatemi, A., 2003. Fatigue crack nucleation and growth in filled natural rubber. *Fatigue and Fracture of Engineering Materials and Structures* 26, 779–789.

Mars, W.,V., Fatemi, A., 2006. Multiaxial stress effects on fatigue behavior of filled natural rubber. *International Journal of Fatigue* 28, 521-529.

Mars, W.V., Fatemi, A., 2008. Fatigue life analysis and predictions for NR and SBR under variable amplitude and multiaxial loading conditions. *International Journal of Fatigue* 30, 1231-1247.

Medalia, A., 1970. Morphology of aggregates: VI. Effective volume of aggregates of carbon black from electron microscopy; Application to vehicle absorption and to die swell of filled rubber. *Journal of Colloid and Interface Science* 32, 115-131.

Medalia, A., 1973. Selecting carbon blacks for Dynamic properties. *Rubber World* 168, 49.

Medalia, A., 1978. Effect of Carbon Black on Dynamic Properties of Rubber Vulcanizates. *Rubber Chemistry and Technology* 51, 437-523.

Medalia, A., 1991. Heat generation in elastomer compounds: causes and effects. *Rubber Chemistry and Technology* 64, 481-492.

Medalia, A., 2001. *Elastomers, Reinforcement of. Dans: Encyclopedia of Materials: Science and Technology*. Pergamon, 2475–2480.

Medalia, A., Kraus, G., 2013. *Science and Technology of Rubber*. 4e ed. ed. Academic Press Inc.

Meinecke, E., 1991. Effect of carbon-black loading and crosslink density on the heat build-up in elastomers. *Rubber Chemistry and Technology* 64, 269-284.

Meo, S., Boukamel, A., Debordes, O., 2002. Analysis of a thermoviscoelastic model in large strain. *Computers and structures* 80, 2085-2098.

Meyer, K., Ferri, C., 1935. Sur l'élasticité du caoutchouc. *Helvetica Chimica Acta* 18, 570-589.

Miehe, C., 1995. Entropic thermoelasticity at finite strains. Aspects of the formulation and numerical implementation. *Computer Methods in Applied Mechanics and Engineering* 120, 243-269.

Molinari, A., 1996. Self heating and thermal failure of polymers sustaining a compressive cyclic loading. *International journal of solids and structure* 33, 3439-3462.

Mooney, M., 1940. A Theory of Large Elastic Deformation. *Journal of Applied Physics* 11, 582-591.

Mooney, M., 1951. The viscosity of a concentrated suspension of spherical particles. *Journal of Colloid Science* 6, 162-170.

Mostafa, A., Abouel-Kasem, A., Bayoumi, M., El-Sebaie, M., 2009. The influence of CB loading on thermal aging resistance of SBR and NBR rubber compounds under different aging temperature. *Materials and Design* 30, 791–795.

MSC.Marc, 2004a. *Volume A: Theory and User Information*. MSC Software Corporation.

MSC.Marc, 2004b. *Volume D: User Subroutines and Special Routines*. MSC Software Corporation.

Mullins, L., 1948. Effect of stretching on the properties of rubber. *Rubber Chemistry and Technology* 21, 281-300.

Mullins, L., 1950. Thixotropic Behavior of Carbon Black in Rubber. *Rubber Chemistry and Technology* 23, 733-743.

Mullins, L., 1969. Softening of rubber by deformation. *Rubber Chemistry and Technology* 42, 339-362.

Mullins, L., Tobin, N., 1957. Theoretical model for the elastic behavior of filler-reinforced vulcanized rubbers. *Rubber Chemistry and Technology* 30, 551-571.

Mullins, L., Tobin, N., 1965. Stress softening in rubber vulcanizates. Part I. Use of a strain amplification factor to describe the elastic behavior of filler-reinforced vulcanized rubber. *Journal of Applied Polymer Science* 9, 2993–3009.

Naït-Abdelaziz, M., Zaïri, F., Qu, Z., Hamdi, A., Aït Hocine, N., 2012. *J* integral as a fracture criterion of rubber-like materials using the intrinsic defect concept. *Mechanics of Materials* 53, 80-90.

Ogden, R., 1972. Large Deformation Isotropic Elasticity - On the Correlation of Theory and Experiment for Incompressible Rubberlike Solids. *Proceedings of the Royal Society of London A* 326, 565-584.

Ovalle Rodas, C., Zaïri, F., Naït-Abdelaziz, M., 2013. Thermo-visco-hyperelastic modeling of the rubber self-heating under fatigue. *Constitutive Models for Rubber VIII – Proceedings of the 8th European Conference on Constitutive Models for Rubbers, ECCMR 2013*, 131-136.

Ovalle Rodas, C., Zaïri, F., Naït-Abdelaziz, M., 2014. A finite strain thermo-viscoelastic constitutive model to describe the self-heating in elastomeric materials during low-cycle fatigue. *Journal of the Mechanics and Physics of Solids* 64, 396-410.

Ovalle Rodas, C., Zaïri, F., Naït-Abdelaziz, M., Charrier, P., 2015. Temperature and filler effects on the relaxed response of filled rubbers: experimental observations on a carbon-filled SBR and constitutive modeling. *International Journal of Solids and Structures*, in press.

Payne, A., 1958. *The Rheology of Elastomers*. Pergamon Press, 86.

Payne, A., 1960. A note on the existence of a yield point in the dynamic modulus of loaded vulcanizates. *Journal of Applied Polymer Science* 3, 127.

Payne, A., 1963a. Dynamic properties of heat-treated Butyl vulcanisates. *Journal of Applied Polymer Science* 7, 873-885.

Payne, A., 1963b. The Dynamic Properties of Carbon Black-Loaded Natural Rubber Vulcanizates. Part I. *Rubber Chemistry and Technology* 36, 432-443.

Payne, A., 1964. Strainwork dependence of filler-loaded vulcanizates. *Journal of Applied Polymer Science* 8, 2661–2686.

Payne, A., 1965. Effect of dispersion on the dynamic properties of filler-loaded rubbers. *Journal of Applied Polymer Science* 9, 2273–2284.

Payne, A., Whittaker, R., Smith, J., 1972. Effect of vulcanization on the low-strain dynamic properties of filled rubbers. *Journal of Applied Polymer Science* 16, 1191–1212.

Pichon, P. G., Boutaous, M., Méchin, F., Sautereau, H., 2012. Measurement and numerical simulation of the self heating of cross-linked segmented polyurethanes under cyclic loading. *European Polymer Journal* 48, 684–695.

Ponte Castañeda, P., 1989. The Overall Constitutive Behaviour of Nonlinearly Elastic Composites. *Proceedings of the Royal Society A* 422, 147-171.

Pramanik, P., Khastgir, D., Saha, T., 1992. Conductive nitrile rubber composite containing carbon fillers: Studies on mechanical properties and electrical conductivity. *Composites Part A: Applied Science and Manufacturing* 23, 183-191.

Privalko, V., Lipatov, Y., 1974. On the folding of the macromolecules in bulk polymers. The structure of interchain "entaglements" in amorphous polymers. *Polymer Science U.S.S.R.* 16, 1809-1816.

Qiu, L., Bae, Y., 2006. Polymer Architecture and Drug Delivery. *Pharmaceutical Research* 23, 1-30.

Rey, T., Chagnon, G., Le Cam, J.-B., Favier, D., 2013. Influence of the temperature on the mechanical behaviour of filled and unfilled silicone rubbers. *Polymer Testing* 32, 492-501.

Rittel, D., 2000. An investigation of the heat generated during cyclic loading of two glassy polymers. Part I: Experimental. *Mechanics of materials* 32, 131-147.

Rittel, D., Rabin, Y., 2000. An investigation of the heat generated during cyclic loading of two glassy polymers; Part II: Thermal Analysis. *Mechanics of materials* 32, 149-159.

Rivlin, R., 1948. Large Elastic Deformations of Isotropic Materials. IV. Further Developments of the General Theory. *Philosophical Transactions of the Royal Society of London A* 241, 379-397.

Samaca Martinez, J., Le Cam, J.-B., Balandraud, X., Toussaint, E., Caillard, J., 2013. Filler effects on the thermomechanical response of stretched rubbers. *Polymer Testing* 32, 835-841.

Schwartz, A., 1907. "Flexibles", with notes on the testing of rubber. *Journal of the Institution of Electrical Engineers* 39, 31-100.

Shedd, J., Ingersol, R., 1904. The Elastic Modulus and Elastic Limit of Rubber and their Relation to Change of Temperature. *Physical Review* 19, 107-116.

Shim, J., Mohr, D., 2011. Rate dependent finite strain constitutive model of polyurea. *International Journal of Plasticity* 27, 868-886.

Sidoroff, F., 1974. Un modèle viscoélastique non linéaire avec configuration intermédiaire. *Journal de Mécanique* 13, 679-713.

Simo, J., 1987. On a fully three-dimensional finite-strain viscoelastic damage model: formulation and computational aspects. *Computer Methods in Applied Mechanics and Engineering* 60, 153-173.

Sircar, A., Lamond, T., 1975a. Strain-Dependent Dynamic Properties of Carbon-Black Reinforced Vulcanizates. I. Individual Elastomers. *Rubber Chemistry and Technology* 48, 79-88.

Sircar, A., Lamond, T., 1975b. Strain-Dependent Dynamic Properties of Carbon-Black Reinforced Vulcanizates. II. Elastomer Blends. *Rubber Chemistry and Technology* 48, 89-96.

Smallwood, H., 1944. Limiting law of the reinforcement of rubber. *Journal of Applied Physics* 15, 758-766.

Sommer, J., Meyer, D., 1974. Factors Controlling the Dynamic Properties of Elastomeric Products. *Journal of Elastomers and Plastics* 6, 49-68.

South, J., Case, S., Reifsnider, K., 2003. Effects of Thermal Aging on The Mechanical Properties of Natural Rubber. *Rubber Chemistry and Technology* 76, 785-802.

Stainier, L., Ortiz, M., 2010. Study and validation of a variation theory of thermo-mechanical coupling in finite visco-plasticity. *International Journal of Solids and Structures* 47, 705-715.

Sullivan, J., Mark, J., Hampton, P., Cohen, R., 1978. Model networks of end-linked polydimethylsiloxane chains. II. Viscoelastic losses. *The Journal of Chemical Physics* 68, 2010-2012.

Thiele, J., Cohen, R., 1980. Thermal expansion phenomena in filled and unfilled natural rubber vulcanizates. *Rubber Chemistry and Technology* 53, 313-320.

Tobolsky, A.V., Prettyman, I.B., Dillon, J.H., 1944. Stress relaxation of natural and synthetic rubber stocks. *Journal of Applied Physics* 15, 380-395.

Tomita, Y., Azuma, K., Naito, M., 2008. Computational evaluation of strain-rate-dependent deformation behavior of rubber and carbon-black-filled rubber under monotonic and cyclic straining. *International Journal of Mechanical Sciences* 50, 856-868.

Trabelsi, S., Albouy, P.-A., Rault, J., 2003. Effective local deformation in stretched filled rubber. *Macromolecules* 36, 9093-9099.

Treloar, L., 1944. Stress-strain data for vulcanised rubber under various types of deformation. *Transactions of the Faraday Society* 40, 59-70.

Treloar, L., 1971. *Viscoelastic properties of polymers*. Br. Polym. J., London: John Wiley & Sons, Ltd.

Treloar, L., 2005. *The Physics of Rubber Elasticity*. 3rd ed. Great Britain: Clarendon Press - Oxford.

Treloar, L.R.G., Riding, G., 1979. A non-Gaussian theory for rubber in biaxial strain. I. Mechanical properties. *Proceedings of the Royal Society of London A* 369, 261-280.

Ulmer, J., Chirico, V., Scott, C., 1973. The Effect of Carbon Black Type on the Dynamic Properties of Natural Rubber. *Rubber Chemistry and Technology* 46, 897-926.

Ulmer, J., Hergenrother, W., Lawson, D., 1998. Hysteresis Contributions in Carbon Black-Filled Rubbers Containing Conventional and Tin End-Modified Polymers. *Rubber Chemistry and Technology* 71, 637-667.

Valanis, K., Landel, R., 1967. The Strain-Energy Function of a Hyperelastic Material in Terms of the Extension Ratios. *Journal of Applied Physics* 38, 2997-3002.

Vand, V., 1948. Viscosity of solutions and suspensions. 1. theory. *Journal of Physical and Colloid Chemistry*, 277-299.

Voet, A., Cook, F., 1967. Mild Stress Softening and Dynamic Properties of Rubber Vulcanizates. *Rubber Chemistry and Technology* 40, 1364-1372.

Wood, L.A., Bekkedahl, N., Roth, F.L. 1943. Density Measurements on Synthetic Rubbers. *Rubber Chemistry and Technology* 16, 244-248.

Wu, P., van der Giessen, E., 1993. On improved network models for rubber elasticity and their application to orientation hardening in glassy polymers. *Journal of the Mechanics and Physics of Solids* 41, 427-456.

Ximenez, F., 1715. *Empiezan las historias del origen de los indios de esta provincia de Guatemala*. Guatemala.

Yang, Q., Stainier, L., Ortiz, M., 2006. A variational formulation of the coupled thermo-mechanical boundary-value problem for general dissipative solids. *Journal of the Mechanics and Physics of Solids* 54, 401-424.

Yeh, G., 1980. Current concepts of morphology of amorphous polymers - II. Degree of local order an overall chain conformation. *Polymer Science U.S.S.R.* 21, 2686-2703.

Yeoh, O., 1993. Some Forms of the Strain Energy Function for Rubber. *Rubber Chemistry and Technology* 66, 754-771.

Zaïri, F., Naït-Abdelaziz, M., Gloaguen, J.M., Lefebvre, J.M., 2008a. Modelling of the elasto-viscoplastic damage behaviour of glassy polymers. *International Journal of Plasticity* 24, 945-965.

Zaïri, F., Naït-Abdelaziz, M., Gloaguen, J.M., Bouaziz, A., Lefebvre, J.M., 2008b. Micromechanical modelling and simulation of chopped random fiber reinforced polymer composites with progressive debonding damage. *International Journal of Solids and Structures* 45, 5220-5236.

Zaïri, F., Naït-Abdelaziz, M., Gloaguen, J.M., Lefebvre, J.M., 2010. Constitutive modelling of the large inelastic deformation behaviour of rubber-toughened poly(methyl methacrylate):

effects of strain rate, temperature and rubber-phase volume fraction. *Modelling and Simulation in Materials Science and Engineering* 18.

Zaïri, F., Naït-Abdelaziz, J.M., Gloaguen, J., Lefebvre, J., 2011a. A physically-based constitutive model for anisotropic damage in rubber-toughened glassy polymers during finite deformation. *International Journal of Plasticity* 27, 25-51.

Zaïri, F., Gloaguen, J.M., Naït-Abdelaziz, M., Mesbah, A., Lefebvre, J.M., 2011b. Study of the effect of size and clay structural parameters on the yield and post-yield response of polymer/clay nanocomposites via a multiscale micromechanical modelling. *Acta Materialia* 59, 3851-3863.